On the impact of non-covalent interactions on the formation of protein-lipid complexes in the gas phase and in solution

Dissertation

zur Erlangung des

Doktorgrades der Naturwissenschaften (Dr. rer. nat.)

der

Naturwissenschaftlichen Fakultät II

Chemie, Physik und Mathematik

der Martin-Luther-Universität

Halle-Wittenberg,

vorgelegt von

Herr **Til Erik Kundlacz**

geboren am [redacted] in [redacted]

Eingereicht am: 11.03.2025 Verteidigt am: 22.10.2025

Gutachter*innen:

1. Prof. Dr. Dariush Hinderberger
2. Prof. Dr. Carla Schmidt
3. Prof. Dr. Michael Landreh

First Reviewer

Prof. Dr. Dariush Hinderberger
MLU Halle-Wittenberg
Institute of Physical Chemistry
Von-Danckelmann-Platz 4
06120 Halle (Saale)
Germany

Second Reviewer

Prof. Dr. Carla Schmidt
JGU Mainz
Department of Chemistry-Biochemistry
Hanns-Dieter-Hüsch-Weg 17
55128 Mainz
Germany

Third Reviewer

Prof. Dr. Michael Landreh
Uppsala University
Department of Cell and Molecular Biology
Husargatan 3
752 37 Uppsala
Sweden

Table of Contents

List of figures

List of abbreviations

AmAc	ammonium acetate
AMP	antimicrobial peptide
BSA	bovine serum albumin
Ca^{2+}	calcium ion
C2A	isolated N-terminal C2 domain of synaptotagmin-1
C2B	isolated C-terminal C2 domain of synaptotagmin-1
C8E4	tetraethylene glycol monooctyl ether
CEM	chain ejection model
CID	collision-induced dissociation
cmc	critical micelle concentration
CRM	charged-residue model
Da	dalton
DLS	dynamic light scattering
DOPC	1,2-dioleoyl-sn-glycero-3-phosphocholine
DOPG	1,2-dioleoyl-sn-glycero-3-phospho-(1'-rac-glycerol)
DOPI	1,2-dioleoyl-sn-glycero-3-phospho-(1'-myo-inositol)
DOPI(4)P	1,2-dioleoyl-sn-glycero-3-phospho-(1'-myo-inositol-4'-phosphate)
DOPI(4,5)P_2	1,2-dioleoyl-sn-glycero-3-phospho-(1'-myo-inositol-4',5'-bisphosphate)
DOPI(3,4,5)P_3	1,2-dioleoyl-sn-glycero-3-phospho-(1'-myo-inositol-3',4',5'-trisphosphate)
DOPS	1,2-dioleoyl-sn-glycero-3-phospho-L-serine
EGTA	ethylene glycol-bis(β-aminoethyl ether)-N,N,N',N'-tetraacetic acid
ESI	electrospray ionisation
GPL	glycerophospholipid
IEM	ion evaporation model
LL-37-neg	negative variant of LL-37
LL-37-pos	positive variant of LL-37
LL-37-wt	wild type LL-37
MALDI	matrix assisted laser desorption/ionisation
MIP	maximum insertion pressure
MD simulation	molecular dynamics simulation
MS	mass spectrometry
MS/MS	tandem mass spectrometry
MWCO	molecular weight cut-off
m/z	mass-to-charge

nano ESI	nanoelectrospray ionisation
native MS	native mass spectrometry
OG	N-octyl-β-D-glycopyranoside
PA	phosphatic acid
PA 14:0/14:0	1,2-dimyristoyl-sn-glycero-3-phosphate
PC	phosphatidylcholine
PC 14:0/14:0	1,2-dimyristoyl-sn-glycero-3-phosphocholine
PE	phosphatidylethanolamine
PE 14:0/14:0	1,2-dimyristoyl-sn-glycero-3-phosphoethanolamine
PG	phosphatidylglycerol
PG 6:0/6:0	1,2-dihexanoyl-sn-glycero-3-phospho-(1'-rac-glycerol)
PG 10:0/10:0	1,2-didecanoyl-sn-glycero-3-phospho-(1'-rac-glycerol)
PG 14:0/14:0	1,2-dimyristoyl-sn-glycero-3-phospho-(1'-rac-glycerol)
PG 18:0/18:0	1,2-distearoyl-sn-glycero-3-phospho-(1'-rac-glycerol)
PI	phosphatidylinositol
$PI(4,5)P_2$	phosphatidylinositol-4,5-bisphosphate
PS	phosphatidylserine
PS 14:0/14:0	1,2-dimyristoyl-sn-glycero-3-phospho-L-serine
RF	response factor
SNAP-25	synaptosome-associated protein of 25 kDa
SNARE	soluble N-ethylmaleimide-sensitive-factor attachment protein receptor
Syt1	synaptotagmin-1
TAP 14:0/14:0	1,2-dimyristoyl-3-trimethylammonium-propane
TOF	time-of-flight

Amino acids letter code

alanine	A
arginine	R
asparagine	N
aspartate (aspartic acid)	D
cysteine	C
glutamate or (glutamic acid)	E
glutamine	Q
glycine	G
histidine	H
isoleucine	I
leucine	L
lysine	K
methionine	M
phenylalanine	F
proline	P
serine	S
threonine	T
tryptophan	W
tyrosine	Y
valine	V

Abstract

Interactions between membrane proteins and lipids are fundamental to many biological processes, making their analysis particularly important. Native mass spectrometry (native MS) emerged as a well-suited tool to characterise these interactions. In this thesis, protein-lipid interactions are characterised by exploring the impact of non-covalent interactions on the formation of protein-lipid complexes. For this, the detergent-mediated lipid transfer from mixed detergent-lipid micelles to the proteins was employed. However, native MS analysis requires the ionisation and gas-phase transfer of the protein-lipid complexes and these processes might distort their non-covalent interactions. Furthermore, a systematic analysis of the detergent-mediated lipid transfer as a method for exploring the interactions between soluble peripheral membrane proteins and lipids is still missing. Accordingly, the two central questions of this thesis are: (i) Do the interactions that are observed in the gas phase reflect interactions formed in solution? (ii) Is detergent-mediated lipid transfer a reliable technique for investigating protein-lipid interactions of peripheral membrane proteins? To address these questions, protein-lipid interactions were systematically investigated by native MS. Specifically, three protein-lipid binding studies were performed, which focused on the impact of specific non-covalent interactions and explored key aspects of the native MS methodology.

In the first part of this thesis, protein-lipid interactions between the amphipathic model peptide LL-37 and glycerophospholipids, containing different head groups or varying in fatty acyl chain lengths, were systematically explored by native MS. The aim of that study was to determine the impact of electrostatic interactions with the lipid head groups and interactions with the fatty acyl chains that are driven by van der Waals interactions and the hydrophobic effect, on the formation of protein-lipid interactions. In addition, the question whether non-covalent interactions formed in solution are reflected by interactions observed in the gas phase was assessed. The interactions of LL-37 with glycerophospholipids containing different head groups revealed a correlation between the ion intensity of complexes and their stability in the gas phase, suggesting that electrostatic interactions drive protein-lipid complex formation in solution and stabilise these complexes in the gas phase. In contrast, interactions with glycerophospholipids varying in fatty acyl chain length revealed a great increase in ion intensity and a minor increase in complex stability with increasing chain lengths. This suggests that interactions driven by the hydrophobic effect in solution contribute to the ion intensity, while van der Waals interactions contribute to the complex stability in the gas phase.

In the second part of this thesis, the effect of peptide surface charge on peptide-lipid interactions was investigated. For this, supercharged cationic (LL-37-pos) and anionic (LL-37-neg) variants of LL-37 were designed. Interactions of the supercharged variants with a variety of lipids were then analysed by native MS in positive and negative ion mode and compared to

interactions formed by the wild type peptide (LL-37-wt). The analysis of interactions formed by LL-37-neg required the use of negative ion mode demonstrating ionisation effects during native MS analysis. In addition to native MS, a Langmuir film balance was used to analyse the interactions of the LL-37 variants with lipid monolayers in solution. Both techniques demonstrate that the surface charge shapes the electrostatically dominated lipid preferences of the LL-37 variants. Specifically, LL-37-pos and LL-37-neg preferred interactions with lipids containing the opposite charge, while LL-37-wt binds negatively charged and zwitterionic lipids with high affinity, likely because it contains anionic and cationic residues.

In the third part of this thesis, the Ca^{2+}-dependent lipid preferences of the isolated cytosolic C2 domains (C2A and C2B) of the Ca^{2+}-sensor Synaptotagmin-1 were characterised. The goal of that study was to investigate the role of Synaptotagmin-1 during synaptic vesicle exocytosis. For this, the lipid preferences of the C2 domains were investigated in the presence and in the absence of Ca^{2+}. Native MS analysis and lipid overlay assays revealed a preference of the C2 domains for negatively charged lipids. Liposome flotation assays employing liposomes that mimic the synaptic vesicle and the presynaptic membrane suggest Ca^{2+}-dependent membrane interactions of the C2 domains and a preference of C2B for the presynaptic membrane. Molecular dynamics simulations of these interactions with synaptic vesicle and presynaptic membrane models demonstrate differences in the binding dynamics, orientation on the membrane and membrane insertion of the C2 domains, suggesting different roles of the C2 domains during exocytosis. The combined results indicate the following mechanism for full-length Synaptotagmin-1: C2B binds to the presynaptic membrane in the presence and in the absence of Ca^{2+}, while C2A associates with the synaptic vesicle membrane and undergoes a Ca^{2+}-dependent shift from a parallel contact angle to a perpendicular orientation. This process places the flexible linker connecting the C2 domains under tension, thereby pulling the two membranes together.

In summary, this thesis contributes to the general understanding of the impact of non-covalent interactions on the formation of interactions between peripheral membrane proteins and lipids. Furthermore, this thesis addresses key questions that arise when studying protein-lipid interactions by native MS analysis.

Zusammenfassung

Wechselwirkungen zwischen Membranproteinen und Lipiden sind essenziell für viele biologische Prozesse, was ihre Analyse besonders bedeutend macht. Native Massenspektrometrie (MS) etablierte sich als geeignete Methode um diese Interaktionen zu untersuchen. In dieser Arbeit wurden die Interaktionen zwischen Proteinen und Lipiden charakterisiert und der Einfluss nicht-kovalenter Wechselwirkungen auf die Bildung von Protein-Lipid-Komplexen untersucht. Hierfür wurde der durch Detergens vermittelte Lipidtransfer von gemischten Detergens-Lipid-Mizellen auf die Proteine genutzt. Die Analyse mittels nativer MS erfordert jedoch die Ionisierung und den Transfer der Protein-Lipid-Komplexe in die Gasphase. Beide Prozesse können die nicht-kovalenten Wechselwirkungen der Komplexe beeinflussen. Weiterhin gibt es bisher keine systematische Untersuchung des durch Detergens vermittelten Lipidtransfers als Methode zur Analyse der Interaktionen zwischen peripheren Membranproteinen und Lipiden. Die beiden zentralen Fragen dieser Arbeit lauten daher: (i) Spiegeln die in der Gasphase beobachteten Interaktionen die in der Lösung gebildeten Interaktionen wieder? (ii) Ist der durch Detergens vermittelte Lipidtransfer eine geeignete Methode um die Interaktionen peripherer Membranproteine mit Lipiden zu untersuchen? Um diese Fragen zu beantworten, wurden in der vorliegenden Dissertation Protein-Lipid-Wechselwirkungen systematisch mittels nativer MS untersucht. Hierfür wurden drei Protein-Lipid-Bindestudien durchgeführt, die sich auf die Auswirkungen spezifischer nicht-kovalenter Wechselwirkungen konzentrieren und essentielle Aspekte der nativen MS untersuchen.

Im ersten Teil dieser Arbeit wurden die Protein-Lipid-Interaktionen zwischen dem amphipathischen Modellpeptid LL-37 und Glycerophospholipiden mit unterschiedlichen Kopfgruppen und unterschiedlich langen Fettsäureketten systematisch mittels nativer MS untersucht. Das Ziel dieser Studie war es, den Einfluss von elektrostatischen Wechselwirkungen mit den Kopfgruppen der Lipide sowie den Einfluss von Wechselwirkungen mit den Fettsäureketten auf die Bildung von Protein-Lipid-Interaktionen zu bestimmen. Spezifisch, werden Wechselwirkungen mit den Fettsäureketten durch van der Waals-Wechselwirkungen und den hydrophoben Effekt bedingt. Außerdem wurde die Frage adressiert, ob sich in der Lösung gebildete Interaktionen, in den beobachteten Interaktionen in der Gasphase wiederspiegeln. Die Interaktionen von LL-37 mit Glycerophospholipiden mit unterschiedlichen Kopfgruppen zeigte eine Korrelation zwischen Ionenintensität von Komplexen und ihrer Stabilität in der Gasphase. Diese Korrelation weist darauf hin, dass elektrostatische Wechselwirkungen die Bildung von Protein-Lipid-Komplexen in Lösung bestimmen und diese Komplexe in der Gasphase stabilisieren. Im Gegensatz dazu wurde für Interaktionen mit Glycerophospholipiden mit unterschiedlicher Fettsäurekettenlänge eine

starke Steigerung der Ionenintensität und eine schwache Zunahme der Stabilität der Komplexe in der Gasphase mit zunehmender Kettenlänge beobachtet. Diese Beobachtung deutet darauf hin, dass Interaktionen, die durch den hydrophoben Effekt in Lösung angetrieben werden, zur Ionenintensität beitragen, während van der Waals-Wechselwirkungen zur Stabilität in der Gasphase beitragen.

Im zweiten Teil dieser Arbeit wurde der Einfluss der Oberflächenladung von Peptiden auf Peptid-Lipid-Wechselwirkungen untersucht. Dafür wurden hochgeladene kationische (LL-37-pos) und anionische (LL-37-neg) Varianten von LL-37 entwickelt. Die Interaktionen der hochgeladenen Varianten mit verschiedenen Lipiden wurden dann mittels nativer MS im positiven und negativen Modus analysiert und mit den Interaktionen des Wildtyps (LL-37-wt) verglichen. Die Analyse der Interaktionen von LL-37-neg erforderte die Messung im negativen Ionenmodus, was auf Ionisierungseffekte während der Analyse durch native MS hindeutet. Zusätzlich zur Analyse mittels nativer MS wurde eine Langmuir Filmwaage verwendet um die Interaktionen der LL-37 Varianten mit Lipid-Monoschichten in Lösung zu untersuchen. Beide Techniken zeigten, dass die Oberflächenladung der LL-37 Varianten die elektrostatisch dominierten Lipidpräferenzen bestimmt. Im Detail bevorzugten LL-37-pos und LL-37-neg Interaktionen mit Lipiden entgegengesetzter Ladung, während LL-37-wt eine hohe Affinität für negativ geladene und zwitterionische Lipide zeigte. Der Grund dafür ist wahrscheinlich, dass LL-37-wt anionische und kationische Aminosäuren enthält.

Im dritten Teil dieser Arbeit wurden Ca^{2+}-abhängige Lipidpräferenzen der isolierten cytosolischen C2-Domänen (C2A und C2B) des Ca^{2+}-Sensors Synaptotagmin-1 charakterisiert. Das Ziel dieser Studie war es, die Rolle von Synaptotagmin-1 in der Exozytose synaptischer Vesikel zu ermitteln. Dafür wurden die Lipidpräferenzen der C2-Domänen in An- und Abwesenheit von Ca^{2+} untersucht. Native MS Analysen und *lipid overlay assays* zeigten eine Präferenz der C2-Domänen für negativ geladene Lipide. Flotationsanalysen mit Liposomen, die synaptische Vesikel und die präsynaptische Membran nachahmen, deuteten auf Ca^{2+}-abhängige Membraninteraktionen und eine Präferenz von C2B für die präsynaptische Membran hin. Molekulardynamik-Simulationen dieser Interaktionen mit Modellmembranen synaptischer Vesikel- und der präsynaptischen Membran zeigten Unterschiede in der Bindedynamik, Orientierung zur Membran und Membraninsertion der C2-Domänen, was auf unterschiedliche Rollen der C2-Domänen während der Exozytose hinweist. Aus der Kombination der Ergebnisse ergibt sich folgender Mechanismus für Synaptotagmin-1: C2B bindet die präsynaptische Membran in An- und Abwesenheit von Ca^{2+}, während C2A an die Membran der synaptischen Vesikel assoziiert und eine Ca^{2+}-abhängige Positionsänderung von einem parallelen Kontaktwinkel zu einer senkrechten Ausrichtung durchläuft. Durch diesen

Prozess wird der flexible *linker*, der die beiden C2-Domänen verbindet, gespannt, wodurch die beiden Membranen zusammengezogen werden.

Zusammenfassend trägt diese Arbeit zum allgemeinen Verständnis der Auswirkungen nicht-kovalenter Wechselwirkungen auf die Bildung von Interaktionen zwischen peripheren Membranproteinen und Lipiden bei. Darüber hinaus werden wichtige Fragen, die bei der Untersuchung von Protein-Lipid-Wechselwirkungen mittels nativer MS aufkommen, diskutiert.

Publication list

P1 **Til Kundlacz***, Julian Bender*, Carla Schmidt (2021) Effects of non-ionic and zwitterionic detergents on soluble proteins during native mass spectrometry experiments. *International Journal of Mass Spectrometry*, vol. 468, p. 116652, Oct 2021, https://doi.org/10.1016/j.ijms.2021.116652

P2 **Til Kundlacz**, Carla Schmidt (2023) Deciphering Solution and Gas-Phase Interactions between Peptides and Lipids by native Mass Spectrometry. *Anal. Chem.*, 95, 47, 17292-17299. https://doi.org/10.1021/acs.analchem.3c03428

P3 **Til Kundlacz**, Christian Schwieger, Carla Schmidt (2025) Effects of Surface Charge of Amphiphilic Peptides on Peptide-Lipid Interactions in the Gas Phase and in Solutions. *Anal. Chem.*, https://doi.org/10.1021/acs.analchem.5c00283

P4 Julian Bender*, **Til Kundlacz***, Lucas S. P. Rudden, Melissa Frick, Julia Bieber, Matteo T. Degiacomi, Carla Schmidt (2024) Ca^{2+}-dependent lipid preferences shape synaptotagmin-1 C2A and C2B dynamics: Insights from experiments and simulations. *Structure*, vol. 32, issue 10, pages 1691-1704.e5, https://doi.org/10.1016/j.str.2024.07.017

This thesis presents the results of publications **P2**, **P3** and **P4**. Publication **P1** is not reprinted or discussed in detail in this thesis, as the practical work was performed during my Master's thesis and my work as a research assistant at ZIK HALOmem. Details on individual author contributions are provided in the Results chapter. This thesis was performed in the framework of the research training group 2670 "Beyond Amphiphilicity: Self-Organization of Soft Matter via Multiple Noncovalent Interactions" (BEAM).

1. Introduction

Interactions between proteins and lipids are fundamental in many biological processes, including metabolism[1], trafficking[2,3], signal transduction[4] and immune response[5]. They are driven by an interplay of electrostatic interactions such as Coulomb interactions, hydrogen bonds, van der Waals forces and the hydrophobic effect. Protein-lipid interactions involve the interactions of lipids with integral membrane proteins that are embedded in the membrane and with peripheral membrane proteins, which are soluble proteins that are temporarily recruited to the membrane[6]. The structure and type of the membrane protein determines which interactions are dominant. While many peripheral membrane proteins rely mainly on electrostatic interactions with lipid head groups[7], amphipathic peptides contain additional hydrophobic regions for the integration into the hydrophobic core of the membranes[8,9]. An overview of important non-covalent interactions between membrane proteins and lipids is depicted in **Figure 1**. While classical structural methods continue to provide valuable information about the mechanism and the interactions of membrane proteins, they are often not able to resolve specific binding events[10]. Accordingly, native mass spectrometry emerged as a valuable tool to fill this gap, capable of identifying of specific binding partners and determining the complex' stoichiometry[11–14]. However, the analysis by native mass spectrometry requires the ionisation and transfer of the analytes into the gas-phase, where solvent effects are non-existent. This process might distort the non-covalent interactions between proteins and lipids, which leads to one of the central questions of this thesis: Do interactions observed in the gas phase reflect interactions formed in solution? To answer this question, non-covalent interactions between different proteins and lipids will be systematically explored using native mass spectrometry and further compared with interaction studies in solution. This chapter provides a theoretical background about the systems and methods used in this thesis.

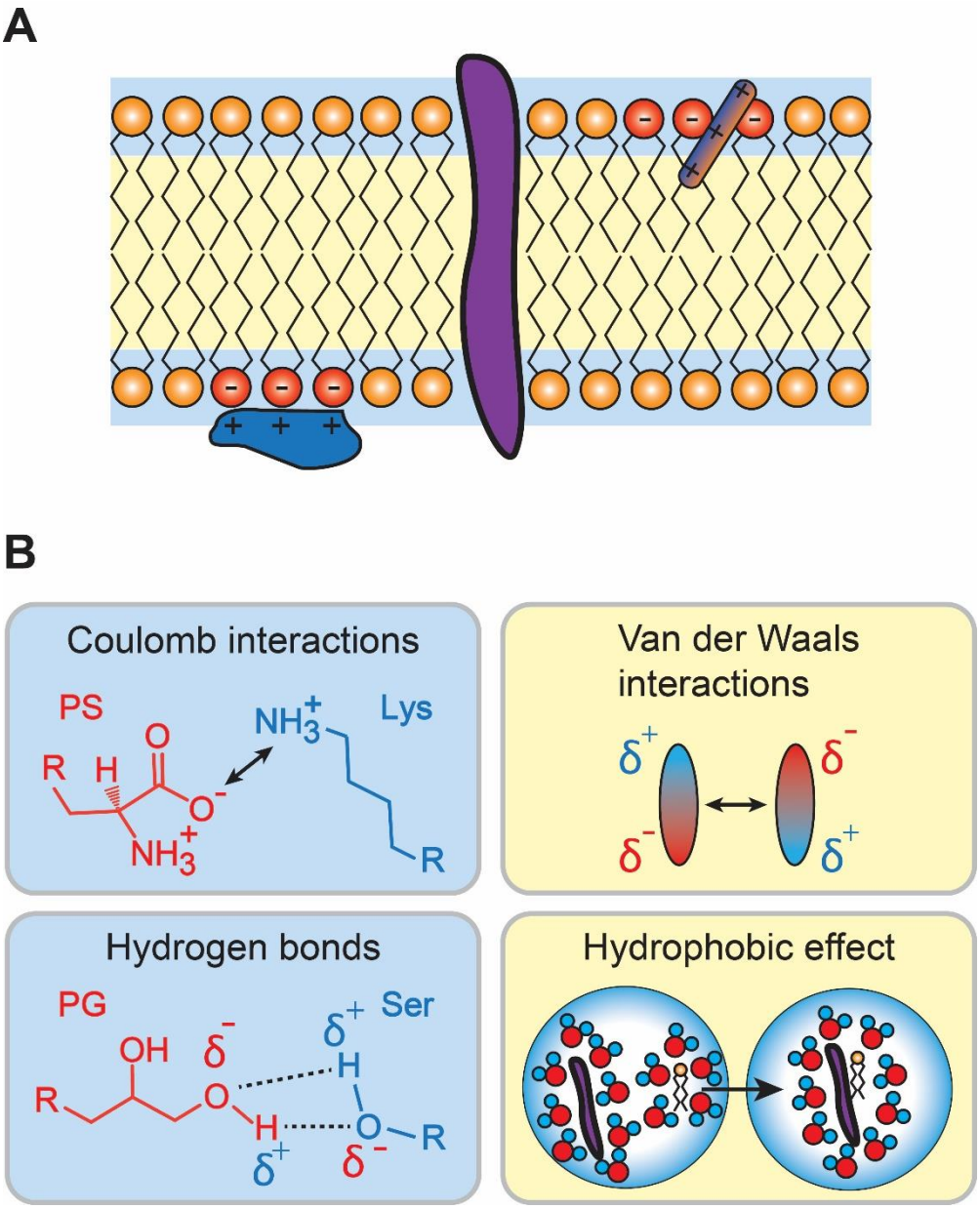

Figure 1: Schematic representation of non-covalent interactions between membrane proteins and lipids within a membrane. (**A**) Biological membranes consist mainly of a phospholipid bilayer including a variety of membrane proteins. Phospholipid bilayers contain a central hydrophobic core region (yellow) and two hydrophilic interfacial regions (blue)[2]. Membrane proteins are classified as integral (purple) or peripheral membrane proteins. Peripheral membrane proteins can be further separated into peripheral membrane proteins that interact with the polar lipid head groups (blue) and amphiphilic peripheral membrane proteins that penetrate into the hydrophobic core region interacting with the lipid head groups and with fatty acyl chains simultaneously (blue and orange). (**B**) Schematic representation of non-covalent interactions that drive protein-lipid interactions in the polar interfacial regions (blue) and in the hydrophobic core region (yellow). PS, phosphatidylserine; Lys, lysine; PG, phosphatidylglycerol; Ser, serine.

1.1 Non-covalent interactions

The formation of complexes between molecules depends on the interplay of their non-covalent interactions. In general, each system adopts an energetically favourable state, i.e. increasing attractive forces and reducing repulsive forces. The interactions between membrane proteins and lipids, which are the central subject of this thesis, are diverse including Coulomb interactions, van der Waals interactions, hydrogen bonds and interactions driven by the hydrophobic effect. Accordingly, in the next paragraph a brief overview on the most important non-covalent interactions between proteins and lipids will be given. In this thesis, protein-lipid interactions are analysed by native mass spectrometry which requires ionisation and gas-phase transfer of the complexes. Therefore, the effects of gas-phase transfer on the non-covalent interactions will be highlighted.

1.1.1 Coulomb interactions

The interactions between two charged particles are best described by Coulomb's law, which quantifies the electrostatic force between two point charges (Q_1 and Q_2) with respect to their distance r, the dielectric permittivity (dielectric constant) of free space ε_0 and the dielectric permittivity of the medium ε[15]:

$$F_C = \frac{Q_1 Q_2}{4\pi\varepsilon_0 \varepsilon r^2}$$

Positive values ($F_C > 0$) signify a repulsive force, while negative values ($F_C < 0$) indicate an attractive force. Accordingly, molecules which are similarly charged experience repulsion while oppositely charged particles (i.e. positive and negative) attract each other. The strength of interaction is proportional to the force of the two charges and inversely proportional to their square distance. The weak distance dependence of Coulomb interactions allows long range interactions between charged molecules. Importantly, the strength of Coulomb interactions is also inversely proportional to the dielectric constant of the medium. Coulomb interactions are one of the driving forces for the association of peripheral membrane proteins to lipid membranes through long-range attractive forces between charged amino acids of the protein and charged lipid head groups[7].

1.1.2 Van der Waals interactions

Van der Waals interactions represent relatively weak, short-range non-covalent interactions between atoms or molecules with induced or permanent dipoles. Dipoles are induced in atoms and molecules, when the electrical centre of the electron cloud does not coincide with the electrical centre of the positive charges of the nuclei[16]. Dipoles can be temporary (also referred

to as instantaneous), induced or permanent. Notably, van der Waals interactions are essential for the interactions between fatty acyl chains of lipids and the nonpolar regions of membrane proteins in the hydrophobic membrane core[17].

Van der Waals forces sum up the following contributing forces:

1. Keesom forces; i.e. interactions between permanent dipoles
2. Debye forces; i.e. interactions between permanent and induced dipoles
3. London dispersion forces; i.e. interactions of temporary dipoles
4. Repulsive potential; i.e. repulsion of atoms with overlapping orbitals due to the Pauli exclusion principle

The total van der Waals forces between two neutral particles are represented as a function of distance in the Lennard-Jones potential[18] (**Figure 2**). The Lennard-Jones potential is a mathematical model to describe the potential energy of the non-covalent interaction between two neutral particles. It combines two terms, a term signifying the repulsion at close proximity $\left(\frac{\sigma}{r}\right)^{12}$ and the attraction $-\left(\frac{\sigma}{r}\right)^{6}$. The repulsion originates from the Pauli exclusion principle, which prevents atoms from having two electrons with the same set of quantum numbers[19]. In contrast, the attractive term reflects the London dispersion forces, one of the major forces making up the van der Waals force[18]. The Lennard-Jones potential is given as

$$W(r) = 4\varepsilon\left[\left(\frac{\sigma}{r}\right)^{12} - \left(\frac{\sigma}{r}\right)^{6}\right]$$

with r = distance between particles, ε = depth of the potential well and σ = distance where the Lennard-Jones potential becomes 0 (i.e. $r = \sigma$ when $W(r) = 0$)[15]. The equilibrium distance at which the potential energy is minimal is defined as $r_{min} = 2^{\frac{1}{6}}\sigma$. Keesom, Debye and London forces will be briefly described in the following paragraphs.

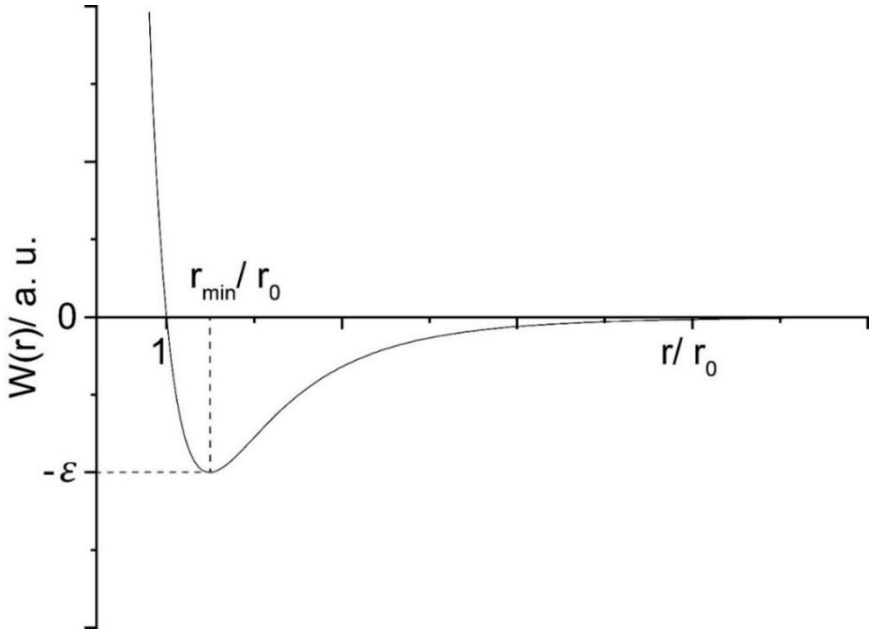

Figure 2: Lennard-Jones potential W(r) as a function of the distance r in the unit r_0. The figure was adapted from Rainer Kimmich 2012[20].

Keesom forces

The force between two freely rotating permanent dipoles (i.e. between two polar molecules) is referred to as Keesom force (**Figure 3**). Permanent dipoles in polar compounds originate from differences in the electronegativity of the atoms, i.e. atoms with higher electronegativity attract electrons and, thereby are partially negatively charged while other atoms are partially positively charged. Due to the thermal motion of particles in solution, dipoles constantly rotate and their relative orientation to each other changes continuously. Therefore, the Keesom energy is determined as the Boltzmann-averaged interaction energy over all possible alignments and it is given as

$$E_K = -\frac{\mu_1^2 \mu_2^2}{3(4\pi\varepsilon\varepsilon_0)^2 k_B T r^6}$$

with μ = permanent dipole moment, ε = dielectric permittivity of the medium, ε_0 = dielectric permittivity of free space k_B = Boltzmann constant, T = absolute temperature and r = distance between particles[15]. Keesom forces are inversely proportional to the square dielectric constant of the medium as well as the temperature. Note that Keesom forces represent the only temperature-dependent forces contributing to the van der Waals forces. In addition, Keesom forces are short ranged having a $1/r^6$ distance dependence.

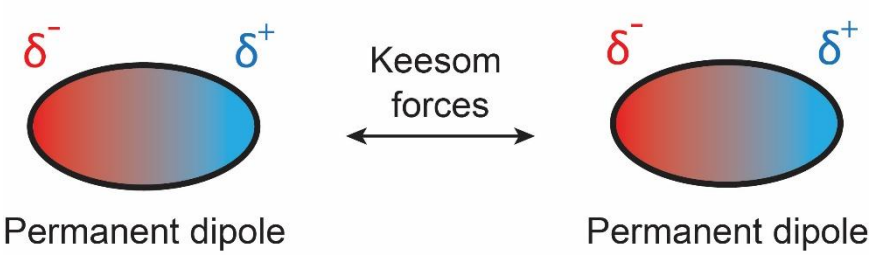

Figure 3: Schematic of Keesom forces. Keesom forces exist between two freely rotating permanent dipoles.

Debye forces

Debye forces determine the interactions between a freely rotating permanent dipole (i.e. a polar molecule) and an induced dipole (i.e. a nonpolar molecule) (**Figure 4**). The electric field of a permanent dipole can induce a dipole in a proximate nonpolar molecule. This process is often referred to as polarisation. Similar to Keesom forces, the orientation of the molecules is not static and an angle-averaged Debye energy is therefore calculated. The effective Debye energy is given as

$$E_D = -\frac{\mu^2 \alpha_0}{(4\pi\varepsilon\varepsilon_0)^2 r^6}$$

with μ = permanent dipole moment, α_0 = polarizability, ε = dielectric permittivity of the medium, ε_0 = dielectric permittivity of free space and r = distance between particles[15]. Note that the equation for the Debye and Keesom energies is very similar with the notable exception that the permanent dipole moment of a second particle within the numerator is replaced by the polarizability term and that the Debye energy is independent of the temperature. The angle-averaged Debye energy is proportional to the dipole moment of the polar molecule and the polarizability of the nonpolar molecule. In addition, it is inversely proportional to ε^2 and r^6. Accordingly, like all van der Waals forces, Debye forces are strongly distance dependent.

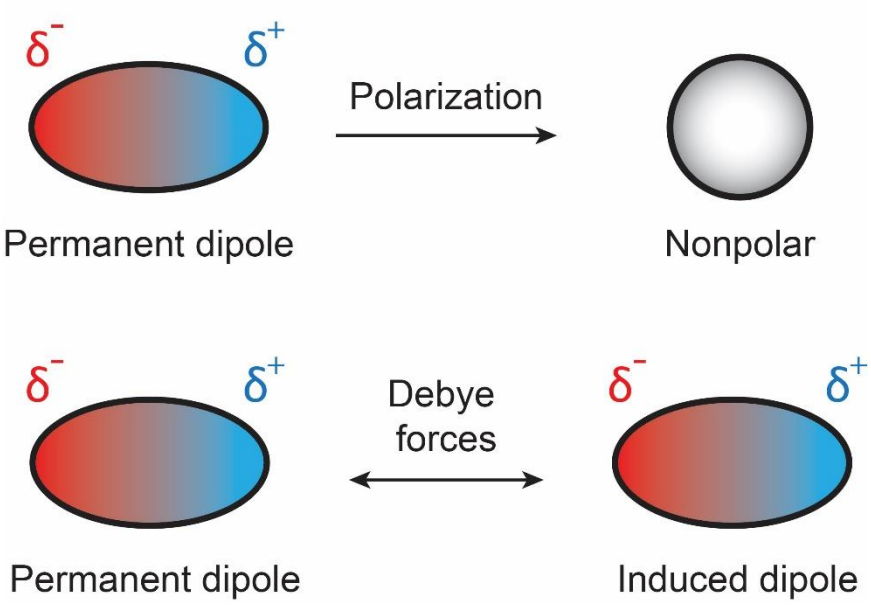

Figure 4: Schematic of Debye forces. Molecules with permanent dipoles induce dipoles in proximate nonpolar molecules (polarization). Debye forces exist between permanent and the induced dipoles.

London dispersion forces

London dispersion forces concern the interactions between atoms or molecules with temporary dipoles (**Figure 5**). They, for instance, contribute to the surface tension of liquids, adhesion forces and the folding of macromolecules[21]. Notably, London forces are present in all atom-atom interactions and allow electrostatic interactions between nonpolar molecules. Although, the time average of the dipole moment μ of nonpolar molecules is zero, random fluctuations of the electron cloud induces temporary dipoles[15]. The electric field of these temporary dipoles can induce dipoles in other proximate atoms (i.e. polarization) resulting in interactions between the atoms[15]. Between two identical particles in vacuum, the London dispersion forces can be estimated by as

$$E_L = -\frac{3h\nu\alpha^2}{4(4\pi\varepsilon\varepsilon_0)^2 r^6}$$

with h = Planck constant, ν = electronic absorption frequency, α = electric polarizability, ε = dielectric permittivity of the medium, ε_0 = dielectric permittivity of free space and r = distance between particles[15].The strength of London dispersion forces increases with (i) atom size, as they are more easily polarised, and (ii) with molecular shape, as larger surface areas of the molecules allow for contacts between the atoms. Characteristic for van der Waals forces, London dispersion forces are strongly dependent on the distance ($\propto \frac{1}{r^6}$) similar to Keesom and Debye forces.

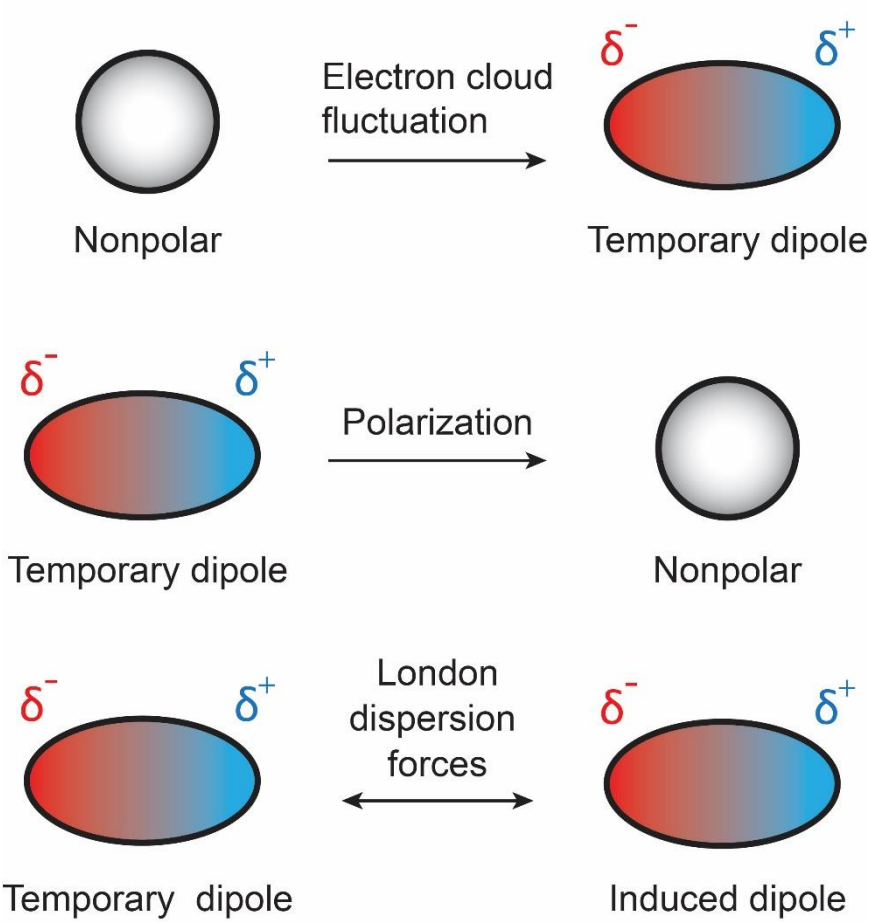

Figure 5: Schematic of London dispersion forces. Random fluctuations in the electron cloud of neutral molecules can induce a temporary dipole. This temporary dipole induces dipoles in proximate nonpolar molecules. London dispersion forces exist between temporary and induced dipoles.

1.1.3 Hydrogen bonds

Hydrogen bonds are a strong, directional dipole-dipole interactions; serving as hydrogen-mediated links between two electronegative groups[15]. A hydrogen bond is formed between an electronegative atom, termed hydrogen bond "acceptor", and a proximate hydrogen atom that is covalently linked to an electronegative atom, which is termed hydrogen bond "donor". Schematically, this is often depicted as D-H···A. Typical electronegative atoms are O, N, F, or Cl. The strength of these interactions can be attributed to the properties of the hydrogen atoms; they are small in size and are easily polarised, thereby allowing close contacts with interaction partners[15]. There are intra- or intermolecular hydrogen bonds with binding energies that are proportional to $\frac{1}{r^2}$. Intramolecular hydrogen bonds are of particular importance in proteins, as they play a major role in the stabilisation of secondary structures[22,23].

1.1.4 The hydrophobic effect and "hydrophobic interactions"

The hydrophobic effect represents the forces behind the clustering of nonpolar particles in aqueous solution and is the reason for the low solubility of nonpolar compounds in water[15,24]. Importantly, the hydrophobic effect drives the formation of micelles and lipid membranes[25]. Water molecules are energetically inclined to form a dynamic hydrogen bond network with neighbouring water molecules or polar groups of other molecules. However, nonpolar particles such as hydrocarbons are unable to form H-bonds, therefore, water molecules in proximity to the nonpolar particles arrange in a way that maximises the number of hydrogen bonds (i.e. up to four hydrogen bonds for each water molecule). The arrangement of the water molecules leads to the formation of Clathrate cages (i.e. solvation shells) around the nonpolar particle. However, this arrangement decreases the mobility of the water molecules reducing the system entropy. To increase the system's entropy, nonpolar molecules cluster and, thereby, reduce the number of water molecules involved in the formation of solvation shells[24]. In summary, the clustering of nonpolar particles in water is not driven by direct "hydrophobic interactions" between the nonpolar particles (which is an often used misleading term) but is instead driven by the difference between the entropy dominated solvation free energy of small individual molecules and the enthalpy dominated solvation free energy of larger clusters[24].

1.1.5 Non-covalent interactions in the gas phase

For the analysis of non-covalent complexes by MS, samples are transferred from solution into the gas phase for analysis. This process has considerable consequences on the stability of the complexes. First, as the dielectric permittivity of the medium (ε) differs in solution (ε = 78.5[15]) and in the gas phase (i.e. vacuum ε = 1), Coulomb forces ($\propto \frac{1}{\varepsilon}$) increase approximately by a factor of 80, while the van der Waals forces ($\propto \frac{1}{\varepsilon^2}$) increase approximately by a factor of 6400[26]. Hydrogen bonds also become stronger in the gas phase, as the absence of solvent molecules eliminates the competition for hydrogen bonds[27,28]. In contrast, as there is no solvent in the gas phase driving the nonpolar particle clustering, complexes formed by the entropy-driven hydrophobic effect are unstable in the gas phase[29]. Furthermore, in the gas phase, dissociation of nonpolar complexes is favoured in terms of entropy. Accordingly, the stability of nonpolar complexes in the gas phase is decreased while the stability of electrostatically dominated complexes is increased, reducing the overall rate of dissociation for electrostatically dominated complexes after ionisation[26,30]. Note that these considerations address the non-covalent interactions in complexes that have undergone ionisation and gas-phase transfer. The direct influence of the ionisation process and the gas-phase transfer on the complexes is still elusive and represents one of the key questions this thesis aims to address.

1.2 Mass spectrometry

Mass spectrometry (MS) is a versatile analytical technique used to measure the mass-to-charge (m/z) ratio of ions in the gas phase. A mass spectrometer consists of three parts: an ion source that ionises the analyte and transfers the ions into the gas phase, a mass analyser that separates ions according to their m/z ratio and a detector that detects the ions. Importantly, the fundamental MS process of ionisation and gas-phase transfer as well as the analysis of ions in the gas phase represent key aspects of this thesis due to their effect on the observed protein-lipid interactions and detergent-mediated lipid transfer as an approach.

1.2.1 Ion sources

The "soft" ionisation techniques for biomolecules are matrix assisted laser desorption/ionisation (MALDI)[31] and electrospray ionisation (ESI)[32]. MALDI involves co-crystallisation of the analyte within a matrix, which is then irradiated by a laser. The matrix material absorbs the energy and transfers it to the analyte leading to its desorption as well as ionisation. During ESI, ions are formed by directly spraying the analyte solution using an ESI emitter to which a high electric potential is applied. In this thesis, ESI was used and the principle behind ESI will be briefly presented in the following paragraphs.

1.2.2 Generation of ions by electrospray ionisation

In ESI, multiply charged ions are produced by spraying the analytes in a volatile solution using an ESI emitter. The application of a high electron potential (up to three kilovolts) to the ESI emitter initiates the ESI process[33] (**Figure 6 A**). Ions are transmitted into the mass spectrometer guided by the electric field applied between the ESI emitter and the oppositely charged mass spectrometer inlet. Due to this strong electric field, the sample solution collects at the tip of the ESI emitter forming a Taylor cone[34]. From the Taylor cone highly charged droplets are released[35]. The polarity of the ESI droplets depends on the polarity applied to the ESI emitter, for the analysis of proteins and protein complexes a positive polarity (i.e. positive ion mode) represents the standard. The droplets shrink in size due to solvent evaporation until the charge on the droplet surface reaches the Rayleigh limit[36] at which the droplets become unstable (i.e. the charge repulsion overcomes the surface tension of the droplet) and undergo fission into a jet of smaller charged progeny droplets (this process is also termed "Coulomb explosion"). The cycle of evaporation and fission events continues until charged droplets with a few nanometres in size are formed[37–39]. For biological applications, nanoelectrospray ionisation (nano ESI)[40,41] is commonly used. Nano ESI differs from conventional ESI in that lower sample flow rates are used leading to lower sample consumption and smaller initial ESI

droplet formation. Smaller ESI droplets lead to a higher ionisation efficiency, salt tolerance and sensitivity.

The final generation of “naked” ions from nanodroplets, has been commonly described using three models: (i) ion evaporation model (IEM)[42], (ii) charged-residue model (CRM)[43,44] and (iii) chain ejection model (CEM)[37] (**Figure 6 B**). The IEM describes the ionisation of small molecules such as small peptides, chemical compounds or metal ions. In this model, single solvated ions are ejected from ESI droplets with radii less than 10 nm driven by the strong electric field of the droplet at the Rayleigh limit[45]. The energy gain from the electric field compensates for the required energy to temporarily enlarge the droplet surface for the ejection process[46]. The ions are ejected with a residual solvation shell[37]. These attached solvent molecules are lost during collisions with background gas while traveling through the sampling stages of the mass spectrometer[47]. The CRM describes the ionisation process of large globular analytes, such as proteins or protein complexes. Therefore, CRM forms the basis for describing the process of ionisation of proteins and protein-lipid complexes in this thesis. Accordingly, Rayleigh-charged nanodroplets, containing in most cases only one large analyte, evaporate to dryness, transferring all droplet charges onto the analyte[48]. During the ionisation process, the droplet charge is maintained at the Rayleigh-limit throughout evaporation by ejecting excess charge likely through IEM[49]. For large globular analytes, the ESI protonation state depends on their surface accessible area and is independent of the analyte charge in solution[50–52]. Accordingly, the dependence of the ESI charge on the surface accessible area of a protein can be used to monitor the folding state of this protein in solution[53]. The CEM describes the ionisation of a nonpolar polymers including unfolded proteins. In unfolded proteins nonpolar residues are exposed, which in turn increases its overall hydrophobicity. Accordingly, the protein migrates to the droplet surface where part of the chain is expelled. This leads to the sequential ejection of the remaining protein during which charge is transferred onto the protein[54].

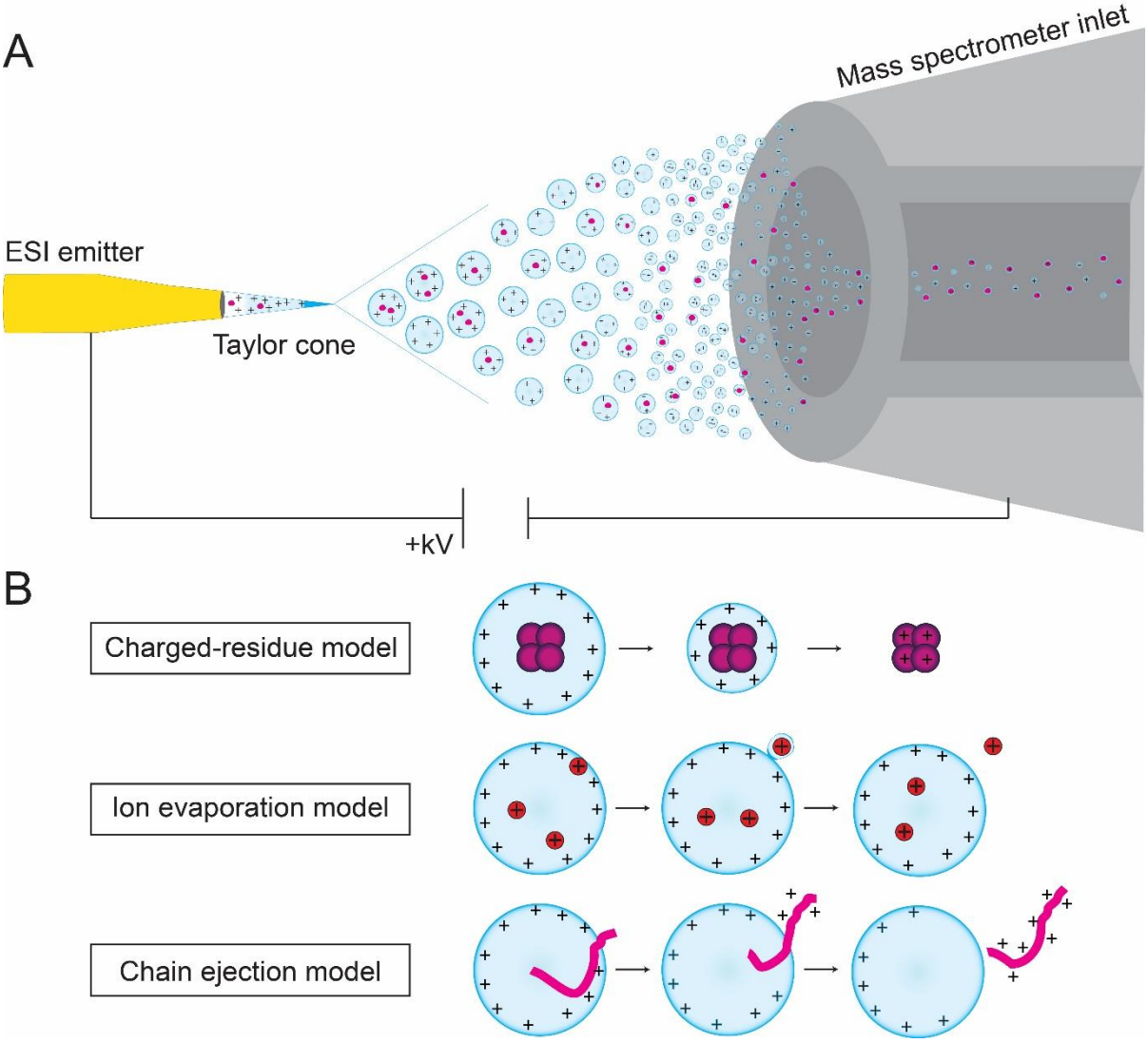

Figure 6: Schematic representation of the ESI process. (A) The sample is sprayed from an ESI emitter to which a high voltage is applied. Due to the electric field which is applied between the ESI emitter and the sampling cone, charges accumulate at the tip of the emitter forming a Taylor cone. From the Taylor cone, highly charged droplets are released that undergo a series of evaporation and fission events. **(B)** Models for the release of gaseous ions from ESI nanodroplets. The CRM describes the ionisation of large globular analytes. The ejection of small charged particles from the ESI droplet is described by the IEM. The mechanism behind the ionisation of unfolded proteins and polymers is best described by the CEM. The figure was adapted from Konermann et al. 2012[54].

1.2.3 Mass analysers and detectors

The mass analyser is separating the ions, produced by the ion source, according to their m/z ratio. Some of the commonly employed mass analysers include the quadrupole[55], the time-of-flight (TOF) mass analyser[56], the Orbitrap mass analyser [57], the ion trap mass analyser[58] and the Fourier Transform Ion Cyclotron Resonance analyser[59]. Decisive for their application are their respective properties, namely, resolution, effective mass range and sensitivity. This work

is limited to the use of quadrupole and TOF mass analysers. A quadrupole is composed of four symmetric metal rods with the same polarity being applied to opposing rods. A combination of a direct current and radio frequency voltage is applied to the rod pairs, constructing an electric field that stabilises ions at defined m/z ratios in their trajectory while passing through the quadrupole. Variation of the direct current and radio frequency voltage can be used to adjust the m/z ratios that are stabilised, defining which ions are selected (i.e. the quadrupole is operated as a "mass filter"). In addition to its function as a mass filter, quadrupoles can be operated in "scanning mode", where instead of selecting ions at a defined m/z ratio, ions of a specific range of m/z ratios are transmitted. For this, the quadrupole is operated without direct current voltage ("RF-only mode"). This application is often used in tandem MS, where more than one mass analyser is coupled within one instrument (see below for details). In the field of native MS, coupling of a quadrupole with a TOF mass analyser is most commonly employed.

In TOF mass analysers, ions are separated based on their m/z ratio by measuring the flight time of ions traversing a field-free drift tube of a defined length under high vacuum. For this, ions are first accelerated using a defined electric potential and their flight times through a drift tube recorded. The recorded flight times are used to directly calculate the m/z ratio of the ions, as the flight time is proportional to the square root of the m/z ratio. Specifically, the relationship between flight time t and m/z ratio is given as

$$t = \frac{d}{\sqrt{2E}}\sqrt{\frac{m}{z}}$$

with d = length of the field-free drift tube and E = strength of electric field which accelerates the ions[60]. For enhancing the mass resolution and mass accuracy of TOF mass analysers, a reflectron is included as part of the TOF analyser. A reflectron creates a retarding electric field that "reflects" ions, thereby, extending the flight path and offsetting minor differences in the kinetic energy of the ions[61]. One major advantage of TOF mass analysers is that their mass range is theoretically unlimited, therefore making them well-suited for analysing high-mass ions[62].

Ions are detected by a detector such as a secondary electron multiplier[63], a multichannel plate[64] or a Orbitrap[57]. An Orbitrap represents a special case, as they are mass analysers and simultaneously detectors. The detected ions are translated into electronic signals and visualised in a mass spectrum with the relative intensity on the y-axis and the m/z ratios on the x-axis.

1.2.4 Tandem MS

Performing tandem MS or MS/MS experiments involves selection of specific precursor ions, the fragmentation or dissociation of the precursor ions and the analysis of the generated product ions. The selected ions are subjected to fragmentation techniques such as high-energy collisional dissociation[65], electron transfer dissociation[66] or collision-induced dissociation (CID)[67,68]. During CID, ions are activated by collisions with inert gas particles (e.g. argon, helium or nitrogen). The collisions increase the internal energy of the ions leading to cleavage of covalent bonds or the disruption of non-covalent interactions depending on the degree of activation. The analysis of the resulting product ions yields an MS2 spectrum. In this thesis, CID was used to probe the gas-phase stability of protein-lipid complexes.

1.3 Native mass spectrometry

Native MS enables the analysis of complexes under non-denaturing conditions, i.e. while preserving their non-covalent interactions in the gas phase. Importantly, this method can be employed to elucidate the topology, stoichiometry and stability of protein(-ligand) complexes. Furthermore, it has been demonstrated that ions analysed in native MS experiments mostly retain their solution conformation in the gas phase[69]. In conclusion, native MS is a valuable and versatile tool in the field of structural biology. In this thesis, native MS techniques were developed to evaluate the influence of ionisation and gas-phase transfer on the non-covalent interactions between LL-37, LL-37 variants and Synaptotagmin-1 with glycerophospholipids.

1.3.1 Sample preparation for native MS

For native MS analysis, analytes need to be transferred into an aqueous volatile solution, which is compatible with native MS analysis and is able to stabilise non-covalent interactions of the analytes. Most commonly, ammonium acetate solution is used because (i) it has a physiological neutral pH around 7, (ii) it acts as an electrolyte (i.e. NH_4^+ and CH_3COO^- ions), thereby stabilising the complexes in solution and (iii) NH_4^+ acts as a proton donor and CH_3COO^- as a proton acceptor, producing ammonia and acetic acid through proton transfer. Both are highly volatile compounds leading to rapid solvent evaporation under ESI conditions. In contrast, the use of non-volatile substances leads to non-specific adduct formation, peak broadening and signal suppression[70,71]. For the transfer of analytes from non-volatile buffers to ammonium acetate solution, small gel filtration columns, filtration devices with defined molecular weight cut-offs (MWCO) or dialysis chambers are employed.

1.3.2 Analysis of protein complexes by native MS

For the analysis of large molecules by native MS, two requirements need to be fulfilled: (i) the ionisation of ions in a volatile and aqueous solution by a soft ionisation technique (see above) and (ii) the employment of a modified mass spectrometer for the analysis of high mass ions. The analysis is typically performed using a quadrupole-TOF tandem mass spectrometer, modified for the transmission for high mass ions[62]. Recently, high resolution native MS, which employs a modified quadrupole-Orbitrap tandem mass spectrometer, gained importance[11]. Modification of these instruments include higher gas pressures in the initial ion stages by reducing the pumping efficiency or introducing a background gas. This leads to increased frequency of collisions between ions entering the mass spectrometer and gas molecules, thereby increasing collisional cooling, ion focusing and ion transmission. Furthermore, the frequency of the radio frequency voltage applied to the quadrupole is decreased by a factor of approximately 3 in order to extend the m/z range that can be transferred[62]. A schematic of the Waters Micromass Q-TOF Ultima mass spectrometer, a modified mass spectrometer used in this thesis, is shown in **Figure 7**.

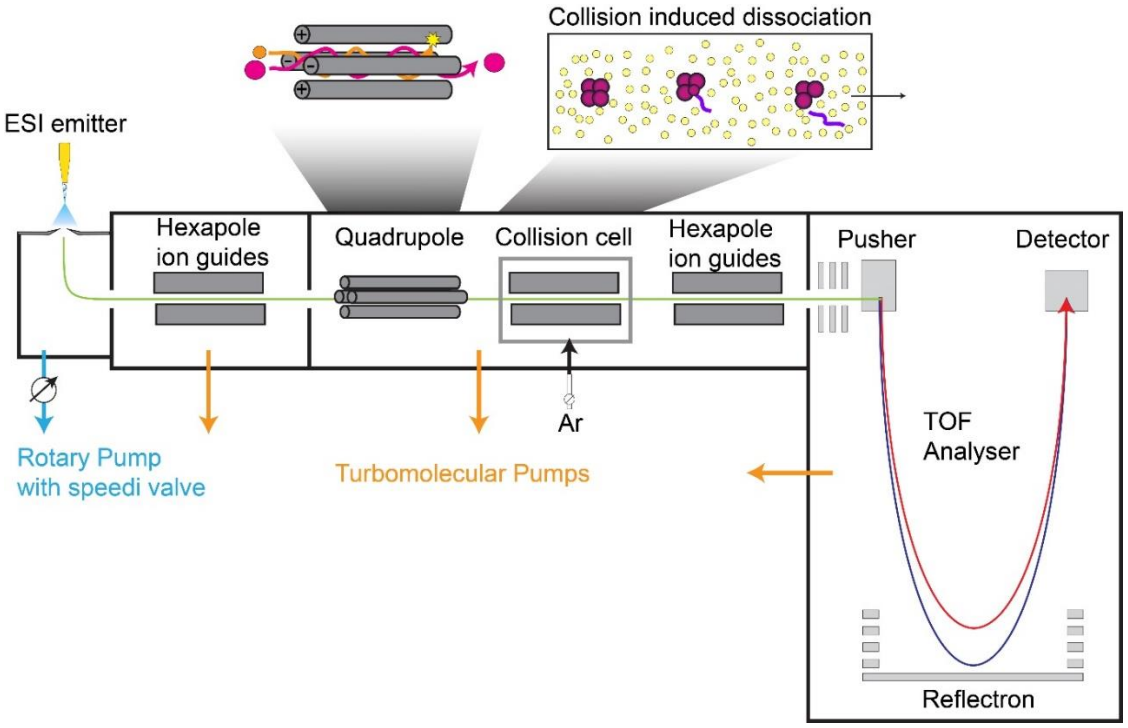

Figure 7: Schematic of the modified Waters Micromass Q-TOF Ultima mass spectrometer. The ion path to the TOF analyser is indicated by a green line. In the TOF analyser the ion path of two ions, which differ in their kinetic energies, is schematically depicted. This instrument contains a quadrupole and a TOF mass analyser. The quadrupole allows selection of ions of specific m/z ratios stabilising their trajectories (inset). CID experiments are performed in the collision cell, which is filled with Argon (inset). In the source region, vacuum pressure is regulated by a speedi valve, which reduces pumping of the rotary pump. Turbomolecular pumps are employed for high-vacuum regions. This figure was adapted from Sobott et al. 2004[72].

To perform native MS, an MS1 spectrum containing all ions, within a specific m/z range, is first recorded. From this spectrum, the masses of the analytes are determined. An example of a native mass spectrum is shown in **Figure 8**. ESI produces multiply charged ions for each mass species, which are observed as charge state distributions in the spectrum. The charge state distributions of folded proteins and protein complexes display a Gaussian distribution. Two neighbouring peaks within a charge state distribution differ by one charge, this allows the assignment of the respective charge states and calculating the corresponding mass from their m/z values. Importantly, the number of charges acquired during ionisation depends on the surface accessible area[50–52]. Therefore, the charge state series can be used to monitor the folding state of the analyte. In general, unfolded proteins tend to acquire more charges and display wider charge state distributions than folded proteins[53]. The deconvolution and annotation of mass spectra is performed manually or by using deconvolution software[73,74]. To validate the topology of complexes, an MS/MS experiment is performed. For this, a precursor ion is selected in the quadrupole and then dissociated by CID. For this, the collisional voltage in the collision cell is increased, leading to collisions of the ions with inert gas particles. These collisions lead to the dissociation of non-covalent complexes but do not cause fragmentation of the proteins. During dissociation, protein oligomers experience an asymmetric distribution of their charge yielding a highly charged monomer and a remaining complex of low charge (also termed “stripped” complex). Accordingly, during ejection of the monomer, the monomer unfolds, thereby increasing its surface area and acquiring a disproportional portion of the charges. This process was described in detail by Benesch et al. 2007[75]. In heterologous complexes the identity of the “stripped” monomer provides valuable information on the topology of the protein complex[12].

Note that in this thesis a technique termed “All ion CID” was employed. In this technique all ions are subjected to CID, rather than selected ions of a defined m/z ratio, to observe the stability of complexes across all charge states. Importantly, ion activation at low collisional voltages of 30 V and below tend to preserve non-covalent complexes but facilitate the desolvation process as well as the removal of unspecific adducts.

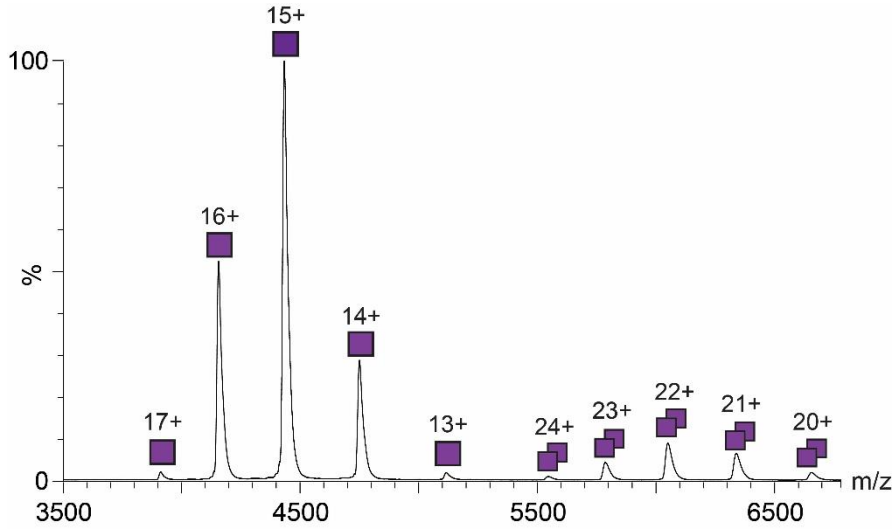

Figure 8: Native MS spectrum of bovine serum albumin (BSA). The y-axis shows the relative intensity and the x-axis the m/z ratio. Native MS of 5 µM BSA in 200 mM ammonium acetate reveals two Gaussian charge state distributions: one at lower m/z ratios ranging from 13+ to 17+, corresponding in mass to the BSA monomer (purple square), and one at higher m/z ratios ranging from 20+ to 24+ corresponding to the BSA dimer (two purple squares).

1.3.3 Exploring protein-lipid interactions by native MS

In recent years, native MS has been established as a valuable tool to explore the interactions between proteins and lipids. For the analysis of membrane proteins, the standard procedure involves the purification in or transfer into an MS compatible detergent solution[76]. Note that non-ionic detergents (e.g. DDM, OG, or C8E4) are in general more compatible with MS analysis than ionic detergents. After the ionisation of the membrane proteins in the detergent micelles, membrane proteins are subjected to high collisional activation to strip the attached detergent molecules[77]. Despite this, the overall stability of the membrane proteins is retained throughout the process as the detergent micelle acts as a "shield" for the proteins during the ionisation process[78,77]. Notably, co-purified tightly bound lipids can be identified[12]. In addition, more recently, a protocol was also presented to identify key lipid interactions of co-purified lipids by stepwise delipidation[79]. Lipid binding preferences of membrane proteins can also be probed after the addition of lipids solubilised in detergent micelles[76,80,81]. Following an unknown mechanism, lipids are transferred from mixed detergent-lipid micelles to the membrane protein, thereby forming protein-lipid complexes. Importantly, this methodology is not limited to membrane proteins but was also applied for soluble proteins[82]. It was proposed that, during the ionisation process by ESI, soluble proteins interact with the lipid head groups on the surface of detergent-lipid micelles. The proposed mechanism for the formation or protein-lipid complexes using mixed detergent-lipid micelles is shown in **Figure 9**. In this thesis, the transfer

of lipids from detergent-lipid micelles was used to identify the lipid preferences of the soluble protein Synaptotagmin-1, the amphipathic peptide LL-37 and the LL-37 variants.

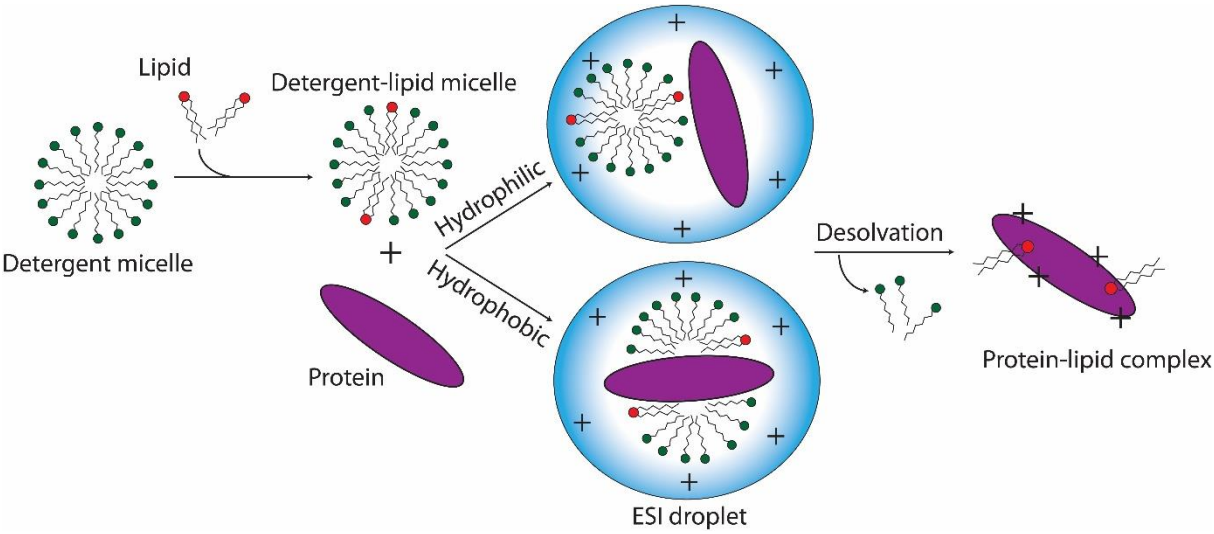

Figure 9: Mechanism for the detergent-mediated protein-lipid complex formation. Mixed detergent-lipid micelles are formed through the solubilisation of lipids (red head group) in detergent (green head group) solutions. The detergent-lipid micelles are incubated with a protein (purple). At sufficiently high concentration of the detergent-lipid micelles, the protein and a detergent-lipid micelle share the same ESI droplet during ionisation. Depending on the protein's hydrophobicity, the protein integrates into the micelle (hydrophobic) or interacts with lipids on the micelle surface (hydrophilic). Specific lipid contacts are retained while unbound lipid species and detergent molecules are removed during desolvation and collisional activation, finally releasing protein-lipid complexes for analysis. The figure was adapted from Landreh et al. 2017[82].

1.4 Biophysical methods

In this section, the principles behind dynamic light scattering and surface pressure measurements using a Langmuir film balance will be briefly described. In this thesis, the former was used to evaluate formation of liposomes and detergent-(lipid) micelles while the latter was used to determine the surface activity of LL-37 variants and to study their interactions with lipids monolayers at the air-water interface. A Langmuir film balance was used to evaluate protein-lipid interactions in solution and the results were compared with the interactions observed using native MS, where complexes are observed in the gas phase.

1.4.1 Dynamic light scattering

Dynamic light scattering (DLS) is an analytical technique which makes use of the Brownian motion of particles to determine their size (within nanometre to micrometre range) in solution. Brownian motion describes the continuous random movement of particles in solution caused

by collisions with the fluid molecules[83]. The speed of Brownian motion depends on the temperature, solvent viscosity and the particles size, with smaller particles moving faster than larger ones. The principle behind DLS was described in detail by several reviews[84–86]. Briefly, for DLS measurements, the particles are irradiated by a monochromatic beam of light (e.g. a laser), which is scattered by the particles. The scattering of the light is influenced by both the size and the shape of the particles. Fluctuations in intensity of the scattered light over time (due to the diffusion of particles driven by Brownian motion) are analysed to obtain the diffusion coefficient of the particles, which is directly related to the size of the particles. Using the Stokes-Einstein equation, the hydrodynamic diameter of particles can then be determined from their diffusion coefficient[87]. In this work, DLS was used to validate the formation of detergent-lipid micelles as well as to verify the size of liposomes. In conclusion, DLS represents a fast technique for the determination of particles sizes.

1.4.2 Surface pressure measurements using a Langmuir film balance

To study the interactions between proteins and membranes, a variety of membrane model systems have been established. Lipid monolayers at the air-water interface are a model system predominantly used for studying the interactions of soluble proteins, peptides or polymers with lipid membranes. Lipid monolayers, also known as Langmuir monolayers, mimic half of a lipid membrane[88–90]. This model system allows to control the phase properties as well as the monolayer composition. Monolayers are prepared by gradually spreading lipids dissolved in chloroform or chloroform-methanol mixtures at the air-water interface. The lipids self-assemble at the air-water interface due to their amphipathic properties (i.e. they contain hydrophobic fatty acyl chains and a hydrophilic head group). Insertion of soluble proteins into the monolayer can be studied either by monitoring changes in surface area at a constant surface pressure or changes in surface pressure at a constant area[91].

For measuring the changes in surface pressure at a constant area, as was done in this study, (**Figure 10**) small circular Teflon troughs without movable barriers for film compression are employed. These troughs are constantly stirred during the measurements and a constant temperature is maintained. Changes in surface pressure over time are typically monitored using a Wilhelmy plate. The surface pressure is defined as the difference between the surface tension of water and the surface tension in the presence of a lipid monolayer ($\pi = \gamma_0 - \gamma$). Due to the attractive cohesion forces between water molecules, the surface tension of water is very high, i.e. 72 mN/m. Attractive forces between the lipids of the lipid monolayer are much lower leading to a decrease in surface tension and an increase in surface pressure with an increasing amount of lipid at the air-water interface.

The insertion of a protein into a lipid monolayer is followed after direct injection of defined amounts of protein into the subphase underneath the lipid monolayer and subsequently monitoring the changes in surface pressure over time (Δπ). For data analysis, Δπ is determined as a function of the initial surface pressure π_0, which can be adjusted by the amount of spread lipids. Plotting Δπ against π_0 results in a linear graph, which allows the determination of the maximum insertion pressure (MIP) at the intersect with the x-axis. The MIP defines the maximal surface pressure at which insertion is energetically favourable[92]. The MIP value is characteristic for the studied protein and indicates the insertion efficiency into the respective lipid monolayer and the specificity towards the lipids[91,92]. Importantly, a surface pressure of 30 mN/m corresponds to the monolayer-bilayer equivalence pressure, i.e. the surface pressure at which the properties of the monolayer resemble that of a bilayer[93–96]. Accordingly, proteins with MIPs over 30 mN/m likely insert into lipid bilayers with the same composition. Notably, the MIP also depends on the concentration of the protein in the subphase, as the MIP increases until the air-water interface is saturated with the protein. The saturation concentration and the surface pressure at which protein saturation is reached can also be used as a measure for the hydrophobicity of the compound[90–92,97]. In conclusion, Langmuir monolayers represent a valuable membrane model system, providing control about the monolayer properties and composition, thereby allowing the study of a wide range of soluble molecules with different lipids.

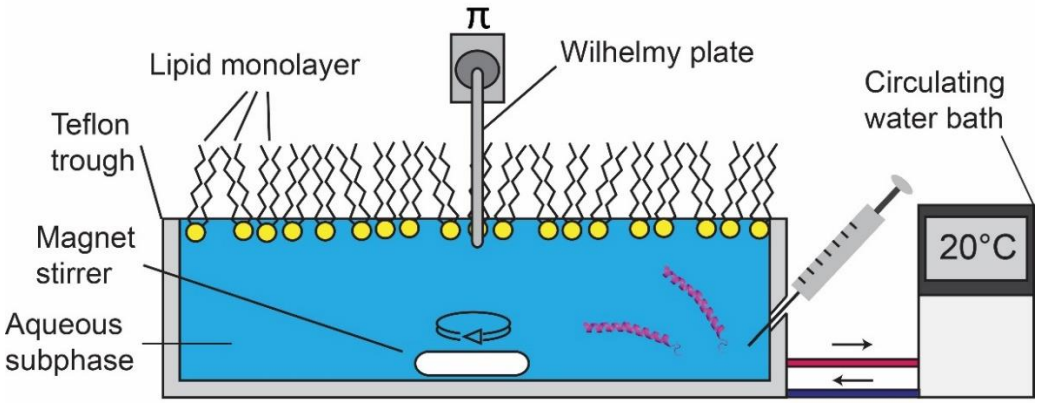

Figure 10: Schematic representation of a Langmuir film balance. Lipids are spread on an aqueous subphase within a Teflon trough. Due to their amphipathic structure, the lipids assemble at the air-water interface as a lipid monolayer. The aqueous subphase is constantly stirred during the experiments. Insertion of a protein into the monolayer is monitored through changes in surface pressure using a Wilhelmy plate. The temperature is controlled at 20 °C by an external circulating water bath.

1.5 Proteins and lipids

To explore the non-covalent interactions between proteins and lipids, the antimicrobial peptide LL-37 was chosen as a model protein (model peptide). Note that the focus of this thesis is not the study of the biological function of LL-37 and, therefore, the following section will focus on its structural properties. Furthermore, established native MS workflows were further applied to study the lipid preference of the Ca^{2+}-sensor protein Synaptotagmin-1, allowing detailed insights into its role in the synaptic vesicle exocytosis at the synapse. A brief introduction to the structure and interactions of Synaptotagmin-1 is provided in the corresponding paragraph below.

Lipids are a chemically and functionally diverse class of biomolecules. They fulfil three major functions[98]: (i) they serve as an energy storage for organisms, (ii) together with proteins they form the cellular membranes which act as a barriers, separating the cell and cellular organelles from their outer environment and (iii) they act as chemical messengers in signal transduction. In this thesis, the focus was on the interactions of proteins with glycerophospholipids, which represent one of the major components of membranes[99].

1.5.1 The antimicrobial peptide LL-37

Interactions of soluble peripheral membrane proteins with lipids range from specific interactions of protein domains that target certain head groups (e.g. the pleckstrin homology domain specifically targets phosphatidylinositol-4,5-bisphosphate[100]) to non-specific long-range electrostatic interactions between the charged amino acids of the proteins and charged lipid head groups on the membrane surface[7]. In this thesis, the human LL-37 serves as a model peptide for exploring protein-lipid complexes formed by electrostatic non-covalent interactions and by the hydrophobic effect in solution. LL-37 belongs to the class of alpha-helical antimicrobial peptides (AMP), which are part of the innate defence system against bacteria, viruses and fungi[101,102]. AMPs are typically small (i.e. 10 to 60 amino acids), cationic and amphipathic, i.e. they contain a hydrophilic and a hydrophobic interface[103]. These properties facilitate their specificity for bacterial membranes, which contain a high proportion of negatively charged lipids[104,105]. Interestingly, AMPs are able to bypass the defence mechanisms of antibiotic-resistant bacteria by directly targeting and disrupting their cell membrane[106–109]; making them interesting alternatives to antibiotics. LL-37 is part of the human cathelicidin family and is derived through cleavage of the cathelicidin hCAP18 proprotein[110]. It consists of 37 amino acids of which 5 are negatively and 11 are positively charged resulting in a solution net-charge of 6+. LL-37 consists of a single amphipathic alpha-helix ranging from residues 2 to 32 and a short C-terminal coil region ranging from residues 33 to 37 (**Figure 11**)[111]. As demonstrated for many AMPs, LL-37 can adapt an alpha-helical structure in a hydrophobic

environment, for instance a phospholipid membrane or a detergent micelle[9,111–114]. However, compared to many other alpha-helical AMPs, which are unstructured in aqueous solution, the conformation of LL-37 is sensitive to ionic strength and adopts at sufficiently high salt concentrations an alpha-helical conformation[115]. In aqueous solution, aggregation of alpha-helical LL-37 is driven by its hydrophobic interface[110]. For its main biological function, LL-37 directly interacts and disrupts membranes of pathogens presumably through pore formation[109,116]. Before pore formation, LL-37 initially inserts in the membrane interface between the polar lipid head groups and the hydrophobic membrane core oriented in parallel to the lipid bilayer[117,118]. Thus, its hydrophobic interface allows for interactions with the hydrophobic membrane core, while its hydrophilic interface allows electrostatic interactions with the lipid head groups, making it a suitable model peptide for exploring the impact of non-covalent interactions on the formation of protein-lipid interactions. Compared to other AMPs, which are selective towards anionic bacterial membranes, interactions of LL-37 with zwitterionic eukaryotic membranes (i.e. cytotoxic activity) were also observed[5,115,117].

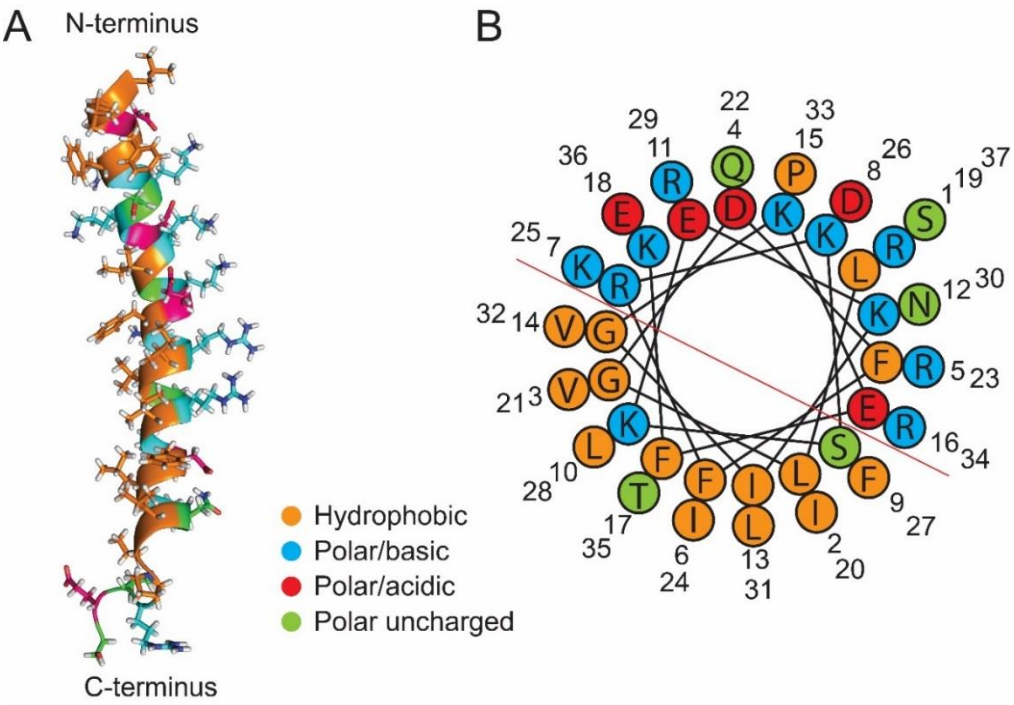

Figure 11: Structure of the antimicrobial peptide LL-37. (**A**) NMR structure of LL-37 in sodium dodecyl sulphate micelles (PDB ID: 2K6O). Hydrophobic (orange), polar basic (blue), polar acidic (red) and polar uncharged (green) amino acids are indicated. Amino acids with positive values according to the Eisenberg scale were classified as hydrophobic[119]. (**B**) Helical wheel projection of LL-37 created using Heliquest[120]. The hydrophobic (bottom) and the hydrophilic interfaces (top) are separated by a red line. Figure adapted from Kundlacz et al. 2023[121].

1.5.2 The Ca^{2+}-sensor Synaptotagmin-1

For signal transmission at the synapse, synaptic vesicles loaded with neurotransmitters (e.g. glutamate) fuse with the presynaptic membrane of the synapse, thereby, releasing the neurotransmitters into the synaptic cleft[122–124]. The fusion process is initiated by the arrival of an action potential inducing Ca^{2+}-influx through voltage-gated membrane channels[122,124]. The driving force behind the exocytosis of neurotransmitters is provided by the formation of the soluble N-ethylmaleimide-sensitive-factor attachment protein receptor (SNARE) complex[125]. This fusion machinery consists of one synaptic vesicle protein, synaptobrevin-2, and two presynaptic membrane proteins, syntaxin-1A and the synaptosome-associated protein of 25 kDa (SNAP-25)[126,127]. Many proteins are involved in the regulation of SNARE complex formation. One such regulator is the synaptic vesicle protein Synaptotagmin-1 (Syt1), which functions as a Ca^{2+}-sensor and is directly involved in the process of exocytosis[124,128,129].

Syt1 is anchored to synaptic vesicles by a short N-terminal transmembrane helix. Syt1 contains two cytoplasmic C2 domains (C2A and C2B) connected by a flexible linker[130,131]. Both C2 domains are composed of a β-sandwich structure with flexible loops connecting the β-strands in C2A and C2B[132–134]. These aspartate rich loops are referred to as Ca^{2+}-binding loops, binding up to three and up to two Ca^{2+}-ions in C2A and C2B[134,135]. Together with a polybasic stretch on the surface of the C2B domain, the Ca^{2+}-binding loops are responsible for electrostatically dominated interactions of the C2 domains with negatively charged lipid membranes[128,136]. Interactions between negatively charged lipids and Ca^{2+}-binding loops are facilitated in the presence of Ca^{2+}-ions, by changing the electrostatic surface potential of the Ca^{2+}-binding loops (i.e. by masking negative charges) and allowing a simultaneous coordination of lipid head groups by the Ca^{2+}-ions and cationic amino acids surrounding the Ca^{2+}-binding loops[128,135,137]. Interactions of Syt1 with phosphatidylinositol-4,5-bisphosphate ($PI(4,5)P_2$) and phosphatidylserine (PS) are likely of functional importance[136,138–140]. However, despite many theories about the mechanism of Syt1 suggesting that Syt1 regulates the synaptic vesicle exocytosis by: (i) tethering the synaptic vesicle to the presynaptic membrane[141,142], (ii) inducing destabilisation within the membranes[143,144], (iii) direct or indirect interaction with the SNARE complex[145–147] or (iv) a combination thereof, the mechanism is still elusive. Here, lipid binding to the individual C2 domains (C2A and C2B) including the N-terminal (C2A) and C-terminal (C2B) linkers was explored following a multidisciplinary approach to determine how interactions with lipids determine the role of Syt1 during synaptic vesicle exocytosis. An overview on the structure of the individual C2 domains is given in **Figure 12**.

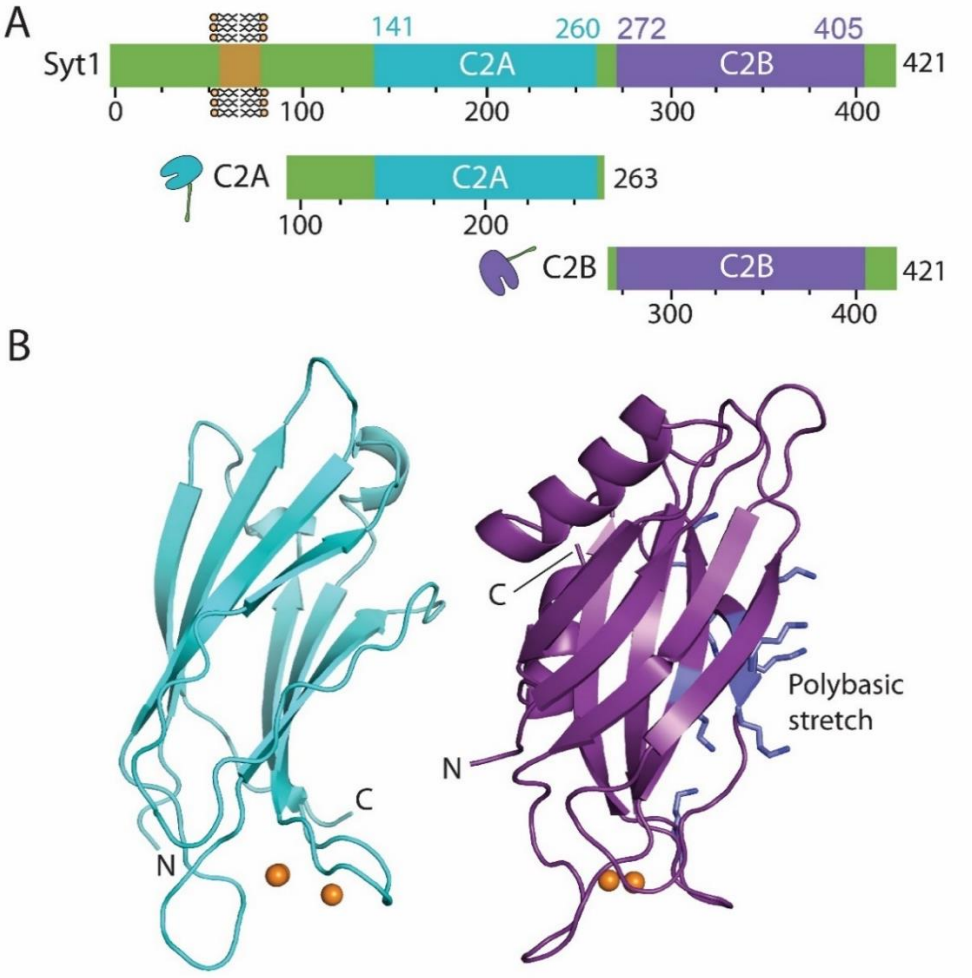

Figure 12: Overview over the structure of the Syt1 C2 domains. (**A**) Schematic of full-length Syt1 including the transmembrane region (brown) and the C2A (blue) and C2B (purple) constructs, which were used in this thesis. (**B**) Cartoon representations of the C2A (PDB ID: 1BYN) and the C2B (PDB ID: 1K5W) domains. The structure of the linkers in the C2A and C2B constructs are not included in the structure. The N- and C-Terminus, bound Ca^{2+}-ions (orange), and residues belonging to the polybasic stretch (blue)[134] were highlighted. The figure was adapted from Bender et al. 2024[148].

1.5.3 Properties of glycerophospholipids

Biological membranes form the basis of cellular life, separating cells and organelles from their outer environment, enabling the formation of chemical gradients and regulated transmembrane transport[98]. Historically, the fluid mosaic model by Singer and Nicolson in 1972[149] served as a basis for describing the organisation of biological membranes. This model has been continuously updated and has become more complex[150]. The structure and composition of these membranes strongly varies between species[151,152] and organelles[98,99,153]. The major structural lipid classes in biological membranes are glycerophospholipids (GPLs), sphingolipids and sterols[98]. GPLs and sphingolipids are polar lipid classes, while sterols are nonpolar. In this thesis, interactions of peripheral membrane proteins with various GPLs of

different properties were investigated in the gas phase and in solution. Exploring the diverse non-covalent interactions between the membrane proteins and the GPLs provided further insights on the effect of ionisation and gas-phase transfer.

GPLs consist of two hydrophobic fatty acyl chains, a glycerol backbone and a hydrophilic head group[99]. The fatty acyl chains are attached to the glycerol backbone through an ester bond at the *sn*-1 and *sn*-2 positions. Fatty acids vary in chain length and can be saturated or unsaturated. Unsaturated fatty acids contain one or more (mostly *cis*) C=C double bonds at varying positions[99]. The degree of fatty acid saturation has a major impact on the properties of lipids membranes. Accordingly, the presence of a double bond increases the volume of fatty acyl chains, thereby changing the 3D-packing parameters of the individual lipids (a concept by Israelachvili et al. 1976[154]). Importantly, unsaturated lipids increase the fluidity of the lipid membrane and favour more fluid packing arrangements[155]. In contrast, saturated lipids and lipids containing *trans* double bonds facilitate tighter membrane packing arrangements[155]. Generally, saturated or monounsaturated fatty acyl chains (i.e. containing one C=C double bond) are located at the *sn*-1 position, while polyunsaturated fatty acyl chains (i.e. containing more than one C=C double bond) are often linked with the *sn*-2 position[152]. The lipid head group is bound to the remaining hydroxyl group of the glycerol backbone and is composed of a phosphate group esterified to an alcohol that defines the type of GPL. GPL classes include phosphatidic acid (PA), phosphatidylglycerol (PG), phosphatidylserine (PS), phosphatidylethanolamine (PE), phosphatidylcholine (PC) and phosphatidylinositol (PI). Notably, PA only contains the phosphate group as a head group. Importantly, the head groups determine the lipid's charge: PC and PE are zwitterionic, while PA, PG, PS and PI are negatively charged. An overview on the structure of GPLs is given in **Figure 13**.

The combination of hydrophobic fatty acyl chains and a hydrophilic head group classifies GPLs as amphiphilic molecules. This amphiphilicity is important as it allows reversible self-assembly into membranes through: (i) aggregation of the hydrophobic fatty acyl chains driven by the hydrophobic effect, (ii) interactions of the head groups with the aqueous environment and with each other, and (iii) the overall low solubility of lipids in aqueous solutions[98].

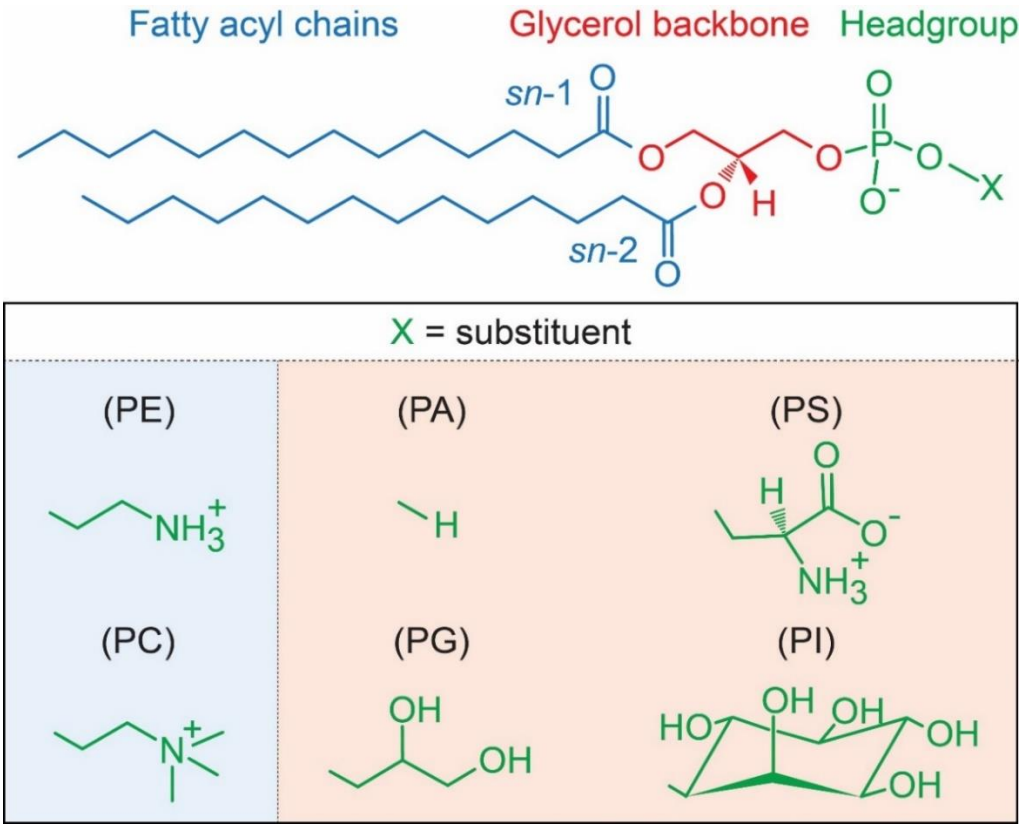

Figure 13: Structure of glycerophospholipids. GPLs consist of two fatty acyl chains, a glycerol backbone and a head group. The hydrophobic fatty acyl chains in GPLs vary in length, degree of saturation and in the position of C=C double bonds. The shown lipid contains myristic acid (14:0) in *sn*-1 and *sn*-2 positions. The hydrophilic head group of GPLs consists of a phosphate group esterified to an alcohol. Common GPLs are phosphatidic acid (PA), phosphatidylglycerol (PG), phosphatidylserine (PS), phosphatidylethanolamine (PE), phosphatidylcholine (PC) and phosphatidylinositol (PI) (see box). Head groups of GPLs can be zwitterionic (blue) or negatively charged (red). The figure was adapted from Harayama et al. 2018[99].

2. Aim of this study

In this thesis, interactions between peripheral membrane proteins and lipids will be characterised to explore the impact of non-covalent interactions on the formation of protein-lipid complexes. Native MS enables the analysis of these complexes, while preserving their non-covalent interactions in the gas phase. However, native MS analysis requires ionisation and gas-phase transfer of the protein-lipid complexes and the effects of these processes are controversially discussed. Of particular importance are the interactions formed by the hydrophobic effect in solution, as solvent effects are absent in the gas phase. Accordingly, the first aim of this thesis was to assess whether interactions that are observed in the gas phase reflect interactions formed in solution. The second aim of this thesis was to characterise the use of native MS employing detergent-mediated lipid transfer from mixed detergent-lipid micelles as an approach for investigating protein-lipid interactions of peripheral membrane proteins. This approach is commonly established as a suitable technique for probing the lipid preferences of integral membrane proteins. However, whether this approach is suitable for exploring protein-lipid interactions of peripheral membrane proteins remained elusive to-date.

In the first part of this thesis, a systematic characterisation of peptide-lipid interactions between the amphipathic LL-37 and GPLs containing different head groups or varying in their fatty acyl chain length will be performed by native MS. By monitoring the changes of ion intensity and gas-phase stability of protein-lipid complexes, this study will provide insights to differentiate between electrostatic interactions in the gas phase and influence of the hydrophobic effect in solution.

The second part of this thesis investigates the effects of peptide surface charge on the formation of peptide-lipid interactions by native MS. More precisely, peptide-lipid interactions between LL-37 and a variety of lipids will be compared to peptide-lipid interactions formed by a supercharged positive (LL-37-pos) and a negative (LL-37-neg) variant of LL-37. In this study, a Langmuir film balance will further be used to explore the interactions of the LL-37 variants with lipid monolayers in solution, thereby, revealing differences between their interactions in the gas phase and in solution. These differences highlight potential effects of the ionisation, gas-phase transfer and the use of detergent-lipid micelles for lipid transfer.

The third part of this thesis investigates how Ca^{2+}-dependent lipid preferences determine the mechanism of the Ca^{2+}-sensor Syt1 during synaptic vesicle exocytosis. For this, the lipid and membrane interactions of the isolated cytosolic C2 domains (C2A and C2B) of Syt1 will be characterised by native MS, lipid overlay assays, liposome flotation assays and molecular dynamics simulations. The combination of these techniques allows an investigation into the

mechanism of Syt1 and provides insights into potential effects of ionisation, gas-phase transfer and detergent-mediated lipid transfer.

3. Results

Short summary of the publications

The main goal of this thesis was to characterise protein-lipid interactions. In detail, the impact of non-covalent interactions on the lipid preferences and the strength of protein-lipid interactions was investigated. For this, native MS employing detergent-mediated lipid transfer as well as complementary techniques were applied and developed for probing the interactions of soluble peripheral membrane proteins with lipids. Accordingly, the publications addressed: (i) the impact of detergents on soluble proteins during native MS and their ability to transfer lipids (**P1**), (ii) the relationship between interactions observed in the gas phase and non-covalent interactions formed in solution (**P2**) and (iii) the impact of surface charge on the peptide-lipid interactions (**P3**). Finally, the same approach was applied, in combination with other techniques, in a biological context to characterise the lipid preferences of the C2A and C2B domains of the Ca^{2+}-sensor Syt1 to determine its role during synaptic vesicle fusion in the neuronal synapse (**P4**).

The goal of **P1** was to explore the influence of detergents on soluble proteins during native MS, as well as their ability to transfer lipids to soluble proteins from mixed detergent-lipid micelles. Notably, tetraethylene glycol monooctyl ether (C8E4) reduced the overall charge of the proteins and was able to stabilise non-covalent interactions. In contrast, N-octyl-β-D-glycopyranoside (OG) increased the overall charge state of the proteins and the protein stability was reduced in the presence of OG. Notably, lipid transfer from mixed detergent-lipid micelles was only observed for C8E4. Therefore, the detergent C8E4 plays a central role in this thesis and all native MS based lipid-binding studies employed C8E4 for the formation of protein-lipid complexes by lipid transfer. Accordingly, although not discussed in detail, **P1** is an important foundation for the thesis.

P2 Deciphering Solution and Gas-phase Interactions between Peptides and Lipids by Native Mass Spectrometry.

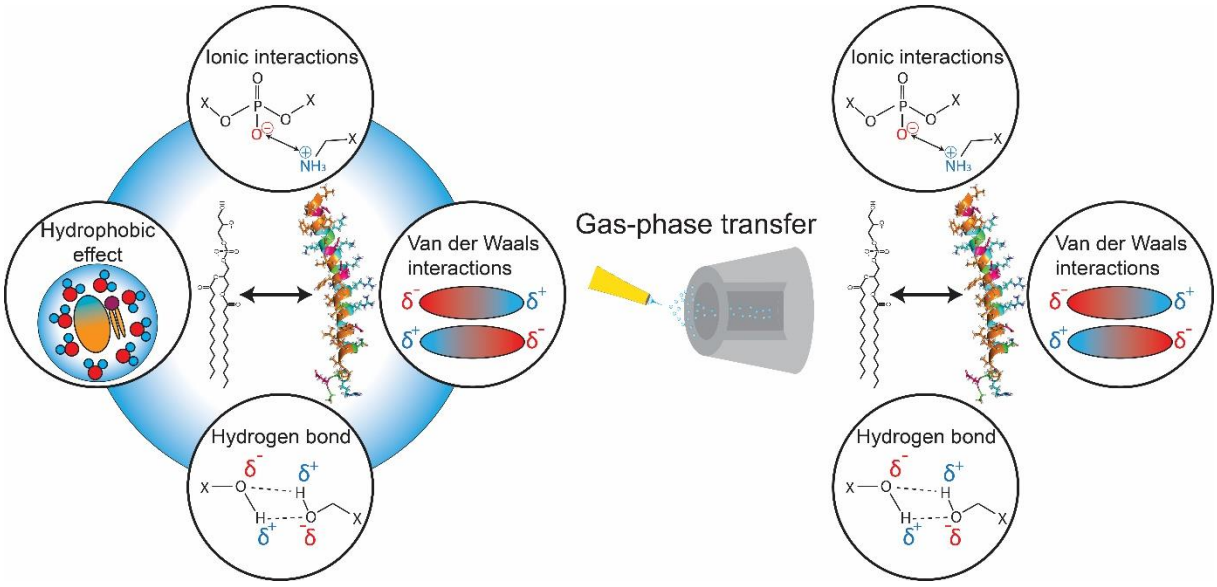

Figure 14: Comparison of non-covalent forces between proteins and lipids in solution and in the gas phase. This graphical abstract was adapted from **P2** Kundlacz et al. 2023[121].

Protein-lipid complexes are formed in solution by electrostatic forces and the hydrophobic effect. However, native MS analysis requires the transfer of the analyte into the gas phase, an environment where electrostatic interactions are enhanced and the hydrophobic effect is absent (**Figure 14**)[29]. Accordingly, in this project, the goal was to determine, whether non-covalent interactions of complexes formed in solution are reflected in the interactions observed in the gas phase by native MS. For this, a systematic study of the interactions between the amphipathic model peptide LL-37 and various GPLs was conducted. Specifically, the intensity of the apo-peptides and the peptide-lipid complexes was analysed, which reflect the solution equilibrium, and the stability of the complexes in the gas phase was assessed via CID.

First, the focus was on the electrostatic interactions of LL-37 with GPLs containing different head groups but the same fatty acyl chains (14:0/14:0), namely two zwitterionic GPLs (PC 14:0/14:0 and PE 14:0/14:0) and three negatively charged GPLs (PA 14:0/14:0, PG 14:0/14:0 and PS 14:0/14:0). Complexes involving negatively charged GPLs displayed high ion intensities and gas-phase stabilities. In contrast, complexes containing zwitterionic lipids were low abundant and showed low stability in the gas phase, indicating that electrostatic interactions with lipid head groups drive the interactions in solution and are also responsible for the relative binding strength in the gas phase.

In the second part of this study, the interactions of LL-37 with PG lipids varying in fatty acyl chain lengths (PG 6:0/6:0 to PG 18:0/18:0) were explored. An increase in the peak intensities and in gas-phase stability with increasing chain length was observed. Given that the

hydrophobic effect is non-existent in the gas phase, the increase in complex intensity and gas-phase stability likely originates from the hydrophobic effect in solution and van der Waals interactions with the fatty acyl chains in the gas phase. Alternatively, gas-phase stabilities could be the result of different binding interfaces between the complexes that formed.

In conclusion, this study demonstrates that the ion intensity does not necessarily correlate with complex stability in the gas phase. Ion intensities reflect interactions formed in solution, including those that are driven by the hydrophobic effect, while electrostatic interactions determine the gas-phase stability.

P3 Effects of Surface Charge of Amphiphilic Peptides on Peptide-Lipid Interactions in the Gas Phase and in Solutions.

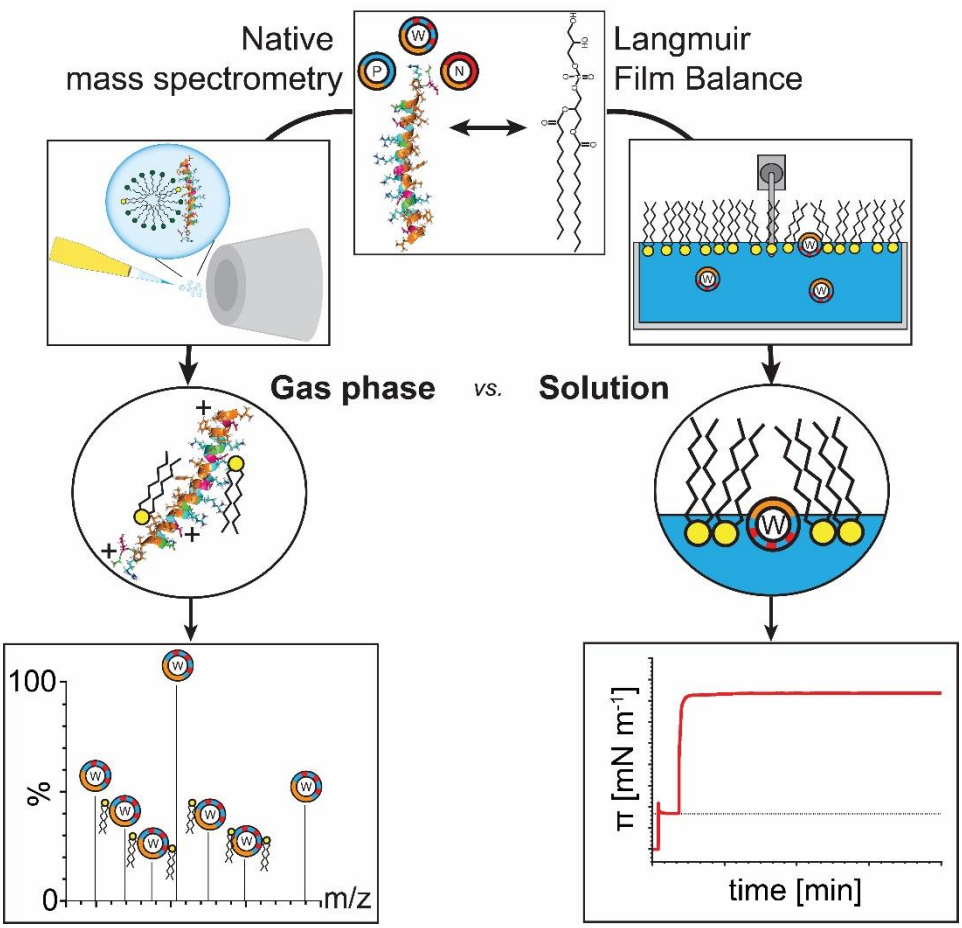

Figure 15: **Overview of the approach followed to analyse the effects of peptide surface charge in the gas phase (lhs) and in solution (rhs).** This graphical abstract is adapted from **P3** Kundlacz et al. 2025.

This study is a continuation of **P2**. Accordingly, one of the central questions was, whether native MS is capable of accurately characterising complexes that were formed by non-covalent interactions in solution. More precisely, the goal was to describe the effects of peptide surface

charge on peptide-lipid interactions with a variety of lipids. For this, a supercharged cationic (LL-37-pos) and a supercharged anionic (LL-37-neg) variant of LL-37 were designed and their interactions were compared with the wild type peptide (LL-37-wt). For native MS analysis, peptide-lipid complexes were formed through lipid transfer from mixed detergent-lipid micelles and analysed in positive and negative ion mode. Importantly, a Langmuir film balance was employed to explore the interactions of the LL-37 variants with lipid monolayers in solution and these findings were compared to the observations in the gas phase (**Figure 15**).

The lipid preferences of the cationic LL-37-wt and LL-37-pos determined by native MS in positive ion mode, correlate well with those determined in solution using the Langmuir film balance. However, for the negatively charged LL-37-neg, only lipid preferences that were determined in negative ion mode correlate with the results from monolayer interactions in solution. Accordingly, observed lipid binding events by native MS are dependent on the ESI ion mode.

Taking the influence of the ion mode into account, analyses by native MS and Langmuir film balance showed a similar trend for the lipid preferences of LL-37-pos and LL-37-neg, with both variants preferring lipids with opposite charge. Intriguingly, LL-37-wt was more flexible in the formation of peptide-lipid interactions. This might arise from LL-37-wt containing negatively and positively charged residues.

In conclusion, both methods revealed a strong impact of peptide surface charge on peptide-lipid interactions. Furthermore, native MS observations reflected the binding preferences observed in solution. Importantly, the influence of the ionisation mode on observed binding events was demonstrated. These findings highlight the importance of careful data evaluation; setting a reference for native MS based binding studies.

P4 Ca^{2+}-dependent lipid preferences shape synaptotagmin-1 C2A and C2B dynamics: Insights from experiments and simulations.

For signal transmission in neurons, synaptic vesicles fuse with the presynaptic membrane, thereby releasing neurotransmitters into the synaptic cleft. The driving force behind the fusion is the formation of the active SNARE complex[124,125]. The formation of the SNARE complex and the process of vesicle fusion is regulated by a large network of proteins including the Ca^{2+}-sensor Syt1[129]. Syt1 contains two cytosolic C2 domains (C2A and C2B), which are responsible for the coordination of Ca^{2+}-ions and the interactions with the membranes. However, although the general function of Syt1 is known[128], the exact mechanism during membrane fusion and the role of Ca^{2+}-(in)dependent membrane interactions are still elusive. Accordingly, in this

study, a multidisciplinary approach was followed to investigate the interactions of the individual C2 domains, C2A and C2B, with lipids and membranes.

First, the lipid preferences of the isolated C2 domains were probed via lipid overlay assay and native MS. Both methods revealed a preference of the C2 domains for negatively charged lipids, especially for phosphatidylinositol phosphates. Significantly, in the lipid overlay assays this preference is enhanced in the presence of Ca^{2+}, while a Ca^{2+}-dependence was not observed during the native MS analysis.

For the second part of this study, liposome flotation assays were employed to explore the interactions of the C2 domains with liposomes, designed to mimic synaptic vesicles and the presynaptic membrane, both in the presence and in the absence of Ca^{2+}. It was previously described that the presence of Ca^{2+} strongly influences membrane association of the C2 domains[136]. Significantly, binding of both C2 domains to the two membrane compositions was observed in the presence of Ca^{2+}, with C2B showing a preference for liposomes mimicking the presynaptic membrane.

Finally, molecular dynamics (MD) simulations were employed to simulate the interactions of the C2 domains with model membranes that correspond to the synaptic vesicle and the plasma membrane, again both in the presence and absence of Ca^{2+}. The analysis revealed similar lipid contacts for the C2 domains but different orientations towards the membrane. Specifically, the C2B domain oriented parallel to the membrane plane in the presence and in the absence of Ca^{2+}, while C2A displayed a Ca^{2+}-dependent shift in orientation from a more parallel contact angle to a perpendicular orientation. Notably, the perpendicular orientation results in deeper membrane insertion causing local membrane rearrangements.

Combining the results obtained from the different techniques, a mechanistic model describing the role of Syt1 during membrane fusion was proposed (**Figure 16**). In the absence of Ca^{2+}, C2B loosely associates with the presynaptic membrane, while C2A binds to the synaptic vesicle membrane. Upon Ca^{2+} binding, C2B's membrane association is enhanced and the C2A domain adopts a perpendicular orientation, placing the flexible linker connecting the C2 domains under tension, thereby generating a pulling force between the two membranes.

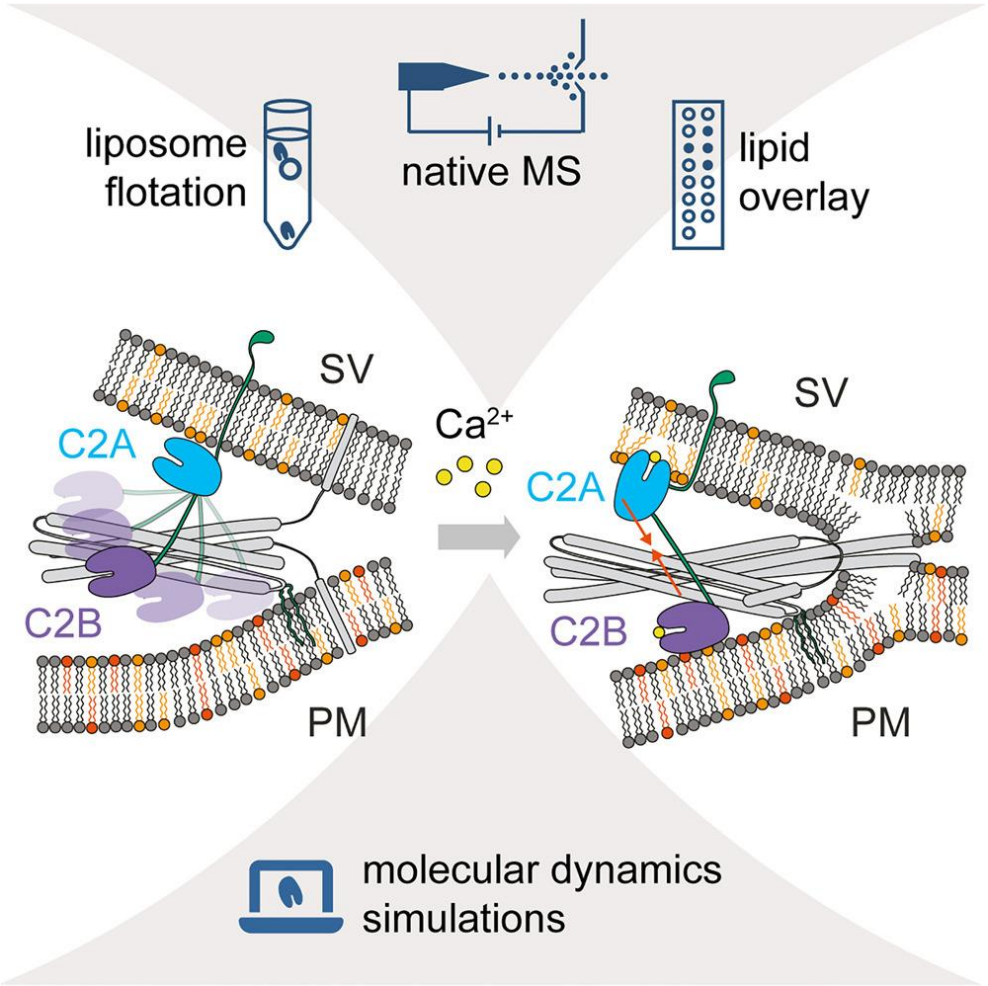

Figure 16: Overview of the proposed mechanism of Syt1 during membrane fusion. The four methods used for investigating the interactions of Syt1 with lipid membranes are depicted. This graphical abstract is taken from **P4** Bender et al. 2024[148].

3.1 Publications

Deciphering Solution and Gas-Phase Interactions between Peptides and Lipids by native Mass Spectrometry.

Til Kundlacz, Carla Schmidt

Anal. Chem. 2023, 95, 47, 17292-17299.

https://doi.org/10.1021/acs.analchem.3c03428

For this publication, I performed all experiments, data evaluation and visualisation of the work. The manuscript was written together with C. Schmidt. Changes to the manuscript as part of the editing and reviewing process were performed by C. Schmidt and me. C. Schmidt guided the research and supervised the project as well as the publication process.

analytical chemistry

pubs.acs.org/ac
Article

Deciphering Solution and Gas-Phase Interactions between Peptides and Lipids by Native Mass Spectrometry

Til Kundlacz and Carla Schmidt*

Cite This: *Anal. Chem.* 2023, 95, 17292−17299
Read Online

ABSTRACT: Many biological processes depend on the interactions between proteins and lipids. Accordingly, the analysis of protein−lipid complexes has become increasingly important. Native mass spectrometry is often used to identify and characterize specific protein−lipid interactions. However, it requires the transfer of the analytes into the gas phase, where electrostatic interactions are enhanced and hydrophobic interactions do not exist. Accordingly, the question remains whether interactions that are observed in the gas phase accurately reflect interactions that are formed in solution. Here, we systematically explore noncovalent interactions between the antimicrobial peptide LL-37 and glycerophospholipids containing different headgroups or varying in fatty acyl chain length. We observe differences in peak intensities for different peptide−lipid complexes, as well as their relative binding strength in the gas phase. Accordingly, we found that ion intensities and gas-phase stability correlate well for complexes formed by electrostatic interactions. Probing hydrophobic interactions by varying the length of fatty acyl chains, we detected differences in ion intensities based on hydrophobic interactions formed in solution. The relative binding strength of these peptide−lipid complexes revealed only minor differences originating from van der Waals interactions and different binding modes of lipid headgroups in solution. In summary, our results demonstrate that hydrophobic interactions are reflected by ion intensities, while electrostatic interactions, including van der Waals interactions, determine the gas-phase stability of complexes.

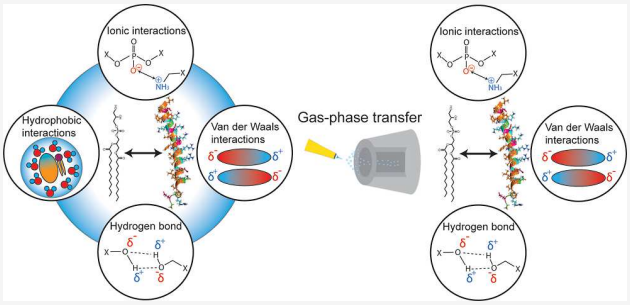

The interactions between membrane proteins and phospholipids rely on two noncovalent forces, namely electrostatic and hydrophobic forces. Whether electrostatic or hydrophobic forces dominate, strongly depends on the structure of the proteins and their lipid environment.[1,2] Importantly, lipid membranes not only provide a stable environment for membrane proteins,[3−5] they are also linked with their function and regulation.[4,6,7] Investigating protein−lipid interactions, therefore, has gained importance over the past years.[8]

Of the available techniques, native mass spectrometry (MS) emerged as a well-suited tool to study protein−lipid interactions.[9−14] Notably, native MS allows identification of the lipids that associate with the proteins as well as determination of their binding stoichiometry.[15−18] Dissociation of the protein−lipid complexes through collision with an inert gas then provides insights into the binding strength of the lipids in the gas phase.[13] However, native MS requires the transfer of biomolecules from solution into the gas phase, and the question of whether interactions observed in the gas phase reflect interactions formed in solution remains. Importantly, in the gas phase, interactions are dominated by electrostatic forces, while hydrophobic forces, which play a major role in solution, are under-represented.[19] A systematic characterization of protein−lipid interactions in the gas phase, i.e., differentiating between electrostatic forces that apply in the gas phase and hydrophobic interactions that form in solution, is still missing.

Here, we explore the interactions of the antimicrobial peptide LL-37 with a range of glycerophospholipids containing different headgroups or varying infatty acyl chain lengths. Using native MS, we systematically probe noncovalent interactions in the gas phase and observe differences in the peak intensities of the complexes that form, providing us with a snapshot of the equilibrium in solution. Dissociation of these complexes through collisions with an inert gas further allows estimation of the relative binding strength of the lipids in the gas phase. In short, we found that interactions in solution are reflected in binding intensities, while the stability of peptide−lipid complexes in the gas phase can be assessed through collisional dissociation.

Received: August 1, 2023
Revised: October 10, 2023
Accepted: October 12, 2023
Published: November 13, 2023

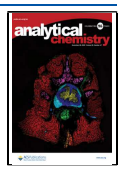

https://doi.org/10.1021/acs.analchem.3c03428
Anal. Chem. 2023, 95, 17292−17299

EXPERIMENTAL SECTION

Materials. Human LL-37 (trifluoroacetate salt, ≥95% purity) was purchased from Sigma-Aldrich (St. Louis, USA). The peptide was dissolved in phosphate-buffered saline (PBS) and stored at −20 °C. 1-*O*-(*n*-Octyl)-tetraethylene glycol (C8E4) was purchased from Glycon Biochem (Luckenwalde, Germany). 7.5 M ammonium acetate (AmAc) solution and PBS tablets were purchased from Sigma-Aldrich (St. Louis, USA). Chloroform (HPLC grade) was purchased from Alfa Aesar (Haverhill, USA). Methanol (LC/MS grade) was purchased from Fisher Scientific (Hampton, USA). 1,2-Dihexanoyl-*sn*-glycero-3-phospho-(1′-*rac*-glycerol) (PG 6:0/6:0), 1,2-dioctanoyl-*sn*-glycero-3-phospho-(1′-*rac*-glycerol) (PG 8:0/8:0), 1,2-didecanoyl-*sn*-glycero-3-phospho-(1′-*rac*-glycerol) (PG 10:0/10:0), 1,2-dilauroyl-*sn*-glycero-3-phospho-(1′-*rac*-glycerol) (12:0/12:0 PG), 1,2-dimyristoyl-*sn*-glycero-3-phospho-(1′-*rac*-glycerol) (PG 14:0/14:0), 1,2-dipalmitoyl-*sn*-glycero-3-phospho-(1′-*rac*-glycerol) (PG 16:0/16:0), 1,2-distearoyl-*sn*-glycero-3-phospho-(1′-*rac*-glycerol) (18:0/18:0 PG), 1,2-dimyristoyl-*sn*-glycero-3-phospho-L-serine (PS 14:0/14:0), 1,2-dimyristoyl-*sn*-glycero-3-phosphoethanolamine (PE 14:0/14:0), 1,2-dimyristoyl-*sn*-glycero-3-phosphocholine (PC 14:0/14:0), and 1,2-dimyristoyl-*sn*-glycero-3-phosphate (PA 14:0/14:0) were purchased from Avanti Polar Lipids (Alabaster, USA). All lipids were dissolved in 2:1 chloroform/methanol and stored in aliquots. For this, the solvent was evaporated under nitrogen, and dried lipids were overlaid with argon. Aliquots were stored at −20 °C. The lipid content was verified by phosphate analysis.[20]

Preparation of Mixed Detergent−Lipid Micelles. For transfer of lipids during electrospray ionization or control experiments, mixed detergent−lipid micelles were prepared. For this, dried lipids were resuspended in 200 mM AmAc, pH 7.5 containing 0.5% (w/v) C8E4, followed by sonication for 30 min at 60 or 70 °C (PG 16:0/16:0) or 90 °C (PG 18:0/18:0).

Dynamic Light Scattering. The mean hydrodynamic diameter of detergent−lipid micelles was determined using a Litesizer 500 particle size analyzer (Anton Paar, Graz, Austria). See the Supporting Information for details.

Circular Dichroism Spectroscopy. Circular dichroism (CD) spectroscopy was performed using a J-810 spectropolarimeter (JASCO, Groß-Umstadt, Germany). See the Supporting Information for details.

Sample Preparation for Native MS. LL-37 was transferred into 200 mM AmAc using Micro Bio-Spin P6-6 gel columns (Bio-Rad, Hercules, USA) according to the manufacturer's instructions. Alternatively, LL-37 was transferred into AmAc using 3 kDa MWCO Amicon ultra centrifugal filters (Merck Millipore, Billerica, USA) according to the manufacturer's instructions. The protein concentration was determined using the Bradford assay.[21] Prior to native MS analysis, LL-37 was mixed with the detergent−lipid micelles to final concentrations of 20 μM LL-37, 25 μM lipid, and 0.5% (w/v) C8E4.

Native MS. Native MS was performed on a Q-TOF Ultima mass spectrometer (Waters, Wilmslow, UK) modified for native MS.[22] For each measurement, 3 μL of sample were loaded into a gold-coated borosilicate emitter needle produced in-house.[23] Typical instrument settings were as follows: capillary voltage, 1.7 kV; capillary temperature, 80 °C; cone voltage, 35 V; collision voltage, 10−100 V; and RF lens voltage, 80 V. Dissociation of peptide−lipid complexes was achieved by increasing the collisional voltage from 10 to 100 V in 10 V increments. Number of replicates: 4 replicates for PG 6:0/6:0, 5 replicates for PG 8:0/8:0, PG 10:0/10:0 and PG 12:0/12:0, 6 replicates for PG 14:0/14:0, 8 replicates for PG 16:0/16:0, 9 replicates for 18:0/18:0 PG, 3 replicates for PS 14:0/14:0 and PA 14:0/14:0, and 4 replicates for PE 14:0/14:0 and PC 14:0/14:0.

Data Analysis. The UniDec[24] software was used for the deconvolution of unprocessed mass spectra using the following settings: m/z range, 820 to 3600; background subtraction, 20; bin size, 2.0; charge range, 1 to 8; mass range, 4400 to 6900 Da; peak full-width half-maximum, <1. The intensity (termed "height" in UniDec settings) of selected peaks was extracted after normalization of the mass spectra to the base peak. The extracted peak intensities of all charge states of LL-37−lipid complexes were summed up and divided by the extracted peak intensity of the total LL-37 monomer peaks, providing the relative abundance of LL-37−lipid complexes. Relative abundances obtained at different collisional voltages were divided by the relative abundance at 10 V. The data points were fitted using the Boltzmann sigmoidal function $y = A_2 + (1 - A_2)/(1 + \exp((x - x_0)/dx))$. CID50 values were obtained from this fit.

For visualization of mass spectra, the raw data was processed using MassLynx v4.1 (Waters, Wilmslow, UK). Accordingly, at least 70 scans were combined and smoothed twice with a smooth window of 20 using the Savitzky−Golay filter,[25] followed by background subtraction applying a 30% reduction under the curve with a polynomial order of 3 and a tolerance of 0.01.

RESULTS AND DISCUSSION

LL-37 as a Model Peptide. To systematically study peptide−lipid interactions in the gas phase, we used the antimicrobial peptide LL-37 as a model peptide. LL-37 is the only human antimicrobial peptide of the cathelicidin family;[26,27] it defends the cell against bacteria or fungi by associating with their membranes causing destabilization and disruption of the membranes.[28,29] LL-37 consists of a single amphipathic helix (Figure S1A) and, therefore, has a hydrophobic and a hydrophilic interface (Figure S1B). The hydrophobic interface allows interactions with the fatty acyl chains in the hydrophobic core of phospholipid bilayers, while the hydrophilic interface electrostatically interacts with the lipid headgroups.

Interactions between LL-37 and phospholipids depend on the correct folding of the amphipathic helix.[30] We, therefore, first assessed the secondary structure of LL-37 by CD spectroscopy (Figure S1C). To reflect the conditions used in native MS, the secondary structure of LL-37 was analyzed in 20 mM AmAc in the presence and in the absence of 0.5% (w/v) C8E4. As high salt concentrations further effect secondary structure formation,[30] LL-37 was also analyzed in PBS (Figure S1C). Note that lower AmAc concentrations were used during CD spectroscopy compared with native MS conditions to reduce the background absorption (20 mM instead of 200 mM AmAc). The CD spectrum of LL-37 in 20 mM AmAc shows a local minimum at 203 nm, indicating that the peptide is unstructured under these conditions.[31] Accordingly, LL-37 was previously described to be disordered at low salt concentrations; a lack of anions showed the strongest effects in these experiments.[30] Note that a higher AmAc concentration, as used in native MS experiments, might induce helix formation.

https://doi.org/10.1021/acs.analchem.3c03428
Anal. Chem. 2023, 95, 17292−17299

As C8E4 detergent was used for lipid transfer to LL-37, the peptide was also analyzed in the presence of 0.5% (w/v) C8E4. The corresponding CD spectrum shows local minima at 208 and 222 nm, which are characteristic for α-helical structures.[32] Our findings indicate that 0.5% (w/v) C8E4 induces transitions of LL-37 from a random coil to an α-helix. This is in agreement with previous studies, showing that many antimicrobial peptides form α-helices in a hydrophobic environment.[33,34] Our findings further suggest direct interactions between LL-37 and C8E4. Similarly, the CD spectrum of LL-37 in the presence of PBS showed local minima at 208 and 222 nm, confirming that α-helical structures form at higher salt concentrations.

Characterization of Detergent−Lipid Micelles. Previous studies showed that detergent micelles stabilize integral membrane proteins in the gas phase[35−38] and allow for lipid transfer from mixed detergent−lipid micelles.[13,39] Here, we analyzed the interactions of the soluble peptide LL-37 with lipids by transferring lipids from detergent−lipid micelles as introduced recently.[40] Although the underlying mechanism of the lipid transfer from detergent−lipid micelles is unknown, this procedure allows the study of lipid binding to soluble proteins and peptides. Importantly, individual lipids are transferred to the protein, providing us with the opportunity to explore the effects of individual lipid species.

To reach this goal, detergent−lipid micelles were prepared in 200 mM AmAc containing 0.5% (w/v) C8E4 and 25 μM of the respective phospholipids. To evaluate solubilization of the lipids, the particle size of these mixed micelles was determined by DLS and compared to C8E4 micelles (Figure S2). PC 14:0/14:0 was completely solubilized showing a particle size of approximately 5 nm similar to C8E4 micelles (Figure S2A). For PE 14:0/14:0, PA 14:0/14:0, and PS 14:0/14:0, additional distributions of large particle sizes were observed, suggesting that these lipids did not solubilize completely and formed higher aggregates. Note that the volume of these aggregates is <1% of the total volume, and these aggregates can, therefore, be neglected. Increasing the C8E4 concentration to 0.75% (w/v) and 2% (w/v) C8E4 resulted in complete solubilization of PS 14:0/14:0 as well as PE 14:0/14:0 and PA 14:0/14:0, respectively (Figure S2A). In contrast, PG lipid species ranging from PG 6:0/6:0 to PG 18:0/18:0 were completely solubilized at 0.5% (w/v) C8E4 with particle sizes similar to C8E4 micelles (Figure S2B); note that PG 16:0/16:0 and PG 18:0/18:0 have higher transition temperatures and required higher sonication temperatures for solubilization. Because populations of larger aggregates were neglectable (see above), the detergent concentration of 0.5% (w/v) was maintained for all measurements.

Exploring Electrostatic Interactions of LL-37 with Different Lipid Headgroups. When interactions that form in solution are explored by the complexes that are observed in the gas phase, the experiments should be carefully designed, and the results should be interpreted with caution. While the equilibrium between the free and the ligand-bound peptide in solution can in principle be maintained in native MS experiments, there are several factors that influence the observed ratio between free and ligand-bound peptide ions:[41−44] (i) optimized settings are required to reduce in-source dissociation (false negatives) and nonspecific complex formation due to high concentration of the ligands in the electrospray droplets (false positives). In addition, the position of the electrospray emitter might affect the ionization of intact complexes.[41] We, therefore, fine-tuned instrument settings to maintain peptide−lipid complexes and kept them constant in all measurements. Note that oligomerization of LL-37 was described previously;[45] we also observed oligomeric states of LL-37 in preliminary experiments; however, we fine-tuned instrumental parameters for the detection of peptide−lipid complexes, and LL-37 oligomers were absent or in low abundance in most mass spectra. (ii) Formation of complexes that is exclusively driven by hydrophobic interactions cannot be followed in the gas phase.[19,46] Accordingly, we do not address interactions with purely hydrophobic molecules. (iii) The response factor describing the ionization and detection efficiency of the analytes depends on the size and structure of the analyte[43,47] and should be comparable between ion species that are analyzed. Accordingly, the response factor of lipids depends on the chemical structure of the lipid headgroup and the length of the fatty acyl chains. In previous studies, the ionization efficiency was found to decrease with increasing length of the fatty acyl chains.[48,49] However, these observations were made for lipids solubilized in chloroform/methanol, and ionization of LL-37−lipid complexes in native MS experiments differs from these experiments.[50] As glycerophospholipids are relatively small molecules when compared to LL-37, the response factor of LL-37−lipid complexes is expected to be comparable to the response factor of free LL-37.

Taking these considerations into account, we first investigated noncovalent interactions of LL-37 with different glycerophospholipid headgroups by native MS. Specifically, we examined interactions of LL-37 with two zwitterionic lipids, namely, PC 14:0/14:0 and PE 14:0/14:0, as well as three negatively charged lipids, namely PA 14:0/14:0, PS 14:0/14:0, and PG 14:0/14:0. To this end, detergent−lipid micelles were prepared as described above and used to transfer the lipids onto LL-37. The formed LL-37−lipid complexes were then analyzed by native MS.

The acquired mass spectra confirmed binding of all 5 phospholipids to LL-37 (Figure S3). Each mass spectrum revealed peaks corresponding in mass to LL-37 with up to 3 associated lipids. Importantly, peak intensities for complexes with zwitterionic lipids, e.g., PC 14:0/14:0, were comparably lower than those observed for complexes with negatively charged lipids, e.g., PS 14:0/14:0 (Figure S3). To determine binding preferences of the different lipid classes, relative abundances of detected complexes were determined as described (Experimental Section) and compared (Figure 1). Accordingly, the relative abundance of LL-37−lipid complexes

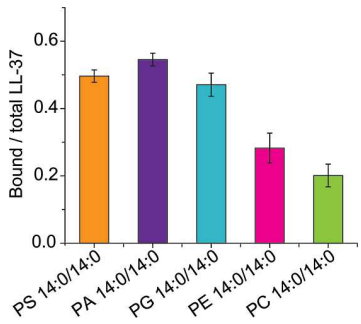

Figure 1. Interactions of LL-37 with lipids of different classes. Relative abundance of LL-37−lipid complexes containing PS 14:0/14:0 (orange), PA 14:0/14:0 (purple), PG 14:0/14:0 (light blue), PE 14:0/14:0 (pink), and PC 14:0/14:0 (light green).

https://doi.org/10.1021/acs.analchem.3c03428
Anal. Chem. 2023, 95, 17292−17299

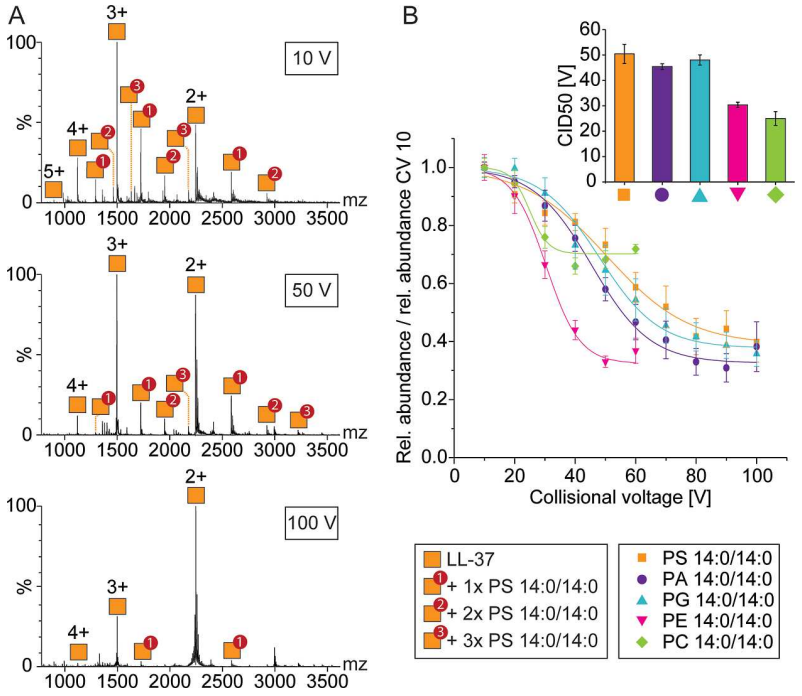

Figure 2. Probing electrostatic interactions in the gas phase by collisional dissociation. (A) Native MS of LL-37 in the presence of C8E4 with PS 14:0/14:0 at different collisional voltages. Charge states and lipid adducts are assigned. Masses of LL-37−lipid complexes are given in Table S1. (B) Collision-induced dissociation of LL-37−lipid complexes. The relative abundance of LL-37−lipid complexes determined for each collisional voltage (CV) was divided by the relative abundance observed at 10 V. The data points were fitted to sigmoidal functions. The CID50 values are plotted for each lipid class.

that contain negatively charged lipids (PG 14:0/14:0, PA 14:0/14:0 or PS 14:0/14:0) was approximately 50%, while the relative abundance of complexes that include zwitterionic lipids (PC 14:0/14:0 or PE 14:0/14:0) was <30%. The lipid binding preference for the different negatively charged lipids was comparable, and only a slight increase of PG 14:0/14:0 < PS 14:0/14:0 < PA 14:0/14:0 was observed. The zwitterionic lipid PE 14:0/14:0 showed slightly higher binding than PC 14:0/14:0. The formation of more hydrogen bonds between the amine group of PE 14:0/14:0 and LL-37 might stabilize the complexes in the gas phase; apart from the phosphate group, the predominantly ionic PC headgroup is not involved in hydrogen bonding. Our results are in agreement with previous findings that revealed a selectivity of LL-37 for negatively charged phospholipids.[51−54] However, it is important to take into account that the approach followed here is limited to the transfer of lipids from detergent−lipid micelles, and the effects of chain packing or lipid−lipid interactions as present in lipid bilayers cannot be assessed.

Electrostatic Interactions Determine the Gas-Phase Stability. Having investigated the formation of LL-37−lipid complexes in solution, we explored the stability of the complexes in the gas phase by collisional dissociation. For this, the collisional voltage in the collision cell was increased from 10 to 100 V in 10 V increments. The peak intensities of the LL-37−lipid complexes decreased with increasing collision voltages (Figure 2A). Comparing the decrease in intensity of different LL-37−lipid complexes (Figure 2B), we estimate the relative binding strength of the lipids in the gas phase. Note that the strength of interactions in the gas phase differs from the strength in solution.[55] For instance, the strength of Coulombic interactions increases by a factor of 80 and van der Waals interactions by a factor of 6400[56] when transferring molecules from solution into the gas phase. Furthermore, desolvation during electrospray ionization not only leads to the loss of hydrophobic interactions but also strengthens hydrogen bonding by eliminating competition with surrounding water molecules.[57] Consequently, rearrangements of the complexes to a gas-phase conformation are possible.[58,59]

Given that the lipids investigated here contain identical fatty acyl chains, differences in binding can be deduced from electrostatic interactions of the lipid headgroups. Since electrostatic interactions are equally enhanced in the gas phase, we are able to compare the relative binding strength in the gas phase and in solution. For this, peak intensities of LL-37−lipid complexes at different collisional voltages were extracted, and the relative abundances of the LL-37−lipid complexes were calculated (see the Experimental Section). The relative abundance obtained for each collisional voltage was then divided by the relative abundance at 10 V. LL-37−lipid complexes containing zwitterionic lipids, i.e., PC 14:0/14:0 and PE 14:0/14:0 showed the lowest binding strength with the lowest intensity at approximately 40 and 50 V, respectively (Figures 2B and S4). Note that the background signal in these measurements was comparably high (Figure S4). The negatively charged lipids, on the contrary, showed high binding strengths with similar dissociation behavior. Accordingly, LL-37−lipid complexes containing PS 14:0/14:0 and PA 14:0/14:0 showed lowest intensities at collisional voltages of approximately 80 V and those containing PG 14:0/14:0 at approximately 100 V. These findings are supported by the CID50 values, i.e., the collisional voltage at which 50% of the complex' intensity is reached. Accordingly, gas-phase stability is reduced for zwitterionic lipids compared with their negatively charged counterparts. These results are in agreement with our own (see above) and previous findings that

https://doi.org/10.1021/acs.analchem.3c03428
Anal. Chem. 2023, 95, 17292−17299

showed preferred interactions of LL-37 with negatively charged lipids.[51−54]

Exploring Hydrophobic Interactions between LL-37 and Fatty Acyl Chains. We next explored hydrophobic interactions of LL-37 with lipids that differ in fatty acyl chain length. For this, we used a range of PG lipids with fatty acyl chains that increased in length by two methylene groups per fatty acyl chain and increment, namely, PG 6:0/6:0, PG 8:0/8:0, PG 10:0/10:0, PG 12:0/12:0, PG 14:0/14:0, PG 16:0/16:0, and PG 18:0/18:0. Native mass spectra confirmed binding of all PG lipids to LL-37 under the conditions applied here (Figure S5). Again, the mass spectra revealed LL-37−lipid complexes with up to 3 associated lipids (Figure S5).

To determine lipid binding preferences, we next evaluated the relative abundance of complexes that were assembled from each LL-37−PG combination (Figure 3). Native mass spectra

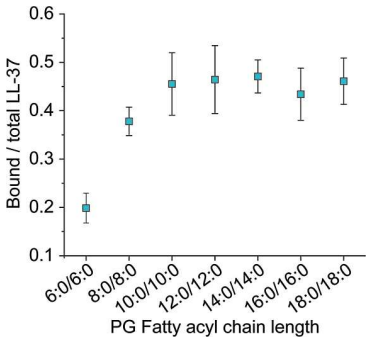

Figure 3. Formation of LL-37−lipid complexes including PG lipids with different fatty acyl chain lengths. The normalized sum of intensities of LL-37−lipid complexes with PG lipids varying in fatty acyl chain length is shown.

revealed a lower relative abundance of complexes containing lipids with short fatty acyl chains. For instance, complexes that contained PG 6:0/6:0 showed an intensity of approximately 20% when compared to total LL-37. In contrast, complexes that contained lipids with longer fatty acyl chains showed higher relative abundances of approximately 45% when compared with total LL-37 (Figure 3). Importantly, only smaller differences were observed between PG 10:0/10:0 and PG 18:0/18:0 lipids; the relative abundance for lipids with fatty acyl chain length >10 carbon atoms reached a plateau.

The increase in the relative abundance of complexes that assemble from PG 6:0/6:0 to PG 10:0/10:0 is likely due to an increase in hydrophobic interactions in solution. The fact that the relative abundance of complexes containing PG lipids with fatty acyl chains >10 carbon atoms does not increase above a certain limit was surprising and might have different reasons: first, the solubility of these lipids in aqueous solutions is low due to their hydrophobicity. Note that DLS analysis revealed complete solubility of these lipids as indicated by micelle formation (Figure S2); however, potential lipid aggregates might not be captured in these measurements due to precipitation. Another explanation might be that LL-37 prefers interactions with fatty acyl chains of a defined length. Due to its amphiphilic structure, the maximum number of hydrophobic contacts likely depends on the size of the hydrophobic interface of LL-37 and longer fatty acyl chains do not increase hydrophobic contacts. Again, the absence of a phospholipid membrane might affect these interactions (see above). As the mechanism behind the transfer of lipids from detergent−lipid micelles remains elusive, the hydrophobicity of the lipids might also influence their transfer. Nonetheless, the increase in relative abundance when forming complexes that contain lipids with longer fatty acyl chains suggests that more hydrophobic interactions are formed in solution resulting in increased complex formation; even though only electrostatic interactions are stabilized in the gas phase, the higher relative abundance of the complexes in solution is visualized in native MS experiments.

Probing Hydrophobic and van der Waals Interactions in the Gas Phase. To gain detailed insights into the interactions between LL-37 and PG lipids that differ in fatty acyl chain length, the formed complexes were dissociated in the gas phase as described above. By correlating the observed binding strength in the gas phase with the detected ion intensities, we are able to distinguish between interactions that drive complex formation in solution and interactions that stabilize the peptide−lipid complexes in the gas phase. For this, the peak intensities of LL-37−lipid complexes at different collisional voltages were extracted to determine the binding strength in the gas phase. Again, peak intensities of LL-37−lipid complexes decrease with increasing collisional voltage; Figure 4A shows an example. The relative abundances of LL-37−lipid complexes at different collisional voltages were subsequently compared (Figure 4B). We observed a similar binding strength for most PG lipids dissociating at approximately 80 to 100 V. Note that PG 6:0/6:0, the lipid with the shortest fatty acyl chain, dissociated at a lower collisional voltage of approximately 60 V. The binding strength of PG 6:0/6:0 might be underestimated due to the low intensity of the complex at low collisional voltages (Figure S5) resulting in a lower signal-to-noise ratio at higher collisional voltages. Only minor differences in binding strength were observed between PG lipids with longer fatty acyl chains. Importantly, a slight increase in the binding strength was observed for increasing fatty acyl chain length (i.e., PG 8:0/8:0 < PG 10:0/10:0 < PG 12:0/12:0 < PG 16:0/16:0 ≈ PG 18:0/18:0). Surprisingly, PG 14:0/14:0 showed the highest binding strength dissociating at approximately 100 V. We assume that the higher binding strength for complexes containing lipids with longer fatty acyl chains results from van der Waals interactions. Accordingly, we assume that the fatty acyl chains of PG lipids are in close contact with LL-37 in the gas phase. We conclude that the binding strength of the same lipid class in the gas phase mostly relies on interactions with the headgroups. Slight differences might be explained by van der Waals interactions that are higher for longer fatty acyl chains than for short-chain lipids. Nonetheless, differences in the binding modes of PG lipids with long or short fatty acyl chains in solution should also be considered; binding of the lipids in different local environments on the protein surface might cause differences in the electrostatic interactions formed through the lipid headgroup and consequently their stabilization in the gas phase.

CONCLUSIONS

In this study, we systematically investigated the interactions of the antimicrobial peptide LL-37 with glycerophospholipids containing different headgroups and varying fatty acyl chain lengths. For this, lipids were transferred from C8E4−lipid micelles as previously described.[40] Using native MS, we explored whether interactions that form in solution are

https://doi.org/10.1021/acs.analchem.3c03428
Anal. Chem. 2023, 95, 17292−17299

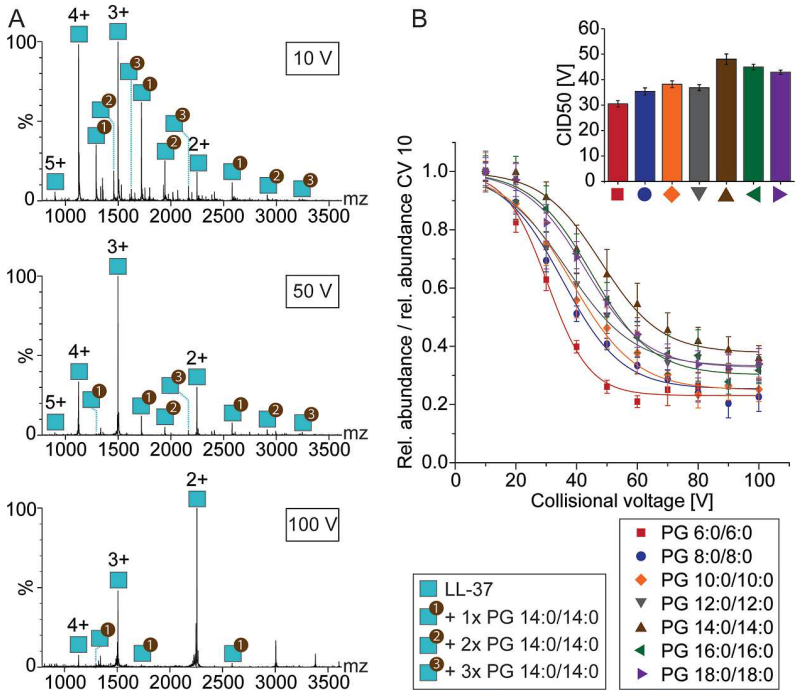

Figure 4. Probing hydrophobic and van der Waals interactions by gas-phase dissociation. (A) Native MS of LL-37 in the presence of C8E4 with PG 14:0/14:0 at different collisional voltages. Charge states and lipid adducts are assigned. Masses of LL-37−lipid complexes are given in Table S1. (B) Collision-induced dissociation of LL-37−lipid complexes. The relative abundance of LL-37−lipid complexes obtained at each collisional voltage (CV) was divided by the relative abundance determined at 10 V. The data points were fitted to sigmoidal functions. The CID50 values are plotted for each lipid class.

reflected in the ion intensities and complex stability in the gas phase.

We found that interactions between LL-37 and negatively charged lipids are preferred; this observation is reflected in the ion intensities and complex stability. Accordingly, electrostatic interactions with the lipid headgroups are responsible for the binding specificity in solution and, furthermore, determine the relative binding strength in the gas phase. Note that the binding strength in solution is less affected by experimental factors such as the response factor and might, therefore, be a more reliable measure for determining the specificity when electrostatic interactions are predominant. Native MS, therefore, is well-suited to investigate electrostatic interactions formed in solution and stabilized in the gas phase.

Probing interactions between LL-37 and PG lipids varying in fatty acyl chain length, we further explored hydrophobic interactions. Even though hydrophobic interactions are not stabilized in the gas phase, we observed differences in the peak intensity of complexes between LL-37 and PG lipids containing shorter or longer fatty acyl chains. We relate these differences to differences in the hydrophobic interactions in solution. Differences in the dissociation of the complexes in the gas phase are further attributed to van der Waals interactions, which, in addition to other electrostatic interactions, contribute to complex stability in the gas phase. The increase in van der Waals interactions suggests the presence of direct contacts between the fatty acyl chains and LL-37 in the gas phase, an observation that cannot be verified by MS, however, might change our understanding of protein structures and protein complexes in the gas phase. Identifying the mechanism of lipid transfer from detergent−lipid micelles to proteins in future studies will further increase our knowledge of protein−lipid and protein−detergent interactions in solution and in the gas phase.

In summary, we show that the peak intensity observed in native mass spectra does not necessarily correlate with the stability of the assemblies in the gas phase. Nonetheless, native MS is a well-suited tool to evaluate interactions that are formed in solution and observed in the gas phase.

■ ASSOCIATED CONTENT

Supporting Information

The Supporting Information is available free of charge at https://pubs.acs.org/doi/10.1021/acs.analchem.3c03428.

Experimental details on dynamic light scattering and CD spectroscopy; structure of LL-37, DLS analysis of detergent−lipid micelles, exploring electrostatic interactions with lipid headgroups, dissociation of LL37−PE and LL-37−PC complexes, exploring hydrophobic interactions of LL-37 with fatty acyl chains; masses of LL-37−lipid complexes (PDF)

■ AUTHOR INFORMATION

Corresponding Author

Carla Schmidt − *Interdisciplinary Research Centre HALOmem, Institute of Biochemistry and Biotechnology, Charles Tanford Protein Centre, Martin Luther University Halle-Wittenberg, 06120 Halle, Germany; Department of Chemistry—Biochemistry, Johannes Gutenberg University Mainz, 55128 Mainz, Germany;* orcid.org/0000-0001-9410-1424; Email: carla.schmidt@uni-mainz.de

https://doi.org/10.1021/acs.analchem.3c03428
Anal. Chem. 2023, 95, 17292−17299

Author

Til Kundlacz − *Interdisciplinary Research Centre HALOmem, Institute of Biochemistry and Biotechnology, Charles Tanford Protein Centre, Martin Luther University Halle-Wittenberg, 06120 Halle, Germany; Institute of Chemistry, Martin Luther University Halle-Wittenberg, 06120 Halle, Germany;* orcid.org/0000-0002-0526-2179

Complete contact information is available at: https://pubs.acs.org/10.1021/acs.analchem.3c03428

Author Contributions

T.K. performed all experiments and analyzed the data. C.S. supervised the experiments and guided the research. T.K. and C.S. wrote the manuscript.

Notes

The authors declare no competing financial interest.

■ ACKNOWLEDGMENTS

We thank Annette Meister (Martin Luther University Halle-Wittenberg) and Julia Bieber (Johannes Gutenberg University Mainz) for helpful discussions and Claudia Müller for analysis of phosphate content. We acknowledge funding from the German Research Foundation (DFG, project number 436494874, RTG 2670 "Beyond Amphiphilicity: Self-Organization of Soft Matter via Multiple Noncovalent Interactions"), the Federal Ministry for Education and Research (BMBF, 03Z22HN22 and 03Z22HI2), and the European Regional Development Funds (EFRE, ZS/2016/04/78115).

■ REFERENCES

(1) Hanshaw, R. G.; Stahelin, R. V.; Smith, B. D. *Chemistry* **2008**, *14*, 1690−1697.
(2) White, S. H.; Wimley, W. C. *Biochim. Biophys. Acta* **1998**, *1376*, 339−352.
(3) von Heijne, G. *Nat. Rev. Mol. Cell Biol.* **2006**, *7*, 909−918.
(4) van Dalen, A.; Hegger, S.; Killian, J. A.; de Kruijff, B. *FEBS Lett.* **2002**, *525*, 33−38.
(5) van Meer, G.; Voelker, D. R.; Feigenson, G. W. *Nat. Rev. Mol. Cell Biol.* **2008**, *9*, 112−124.
(6) Lee, A. G. *Biochim. Biophys. Acta* **2004**, *1666*, 62−87.
(7) Palsdottir, H.; Hunte, C. *Biochim. Biophys. Acta* **2004**, *1666*, 2−18.
(8) Epand, R. M. *Biochim. Biophys. Acta* **1998**, *1376*, 353−368.
(9) Bolla, J. R.; Agasid, M. T.; Mehmood, S.; Robinson, C. V. *Annu. Rev. Biochem.* **2019**, *88*, 85−111.
(10) Frick, M.; Schmidt, C. *Chem. Phys. Lipids* **2019**, *221*, 145−157.
(11) Gupta, K.; Donlan, J. A. C.; Hopper, J. T. S.; Uzdavinys, P.; Landreh, M.; Struwe, W. B.; Drew, D.; Baldwin, A. J.; Stansfeld, P. J.; Robinson, C. V. *Nature* **2017**, *541*, 421−424.
(12) Gupta, K.; Li, J.; Liko, I.; Gault, J.; Bechara, C.; Wu, D.; Hopper, J. T. S.; Giles, K.; Benesch, J. L. P.; Robinson, C. V. *Nat. Protoc.* **2018**, *13*, 1106−1120.
(13) Laganowsky, A.; Reading, E.; Allison, T. M.; Ulmschneider, M. B.; Degiacomi, M. T.; Baldwin, A. J.; Robinson, C. V. *Nature* **2014**, *510*, 172−175.
(14) Landreh, M.; Marty, M. T.; Gault, J.; Robinson, C. V. *Curr. Opin. Struct. Biol.* **2016**, *39*, 54−60.
(15) Barrera, N. P.; Isaacson, S. C.; Zhou, M.; Bavro, V. N.; Welch, A.; Schaedler, T. A.; Seeger, M. A.; Miguel, R. N.; Korkhov, V. M.; van Veen, H. W.; Venter, H.; Walmsley, A. R.; Tate, C. G.; Robinson, C. V. *Nat. Methods* **2009**, *6*, 585−587.
(16) Demmers, J. A. A.; van Dalen, A.; de Kruijff, B.; Heck, A. J. R.; Killian, J. A. *FEBS Lett.* **2003**, *541*, 28−32.
(17) Gault, J.; Donlan, J. A. C.; Liko, I.; Hopper, J. T. S.; Gupta, K.; Housden, N. G.; Struwe, W. B.; Marty, M. T.; Mize, T.; Bechara, C.; Zhu, Y.; Wu, B.; Kleanthous, C.; Belov, M.; Damoc, E.; Makarov, A.; Robinson, C. V. *Nat. Methods* **2016**, *13*, 333−336.
(18) Zhou, M.; Morgner, N.; Barrera, N. P.; Politis, A.; Isaacson, S. C.; Matak-Vinković, D.; Murata, T.; Bernal, R. A.; Stock, D.; Robinson, C. V. *Science* **2011**, *334*, 380−385.
(19) Robinson, C. V.; Chung, E. W.; Kragelund, B. B.; Knudsen, J.; Aplin, R. T.; Poulsen, F. M.; Dobson, C. M. *J. Am. Chem. Soc.* **1996**, *118*, 8646−8653.
(20) Lindberg, O.; Ernster, L. *Methods Biochem. Anal.* **1956**, *3*, 1−22.
(21) Bradford, M. M. *Anal. Biochem.* **1976**, *72*, 248−254.
(22) Sobott, F.; Hernández, H.; McCammon, M. G.; Tito, M. A.; Robinson, C. V. *Anal. Chem.* **2002**, *74*, 1402−1407.
(23) Hernández, H.; Robinson, C. V. *Nat. Protoc.* **2007**, *2*, 715−726.
(24) Marty, M. T.; Baldwin, A. J.; Marklund, E. G.; Hochberg, G. K. A.; Benesch, J. L. P.; Robinson, C. V. *Anal. Chem.* **2015**, *87*, 4370−4376.
(25) Savitzky, A.; Golay, M. J. E. *Anal. Chem.* **1964**, *36*, 1627−1639.
(26) Gennaro, R.; Zanetti, M. *Biopolymers* **2000**, *55*, 31−49.
(27) Ramanathan, B.; Davis, E. G.; Ross, C. R.; Blecha, F. *Microbes Infect.* **2002**, *4*, 361−372.
(28) Shai, Y. *Biochim. Biophys. Acta* **1999**, *1462*, 55−70.
(29) Zasloff, M. *Nature* **2002**, *415*, 389−395.
(30) Johansson, J.; Gudmundsson, G. H.; Rottenberg, M. E.; Berndt, K. D.; Agerberth, B. *J. Biol. Chem.* **1998**, *273*, 3718−3724.
(31) Venyaminov, S.; Baikalov, I. A.; Shen, Z. M.; Wu, C. S.; Yang, J. T. *Anal. Biochem.* **1993**, *214*, 17−24.
(32) Greenfield, N. J. *Nat. Protoc.* **2006**, *1*, 2876−2890.
(33) Dathe, M.; Wieprecht, T. *Biochim. Biophys. Acta* **1999**, *1462*, 71−87.
(34) Sato, H.; Feix, J. B. *Biochim. Biophys. Acta* **2006**, *1758*, 1245−1256.
(35) Barrera, N. P.; Di Bartolo, N.; Booth, P. J.; Robinson, C. V. *Science* **2008**, *321*, 243−246.
(36) Borysik, A. J.; Hewitt, D. J.; Robinson, C. V. *J. Am. Chem. Soc.* **2013**, *135*, 6078−6083.
(37) Reading, E.; Liko, I.; Allison, T. M.; Benesch, J. L. P.; Laganowsky, A.; Robinson, C. V. *Angew. Chem., Int. Ed. Engl.* **2015**, *54*, 4577−4581.
(38) Wang, S. C.; Politis, A.; Di Bartolo, N.; Bavro, V. N.; Tucker, S. J.; Booth, P. J.; Barrera, N. P.; Robinson, C. V. *J. Am. Chem. Soc.* **2010**, *132*, 15468−15470.
(39) Reading, E.; Walton, T. A.; Liko, I.; Marty, M. T.; Laganowsky, A.; Rees, D. C.; Robinson, C. V. *Chem. Biol.* **2015**, *22*, 593−603.
(40) Landreh, M.; Costeira-Paulo, J.; Gault, J.; Marklund, E. G.; Robinson, C. V. *Anal. Chem.* **2017**, *89*, 7425−7430.
(41) Benkestock, K.; Sundqvist, G.; Edlund, P.-O.; Roeraade, J. *J. Mass Spectrom.* **2004**, *39*, 1059−1067.
(42) Kitova, E. N.; El-Hawiet, A.; Schnier, P. D.; Klassen, J. S. *J. Am. Soc. Mass Spectrom.* **2012**, *23*, 431−441.
(43) Peschke, M.; Verkerk, U. H.; Kebarle, P. *J. Am. Soc. Mass Spectrom.* **2004**, *15*, 1424−1434.
(44) Wang, W.; Kitova, E. N.; Klassen, J. S. *Anal. Chem.* **2003**, *75*, 4945−4955.
(45) Walker, L. R.; Marzluff, E. M.; Townsend, J. A.; Resager, W. C.; Marty, M. T. *Anal. Chem.* **2019**, *91*, 9284−9291.
(46) Bich, C.; Baer, S.; Jecklin, M. C.; Zenobi, R. *J. Am. Soc. Mass Spectrom.* **2010**, *21*, 286−289.
(47) Kitova, E. N.; Kitov, P. I.; Paszkiewicz, E.; Kim, J.; Mulvey, G. L.; Armstrong, G. D.; Bundle, D. R.; Klassen, J. S. *Glycobiology* **2007**, *17*, 1127−1137.
(48) Hofmann, T.; Schmidt, C. *Chem. Phys. Lipids* **2019**, *223*, 104782.
(49) Koivusalo, M.; Haimi, P.; Heikinheimo, L.; Kostiainen, R.; Somerharju, P. *J. Lipid Res.* **2001**, *42*, 663−672.
(50) Konermann, L.; Ahadi, E.; Rodriguez, A. D.; Vahidi, S. *Anal. Chem.* **2013**, *85*, 2−9.
(51) Ding, B.; Soblosky, L.; Nguyen, K.; Geng, J.; Yu, X.; Ramamoorthy, A.; Chen, Z. *Sci. Rep.* **2013**, *3*, 1854.

(52) Henzler Wildman, K. A.; Lee, D.-K.; Ramamoorthy, A. *Biochemistry* **2003**, *42*, 6545−6558.
(53) Neville, F.; Cahuzac, M.; Konovalov, O.; Ishitsuka, Y.; Lee, K. Y. C.; Kuzmenko, I.; Kale, G. M.; Gidalevitz, D. *Biophys. J.* **2006**, *90*, 1275−1287.
(54) Zhang, X.; Oglęcka, K.; Sandgren, S.; Belting, M.; Esbjörner, E. K.; Nordén, B.; Gräslund, A. *Biochim. Biophys. Acta* **2010**, *1798*, 2201−2208.
(55) Yin, S.; Xie, Y.; Loo, J. A. *J. Am. Soc. Mass Spectrom.* **2008**, *19*, 1199−1208.
(56) Erba, E. B.; Zenobi, R. *Annu. Rep. Prog. Chem., Sect. C: Phys. Chem.* **2011**, *107*, 199.
(57) Kohtani, M.; Jones, T. C.; Schneider, J. E.; Jarrold, M. F. *J. Am. Chem. Soc.* **2004**, *126*, 7420−7421.
(58) Steinberg, M. Z.; Elber, R.; McLafferty, F. W.; Gerber, R. B.; Breuker, K. *Chembiochem* **2008**, *9*, 2417−2423.
(59) Wang, W.; Kitova, E. N.; Klassen, J. S. *J. Am. Chem. Soc.* **2003**, *125*, 13630−13631.

https://doi.org/10.1021/acs.analchem.3c03428
Anal. Chem. 2023, 95, 17292−17299

Effects of Surface Charge of Amphiphilic Peptides on Peptide-Lipid Interactions in the Gas Phase and in Solutions.

Til Kundlacz, Christian Schwieger, Carla Schmidt

Anal. Chem. 2025

https://doi.org/10.1021/acs.analchem.5c00283

For this publication, I performed all experiments, analysed and visualised the data. I wrote the original manuscript together with C. Schmidt. C. Schwieger helped in planning and supervised the film balance measurements. C. Schmidt, C. Schwieger and I were involved in the editing and the reviewing process. C. Schmidt supervised the project and guided the research as well as the publication process.

analytical chemistry

pubs.acs.org/ac
Article

Effects of Surface Charge of Amphiphilic Peptides on Peptide−Lipid Interactions in the Gas Phase and in Solution

Til Kundlacz, Christian Schwieger, and Carla Schmidt*

Cite This: https://doi.org/10.1021/acs.analchem.5c00283
Read Online

ABSTRACT: The interactions between peptides and lipids are fundamental for many biological processes. Therefore, exploring the noncovalent interactions that govern these interactions has become increasingly important. Native mass spectrometry is a valuable technique for the characterization of specific peptide−lipid interactions. However, native mass spectrometry requires the transfer of the analyte into the gas phase, and noncovalent interactions driven by the hydrophobic effect might be distorted. We, therefore, address the importance of electrostatic interactions for the formation of peptide−lipid interactions. For this, we make use of the amphipathic, antimicrobial peptide LL-37 as well as a positively and a negatively charged variant thereof and study binding of a variety of lipids by native mass spectrometry. We found that the surface charge of the peptides affects the transfer of stable peptide−lipid complexes into the gas phase and that the ionization mode is important to observe these interactions. We further compare our findings observed in the gas phase with interactions formed in solution between the peptides and lipid monolayers using a Langmuir film balance. The two approaches deliver comparable results and reveal a clear trend in the lipid preferences of all variants for those lipids with opposite charge. Notably, the unmodified wild-type peptide was more flexible in the formation of peptide−lipid interactions. We conclude that native mass spectrometry is indeed well-suited to explore the interactions between peptides and lipids and that electrostatic interactions as expressed by the surface charge of the peptides play an important role in the formation and stabilization of peptide−lipid interactions.

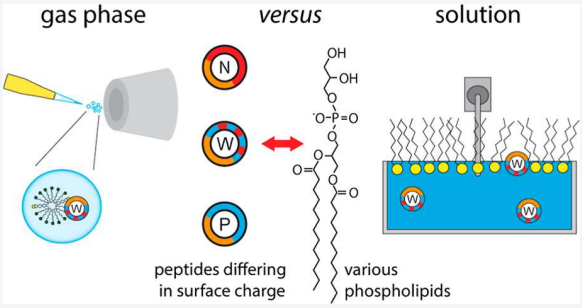

INTRODUCTION

Protein−lipid and protein−membrane interactions are important for various cell functions including, for instance, enzymatic activity, membrane transport, or signaling and trafficking events. They are driven by an interplay of noncovalent interactions, including electrostatic interactions, van der Waals forces, and the hydrophobic effect. Depending on the protein's structure and the binding mode to the lipid bilayer, the different types of noncovalent interactions contribute to its stable association. Importantly, the function of a membrane protein depends not only on correct protein folding but also on a specific lipid environment. The study of protein−lipid interactions, therefore, gained importance during the last decades. While classical structural techniques often fail to provide high-resolution structures of heterogeneous protein−lipid assemblies, other techniques identifying and characterizing the lipid environment of the proteins were introduced.

One such technique is native mass spectrometry (native MS),[1−6] enabling the mass spectrometric analysis of intact protein−lipid complexes under nondenaturing conditions, thereby maintaining noncovalent interactions and resolving individual binding events.[7,8] However, native MS requires the ionization and the transfer of the analyte from solution into the gas phase, where the hydrophobic effect is nonexistent and electrostatic interactions dominate.[9] Accordingly, interactions caused by the hydrophobic effect cannot be stabilized in the gas phase and the question remains whether native MS is capable of accurately describing complexes formed by noncovalent interactions in solution. One approach that is commonly employed when analyzing protein−lipid interactions involves the transfer of lipids from mixed detergent−lipid micelles to soluble or membrane-associated proteins.[5,10,11] Previously, we utilized this approach to analyze interactions between a model peptide, namely, the human antimicrobial peptide LL-37, and a variety of phospholipids.[12] By varying the lipid classes and the length of the fatty acyl chains of the phospholipids, we systematically explored the electrostatic interactions of LL-37 with the lipid head groups as well as interactions with the fatty acyl chains of the lipids that are

Received: January 13, 2025
Accepted: February 7, 2025

driven by the hydrophobic effect. We found that electrostatic interactions are stabilized in the gas phase and that interactions formed in solution are reflected by the intensity of the complexes during native MS measurements.

Here, we follow the same strategy as described above to investigate the effects of the peptide surface charge on peptide−lipid interactions with different lipids. For this, we again chose antimicrobial peptide LL-37 as a model peptide. Antimicrobial peptides are typically short peptides containing a net cationic charge and an amphipathic structure; these properties are essential for their selectivity for bacterial membranes, which contain a high proportion of anionic lipids.[13−15] To study the effects of peptide surface charge, we designed a supercharged cationic (LL-37-pos) and a supercharged anionic (LL-37-neg) variant of LL-37 and compared their lipid interactions with those formed by the wild-type peptide (LL-37-wt). These supercharged variants include additional positively or negatively charged amino acids, altering their solution net charge from 6+ (LL-37-wt) to 14+ (LL-37-pos) or 14− (LL-37-neg). The three variants were investigated with respect to their interactions with negatively charged, zwitterionic, and positively charged lipids. However, as native MS analyses mostly reflect electrostatic interactions that are stable in the gas phase, we further studied the interactions that are formed between the LL-37 variants and lipid monolayers in solution. For this, we employed an adsorption film balance and assembled Langmuir monolayers that are composed of different phospholipids at the air−water interface. Langmuir monolayers represent one leaflet of a phospholipid bilayer and are a widely used as membrane model systems.[16,17] Importantly, interactions between peptides (or proteins) and the monolayers involve hydrophobic as well as electrostatic interactions, therefore allowing the formation of natural binding interfaces including insertion of the peptides into the membrane. Due to their amphipathic structure and natural membrane binding propensity, antimicrobial peptides such as LL-37 are well-suited model peptides to investigate peptide−membrane interactions as well as peptide insertion into the membranes using an adsorption film balance.[18−21]

Using native MS, we first determine the lipid preferences of the three LL-37 variants (i.e., LL-37-wt, LL-37-pos, and LL-37-neg) in the gas phase. While lipid binding of the cationic variants LL-37-wt and LL-37-pos was successfully assessed in positive ion mode, which is commonly employed for proteins and peptides, the analysis of the anionic variant (LL-37-neg) required the application of the negative ion mode, demonstrating that the ionization affects lipid binding and stabilization of peptide−lipid complexes in the gas phase. Importantly, by making use of an adsorption film balance, lipid binding preferences of the variants in solution were explored and compared with the results obtained in the gas phase. Accordingly, gas phase and solution measurements correlate well when considering the surface charge of the peptides and the required ion modes during native MS experiments.

EXPERIMENTAL METHODS

Materials. 1-*O*-(*n*-Octyl)-tetraethylene glycol (C8E4) was purchased from Glycon Biochem (Luckenwalde, Germany). 7.5 M ammonium acetate (AmAc) solution (7.5 M) and PBS tablets were purchased from Sigma-Aldrich (St. Louis, USA). Ammonium bicarbonate (≥99%) was purchased from Carl Roth (Karlsruhe, Germany). Chloroform (HPLC grade) was purchased from Alfa Aesar (Haverhill, USA). Methanol (LC/MS grade) and acetic acid (LC/MS grade) were purchased from Fisher Scientific (Hampton, USA).

Human LL-37 (trifluoroacetate salt, ≥95% purity, Sigma-Aldrich (St. Louis, USA)) was dissolved in phosphate-buffered saline (PBS) from Sigma-Aldrich (St. Louis, USA) and stored at −20 °C. A positively (LL-37-pos) and a negatively (LL-37-neg) charged variant of LL-37 were obtained from Thermo Scientific Custom Peptide synthesis service (Waltham, USA) as lyophilized trifluoroacetate salts: LL-37-pos (amino acid sequence: LLGKFFRKSKKKIGKKWKRIVQ-RIKKFLRNLVPRTES) and LL-37-neg (amino acid sequence: LLGDFFEESEEEIGEEWEEIVQEIEDFLENLVPRTES). Note that a phenylalanine at position 17 was substituted for tryptophan to provide the variants with spectroscopic properties. Notably, single phenylalanine to tryptophan LL-37 mutants display similar behavior to the wild-type.[20] LL-37-pos was dissolved in 25% (v/v) acetic acid, further diluted with water to a final peptide concentration of 1 mg/mL, and stored at −20 °C. LL-37-neg was dissolved with 0.1 M ammonium bicarbonate (Carl Roth GmbH, Karlsruhe, Germany), further diluted with water to a final peptide concentration of 1 mg/mL, and stored at −20 °C.

1,2-Dimyristoyl-*sn*-glycero-3-phospho-(1′-rac-glycerol) (PG 14:0/14:0), 1,2-dimyristoyl-*sn*-glycero-3-phospho-L-serine (PS 14:0/14:0), 1,2-dimyristoyl-*sn*-glycero-3-phosphoethanolamine (PE 14:0/14:0), 1,2-dimyristoyl-*sn*-glycero-3-phosphocholine (PC 14:0/14:0), 1,2-dimyristoyl-*sn*-glycero-3-phosphate (PA 14:0/14:0), and 1,2-dimyristoyl-3-trimethylammonium-propane (TAP 14:0/14:0) were purchased from Avanti Polar Lipids (Alabaster, USA). The lipids were dissolved in pure chloroform or 2:1 chloroform:methanol (v/v) and stored in aliquots. For this, the solvent was evaporated under a nitrogen stream, and dried lipids were overlaid with argon. Aliquots were stored at −20 °C. The lipid content was verified by photometric phosphate analysis.[22] An overview of the lipid structures is given in Figure S1.

Preparation of Mixed Detergent−Lipid Micelles. For transfer of lipids to peptide variants during electrospray ionization (ESI), mixed detergent−lipid micelles were prepared as follows: dried lipids were resuspended in 200 mM AmAc, pH 7.5 containing 0.5% (w/v) C8E4 and sonicated for 30 min at 60 °C. For complete solubilization of TAP 14:0/14:0, sonication was performed at 70 °C followed by two freeze/thaw cycles.

Dynamic Light Scattering. The mean hydrodynamic diameter of detergent−lipid micelles and C8E4 micelles was determined using a Litesizer 500 particle size analyzer (Anton Paar, Graz, Austria). For this, 100 μL of a detergent−lipid micelle suspension were analyzed in a 3 × 3 mm ultra-microcuvette (Hellma Analytics, Müllheim, Germany). The particles were irradiated with a semiconductor laser diode at 658 nm by employing the following instrument settings: measuring angle, side scatter (90°); temperature, 25 °C; measurement time, automatic; filter, automatic; focus, automatic; material, phospholipids. The mean hydrodynamic diameter was determined from size distribution histograms using Kalliope (Anton Paar, Graz, Austria).

Circular Dichroism Spectroscopy. For UV−vis circular dichroism (CD) spectroscopy, 50 μL of a 1 mg/mL peptide solution in PBS and 200 mM AmAc in the presence and absence of 0.5% (w/v) C8E4 were analyzed in a 0.1 mm quartz cuvette at 20 °C using a J-810 spectropolarimeter (JASCO, Groß-Umstadt, Germany). The following instrument param-

https://doi.org/10.1021/acs.analchem.5c00283
Anal. Chem. XXXX, XXX, XXX−XXX

eters were applied: wavelength, 190−240 nm; scanning mode, continued; scan number, 64 scans; scan speed, 50 nm/min; response, 1 s; data pitch, 1 nm. The raw data was reduced to data points at HT voltage below 600 V as the signal-to-noise ratio is lower at high dynode voltages. CD spectra were smoothed using a binomial filter, and a reference spectrum was subtracted using the Spectra Manager software (JASCO). The ellipticity was converted to mean residue ellipticity ($\Delta\varepsilon$) as described previously.[23]

Sample Preparation for Native MS. LL-37 variants were transferred to 200 mM AmAc using Micro Bio-Spin P6-6 gel columns (Bio-Rad, Hercules, USA) according to the manufacturer's instructions. The peptide concentration was subsequently determined using the Bradford assay[24] (LL-37-wt) or by UV−vis spectroscopy at 280 nm (LL-37-pos and LL-37-neg). Prior to native MS analysis, 20 μM of the LL-37 variants was mixed with the detergent−lipid micelles to final concentrations of 25 μM lipid and 0.5% (w/v) C8E4.

Native MS. All measurements were performed using a Q-TOF Ultima mass spectrometer (Waters, Wilmslow, UK) modified for native MS.[25] For each individual measurement, 3 μL of the sample were loaded into a gold-coated borosilicate emitter needle produced in-house.[26] The analysis was performed in positive or negative ion mode.

Instrument settings for positive ion mode were as follows: capillary voltage, 1.7 kV; capillary temperature, 80 °C; cone voltage, 35 V; collisional voltage, 30 V; and RF lens voltage, 80 V. Four replicates were performed for each measurement.

Instrument settings for negative ion mode: capillary voltage, 1.0 kV; capillary temperature, 80 °C; cone voltage, 35 V; collisional voltage, 30 V; and RF lens voltage, 80 V. Four replicates were performed for the interaction of LL-37-neg with TAP 14:0/14:0 and three replicates for the interaction with PC 14:0/14:0 and PG 14:0/14:0, respectively.

Data Analysis. The UniDec[27] software was used for deconvolution of unprocessed mass spectra. The following settings were employed: m/z range, 750 to 4600; Gaussian smoothing, 20; background subtraction, 20; charge range, 1 to 8; mass range, 4400 to 6900 Da; peak full width half-maximum, ∼3.4. The intensity (termed "height" in UniDec settings) of selected peaks was extracted after normalization of the mass spectra to the base peak. Extracted peak intensities of all charge states of the peptide−lipid complexes were summed and divided by the extracted peak intensity of the total peptide monomer peaks, yielding relative abundances of the peptide−lipid complexes.

For visualization of mass spectra, raw data were processed using MassLynx v4.1 (Waters, Wilmslow, UK). At least 70 scans were combined and smoothed twice with a smooth window of 20 using the Savitzky−Golay filter[28] followed by background subtraction applying a 30% reduction under the curve with a polynomial order of 3 and a tolerance of 0.01.

Film Balance Measurements. Film balance experiments were performed using a DeltaPi-4x Langmuir Tensiometer (Kibron, Helsinki, Finland). PBS was used as the aqueous phase for all experiments (2.1 mL of PBS per trough). All experiments were performed at 20 °C; the temperature was controlled by using an external circulating water bath. During the measurements, the film balance was covered with an acrylic glass cover to avoid dust accumulation, as well as evaporation of the subphase. Small water reservoirs under the acrylic glass cover further reduced sample evaporation during the measurements. The subphases were gently stirred throughout the measurements.

Before the analysis, the instrument was calibrated against the known surface pressure (π) of water at 20 °C (72.8 mN/m). Subsequently, the surface pressure of the subphase was measured for at least 10 min to detect potential surface contaminants. The peptide samples were prepared as follows: LL-37 variants were transferred to PBS using 3 kDa MWCO Amicon Ultra Centrifugal Filters (Merck Millipore, Billerica, USA). The protein concentration was determined using the Bradford assay[24] (LL-37-wt) or by UV−vis spectroscopy at 280 nm (LL-37-pos and LL-37-neg).

Determination of the Surface Activity. To determine the surface activity of the individual LL-37 variants as well as appropriate peptide concentrations for monolayer adsorption studies, the adsorption at the air−water interface was analyzed. For this, peptide concentrations of 100−900 nM (LL-37-wt), 25−500 nM (LL-37-pos), and 25−750 nM (LL-37-neg) were injected into the subphase, and the increase in surface pressure ($\Delta\pi$), caused by accumulation of the peptides at the air−water interface, was measured as a function of time for 3−6 h. For data analysis, $\Delta\pi$ was plotted against the peptide bulk concentration and fitted using an exponential association function $[y = y_0 + A_1\ (1 - e^{-x/t1}) + A_2\ (1 - e^{-x/t2})]$. $\Delta\pi$ increases with the peptide concentration until a plateau, indicating surface saturation, is reached. The peptide concentration for monolayer adsorption studies was chosen such that saturation is assured.

Adsorption of Peptides to Lipid Monolayers. To determine the adsorption of LL-37 variants to a lipid monolayer, lipid monolayers were prepared by gradually spreading different lipids (PC 14:0/14:0, PG 14:0/14:0, or TAP 14:0/14:0) dissolved at 0.1 mg/mL in chloroform or 2:1 chloroform:methanol (v/v) at the air−water interface until the desired initial surface pressure (π_0) is reached. The lipid film was then equilibrated for approximately 30 min. Subsequently, the peptides were injected into the subphase underneath the lipid film. The final peptide concentration in the subphase was 400 nM for all variants. After peptide injection, the surface pressure was measured as a function of time for 4 to 8 h until the surface pressure reached an equilibrium value (π_{eq}). The change in surface pressure ($\Delta\pi$), caused by insertion of the peptides into the lipid monolayer, is calculated as $\Delta\pi = \pi_{eq} - \pi_0$. For each LL-37 variant and each lipid monolayer, several measurements at different initial surface pressures π_0 were performed. For data analysis, $\Delta\pi$ was plotted against π_0 and fitted with a linear function $\Delta\pi = A{\cdot}\pi_0 + B$. The maximum insertion pressure (MIP) was determined by extrapolating the plot of $\Delta\pi$ as a function of π_0 to $\Delta\pi = 0$. The MIP equals the intercept of the linear plot with the x axis. Error bars of the MIP values were calculated using the Binding Parameter Calculator software.[29]

RESULTS AND DISCUSSION

Generation and Characterization of Surface-Charge Variants. In a previous study, we explored the noncovalent interactions of a peptide with lipids of different electrostatic and hydrophobic properties to determine whether observations in the gas phase reflect interactions that are formed in solution.[12] In that study, we showed that electrostatic interactions formed between the lipid head groups and the peptide in solution are stabilized in the gas phase. However, these experiments only addressed the effects of different lipid

https://doi.org/10.1021/acs.analchem.5c00283
Anal. Chem. XXXX, XXX, XXX−XXX

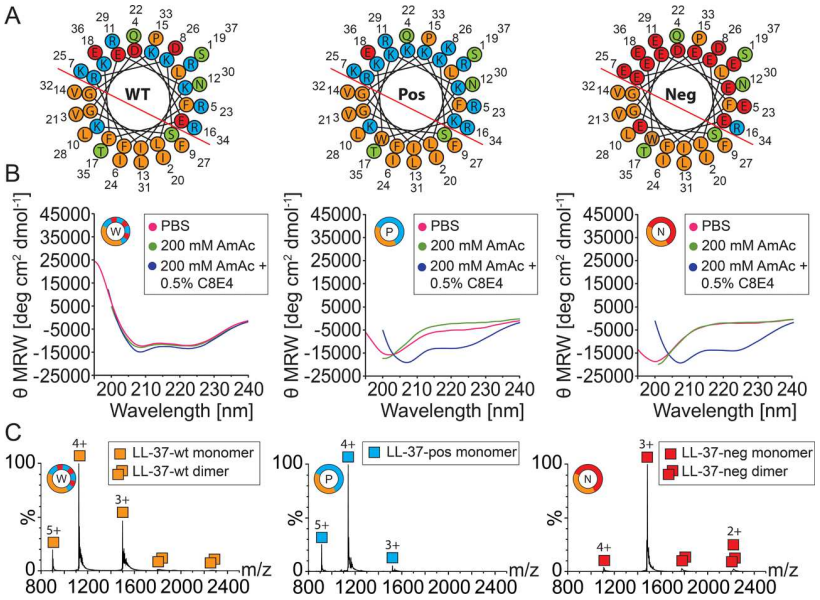

Figure 1. Characterization of LL-37 variants. (A) Helical wheel projection of LL-37-wt (lhs), LL-37-pos (middle), and LL-37-neg (rhs) created with HeliQuest.[51] Hydrophobic (orange), basic (blue), acidic (red), and polar uncharged residues (green) are shown. The hydrophobic−hydrophilic interface is indicated (red line). (B) CD spectra of LL-37-wt (lhs), LL-37-pos (middle), and LL-37-neg (rhs) acquired in PBS (pink), 200 mM AmAc (green), and 200 mM AmAc, 0.5% (w/v) C8E4 (blue). (C) Native mass spectra of 10 μM LL-37-wt (lhs), LL-37-pos (middle), and LL-37-neg (rhs) in 200 mM AmAc. Charge states as well as monomeric (squares) and dimeric (two squares) species are assigned. For masses of determined species, see Table S2.

head groups and the question remains whether the surface charge of a peptide affects the formation of peptide−lipid complexes in solution and in the gas phase. We, therefore, set out to investigate the influence of the surface charge of peptides on peptide−lipid interactions formed in solution and observed in the gas phase.

For this, we designed a systematic study using antimicrobial peptide LL-37 as a model peptide. According to its function, LL-37 forms an amphipathic helix required for membrane integration during antimicrobial defense.[13,30,31] This mechanism involves interactions between the hydrophobic interface of the amphipathic helix and the fatty acyl chains of the phospholipids as well as electrostatic interactions between the hydrophilic interface of LL-37 and the lipid head groups. To study the effects of surface charge on these interactions, we designed a positively and negatively charged variant of LL-37 in addition to the wild-type peptide. Accordingly, aspartate and glutamate residues of LL-37 residing in the amphipathic helix were replaced by lysine residues (positively charged variant, LL-37-pos) or lysine and arginine residues of the LL-37 sequence were substituted with glutamate residues (negatively charged variant, LL-37-neg). By replacing a multitude of residues rather than individual amino acids, we generated supercharged variants of LL-37 that differed significantly in their solution net charge, allowing us to attribute observed effects to differences in surface charge of the peptides. Importantly, while the physiochemical properties of the three LL-37 variants (i.e., LL-37-wt, LL-37-pos, and LL-37-neg) differ significantly (Table S1), the amphipathic structure of LL-37 consisting of a hydrophobic and a hydrophilic interface is maintained as shown in the helical wheel projections (Figure 1A).

To investigate the influence of the modifications onto helix formation of the LL-37 variants, the secondary structure content of both LL-37-pos and LL-37-neg was assessed by CD spectroscopy and compared with the wild-type peptide (Figure 1B). To mimic the experimental conditions employed in native MS and in film balance experiments, we used PBS or 200 mM AmAc with and without 0.5% (w/v) C8E4. The CD spectrum of LL-37-wt was acquired in the presence of PBS and revealed local minima at 208 and 222 nm, which are characteristic for alpha helical structures.[32] In contrast, LL-37-pos and LL-37-neg showed a local minimum at 203 nm indicating that both variants are unstructured in PBS.[33] Similarly, in the presence of 200 mM AmAc, LL-37-wt adopts a helical conformation, while LL-37-pos and LL-37-neg are unfolded. Notably, when 0.5% (w/v) C8E4 was added to 200 mM AmAc, all LL-37 variants adopted an α helix indicating that the C8E4 detergent induces a transition of LL-37-pos and LL-37-neg from an unstructured to an α-helical conformation; accordingly, the helical content of LL-37-wt increased in the presence of C8E4. This is in agreement with previous findings showing that the formation of alpha helices in a hydrophobic environment has been described for many antimicrobial peptides.[34−37] Interestingly, the ionic strength of PBS or 200 mM AmAc is not sufficient to induce structure formation of LL-37-pos and LL-37-neg as proposed for LL-37-wt earlier.[13] Importantly, buffer conditions as employed during native MS induce the formation of an α helix, guaranteeing that observed effects are not an effect of structural differences between the variants. In addition, helix formation is a prerequisite for biological function of the peptides[13] and functional activity of the peptides is, therefore, anticipated.

Next, we assessed the ionization behavior of the three variants during native MS in positive ion mode, as commonly employed for proteins and peptides (Figure 1C). The acquired mass spectra showed three charge states for all variants. For LL-37-wt and LL-37-pos, charge states ranging from 3+ to 5+ corresponding to the monomeric peptide were observed. LL-37-neg showed a small shift toward lower charge states

https://doi.org/10.1021/acs.analchem.5c00283
Anal. Chem. XXXX, XXX, XXX−XXX

resulting in charge states from 2+ to 4+. In all cases, the monomeric peak distribution was predominant; LL-37-wt and LL-37-neg showed a minor distribution (<5%) of the dimeric peptide. Note that the charge states observed in these measurements do not correlate with the charges of the peptides in solution (Table S1); this phenomenon was previously discussed in detail.[38−40] As the ionization of peptides is best described by the charged residue model,[41] the number of acquired charges of peptides correlates with the Rayleigh charge of the ESI droplet and, therefore, the surface-accessible area of the peptides.[42−45] Accordingly, LL-37-wt and LL-37-pos contain more potential protonation sites (i.e., basic amino acid residues) than the number of charges observed by native MS,[46] and a similar charge state distribution was observed for the two variants. The small shift in the charge state distribution observed for LL-37-neg might be explained by the fact that a lack of protonation sites has only minor effects on the observed charge states[47,48] and, therefore, positive charges during ionization are less stabilized (resulting in a reduction of only one acquired charge). Accordingly, in positive ion mode, carboxyl groups do not contribute to the charges acquired during ESI as they are neutralized by proton transfer during the ionization process.[49,50] In addition, LL-37-neg might adopt a conformation different from that of LL-37-wt and LL-37-pos.

Effects of Surface Charge on Peptide−Lipid Interactions in the Gas Phase. To assess protein−lipid interactions in the gas phase, we carefully optimized the instrument settings, including cone and collisional voltages. Accordingly, due to adduct formation of C8E4, collisional voltages below 30 V were not applied. The same optimized settings were employed for native MS measurements of all three variants. In addition, as the position of the ESI emitter significantly affects the ionization of analytes,[52] the position of the ESI emitter was maintained in a similar position in relation to the cone in all measurements.

Before transferring lipids to the LL-37 variants, we first studied the effect of the C8E4 detergent on their ionization properties (Figure S2). For this, the three variants were mixed with C8E4 detergent micelles and subsequently analyzed by native MS. As reported previously,[53,54] charge reduction was observed in the presence of C8E4. Accordingly, for LL-37-wt and LL-37-neg, average charge states of 3.1+ (LL-37-wt) and 2.3+ (LL-37-neg) were observed in comparison to average charge states of 3.8+ (LL-37-wt) and 3.0+ (LL-37-neg) in the absence of C8E4 (Figures 1 and S2). On the contrary, this effect was not as obvious for LL-37-pos, which showed similar average charge state in the absence (4.2+) and presence (3.9+) of C8E4. Presumably, LL-37-pos stabilizes positive charges on the surface of the ESI droplet; due to its high gas phase basicity, charge reducing effects of C8E4 are minimized. This is in agreement with a recent study proposing that proteins with a higher gas phase basicity, i.e., proteins that contain more basic residues with high-affinity protonation sites, are more resistant to charge reduction.[47] Interestingly, in the presence of this charge-reducing detergent, the three variants reflect the expected distribution of charges with the most intense charge state observed for LL-37-pos and the lowest for LL-37-neg.

Next, we analyzed the interactions of the three LL-37 variants with three negatively charged phospholipids (PA 14:0/14:0, PG 14:0/14:0, and PS 14:0/14:0) and two zwitterionic phospholipids (PC 14:0/14:0 and PE 14:0/14:0) as well as one positively charged, non-natural lipid analogue (TAP 14:0/14:0) by native MS (see Figure S1 for an overview of the lipid structures). For transfer of lipids to the peptides, detergent−lipid micelles were prepared (see Section Experimental Methods), mixed with the LL-37 variants and subsequently subjected to ESI and native MS. Note that detergent−lipid micelles including TAP showed a typical hydrodynamic diameter of approximately 6 nm comparable with C8E4 micelles (Figure S3). The acquired mass spectra revealed interactions of all LL-37 variants with the three negatively charged phospholipids (Figure S4); charge state distributions corresponding in mass to the LL-37 variant with up to three (LL-37-wt and LL-37-pos) or two (LL-37-neg) associated lipids were observed. The mass spectra acquired with the zwitterionic phospholipids and the cationic lipid analogue (Figure S5) revealed the binding of up to two zwitterionic lipids to all variants. Interestingly, binding of TAP 14:0/14:0 was observed only to LL-37-neg, while LL-37-wt and LL-37-pos did not bind this lipid. In summary, the complexes formed between negatively charged lipids and LL-37-wt and LL-37-pos showed higher intensities and higher numbers of associated lipids (up to three) than those of the complexes formed with zwitterionic lipids (up to two). In contrast, intensities and numbers of associated lipids observed for peptide−lipid complexes including LL-37-neg were low for all lipids employed.

In order to determine lipid binding preferences of the three LL-37 variants, we determined and compared relative abundances of peptide−lipid complexes as described (Section Experimental Methods and Figure 2). The relative abundances

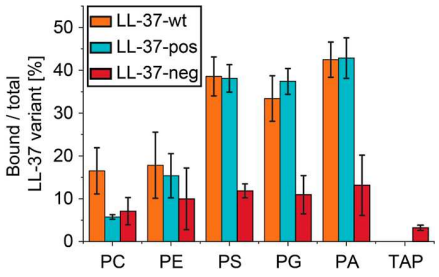

Figure 2. Interactions of LL-37 variants with different glycerophospholipids and TAP. Relative abundances of the complexes formed between LL-37-wt (orange), LL-37-pos (cyan), or LL-37-neg (red) and PC 14:0/14:0, PE 14:0/14:0, PS 14:0/14:0, PG 14:0/14:0, PA 14:0/14:0, and the lipid analogue TAP 14:0/14:0 were determined and compared. Error bars show the standard deviations between replicates (n = 4).

of detected peptide−lipid complexes for LL-37-wt and LL-37-pos were mostly comparable with the exception of peptide−lipid complexes containing PC 14:0/14:0, which showed higher abundances for LL-37-wt. In detail, complexes containing negatively charged phospholipids (i.e., PS 14:0/14:0, PG 14:0/14:0, and PA 14:0/14:0) showed relative intensities of up to 40%, while the intensities of complexes containing zwitterionic lipids (i.e., PC 14:0/14:0 and PE 14:0/14:0) were lower than 20%. Complexes containing the cationic lipid analogue TAP 14:0/14:0 were not detected. These results are in agreement with previous studies demonstrating the preference of LL-37-wt for negatively charged glycerophospholipids.[21,55−57] For LL-37-neg, relative abundances of peptide−lipid complexes were generally low (<15%). Despite its negative charge in solution, binding of the cationic TAP

https://doi.org/10.1021/acs.analchem.5c00283
Anal. Chem. XXXX, XXX, XXX−XXX

14:0/14:0 was less abundant. Notably, slightly higher intensities were determined for complexes containing negatively charged lipids when compared to zwitterionic lipids.

Nonetheless, we observed the following trend of lipid preferences for all LL-37 variants: negatively charged > zwitterionic > positively charged. Considering the different electrostatic properties of the LL-37 variants, these results were surprising. We, therefore, hypothesize that the observed peptide−lipid interactions are determined by the following factors: (i) The transfer of lipids from detergent−lipid micelles does not reflect conditions of a lipid bilayer such as chain packing, membrane curvature, or lipid−lipid interactions. In addition, the transfer efficiency of the lipids might also differ. (ii) Interactions with the accessible negative charge of the phosphate group in phospholipids likely enhance the binding to LL-37-wt and LL-37-pos. (iii) During native MS measurements, interactions with negatively charged lipids are likely stabilized in positive ion mode. Presumably, the ionization of cationic and zwitterionic lipids is more efficient and dissociation of these lipids is facilitated; accordingly, their ionization is best explained by the ion evaporation model. (iv) The neutralization of carboxyl groups by proton transfer during ESI in positive ion mode[49,50] results in a lack of negative charges that stabilize interactions with positively charged functional groups in the gas phase.

Exploring the Influence of Ionization Mode on Observed Peptide−Lipid Interactions. Hypothesizing that binding of negatively charged lipids is favored in positive ion mode, we next analyzed peptide−lipid interactions of the LL-37 variants in negative ion mode to uncover potential differences in the binding behavior. For this, we first optimized the MS conditions for measurements in negative ion mode. However, while the analysis of LL-37-neg revealed a narrow charge state distribution and a low degree of adduct formation, we were not able to analyze LL-37-wt and LL-37-pos in negative ion mode due to low ionization. We, therefore, only proceeded by fine-tuning instrument parameters for the analysis of LL-37-neg and its complexes.

Applying the optimized instrument parameters for negative ion mode, we analyzed LL-37-neg in 200 mM AmAc in the presence and absence of 0.5% (w/v) C8E4 as well as with three lipids, namely, zwitterionic PC 14:0/14:0, negatively charged PG 14:0/14:0, and the cationic TAP 14:0/14:0. Native mass spectra revealed a shift in the charge state distribution to higher charge states in the presence of C8E4 (Figure S5). Remarkably, despite similar cone and collision voltages, we did not observe unspecific fragmentation of LL-37-neg in negative ion mode, indicating stabilization of the peptide similar to membrane proteins as described before.[58] These measurements revealed binding of PC 14:0/14:0 and TAP 14:0/14:0 to LL-37-neg with a maximum of two associated lipids (Figure S6). Interestingly, the binding of PG 14:0/14:0 to LL-37-neg was not observed.

To compare binding of lipids to LL-37-neg in positive and negative ion modes, we determined the relative abundances of the peptide−lipid complexes for LL-37-neg with all of the tested lipids (Figure 3). In negative ion mode, we observed higher abundances for complexes containing PC 14:0/14:0 (approximately 12%) and TAP 14:0/14:0 (approximately 17%) compared to abundances observed in positive ion mode (approximately 7 and 3%, respectively). Importantly, binding of PG 14:0/14:0 was not detected in negative ion mode, while an abundance of LL-37-neg-PG complexes of

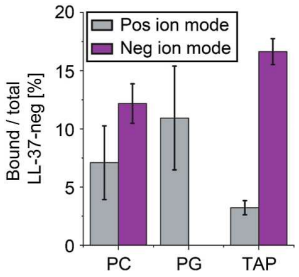

Figure 3. Interactions of LL-37-neg with lipids analyzed by native MS in negative ion mode. The relative abundance of LL-37-neg−lipid complexes containing PC 14:0/14:0, PG 14:0/14:0, or TAP 14:0/14:0 is given for positive (gray) and negative (purple) ion modes. Relative abundances were obtained from native mass spectra acquired in positive (Figures S3 and S4) and negative (Figure S5) ion modes. Error bars show the standard deviations between replicates (n = 3 for PC and PG negative ion mode; n = 4 for TAP in negative ion mode and PC, PG, and TAP in positive ion mode).

approximately 11% was obtained in positive ion mode. The differences observed in relative abundances of the LL-37-neg−lipid complexes indicate that the ion mode has major influences on the lipid preferences of LL-37-neg. Neutralization of negative charges during ESI in positive ion mode might reduce interactions with zwitterionic lipids and the positively charged lipid analogue in the gas phase. Accordingly, LL-37-neg-lipid complexes are not sufficiently stabilized and, therefore, not observed in the mass spectra. Furthermore, the ionization efficiency of the peptide and the lipids in the different ion modes might also influence the observed interactions (see above); however, it is challenging to determine the degree of unspecific association and dissociation in these measurements.

Investigating the Surface Activity of LL-37 Variants. Having investigated the lipid preferences of the LL-37 variants in the gas phase by native MS, we aimed to investigate the interactions of the variants with lipids in solution. For this, we made use of a Langmuir film balance and studied the adsorption of the LL-37 variants to single component lipid monolayers in solution. Lipid monolayers mimic one leaflet of a phospholipid bilayer and, therefore, represent a suitable model system for analyzing peptide−membrane interactions including binding and insertion of the peptides. These interactions are observed as changes in the surface pressure of the lipid film, i.e., peptide insertion leads to an increase in surface pressure.[59,60]

Before exploring the interactions of the LL-37 variants with different lipid monolayers, we first studied their adsorption at the air−water interface (i.e., without lipid film) as a function of peptide concentration. For this, different peptide concentrations were directly injected into the subphase consisting of PBS buffer (see Figure 4A for the experimental setup) and the adsorption of the peptide to the air−water interface was determined by monitoring the increase in surface pressure (π) (Figure 4B). Adsorption of the peptide at the air−water interface proceeds until reaching a plateau of equilibrium surface pressure (π_{eq}). The increase in surface pressure ($\Delta\pi$) is determined for the individual LL-37 variants at varying concentrations from these plateaus (Figure S7). To determine the surface activity of the individual LL-37 variants, $\Delta\pi$ is plotted against the peptide concentration (Figure 4C). An increase in $\Delta\pi$ with increasing peptide concentration was

https://doi.org/10.1021/acs.analchem.5c00283
Anal. Chem. XXXX, XXX, XXX−XXX

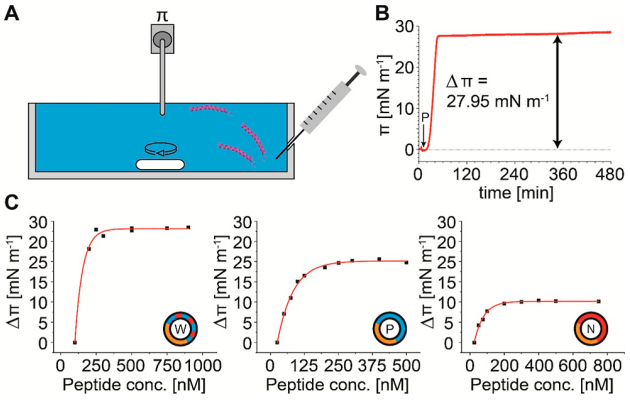

Figure 4. Surface activity of the three LL-37 variants. (A) Schematic of the experimental setup. Peptides were directly injected into the subphase (PBS). The increase in surface pressure resulting from the adsorption of peptides at the air−water interface is measured by a metal probe. (B) The surface pressure is plotted against time for the adsorption of 250 nM of LL-37-wt as an example. The time point of peptide injection (P) and the increase in surface pressure ($\Delta\pi$) are indicated. (C) $\Delta\pi$ was plotted against the peptide concentration of LL-37-wt (lhs), LL-37-pos (middle), and LL-37-neg (rhs).

observed for all of the LL-37 variants. At peptide concentrations of approximately 350 nM (LL-37-wt) or 300 nM (LL-37-pos and LL-37-neg), $\Delta\pi$ reaches its maximum, indicating the subphase concentrations at which the air−water interface is saturated with adsorbed peptide. This pressure is related to the surface activity of the peptides. Following this approach, we determined surface saturation pressures of approximately 28 mN/m for LL-37-wt, 20 mN/m for LL-37-pos, and 10 mN/m for LL-37-neg, indicating that LL-37-wt has the highest and LL-37-neg the lowest surface activity. To test weather surface activity correlates with the hydrophobicity of peptides, the GRAVY score[61,62] of the peptides was calculated (Table S1). In contrast to the observed surface activities (LL-37-neg < LL-37-pos < LL-37-wt), the GRAVY, describing the hydrophobicity of the peptides, increases in the order LL-37-pos < LL-37-wt < LL-37-neg. Therefore, the surface activity is not only defined by the net hydrophobicity of the peptides but also influenced by other factors. For instance, a correct secondary structure formation is required for the peptides to obtain their amphipathic properties.[63] Accordingly, the secondary structure analysis of the LL-37 variants in PBS by CD spectroscopy (see above, Figure 1B) revealed that only LL-37-wt formed an α helix in PBS, while LL-37-pos and LL-37-neg were unfolded in solution. The lack of a secondary structure in the absence of a detergent might explain the low surface activities observed for LL-37-pos and LL-37-neg. Notably, many amphipathic peptides are known to fold only in a hydrophobic environment;[20,34−37] we, therefore, expect the LL-37 variants to adopt an α-helical conformation in the presence of lipid monolayers. Nonetheless, based on the described experiments, we selected a peptide concentration of 400 nM for exploring the interactions of the LL-37 variants with lipid monolayers. This assures that the subphase concentration does not limit the potential adsorption to the lipid monolayers, and the observed effects can be attributed to lipid−peptide interactions.

Interaction of LL-37 Variants with Lipid Monolayers. Having explored the surface activity of the three LL-37 variants, we proceeded to investigate their interactions with zwitterionic, negatively, and positively charged lipid monolayers. As the results obtained for native MS measurements were comparable between different zwitterionic or negatively charged lipids, we prepared three exemplary lipid monolayers using the negatively charged lipid PG 14:0/14:0, the zwitterionic lipid PC 14:0/14:0, and the cationic lipid analogue TAP 14:0/14:0. To study insertion of peptides, lipid monolayers were prepared at different surface pressures by spreading lipids dissolved in chloroform or chloroform/methanol mixtures at the air−water interface (Figure 5A).

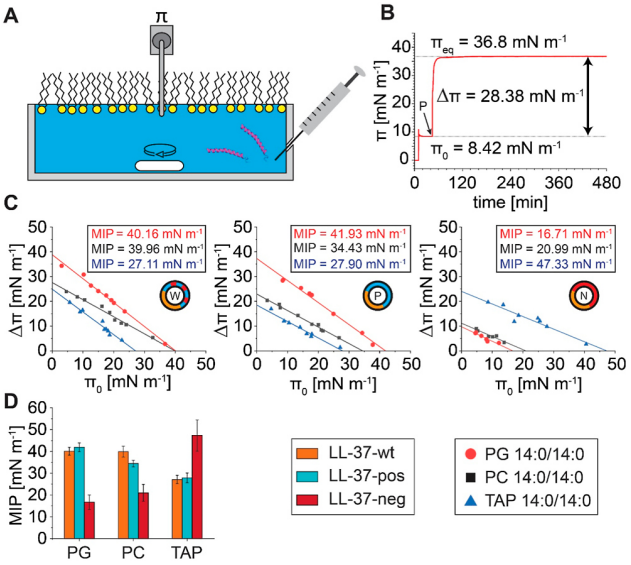

Figure 5. Exploring interactions of LL-37 variants with lipid monolayers. (A) Schematic of the experimental setup. Peptides were directly injected into a subphase (PBS) underneath the lipid monolayer. (B) The surface pressure was plotted against time for the insertion of 400 nM LL-37-pos into a PG 14:0/14:0 monolayer. The time point of peptide insertion (P), the initial surface pressure (π_0), the increase in surface pressure ($\Delta\pi$), and the equilibrium adsorption pressure (π_{eq}) are given. (C) $\Delta\pi$ was plotted against π_0 for the interaction of LL-37-wt (lhs), LL-37-pos (middle), and LL-37-neg (rhs) with PG 14:0/14:0 (red circles), PC 14:0/14:0 (black squares), and TAP 14:0/14:0 (blue triangles). Determined MIPs for the respective lipids are given in the insets. (D) The MIPs of LL-37-wt (orange), LL-37-pos (cyan), and LL-37-neg (red) for PG 14:0/14:0, PC 14:0/14:0, and TAP 14:0/14:0 monolayers are compared.

After injection of the peptide into the subphase underneath the lipid monolayer, we monitored the change in surface pressure caused by insertion of the peptides into the lipid monolayers. A peptide concentration of 400 nM (see above, Figure 4C) was selected for these experiments.

To characterize lipid preferences of the LL-37 variants in solution, the MIP was determined for different lipid monolayers. The MIP corresponds to the maximum surface pressure at which peptide insertion is energetically favorable.[29] Notably, a π = 30 mN/m is commonly defined as the bilayer−monolayer equivalence pressure, i.e., the pressure at which the structure of a lipid monolayer resembles that of one phospholipid bilayer leaflet.[64−67] Accordingly, if a MIP ≥ 30 mN/m is observed for a specific monolayer, the peptide inserts into a self-assembled bilayer of the same lipid. To determine the MIP values, we analyzed the change in surface pressure after peptide insertion ($\Delta\pi$) at various initial surface pressures (π_0) for the three different lipids in combination with each

https://doi.org/10.1021/acs.analchem.5c00283
Anal. Chem. XXXX, XXX, XXX−XXX

individual LL-37 variant (Figures 5B and S8). Next, we plotted $\Delta\pi$ as a function of π_0 for each peptide−lipid combination (Figure 5C). The MIPs were obtained by extrapolating the linear regressions to determine the intercept with the x axis (see Section Experimental Methods).

For each LL-37 variant, the MIP values were extracted (Figure 5C) and compared (Figure 5D). For LL-37-wt, we observed a similar extent of penetration into PG 14:0/14:0 and PC 14:0/14:0 monolayers with MIPs of approximately 40 mN/m. These findings are in agreement with previous reports demonstrating similar binding and penetration of LL-37 into zwitterionic and anionic lipid membranes.[31] In contrast, a lower MIP of approximately 27 mN/m was determined for the interaction with a TAP 14:0/14:0 monolayer, suggesting a preference for PG 14:0/14:0 and PC 14:0/14:0 over TAP 14:0/14:0. We postulate that these preferences are mainly defined by two factors: (i) Interactions with the negative charge of the phosphate group in PG 14:0/14:0 and PC 14:0/14:0 likely enhance the binding affinity of LL-37-wt. (ii) The position of the cationic functional group of TAP 14:0/14:0 relative to the hydrophilic binding interface of LL-37-wt is less favorable for the interactions. Accordingly, LL-37-wt was previously proposed to locate in the interfacial region between the lipid head groups and the hydrophobic core.[20] Therefore, the interactions between PG 14:0/14:0 and PC 14:0/14:0 are similar, while interactions with TAP 14:0/14:0 are affected by the charge repulsion of LL-37-wt. In a similar fashion, several Gram-positive bacteria contain cationic lipid lysyl-phosphatidylglycerol in their outer layer membranes enhancing resistance against antimicrobial peptides via charge repulsion.[68]

For LL-37-pos with PG 14:0/14:0 monolayers, a MIP of approximately 42 mN/m was obtained. In contrast, MIPs for the interaction of LL-37-pos with PC 14:0/14:0 and TAP 14:0/14:0 were lower (approximately 34 and 28 mN/m, respectively). These findings indicate a higher selectivity of LL-37-pos for negatively charged lipids, likely caused by attractive interactions with the negatively charged PG 14:0/14:0 headgroup on the one hand and an increased charge repulsion between the positively charged amino acids and the positively charged choline groups of PC 14:0/14:0 and TAP 14:0/14:0 on the other hand. Note that MIP values obtained for LL-37-pos with PG 14:0/14:0 and TAP 14:0/14:0 monolayers are comparable to MIPs determined for LL-37-wt, while interactions with PC 14:0/14:0 are less favored for LL-37-pos than for LL-37-wt. Again, the enhanced charge repulsion of LL-37-pos might be the reason for this observation.

For LL-37-neg, low MIPs of approximately 17 and 21 mN/m were determined for the interactions with PG and PC monolayers, respectively. However, interactions of LL-37-neg with a TAP 14:0/14:0 monolayer resulted in the highest MIP of approximately 47 mN/m, indicating that LL-37-neg prefers cationic lipids over zwitterionic and negatively charged lipids. Considering a similar insertion mode of LL-37-neg into a the lipid membrane as described for LL-37-wt,[20] interactions with negatively charged phosphate groups of PG 14:0/14:0 and PC 14:0/14:0 are less favored than with the positively charged functional group of TAP 14:0/14:0. Again, differences in the formation of the secondary structure might also affect the insertion of LL-37-neg and therefore the observed MIP values.

CONCLUSIONS

In this study, we employed three LL-37 variants with different electrostatic properties to systematically investigate the impact of the surface charge of peptides on their interactions with different lipids in the gas phase and in solution. For this, we analyzed peptide−lipid interactions, formed through the transfer of lipids from mixed detergent−lipid micelles, by native MS in positive and negative ion modes. Making use of a film balance, we compared these results to interactions of the different peptide variants with lipid monolayers composed of exemplary lipids that were also used during native MS.

Native MS in positive ion mode revealed a preference of LL-37-wt and LL-37-pos for negatively charged lipids. A lower affinity was determined for PC 14:0/14:0, while interactions with a cationic lipid analogue (i.e., TAP 14:0/14:0) were not detected. Interestingly, in positive ion mode, interactions of LL-37-neg with all lipids employed in this study were of low abundance when compared with LL-37-wt and LL-37-pos. In contrast, when using negative ion mode, LL-37-neg showed a higher affinity for the cationic lipid TAP 14:0/14:0, a comparably low affinity for the zwitterionic lipid PC 14:0/14:0 and no affinity for the negatively charged lipid PG 14:0/14:0. Adsorption measurements using a Langmuir film balance revealed similar binding preferences of LL-37-wt and LL-37-pos for PG 14:0/14:0 and PC 14:0/14:0 as well as low binding affinity for TAP 14:0/14:0. Similar to native MS, LL-37-neg showed a low binding affinity for PG 14:0/14:0 and PC 14:0/14:0 (as observed in positive ion mode) and a high binding affinity for TAP 14:0/14:0 (as observed in negative ion mode).

Comparing the lipid preferences of LL-37-wt and LL-37-pos determined by native MS and by Langmuir film balance, the overall trend observed by both methods is similar, with the only exception that interactions of LL-37-wt with PC 14:0/14:0 were higher with a Langmuir film balance. For LL-37-neg, only lipid preferences determined in negative ion mode correlate with the preferences determined in solution, indicating that the positive ion mode is not suited for the analysis of interactions between peptides with negative solution charge and their ligands. Note that the interactions of LL-37-neg with PG 14:0/14:0 might also be underestimated because the ionization of PG 14:0/14:0 is more efficient in negative ion mode. In agreement, interactions with PG 14:0/14:0 and PC 14:0/14:0 monolayers resulted in low MIPs around 20 mN/m, while interactions with TAP 14:0/14:0 resulted in a high MIP (47 mN/m).

Our findings are in agreement with previous studies showing that LL-37 is sensitive to the composition of the target membranes. For instance, a bacterial defense mechanism against LL-37 includes the expression of untypical phosphorylcholine modulating LL-37−membrane interactions and decreasing the antimicrobial activity of the peptide.[69] Furthermore, aggregation of LL-37 is higher in zwitterionic PC membranes when compared with negatively charged PC/PS membranes.[31] Accordingly, both studies confirm that the preferred natural membrane environment of LL-37 includes negatively charged phospholipids.

From a technical point of view, although relative abundances of complexes identified in the gas phase by native MS and MIPs determined through adsorption at lipid monolayers using a Langmuir film balance cannot be directly compared, both approaches reveal potential differences in the electrostatic interactions of peptides and lipids. The relative complex abundances and MIP values correlate well for the interactions of cationic peptides LL-37-wt and LL-37-pos. Importantly, a correlation of gas phase and solution interactions was also observed for LL-37-neg, however, only when employing the

https://doi.org/10.1021/acs.analchem.5c00283
Anal. Chem. XXXX, XXX, XXX−XXX

negative ion mode. Interestingly, discrepancies were identified for interactions of the two variants LL-37-wt and LL-37-pos with the zwitterionic lipid PC 14:0/14:0. We assume that, in addition to potentially different binding interfaces between peptides and lipids in these two approaches, ionization effects might lead to an underestimation of complex formation containing cationic peptides and positively charged ligands in positive ion mode. Our findings underline the need for uncovering the mechanism of lipid transfer from detergent−lipid micelles; this procedure appears to be influenced by the ionization mechanism during native MS and potentially the binding interface between the peptide and the ligand. Nonetheless, we demonstrate the capability of native MS for determining the general binding preferences of peptides; however, the ion mode influences the observed interactions and should be selected with care. Accordingly, the positive ion mode is applicable for the analysis of cationic peptides, while the analysis of negatively charged peptides might require the negative ion mode.

In summary, our comparison reveals, for both approaches, strong effects of electrostatic interactions on peptide−lipid interactions. Accordingly, the highly charged peptide variants (i.e., LL-37-pos and LL-37-neg) show preferences for lipids with opposite charge, while the wild-type variant contains positively charged and negatively charged amino acid residues and, therefore, is more flexible in the formation of interactions with various (phospho-) lipids. The effects of the structural content as well as structure formation during membrane insertion remain to be elucidated in future experiments. Importantly, our study together with other previous and potential future studies further contributes to the general understanding of peptide−membrane interactions. These findings will therefore be of interest for different lines of research, for instance, in pharmaceutical applications designing artificial antimicrobial peptides.

■ ASSOCIATED CONTENT

Supporting Information

The Supporting Information is available free of charge at https://pubs.acs.org/doi/10.1021/acs.analchem.5c00283.

Figures of structures of lipids employed in this study, effects of C8E4 on the ionization properties of the LL-37 variants, DLS analysis of detergent−lipid micelles, exploration of electrostatic interactions between the LL-37 variants and negatively charged lipids, explorarion of interactions between the LL-37 variants and zwitterionic and positively charged lipids, exploration of interactions between LL-37-neg and lipids in negative ion mode, investigation of surface activity of the LL-37 variants by adsorption film balance, and interactions of the LL-37 variants with lipid monolayers studied by adsorption film balance and tables of properties of the used LL-37 variants and masses of LL-37 variants and peptide−lipid complexes determined by native MS (PDF)

■ AUTHOR INFORMATION

Corresponding Author

Carla Schmidt − *Department of Chemistry—Biochemistry, Biocenter II, Johannes Gutenberg University Mainz, 55128 Mainz, Germany;* orcid.org/0000-0001-9410-1424; Email: carla.schmidt@uni-mainz.de

Authors

Til Kundlacz − *Institute of Chemistry, Martin Luther University Halle-Wittenberg, 06120 Halle, Germany;* orcid.org/0000-0002-0526-2179

Christian Schwieger − *Institute of Chemistry, Martin Luther University Halle-Wittenberg, 06120 Halle, Germany;* orcid.org/0000-0001-8327-1233

Complete contact information is available at: https://pubs.acs.org/10.1021/acs.analchem.5c00283

Notes

The authors declare no competing financial interest.

■ ACKNOWLEDGMENTS

We thank Annette Meister and Dariush Hinderberger (Martin Luther University Halle-Wittenberg) for helpful discussions. We acknowledge funding from the German Research Foundation (DFG, project number 436494874, RTG 2670 “Beyond Amphiphilicity: Self-Organization of Soft Matter via Multiple Noncovalent Interactions”), the Federal Ministry for Education and Research (BMBF, 03Z22HN22 and 03Z22HI2), and the European Regional Development Funds (EFRE, ZS/2016/04/78115).

■ REFERENCES

(1) Bolla, J. R.; Agasid, M. T.; Mehmood, S.; Robinson, C. V. *Annu. Rev. Biochem.* **2019**, *88*, 85−111.
(2) Frick, M.; Schmidt, C. *Chem. Phys. Lipids* **2019**, *221*, 145−157.
(3) Gupta, K.; Donlan, J. A. C.; Hopper, J. T. S.; Uzdavinys, P.; Landreh, M.; Struwe, W. B.; Drew, D.; Baldwin, A. J.; Stansfeld, P. J.; Robinson, C. V. *Nature* **2017**, *541*, 421−424.
(4) Gupta, K.; Li, J.; Liko, I.; Gault, J.; Bechara, C.; Wu, D.; Hopper, J. T. S.; Giles, K.; Benesch, J. L. P.; Robinson, C. V. *Nat. Protoc.* **2018**, *13*, 1106−1120.
(5) Laganowsky, A.; Reading, E.; Allison, T. M.; Ulmschneider, M. B.; Degiacomi, M. T.; Baldwin, A. J.; Robinson, C. V. *Nature* **2014**, *510*, 172−175.
(6) Landreh, M.; Marty, M. T.; Gault, J.; Robinson, C. V. *Curr. Opin. Struct. Biol.* **2016**, *39*, 54−60.
(7) Loo, J. A. *Mass Spectrom. Rev.* **1997**, *16*, 1−23.
(8) Barth, M.; Schmidt, C. *J. Mass Spectrom.* **2020**, *55*, No. e4578.
(9) Robinson, C. V.; Chung, E. W.; Kragelund, B. B.; Knudsen, J.; Aplin, R. T.; Poulsen, F. M.; Dobson, C. M. *J. Am. Chem. Soc.* **1996**, *118*, 8646−8653.
(10) Reading, E.; Walton, T. A.; Liko, I.; Marty, M. T.; Laganowsky, A.; Rees, D. C.; Robinson, C. V. *Chem. Biol.* **2015**, *22*, 593−603.
(11) Landreh, M.; Costeira-Paulo, J.; Gault, J.; Marklund, E. G.; Robinson, C. V. *Anal. Chem.* **2017**, *89*, 7425−7430.
(12) Kundlacz, T.; Schmidt, C. *Anal. Chem.* **2023**, *95*, 17292−17299.
(13) Johansson, J.; Gudmundsson, G. H.; Rottenberg, M. E.; Berndt, K. D.; Agerberth, B. *J. Biol. Chem.* **1998**, *273*, 3718−3724.
(14) Brogden, K. A.; Ackermann, M.; McCray, P. B.; Tack, B. F. *Int. J. Antimicrob. Agents* **2003**, *22*, 465−478.
(15) Sohlenkamp, C.; Geiger, O. *FEMS Microbiol. Rev.* **2016**, *40*, 133−159.
(16) Möhwald, H. *Annu. Rev. Phys. Chem.* **1990**, *41*, 441−476.
(17) Brockman, H. *Curr. Opin. Struct. Biol.* **1999**, *9*, 438−443.
(18) Maget-Dana, R. *Biochim. Biophys. Acta* **1999**, *1462*, 109−140.
(19) Volinsky, R.; Kolusheva, S.; Berman, A.; Jelinek, R. *Biochim. Biophys. Acta* **2006**, *1758*, 1393−1407.
(20) Sood, R.; Domanov, Y.; Pietiäinen, M.; Kontinen, V. P.; Kinnunen, P. K. J. *Biochim. Biophys. Acta* **2008**, *1778*, 983−996.
(21) Neville, F.; Cahuzac, M.; Konovalov, O.; Ishitsuka, Y.; Lee, K. Y. C.; Kuzmenko, I.; Kale, G. M.; Gidalevitz, D. *Biophys. J.* **2006**, *90*, 1275−1287.

(22) Ernster, L.; Lindberg, O. *Methods Biochem. Anal.* **1956**, *3*, 1−22.
(23) Kelly, S. M.; Jess, T. J.; Price, N. C. *Biochim. Biophys. Acta* **2005**, *1751*, 119−139.
(24) Bradford, M. M. *Anal. Biochem.* **1976**, *72*, 248−254.
(25) Sobott, F.; Hernández, H.; McCammon, M. G.; Tito, M. A.; Robinson, C. V. *Anal. Chem.* **2002**, *74*, 1402−1407.
(26) Hernández, H.; Robinson, C. V. *Nat. Protoc.* **2007**, *2*, 715−726.
(27) Marty, M. T.; Baldwin, A. J.; Marklund, E. G.; Hochberg, G. K. A.; Benesch, J. L. P.; Robinson, C. V. *Anal. Chem.* **2015**, *87*, 4370−4376.
(28) Savitzky, A.; Golay, M. J. E. *Anal. Chem.* **1964**, *36*, 1627−1639.
(29) Calvez, P.; Bussières, S.; Eric, D.; Salesse, C. *Biochimie* **2009**, *91*, 718−733.
(30) Shai, Y. *Biochim. Biophys. Acta* **1999**, *1462*, 55−70.
(31) Oren, Z.; Lerman, J. C.; Gudmundsson, G. H.; Agerberth, B.; Shai, Y. *Biochem. J.* **1999**, *341* (3), 501−513.
(32) Greenfield, N. J. *Nat. Protoc.* **2006**, *1*, 2876−2890.
(33) Venyaminov, S.; Baikalov, I. A.; Shen, Z. M.; Wu, C. S.; Yang, J. T. *Anal. Biochem.* **1993**, *214*, 17−24.
(34) Dathe, M.; Wieprecht, T. *Biochim. Biophys. Acta* **1999**, *1462*, 71−87.
(35) Sato, H.; Feix, J. B. *Biochim. Biophys. Acta* **2006**, *1758*, 1245−1256.
(36) White, S. H.; Wimley, W. C. *Biochim. Biophys. Acta* **1998**, *1376*, 339−352.
(37) Ladokhin, A. S.; White, S. H. *J. Mol. Biol.* **1999**, *285*, 1363−1369.
(38) Konermann, L.; Ahadi, E.; Rodriguez, A. D.; Vahidi, S. *Anal. Chem.* **2013**, *85*, 2−9.
(39) Kelly, M. A.; Vestling, M. M.; Fenselau, C. C.; Smith, P. B. *Org. Mass Spectrom.* **1992**, *27*, 1143−1147.
(40) Wang, G.; Cole, R. B. *Org. Mass Spectrom.* **1994**, *29*, 419−427.
(41) Dole, M.; Mack, L. L.; Hines, R. L.; Mobley, R. C.; Ferguson, L. D.; Alice, M. B. *J. Chem. Phys.* **1968**, *49*, 2240−2249.
(42) Kebarle, P.; Verkerk, U. H. *Mass Spectrom. Rev.* **2009**, *28*, 898−917.
(43) Fernandez de la Mora, J. *Anal. Chim. Acta* **2000**, *406*, 93−104.
(44) McAllister, R. G.; Metwally, H.; Sun, Y.; Konermann, L. *J. Am. Chem. Soc.* **2015**, *137*, 12667−12676.
(45) Testa, L.; Brocca, S.; Grandori, R. *Anal. Chem.* **2011**, *83*, 6459−6463.
(46) Felitsyn, N.; Peschke, M.; Kebarle, P. *Int. J. Mass Spectrom.* **2002**, *219*, 39−62.
(47) Abramsson, M. L.; Sahin, C.; Hopper, J. T. S.; Branca, R. M. M.; Danielsson, J.; Xu, M.; Chandler, S. A.; Österlund, N.; Ilag, L. L.; Leppert, A.; Costeira-Paulo, J.; Lang, L.; Teilum, K.; Laganowsky, A.; Benesch, J. L. P.; Oliveberg, M.; Robinson, C. V.; Marklund, E. G.; Allison, T. M.; Winther, J. R.; Landreh, M. *JACS Au* **2021**, *1*, 2385−2393.
(48) Kaltashov, I. A.; Mohimen, A. *Anal. Chem.* **2005**, *77*, 5370−5379.
(49) Grandori, R. *J. Mass Spectrom.* **2003**, *38*, 11−15.
(50) Cole, R. B. *Electrospray ionization mass spectrometry: fundamentals, instrumentation, and applications*; Cole, R. B., Ed., Wiley-Interscience; 1997; p 577.
(51) Gautier, R.; Douguet, D.; Antonny, B.; Drin, G. *Bioinformatics* **2008**, *24*, 2101−2102.
(52) Benkestock, K.; Sundqvist, G.; Edlund, P.-O.; Roeraade, J. *J. Mass Spectrom.* **2004**, *39*, 1059−1067.
(53) Reading, E.; Liko, I.; Allison, T. M.; Benesch, J. L. P.; Laganowsky, A.; Robinson, C. V. *Angew. Chem., Int. Ed. Engl.* **2015**, *54*, 4577−4581.
(54) Kundlacz, T.; Bender, J.; Schmidt, C. *Int. J. Mass Spectrom.* **2021**, *468*, 116652.
(55) Ding, B.; Soblosky, L.; Nguyen, K.; Geng, J.; Yu, X.; Ramamoorthy, A.; Chen, Z. *Sci. Rep.* **2013**, *3*, 1854.
(56) Henzler Wildman, K. A.; Lee, D.-K.; Ramamoorthy, A. *Biochemistry* **2003**, *42*, 6545−6558.
(57) Zhang, X.; Oglęcka, K.; Sandgren, S.; Belting, M.; Esbjörner, E. K.; Nordén, B.; Gräslund, A. *Biochim. Biophys. Acta* **2010**, *1798*, 2201−2208.
(58) Liko, I.; Hopper, J. T. S.; Allison, T. M.; Benesch, J. L. P.; Robinson, C. V. *J. Am. Soc. Mass Spectrom.* **2016**, *27*, 1099−1104.
(59) Blume, A. *ChemTexts* **2018**, *4*, 3.
(60) Papahadjopoulos, D.; Moscarello, M.; Eylar, E. H.; Isac, T. *Biochim. Biophys. Acta* **1975**, *401*, 317−335.
(61) Kyte, J.; Doolittle, R. F. *J. Mol. Biol.* **1982**, *157*, 105−132.
(62) Gasteiger, E.; Hoogland, C.; Gattiker, A.; Duvaud, S. . 'e.; Wilkins, M. R.; Appel, R. D.; Bairoch, A. *The Proteomics Protocols Handbook*; Walker, J. M., Ed.; Humana Press: Totowa, NJ, 2005; pp 571−607.
(63) Arouri, A.; Kerth, A.; Dathe, M.; Blume, A. *Langmuir* **2011**, *27*, 2811−2818.
(64) Demel, R. A.; Geurts van Kessel, W. S.; Zwaal, R. F.; Roelofsen, B.; van Deenen, L. L. *Biochim. Biophys. Acta* **1975**, *406*, 97−107.
(65) Marsh, D. *Biochim. Biophys. Acta* **1996**, *1286*, 183−223.
(66) Seelig, A. *Biochim. Biophys. Acta* **1987**, *899*, 196−204.
(67) Blume, A.; Eibl, H. *Biochim. Biophys. Acta* **1979**, *558*, 13−21.
(68) Sohlenkamp, C.; Galindo-Lagunas, K. A.; Guan, Z.; Vinuesa, P.; Robinson, S.; Thomas-Oates, J.; Raetz, C. R. H.; Geiger, O. *Mol. Plant-Microbe Interact.* **2007**, *20*, 1421−1430.
(69) Lysenko, E. S.; Gould, J.; Bals, R.; Wilson, J. M.; Weiser, J. N. *Infect. Immun.* **2000**, *68*, 1664−1671.

https://doi.org/10.1021/acs.analchem.5c00283
Anal. Chem. XXXX, XXX, XXX−XXX

Ca^{2+}-dependent lipid preferences shape synaptotagmin-1 C2A and C2B dynamics: Insights from experiments and simulations.

Julian Bender*, Til Kundlacz*, Lucas S. P. Rudden, Melissa Frick, Julia Bieber, Matteo T. Degiacomi, Carla Schmidt

*contributed equally

Structure 2024, 32, 10, 1691-1704.e5

https://doi.org/10.1016/j.str.2024.07.017

In this publication, I performed all native MS experiments in the absence of Ca^{2+}, including sample preparation as well as data analysis. In addition, I conducted and evaluated protein-lipid-binding studies by lipid overlay assays. I contributed to the visualisation of the work, assisted in the writing and editing of the manuscript as well as in changes during the reviewing process. Furthermore, I performed additional experiments that were not included in the publication. J. Bender wrote the software script for the MD simulation together with L. S. P. Rudden. J. Bender planned and performed the MD simulations, wrote the original manuscript together with C. Schmidt, and was involved in the editing, visualization and reviewing process of the manuscript. L. S. P. Rudden and M. T. Degiacomi were involved in designing the methodology as well as the editing and reviewing process. M. Frick performed the liposome flotation assays. J. Bieber performed the native MS binding studies in the presence of Ca^{2+}, analysed the respective data and contributed during the reviewing process. C. Schmidt guided the research and supervised the project as well as the publication process.

Article

Structure

Ca^{2+}-dependent lipid preferences shape synaptotagmin-1 C2A and C2B dynamics: Insights from experiments and simulations

Graphical abstract

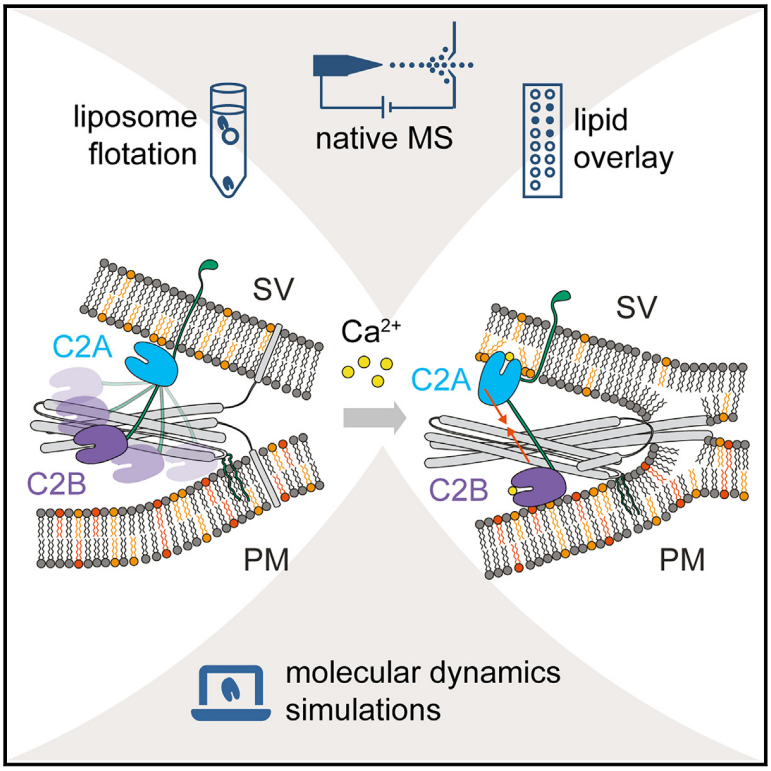

Authors

Julian Bender, Til Kundlacz, Lucas S.P. Rudden, Melissa Frick, Julia Bieber, Matteo T. Degiacomi, Carla Schmidt

Correspondence

carla.schmidt@uni-mainz.de

In brief

The role of the calcium sensor synaptotagmin-1 during membrane fusion is still controversially discussed. Bender et al. follow a multidisciplinary approach and characterize lipid and membrane binding of its isolated C2 domains in the absence and presence of Ca^{2+}. Similarities and differences between the two domains are described.

Highlights

- The C2A and C2B domains of synaptotagmin-1 interact with individual phospholipids
- Specific interactions of C2A and C2B with phospholipid membranes are Ca^{2+}-dependent
- C2A and C2B adopt a different orientation on phospholipid membranes
- A mechanism for synaptotagmin-1 during membrane fusion is proposed

Bender et al., 2024, Structure *32*, 1691–1704
October 3, 2024
https://doi.org/10.1016/j.str.2024.07.017

CellPress

Structure

CellPress
OPEN ACCESS

Article

Ca^{2+}-dependent lipid preferences shape synaptotagmin-1 C2A and C2B dynamics: Insights from experiments and simulations

Julian Bender,[1,5,7] Til Kundlacz,[1,2,7] Lucas S.P. Rudden,[3,6] Melissa Frick,[1] Julia Bieber,[4] Matteo T. Degiacomi,[3] and Carla Schmidt[1,4,8,*]

[1]Interdisciplinary Research Center HALOmem, Institute of Biochemistry and Biotechnology, Charles Tanford Protein Center, Martin Luther University Halle-Wittenberg, Kurt-Mothes-Straße 3a, 06120 Halle, Germany
[2]Institute of Chemistry, Martin Luther University Halle-Wittenberg, Von-Danckelmann-Platz 4, 06120 Halle, Germany
[3]Department of Physics, Durham University, South Road, Durham DH1 3LE, UK
[4]Department of Chemistry - Biochemistry, Johannes Gutenberg University Mainz, Hanns-Dieter-Hüsch-Weg 17, 55128 Mainz, Germany
[5]Present address: Chair of Biochemistry II, Theodor Boveri-Institute, University of Würzburg, Biocenter, Am Hubland, 97074 Würzburg, Germany
[6]Present address: Institute of Bioengineering, Swiss Federal Institute of Technology (EPFL), Lausanne 1015, Switzerland
[7]These authors contributed equally
[8]Lead contact
*Correspondence: carla.schmidt@uni-mainz.de
https://doi.org/10.1016/j.str.2024.07.017

SUMMARY

Signal transmission between neurons requires exocytosis of neurotransmitters from the lumen of synaptic vesicles into the synaptic cleft. Following an influx of Ca^{2+}, this process is facilitated by the Ca^{2+} sensor synaptotagmin-1. The underlying mechanisms involve electrostatic and hydrophobic interactions tuning the lipid preferences of the two C2 domains of synaptotagmin-1; however, the details are still controversially discussed. We, therefore, follow a multidisciplinary approach and characterize lipid and membrane binding of the isolated C2A and C2B domains. We first target interactions with individual lipid species, and then study interactions with model membranes of liposomes. Finally, we perform molecular dynamics simulations to unravel differences in membrane binding. We found that both C2 domains, as a response to Ca^{2+}, insert into the lipid membrane; however, C2A adopts a more perpendicular orientation while C2B remains parallel. These findings allow us to propose a mechanism for synaptotagmin-1 during membrane fusion.

INTRODUCTION

Signal transmission in neurons is accomplished by exocytosis of neurotransmitters from the lumen of synaptic vesicles into the synaptic cleft and subsequent binding of the neurotransmitters to neurotransmitter receptors at the postsynaptic membrane. To achieve this, a subset of synaptic vesicles docks at the presynaptic plasma membrane forming a pool of vesicles ready to fuse with the plasma membrane. Arrival of an action potential then causes influx of Ca^{2+} into the cytoplasm triggering membrane fusion.[1,2]

Docking of the vesicles and fusion of the vesicle and plasma membranes requires formation of the SNARE (i.e., soluble N-ethylmaleimide-sensitive-factor attachment receptor) complex, the neuronal membrane fusion machinery.[3] The SNARE complex assembles from three SNARE proteins, namely synaptobrevin-2, SNAP25, and syntaxin-1A, by formation of a tight four-helix bundle.[4–6] Zippering of the helices proceeds from their N-termini toward their C-termini through interactions of their SNARE motifs.[7,8] As a result, the two lipid bilayers are pulled together resulting in fusion of the membranes. Formation of the SNARE complex and fusion of the membranes is regulated by various proteins including, for instance, the complexins[9,10] or synaptotagmin-1, the primary Ca^{2+} sensor of synaptic vesicles.[11]

Synaptotagmin-1 contains a short luminal domain, an α-helical transmembrane anchor, as well as two cytosolic C2 domains (i.e., C2A and C2B) connected through flexible linkers.[12,13] The C2A and C2B domains form β-sandwich structures accommodating aspartate-containing Ca^{2+} binding loops that coordinate three (C2A) and two (C2B) Ca^{2+} ions.[14–17] C2B contains an additional polybasic region close to the Ca^{2+} binding loops.[14] Ca^{2+} binding alters the electrostatic surface potential of synaptotagmin-1 resulting in membrane binding of the C2 domains through the head groups of anionic phospholipids.[18,19] Ca^{2+}-dependent interactions with the membrane are further mediated by penetration of the C2 domains into the hydrophobic core of the lipid membrane[20,21] as well as electrostatic interactions of the polybasic stretch and two arginine residues with multivalent phosphoinositides.[22–24] Likewise, an increase in membrane affinity upon Ca^{2+} binding was reported.[25–27]

Recently, the membrane binding characteristics of the C2A and C2B domains were described as follows: C2A does not bind membranes containing phosphatidylserine (PS) or phosphatidylinositide in the absence of Ca^{2+}. In the presence of Ca^{2+}, C2A preferably binds PS-containing membranes. C2B, on the other hand, preferentially binds to and inserts into membranes containing phosphatidylinositol 4,5 bisphosphate ($PI(4,5)P_2$).[28] Therefore, a "bridging" mechanism of synaptotagmin-1 implying a preference of C2A for the *cis* membrane, i.e., the membrane it is anchored to, and of C2B for the target *trans* membrane was reasoned.[28]

Even though the general function of synaptotagmin-1 is well understood, the exact working principle is still controversially discussed.[29] This includes, among other aspects, the lipid preferences of the two C2 domains that govern membrane binding. We, therefore, follow a multidisciplinary approach and study interactions of C2A and C2B with specific lipids and lipid membranes of defined composition in the absence and in the presence of Ca^{2+}. Specifically, we characterize binding of specific lipid classes by lipid overlay assays and native mass spectrometry and then explore association of the C2A and C2B domains to lipid bilayers in liposome flotation assays. We found that both C2 domains bind a variety of individual lipids; in solution, these interactions were enhanced in the presence of Ca^{2+}, while interactions that were captured in the gas phase occurred independently of Ca^{2+} binding. Importantly, the C2A and C2B domains require Ca^{2+} to associate with a phospholipid bilayer of specific composition. Finally, we make use of molecular dynamics simulations of C2A and C2B in the presence of model membranes resembling the vesicle and plasma membranes to gain detailed insight on the structural dynamics, lipid contacts, membrane penetration and contact angles of synaptotagmin-1. Our simulations unravel differences between the C2A and C2B domains in their membrane orientation and insertion depth, allowing us to provide a mechanistic model for membrane fusion facilitated by synaptotagmin-1.

RESULTS

C2A and C2B preferably bind negatively charged phospholipids

To study lipid and membrane binding of the individual C2 domains of synaptotagmin-1, we chose two variants including the sequences of the individual C2A and C2B domains, respectively, as well as parts of the N-terminal (C2A) and C-terminal (C2B) linkers (Figure 1A). Both proteins were purified through an affinity strategy using an N-terminal His-tag (see STAR Methods for details). Following purification, the His-tag was cleaved with thrombin as confirmed by gel electrophoresis showing a mass difference of approximately 1 kDa between the tagged and the untagged protein (Figure 1B). The molecular weight of the C2A and C2B domains was then confirmed by native mass spectrometry revealing charge state distributions corresponding in mass to 19.5 kDa (C2A) and 17.6 kDa (C2B), respectively (Figure 1B).

As lipid binding depends on the correct folding of the C2 domains, we analyzed their secondary structure by far-UV circular dichroism (CD) spectroscopy and compared experimentally observed with theoretically calculated CD spectra (STAR Methods). The spectra of C2A and C2B both showed a local minimum at 218 nm, which is characteristic for the anti-parallel β-sheet structure of the C2A and C2B domains (Figure 1C).

Having confirmed formation of secondary structure elements of the C2A and C2B domains comparable to existing high-resolution structures, we next explored their binding specificity for the head groups of specific lipid classes. For this, membrane lipid strips spotted with 100 pmol of different lipids were incubated with C2A and C2B in the absence or in the presence of Ca^{2+} and bound protein was detected using specific primary and secondary antibodies. To mimic native conditions, we either removed free Ca^{2+} ions by addition of 1 mM EGTA providing a Ca^{2+}-free environment similar to the pre-fusion state or we added 500 μM $CaCl_2$ representing a high Ca^{2+} concentration as observed during an action potential. Note that the intracellular Ca^{2+} concentration increases locally approximately thousand-fold during an action potential (reaching up to 300 μM[30]); we compensate for this by adding 500 μM in these *in vitro* experiments. In the absence of Ca^{2+}, C2A and C2B specifically bound phosphatidylinositol phosphate (PI(4)P), phosphatidic acid (PA) and, at very low intensities, sulfatides (Figure 2A). C2B further showed weak binding to PS and strong binding to cardiolipin. In the presence of Ca^{2+}, binding to PI(4)P significantly increased and binding to phosphatidylinositol bisphosphate ($PI(4,5)P_2$; C2A and C2B domains) and phosphatidylinositol trisphosphate ($PI(3,4,5)P_3$; only C2B domain) was observed in addition to the previously detected lipids (Figure 2A). These binding assays confirm that Ca^{2+} indeed affects the interactions of synaptotagmin-1 with phosphatidylinositol phosphates.

We then explored interactions of C2A and C2B with different lipids in solution following a strategy presented recently.[31] For this, mixed detergent-lipid micelles serve as vehicles of lipids in solution during electrospray ionization for native mass spectrometry, transferring lipids onto the protein surface upon contacts with the micelle in the electrospray droplet.[31] To achieve this, we incubated the C2A and C2B domains with mixed detergent-lipid micelles and subsequently analyzed the protein-lipid complexes that formed by native mass spectrometry (Figure 2B). We first explored lipid transfer of negatively charged dioleoyl (DO) phospholipids including DOPS, DOPI, DOPI(4)P, $DOPI(4,5)P_2$ and $DOPI(3,4,5)P_3$ (Figures 2B and S1). As expected, binding of all lipids was observed, and intensities of protein-lipid complexes increased at higher concentration of the lipids. Native mass spectra further reveal binding of up to three lipids per C2 domain. In agreement with the observed specificity for negatively charged lipids (see previous text), highest intensities were observed for $DOPI(3,4,5)P_3$ (Figure S1). In addition to negatively charged phospholipids, we also explored binding of zwitterionic DOPC. Again, binding of up to three lipid molecules was observed at high lipid concentration (Figure S1); we assume that electrostatic interactions between the positively charged choline head group and negatively charged Ca^{2+}-binding loops are stabilized in the gas-phase during native mass spectrometry experiments.[32] Importantly, increasing the collisional voltage in the collision cell of the mass spectrometer to only 30 V caused dissociation of DOPC, while $DOPI(4,5)P_2$ remained stably associated with C2B even at a collisional voltage of 60 V (Figure S2). Presumably, electrostatic interactions between the positively charged residues of the C2 domains and negatively charged $DOPI(4,5)P_2$ are stronger than

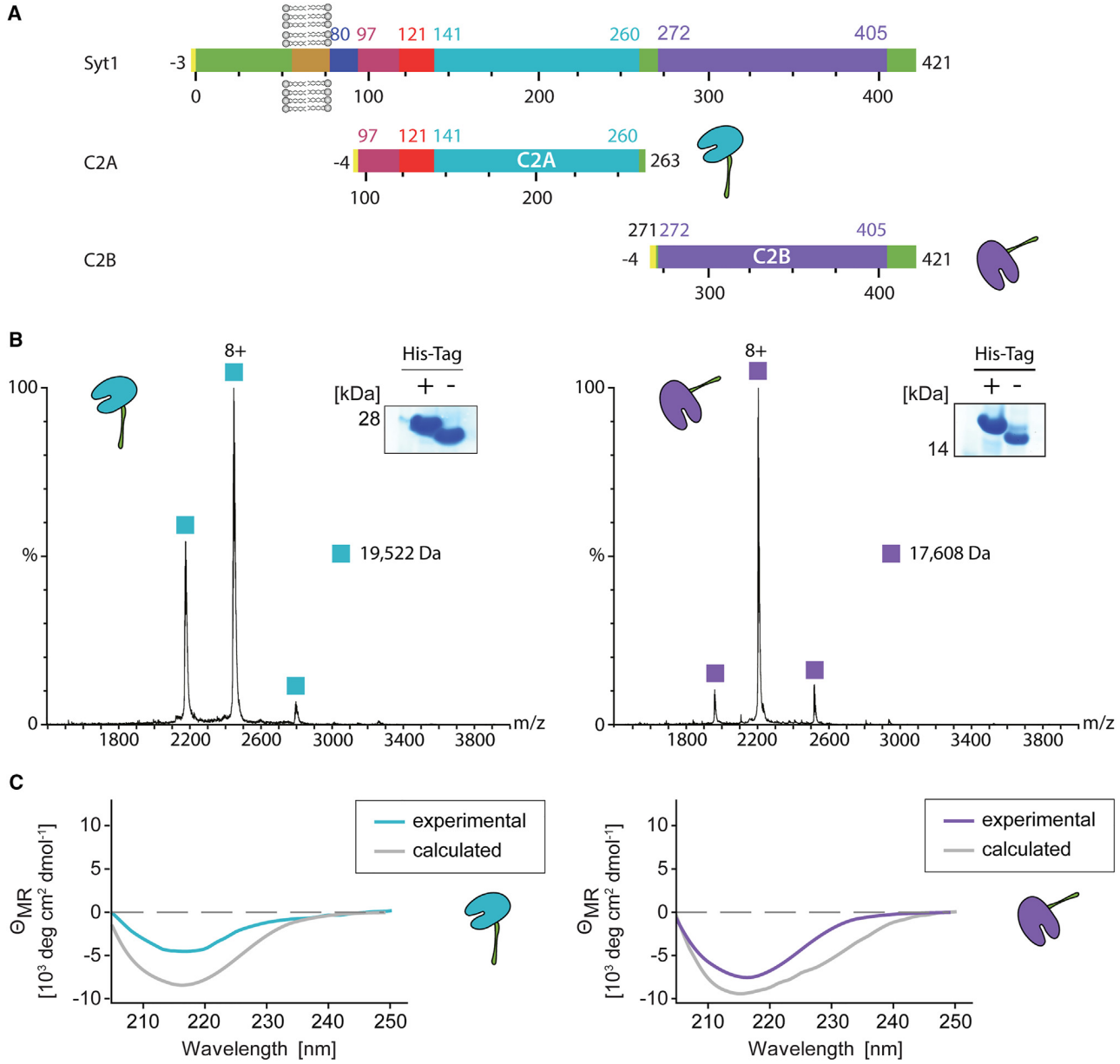

Figure 1. Purified C2A and C2B domains

(A) Schematic of full-length synaptotagmin-1 (Syt1) as well as the C2A (cyan) and C2B (purple) constructs used in this study.

(B) Native mass spectrometry of C2A (cyan) and C2B (purple). Successful cleavage of the His-tag was verified by gel electrophoresis (inserts).

(C) Far-UV CD spectroscopy of C2A (cyan) and C2B (purple) domains confirmed β-sheet formation of the purified proteins. Experimentally determined CD spectra (cyan, purple) are compared to calculated, theoretical spectra (gray).

those between the negatively charged Ca^{2+}-binding loops and zwitterionic DOPC.

As reported previously, synaptotagmin-1 binds phospholipids in the presence and in the absence of Ca^{2+}, and importantly, Ca^{2+} and phospholipid binding modulate the strength of these interactions cooperatively.[22–24] We, therefore, compared phospholipid binding to the C2A and C2B domains in the presence and in the absence of Ca^{2+}. For this, the proteins were pre-incubated with Ca^{2+} or EGTA (to mimic the Ca^{2+}-free state) and phospholipids were transferred to the domains as described (see previous text). The analysis of proteins by native mass spectrometry in the presence of high salt concentrations is not trivial, and instrument conditions were adjusted carefully (method details). First, Ca^{2+} binding was confirmed for the two domains in the absence of phospholipids. Indeed, as reported previously,[14–17] binding of three or two Ca^{2+} ions was observed for the C2A and C2B domains, respectively (Figure S3). We then compared lipid binding to the C2 domains in the presence of

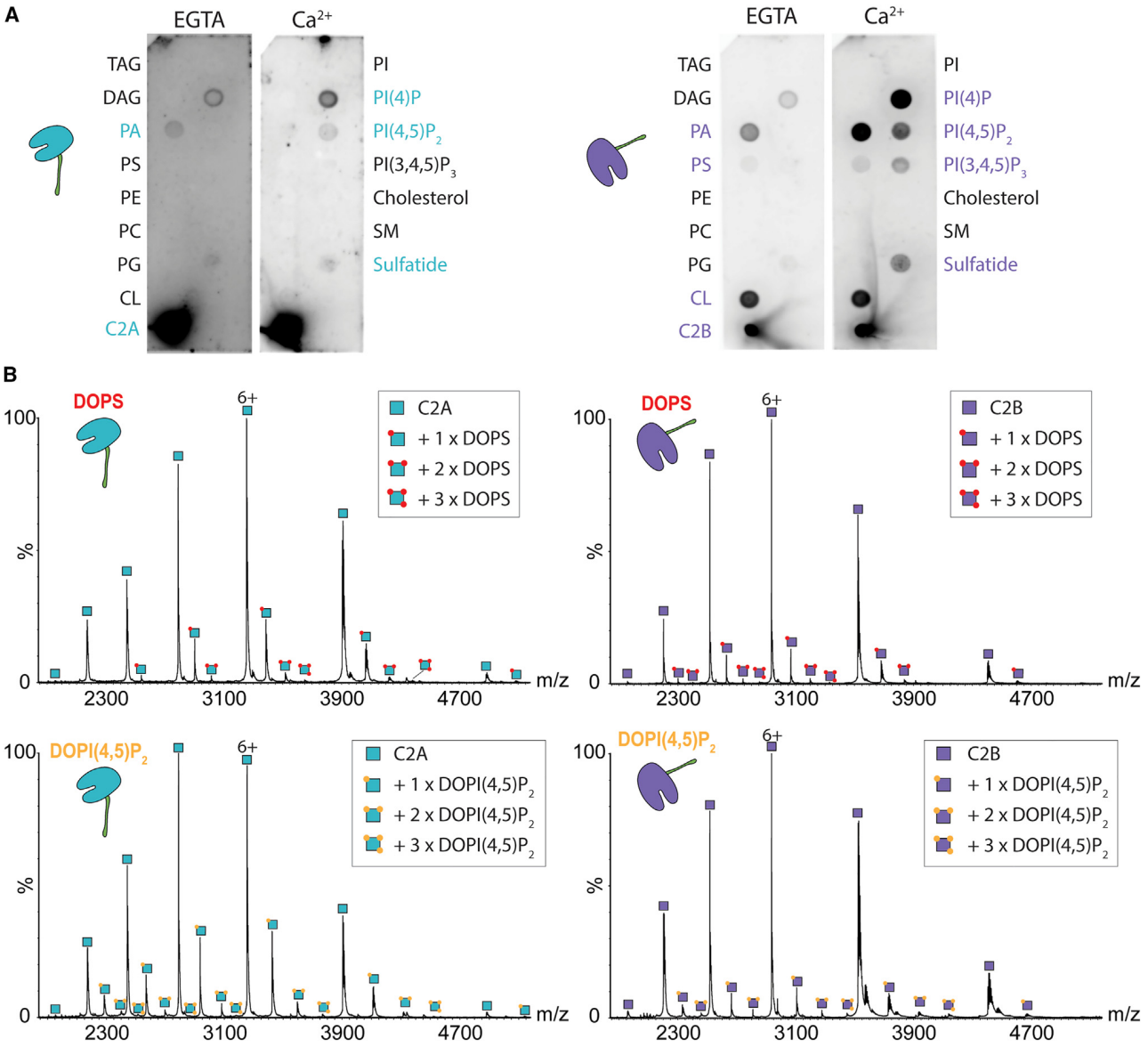

Figure 2. C2A and C2B domains bind negatively charged phospholipids

(A) Lipid overlay assays. Membrane lipid strips spotted with different membrane lipids were incubated with C2A (lhs, cyan) and C2B (rhs, purple). Protein binding was visualized using specific antibodies.

(B) Native mass spectrometry reveals binding of C2A (lhs, cyan) and C2B (rhs, purple) to up to three DOPS (red) and DOPI(4,5)P_2 (yellow) molecules.

See also Figures S1 and S2.

EGTA or Ca^{2+}. We specifically focused on two negatively charged phospholipids, namely DOPS and DOPI(4,5)P_2, as well as zwitterionic DOPC. Native mass spectra revealed lipid adducts for all phospholipids in the absence and in the presence of Ca^{2+} (Figure S4). As the analysis of the proteins in the presence of Ca^{2+} required higher collisional voltages (method details), lipid adducts partially dissociated resulting in loss of lipid adducts from higher charge states as well as lower intensities of the protein-lipid complexes in general. Nonetheless, interactions of C2A and C2B with all phospholipids were observed, independent on the presence of Ca^{2+} or EGTA. Interestingly, we again found lipid adducts of zwitterionic DOPC albeit at low intensity and only with low charge states. In addition, DOPC easily dissociates from the protein-lipid complexes (Figure S4A) confirming that interactions in the gas phase are weaker with DOPC than with negatively charged lipids. We reason that both C2 domains interact with mixed detergent-lipid micelles independently of Ca^{2+} binding, and that these interactions are captured during ionization when the proteins are transferred into the gas phase.

Ca^{2+} affects membrane binding of C2A and C2B

Having explored lipid binding to the C2 domains of synaptotagmin-1 in solution through contacts with detergent-lipid

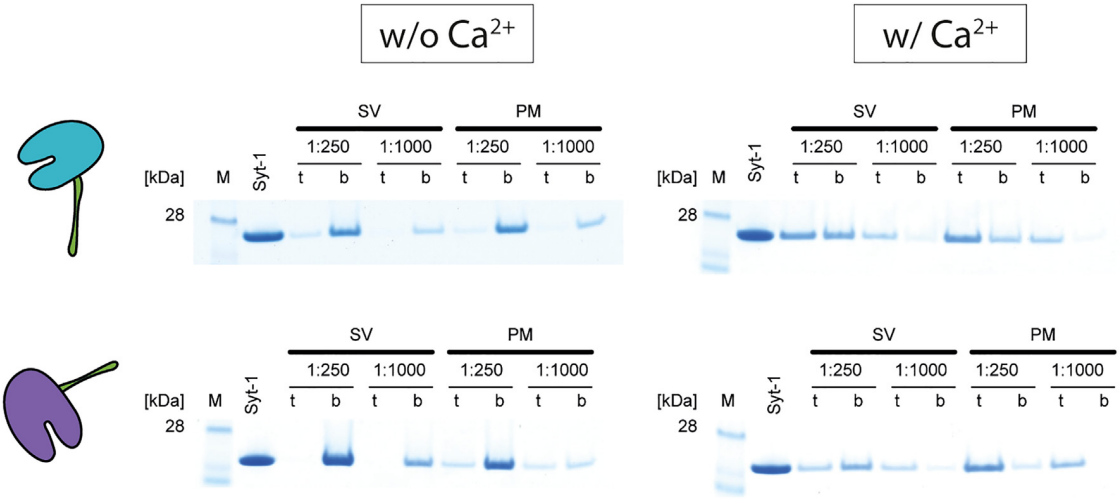

Figure 3. Binding of C2A and C2B to phospholipid bilayers is affected by Ca^{2+}

C2A (cyan) and C2B (purple) were incubated with liposomes resembling the synaptic vesicle membrane (SV) or the presynaptic plasma membrane (PM). Binding to the liposome membranes was then analyzed by liposome flotation on a sucrose gradient. Top (t) and bottom (b) fractions were collected, and protein binding was monitored by gel electrophoresis.

micelles and immobilized lipids, we next explored binding of C2A and C2B to phospholipid bilayers. For this, we made use of liposomes of different composition resembling the synaptic vesicle membrane and the presynaptic plasma membrane, respectively.[33] Accordingly, liposomes containing DOPC:DOPS:DOPE:cholesterol at a molar ratio of 38:12:20:20 (synaptic vesicle membrane) or DOPC:DOPS:DOPE:$PI(4,5)P_2$:DAG:cholesterol at a molar ratio of 38:12:20:2:2:20 (presynaptic plasma membrane; DAG, diacylglycerol) were prepared as described (see method details). The C2A and C2B domains were then incubated with the liposomes and, subsequently, overlaid with a sucrose gradient. After centrifugation, top and bottom fractions of the gradient were collected and analyzed by gel electrophoresis for their protein content. Proteins that associate with the liposome membrane will be identified in the top fractions together with the liposomes, which float on the sucrose gradient. Proteins that do not bind the liposome membrane ("free protein") will be identified in the bottom fractions.

We compared binding of the C2A and C2B domains to liposomes resembling the synaptic vesicle and the presynaptic plasma membranes in the absence and in the presence of Ca^{2+} at two protein:lipid ratios (1:250 and 1:1,000). In the absence of Ca^{2+}, C2A and C2B were mostly identified in the bottom fractions and only a small proportion of both domains was observed in the top fractions when using liposomes that were composed of the presynaptic plasma membrane lipid mixture (Figure 3). However, when performing these experiments in the presence of Ca^{2+}, the majority of both proteins were identified in the top fractions, i.e., both domains associated with the liposome membranes in the presence of Ca^{2+}. These effects were most prevalent for the C2B domain, binding liposomes that resemble the presynaptic plasma membrane. In addition, binding of C2A to synaptic vesicle and plasma membrane liposomes as well as binding of C2B to synaptic vesicle liposomes was also observed, albeit at lower intensity. When comparing the two protein:lipid ratios, we did not observe major differences; however, the results were more distinct when using a higher protein:lipid ratio (i.e., 1:1,000).

In summary, we found that Ca^{2+} affects the binding of the C2A and C2B domains to phospholipid membranes. While both domains appear to associate in the presence of Ca^{2+} with the two membrane compositions employed here, C2B appears to be particularly selective to the presynaptic plasma membrane mimetic.

Molecular dynamics simulations assess structural flexibility of C2A and C2B

To advance our *in vitro* findings and develop a model elucidating the molecular details of C2 lipid-preferences, we simulated the interactions of C2A and C2B with model membranes corresponding to the synaptic vesicle and the plasma membrane in the presence and in the absence of Ca^{2+}. Briefly, we extracted the structures of Ca^{2+}-bound C2A and C2B from an available high-resolution structure of Synaptotagmin-1 C2AB (PDB: 5KJ7 [34]) and removed the Ca^{2+} ions to generate Ca^{2+}-free structures (see STAR Methods for details). The initial lipid membrane model was generated *in silico* using the CHARMM-GUI membrane-builder.[35] After relaxation of the proteins and the membrane models, we assembled protein-membrane models. For this, we placed each C2 model in three different initial orientations above the lipid membrane (Figure S5) to minimize influence by the starting orientation as reported previously.[36] Performing simulations of C2A and C2B with model membranes mimicking the synaptic vesicle and plasma membrane in the presence and absence of Ca^{2+}, and with three starting orientations, we composed a total of 24 arrangements. Each arrangement was then simulated for 1.5 μs (see STAR Methods for details).

Obtained trajectories confirm that the C2A and C2B domains retain a stable tertiary structure (average Cα root-mean-square deviation <2 Å for all simulations, Figures S6A and S6B). Moreover, inspecting the local flexibility of C2A and C2B, we identified a Ca^{2+}-dependent difference of root-mean-square fluctuation in

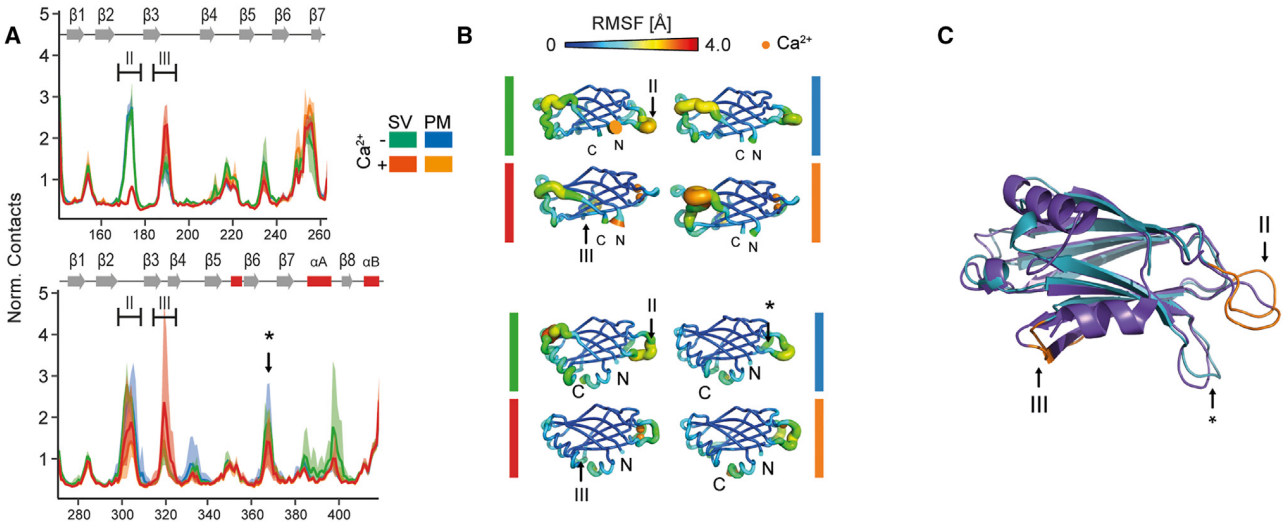

Figure 4. Studying the flexibility of the C2A and C2B domains

(A) Root-mean-square fluctuation (RMSF) of the C2A (top) and C2B (bottom) domains of simulations involving the synaptic vesicle membrane (SV, green, red) and the plasma membrane (PM, blue, orange) in the absence (green, blue) and in the presence (red, orange) of Ca^{2+}. Loop II (residues 169–176 in C2A and residues 300–308 in C2B) and loop III (residues 187–192 in C2A and residues 317–324 in C2B) as well as residues 365–370 in C2B (*) are highlighted. The secondary structure annotation is shown on top of each plot.

(B) RMSF mapped on the structures of the C2 domains of synaptotagmin-1 for selected examples. Higher diameters and warmer colors indicate higher RMSF (see legend).

(C) Structural alignment of the C2A and C2B domains. Regions of flexibility (i.e., loops II, III and * (C2B)) are indicated.

loops II and III of both, C2A and C2B (Figures 4A and 4B). Loop II (residues 169–176 in C2A and residues 300–308 in C2B) represents the calcium-binding region of the C2 domain and a reduced flexibility is in line with binding of Ca^{2+} to this loop. Loop III (residues 187–192 in C2A and residues 317–324 in C2B) showed an increase in root-mean-square fluctuation in the presence of Ca^{2+}; this loop is located on the opposite side of the domain suggesting that Ca^{2+} influences its dynamics indirectly (Figure 4C).

C2A and C2B specifically interact with negatively charged lipids in silico

Having described the structural flexibility of the C2 domains in the absence and presence of Ca^{2+}, we explored their specific interactions with lipids in the simulation. For this, we identified lipid molecules within 2.6 Å (i.e., the distance of a hydrogen bond) of each amino acid residue for each time frame of the simulation and counted the number of residue-lipid contacts throughout the simulation. To eliminate transient, unspecific interactions, we retained only protein-lipid interactions that were observed continuously for at least 10 ns. Contact counts were then normalized by the relative number of lipids in the model membrane excluding stochastic matches and by the total number of lipid contacts in a simulation accounting for varying contact times in different simulations.

Normalized lipid contacts confirm a lipid preference for negatively charged lipids as observed previously *in vitro* (Figure 5A, lhs). Notably, preferential binding was observed to $PI(4,5)P_2$, followed by contacts with PS. Intriguingly, close contacts with PE lipids were also identified, which were not anticipated based on our *in vitro* results. This difference may be attributed to interactions that form in a mixed model membrane, in contrast to the pure lipid compositions as used in native mass spectrometry or lipid overlay experiments, thereby allowing close contacts of the C2 domains with neighboring lipids. Our simulations did not reveal different lipid preferences of the C2A and C2B domains as observed during liposome flotation; however, these differences might originate from binding and unbinding events on a timescale inaccessible to the present simulation. To exploit the atomistic resolution of the simulations, we mapped the residues involved in lipid-contacts on the structural models of C2A and C2B. Binding of $PI(4,5)P_2$ and PS to C2A and C2B predominantly occurred through the calcium-binding loops and the polybasic region for both model membranes in the presence and in the absence of Ca^{2+} (Figure 5A, rhs; Figure 6).

C2A and C2B insert into model membranes

We next examined the insertion of C2A and C2B into the membrane, a phenomenon previously described.[37–39] For this, the closest distance between the C2 domains and the phosphorous atoms of the proximal membrane leaflet was calculated over the last 800 ns of the 1.5 μs simulation time (Figure 5B). Throughout this period, the distances between the C2 domains and the model membrane remained constant, suggesting that the considered time frame represents a (local) energy minimum. Distances >0 Å (see STAR Methods for details on computing the distance) indicate that the protein is located below the phosphate headgroups, i.e., integrates into the membrane, whereas distances <0 Å refer to proteins that do not insert. The histogram of these distances reveals that the insertion depth of C2A shifts from 2.8 to 4.4 Å when Ca^{2+} is included in the simulation, suggesting a tight insertion of C2A into the membrane when Ca^{2+} is present. Importantly, a significant difference in insertion depth of C2A

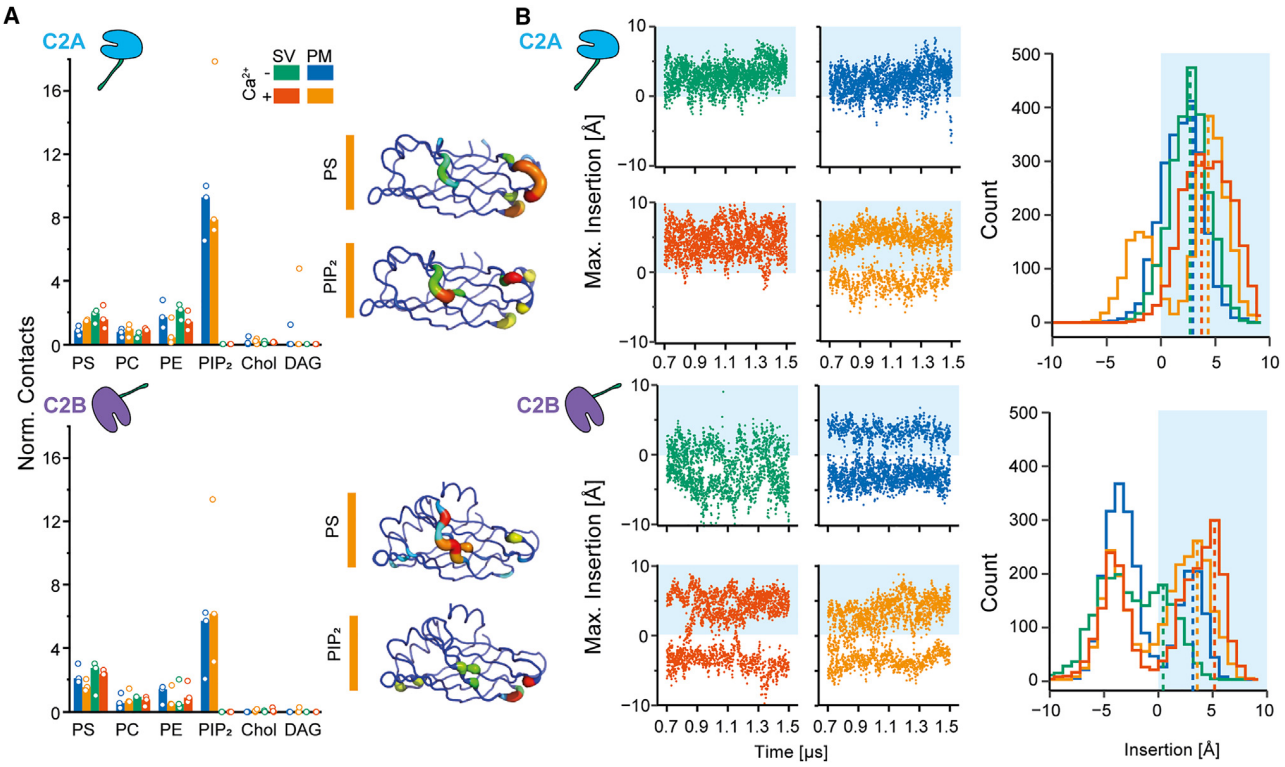

Figure 5. Lipid specificity and membrane insertion of C2A and C2B as identified by molecular dynamics simulations

(A) Normalized lipid contacts of C2A (top) and C2B (bottom) interacting with the synaptic vesicle membrane (SV, green and red) and plasma membrane (PM, blue and orange) in the absence (green and blue) and in the presence (red and orange) of Ca^{2+}. The bar plots (lhs) show the median normalized lipid contacts for C2A (top) and C2B (bottom). Data points indicate summed contacts for each starting condition. Interactions with PS and PIP_2 lipids were mapped on the structural models of C2A (top) and C2B (bottom) domains revealing their contact surfaces. Higher number of lipid contacts is indicated by warmer colors and a larger diameter of the protein backbone representation.

(B) Maximum insertion of the C2 domains during the last 800 ns of the molecular dynamics simulations involving the SV (green and red) and plasma (blue and orange) model membranes in the absence (green and blue) and in the presence (red and orange) of Ca^{2+} (lhs). The corresponding histograms of C2A (top) and C2B (bottom) are shown (rhs). The insertion depth with the highest count is indicated for each condition (dashed lines). The position of the lipid membrane is indicated (blue shaded area).

when interacting with the synaptic vesicle or plasma membrane was not observed. C2B, on the other hand, showed a bimodal distance distribution. Considering only simulation frames in which C2B inserted into the membrane, an increase in insertion depth, similar to C2A, was observed in the presence of Ca^{2+}. Considering the observed counts, a clear trend toward membrane insertion is observed upon Ca^{2+} binding; more precisely, the counts of the bimodal distribution were higher for distances <0 Å in the absence of Ca^{2+} (green and blue simulations in Figure 5B) and higher for distances >0 Å for simulations in the presence of Ca^{2+} (red and orange simulations in Figure 5B). Notably, the insertion depth of C2B into the plasma membrane, when compared with the insertion into the synaptic vesicle membrane, in the absence of Ca^{2+} was comparably high (approximately 3.2 Å) and a stable association with the plasma membrane even in the absence of Ca^{2+} might explain these differences.

Ca^{2+} binding modulates the orientation of C2A and C2B interacting with model membranes

Our analyses showed that the presence of Ca^{2+} leads to a slightly deeper insertion of the C2 domains into both the synaptic vesicle and plasma membranes. We, therefore, further investigated how Ca^{2+} influences the relative orientation of the C2 domains with respect to the membrane. To address this question, we calculated the angle between a vector along the main axis of the C2 domains (Figure 7A; see method details). To exclude the initial annealing phase, we only analyzed the last 800 ns of the simulation time.

This analysis revealed a distinct trend for C2A: in the presence of Ca^{2+}, simulations with either the synaptic vesicle or plasma membrane showed lower contact angles of approximately 45°, corresponding to a more perpendicular orientation on the membrane, while Ca^{2+}-free simulations exhibited average angles of 60°–70°. This finding was consistent across all simulations. Membrane interaction angles observed for C2B, on the other hand, were consistently higher for all membrane systems. A median value of approximately 90° indicates parallel orientation of the C2B main axis to the membrane. Furthermore, in contrast to C2A, distributions of interaction angles were observed for different initial orientations of C2B. For instance, C2B interacting with the plasma membrane in the absence of Ca^{2+} showed an average interaction angle of approximately 95° in simulations

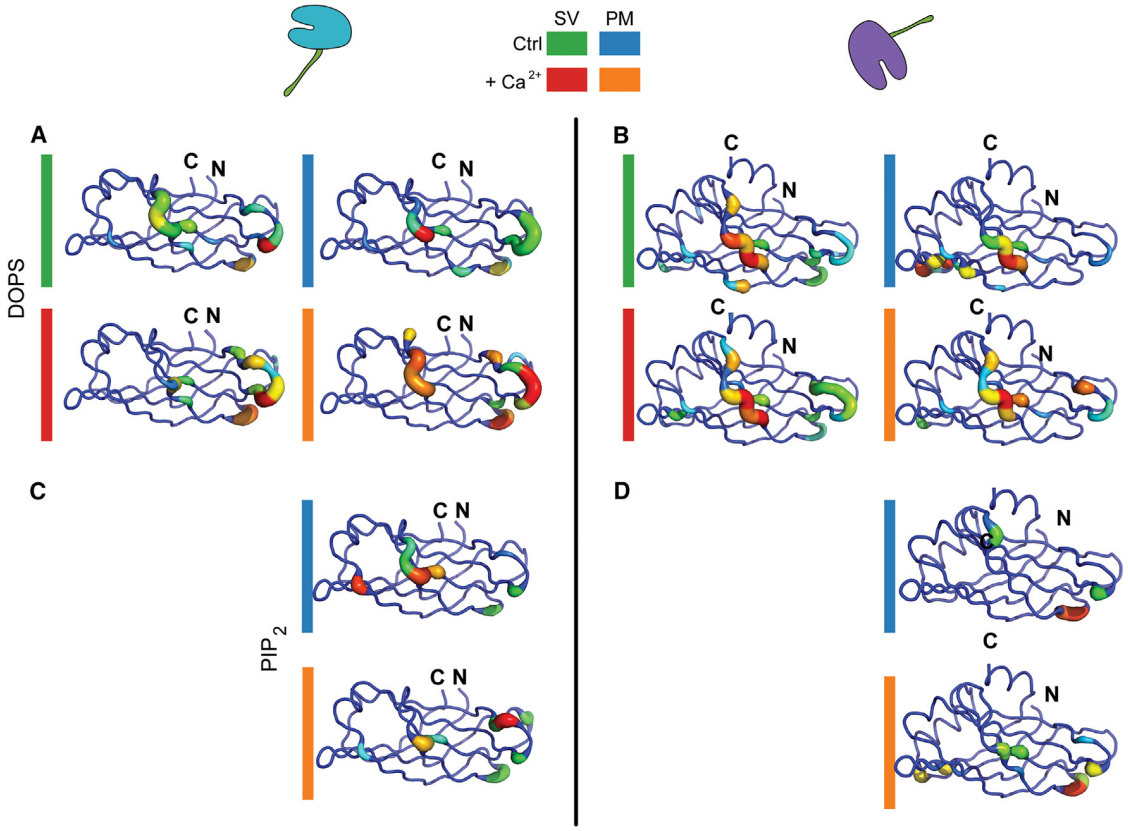

Figure 6. Residues involved in protein-lipid contacts of C2A (cyan, lhs) and C2B (purple, rhs)

The structures of C2A and C2B are shown. Lipid contacts observed in simulations including two model membranes mimicking the synaptic vesicle membrane (SV, green and red) or the plasma membrane (PM, blue and orange) in the absence of Ca^{2+} (Ctrl, green and blue) or in the presence of Ca^{2+} (red and orange). The sum of lipid contacts of three simulations starting with different initial orientations is shown as sausage representation. Warmer colors indicate a higher number of lipid contacts.

(A) Contacts of C2A with DOPS.

(B) Contacts of C2B with DOPS.

(C) Contacts of C2A with PIP_2. Note that PIP_2 is not present in the SV model membrane.

(D) Contacts of C2B with PIP_2. Note that PIP_2 is not present in the SV model membrane.

with 0° or 60° initial orientation, while simulations starting at a 30° angle showed an average final angle of approximately 75° suggesting that C2B interactions with the membrane are more dynamic and at least two membrane orientations, both characterized by higher contact angles than that of C2A, are adopted.

To further investigate the effect of Ca^{2+} binding to the C2 domains on the membrane plane, we analyzed the positions of the membrane phosphorus atoms after binding of C2A or C2B (Figure 7B). For this, we oriented the membrane on the *xy*-plane and centered the C2 domain on the membrane. We then calculated the difference between the *z*-coordinates of the lowest membrane phosphor atom and all other phosphor atoms (see STAR Methods for details). Low distances indicate a planar membrane system, while higher distances suggest local invagination of the membrane. Interestingly, in simulations of C2A, we observed an increase in distance around a central indentation for the proximal leaflet; this effect was pronounced in simulations including Ca^{2+}. Analyzing simulations of C2B revealed a less pronounced effect, even though the indentation for C2B was generally higher in the presence of Ca^{2+}. As a control, we analyzed the phosphorus atoms of the distal leaflet and detected a planar membrane in all simulations (Figure 7B). As expected, the C2 domains appear to affect only one of the two leaflets. These findings agree well with the perpendicular orientation of C2A on the two membrane systems in the presence of Ca^{2+}.

DISCUSSION

In this study, we characterized lipid and membrane binding of the C2A and C2B domains of synaptotagmin-1 in the presence and in the absence of Ca^{2+}. For this, we followed a multidisciplinary approach including lipid overlay assays, native mass spectrometry and liposome flotation assays as well as extensive molecular dynamics simulations. Lipid overlay assays and native mass spectrometry revealed a clear preference for negatively charged phospholipids; of particular interest are PIP_2s, which were previously described to drive Ca^{2+}-dependent interactions of synaptotagmin-1 with the vesicular and the plasma membranes.[28] Employing liposomes as model membranes for synaptic vesicles and the plasma membrane revealed preferences of

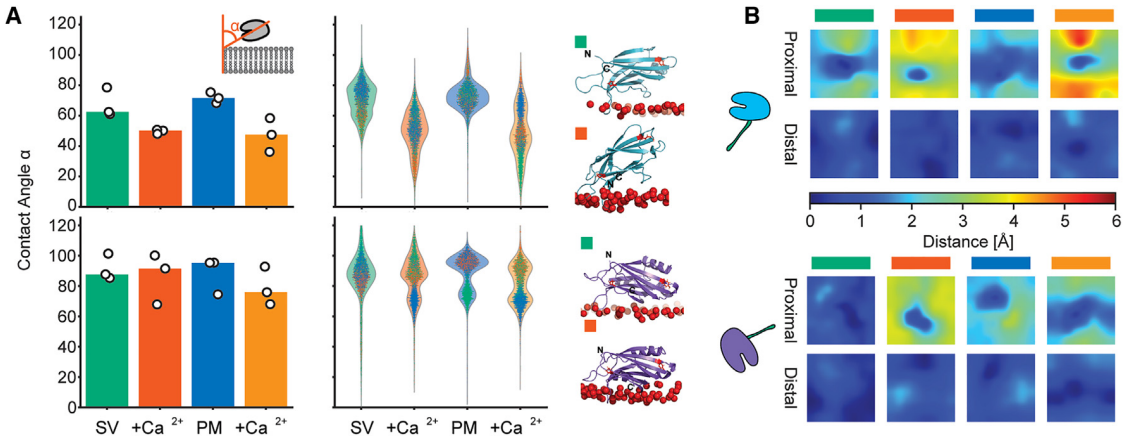

Figure 7. Orientation of C2A and C2B on the SV and plasma model membranes

(A) Median contact angles of C2A (top) and C2B (bottom) with the synaptic vesicle (red and green) and plasma (blue and orange) model membranes (lhs). Angles were averaged over the last 800 ns of the simulation (data points correspond to individual averages for the three initial starting orientations). Violin plots detailing the distributions of contact angles for 0° (violet), 30° (green) and 60° (blue) initial starting orientation (middle panel, data points correspond to individual frames of the simulations). Models representing the orientation of the C2 domains on the SV membrane in the absence (green) and in the presence (red) of Ca^{2+} are shown (rhs).

(B) z-positions of the phosphor atoms of the membrane lipid headgroups in the proximal and distal membrane leaflet of the SV (green and red) and plasma (blue and orange) model membranes when binding C2A (cyan, top) and C2B (purple, bottom) in the absence (green and blue) and in the presence (red and orange) of Ca^{2+}.

C2A and C2B for specific membrane compositions. As described previously, this preference was strongly affected by the presence or absence of Ca^{2+}.[39] Finally, molecular dynamics simulations provided detailed insight into the dynamics of the proteins, the protein-lipid contacts, membrane insertion and local changes in the membrane environment after membrane penetration. While both C2 domains showed very similar lipid contacts and membrane binding behavior during the simulations, differences were mostly observed in the orientation of the domains on the model membranes as well as the effects on the local membrane environment when intruding into the membrane.

Lipid binding to synaptotagmin-1 was assessed in many previous studies, mostly using the cytosolic C2AB construct. To deduce lipid and membrane contacts to the individual C2 domains, we preformed all experiments with isolated C2A and C2B domains. As reported previously, we observed a clear preference for negatively charged phospholipids for both, the C2A and C2B domains, in lipid overlay assays and by native mass spectrometry (Figures 2, 3, and S1). While previous studies mostly targeted PS and PIP_2s, we also observed binding of the C2 domains to additional negatively charged phospholipids such as sulfatides or cardiolipin in lipid overlay assays (Figure 2) or DOPI, DOPI(4)P or DOPI(3,4,5)P3 (Figure S1) in native mass spectrometry measurements. As most of these lipids are physiologically not relevant for synaptotagmin-1, we assume that the C2 domains electrostatically interact with negative charges. Accordingly, using native mass spectrometry, binding of $PI(3,4,5)P_3$ was most pronounced, presumably due to the high negative charges. Importantly, after addition of Ca^{2+}, the preference for negatively charged lipids, in particular for PI(4)P and $PI(4,5)P_2$s, increased in lipid overlay assays; this effect was pronounced for C2B.

Native mass spectrometry, on the other hand, revealed binding of C2A and C2B to all lipids employed here, including zwitterionic DOPC (Figures S1). This interaction was unexpected and might be the result of the experimental approach followed: as the C2A and C2B domains are soluble variants of synaptotagmin-1, we transferred lipids from mixed detergent-lipid micelles onto the proteins during ionization for mass spectrometry experiments.[31] Recently, we characterized protein-lipid interactions that form in solution and are stabilized in the gas-phase and found that protein-lipid interactions in the gas-phase are predominantly stabilized through electrostatic interactions[40]; we therefore assume that interactions with DOPC form through negatively charged residues, e.g., of the Ca^{2+} binding loops, in the presence and in the absence of Ca^{2+} and are, therefore, not relevant for stable protein-lipid contacts. Accordingly, the complexes that formed between the C2 domains and DOPC readily dissociated at low collisional energies in contrast to the complexes that formed with negatively charged phospholipids (Figures S2 and S4A).

Surprisingly, in contrast to a recent study,[41] pre-incubation of the C2 domains with Ca^{2+} or EGTA (to mimic a "real" Ca^{2+}-free state) did not affect the degree of phospholipid binding (Figure S4). Methodological limitations might be the reason for this discrepancy: (1) solvent molecules evaporate during electrospray ionization, and non-covalent interactions in the gas phase are stabilized through electrostatic interactions,[40] i.e., even transient interactions might be captured and stabilized; (2) unspecific interactions between proteins and detergent-lipid micelles might be induced due to shrinking of the electrospray droplet during the ionization process; and (3) instrument parameters had to be adjusted for the analysis in the presence of Ca^{2+} (or EGTA). These analyses required a high collisional voltage at which protein-lipid complexes (at least partially) dissociate; consequently, phospholipid binding is not quantitative under these conditions. The applicability of native mass spectrometry to study Ca^{2+}-dependent phospholipid binding remains to be evaluated in future studies.

Nonetheless, interactions of synaptotagmin-1 with phospholipids are mainly based on electrostatic interaction (e.g., studies by Striegel et al.,[18] Bai et al.,[25] and Brose et al.[42]) and, therefore, native mass spectrometry appears to be well-suited to assess the stability of phospholipid binding. Our findings are in accordance with the commonly accepted hypothesis that synaptotagmin-1 stably binds PS and PIPs/PIP_2s.

Using native mass spectrometry, we further observed binding of up to three lipid molecules per C2 domain (Figures 2 and S1). Assuming membrane binding through the Ca^{2+}-binding loops and the polybasic lysine patches, this binding stoichiometry agrees well with few lipid contacts per domain. In addition to the number of available contact sites on the protein surface, the number of lipid adducts increased with lipid concentration (Figure S1) suggesting a concentration-dependent association.

Having characterized binding of specific lipid molecules, we further assessed binding of the C2 domains to phospholipid bilayers of liposomes mimicking the synaptic vesicle or plasma membrane. While both, C2A and C2B, showed only minimal binding to the liposomes in the absence of Ca^{2+}, clear differences in the preferences for the lipid composition were observed when Ca^{2+} was added. Accordingly, C2A was not selective in the membrane composition, however, C2B showed enhanced binding to the PI(4,5)P_2-containing plasma membrane and only minimal interactions with the synaptic vesicle membrane (Figure 3). This observation agrees well with previous studies suggesting preferred binding of C2B to PI(4,5)P_2 through the polybasic lysine patch.[22,25,39,43–48] Importantly, a different Ca^{2+}-dependent lipid binding behavior was described for the C2A/C2B domains of Rab3A and synaptotagmin-1[48] suggesting that different C2 domains are fine-tuned for their environment (i.e., the lipid composition of the membranes) and for their function (slow versus fast Ca^{2+} sensors). Accordingly, Rab3A is a slow Ca^{2+} sensor (low Ca^{2+} affinity), located at the fusion site, which does not compete with synaptotagmin-1. The different lipid binding properties of the C2 domains are adjusted to their function, i.e., to their target membranes.[48] Our results further support a bridging model, in which C2A interacts with the synaptic vesicles membrane and C2B contacts the plasma membrane.[22,28] While the interface between C2B and the plasma membrane requires specific interactions, C2A is anchored to the vesicle membrane and, therefore, spatially oriented toward the vesicle membrane.

To gain detailed insight into these interactions, molecular dynamics simulations were widely used in the last two decades. However, a direct comparison of the results obtained from these studies is difficult as they differ, for instance, in lipid composition of the model membranes, protein variants (most studies used the C2AB fragment), additional binding partners such as SNARE proteins and, importantly, the simulation time.[37,49,50] In this work, we simulated isolated C2 domains with and without Ca^{2+} to characterize their binding to a complex membrane, designed to mimic the lipid composition employed in membrane fusion experiments.[33] To obtain robust statistics, we simulated each model system in 1.5 μs-long triplicates, initializing the C2 domains at different angles with respect to the membranes (Figure S5). Our resulting description of C2A and C2B interactions with the membrane agrees well with a recent study also including the isolated C2A and C2B domains.[37] Notably, our observation that the C2A domain is not selective in the membrane composition and rather responds to Ca^{2+} binding, while the C2B domain stably associates with the PI(4,5)P_2-containing plasma membrane even in the absence of Ca^{2+} (Figure 5) was previously described experimentally[24,44,45] confirming a good agreement between our simulations and experimental studies.

While the binding behavior of C2A and C2B was comparable in terms of lipid contacts, differences were observed in the orientation of the two domains on the membrane. As suggested previously,[37] C2B adopted a rather flat orientation allowing contacts with lipids through the Ca^{2+}-binding loops and the polybasic patch (Figure 7A). This orientation agrees well with a previous study reporting an orientation parallel to the membrane for C2 domains with type II topology.[51] Notably, a bimodal distribution was observed for the orientation of C2B suggesting a more transient association with the membrane. C2A, on the other hand, adopted a more upright orientation perpendicular to the membrane plane in the presence of Ca^{2+} (Figure 7A). In addition, this upright position induced deeper insertion into the membrane causing local rearrangements of the membrane in the direct neighborhood of the protein (Figure 7B). C2A, therefore, appears to adopt the typical orientation of type I C2 domains in the absence of Ca^{2+}, while the upright orientation in the presence of Ca^{2+} resembles the orientation of type II C2 domains.[51] The change in orientation in the presence of Ca^{2+} suggests a role during membrane fusion by stretching the linker connecting the C2A and C2B domains and, as a consequence, pulling the vesicular and the plasma membranes together. Considering that synaptotagmin-1 contains two C2 domains, while one C2 domain would be sufficient to bridge the two membranes, we propose that this structural change represents an additional regulatory element during membrane fusion.

Finally, our results allow us to propose a mechanistic model showing how membrane interactions of C2A and C2B contribute to membrane fusion (Figure 8). In this model, C2A is binding the synaptic vesicle membrane, while C2B, which is connected through a flexible linker, is moving toward the PI(4,5)P_2-containing plasma membrane. The flexible linker further allows membrane contacts prior to Ca^{2+} binding. Flexibility of C2B allows additional contacts with the SNARE complex as proposed previously.[52,53] Upon Ca^{2+} binding, the C2B domain stably associates with the plasma membrane and C2A adopts an upright orientation at the vesicle membrane. These binding effects cause tension at the connecting flexible linker, thereby pulling the two membranes together (Figure 8). All in all, our model agrees well with previously published models: It includes a bridging mechanism of full-length synaptotagmin-1,[22,28] it allows for contacts with the SNARE complex,[54,55] it involves contacts of C2B with the plasma membrane in the absence of Ca^{2+},[24,44,45] it requires both C2A and C2B domains for membrane fusion[56] and it allows regulation by additional factors such as complexin-1 that interact with the SNARE complex or synaptotagmin-1.[57–59]

STAR★METHODS

Detailed methods are provided in the online version of this paper and include the following:

- KEY RESOURCES TABLE
- RESOURCE AVAILABILITY

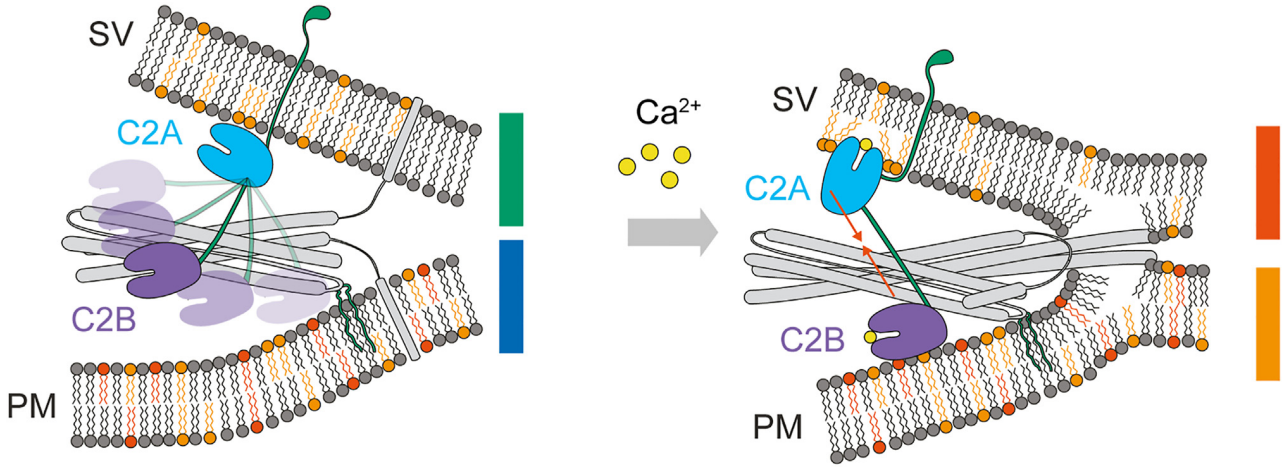

Figure 8. Model summarizing the effects of Ca^{2+} binding on the interactions between C2A and C2B with the membranes

In the absence of Ca^{2+}, C2A interacts with the synaptic vesicle (SV) membrane, while C2B is flexible making contacts with the SNARE complex as well as the plasma membrane (PM). Binding of Ca^{2+} then leads to a perpendicular orientation of C2A and partial penetration into the membrane leaflet, as well as enhanced interactions of C2B with the PM. These structural rearrangements of the C2 domains induce tension on the linker connecting C2A and C2B, thereby, pulling the SV membrane and the PM together.

SUPPLEMENTAL INFORMATION

Supplemental information can be found online at https://doi.org/10.1016/j.str.2024.07.017.

ACKNOWLEDGMENTS

We thank Reinhard Jahn (MPI for Multidisciplinary Sciences, Göttingen, Germany) for providing synaptotagmin-1 plasmids. We acknowledge funding from the Federal Ministry of Education and Research (BMBF, 03Z22HN22 and 03Z22HI2), the European Regional Development Funds (EFRE, ZS/2016/04/78115) and the German Research Foundation (DFG, project number 436494874, RTG 2670 "Beyond Amphiphilicity: Self-Organization of Soft Matter via Multiple Noncovalent Interactions" and project number 391498659, RTG 2467 "Intrinsically Disordered Proteins – Molecular Principles, Cellular Functions, and Diseases"). J. Bender acknowledges funding from the Studienstiftung des Deutschen Volkes. J. Bieber is a Joachim Herz Add-on Fellow. M.T.D. acknowledges funding from the Engineering and Physical Sciences Research Council (fellowship EP/P016499/1).

AUTHOR CONTRIBUTIONS

Conceptualization, J. Bender and C.S.; methodology, J. Bender, L.S.P.R., M.T.D., and C.S.; software, J. Bender and L.S.P.R.; investigation, J. Bender, T.K., M.F., J. Bieber; writing – original draft, J. Bender and C.S.; writing – review & editing, J. Bender, T.K., L.S.P.R., J. Bieber, M.T.D., and C.S.; visualization, J. Bender, T.K., and C.S.; supervision, M.T.D. and C.S.; funding acquisition, M.T.D. and C.S.

DECLARATION OF INTERESTS

The authors declare no competing interest.

Received: February 7, 2024
Revised: July 4, 2024
Accepted: July 28, 2024
Published: August 21, 2024

REFERENCES

1. Jahn, R., and Südhof, T.C. (1994). Synaptic vesicles and exocytosis. Annu. Rev. Neurosci. *17*, 219–246. https://doi.org/10.1146/annurev.ne.17.030194.001251.
2. Sudhof, T.C. (2004). The synaptic vesicle cycle. Annu. Rev. Neurosci. *27*, 509–547. https://doi.org/10.1146/annurev.neuro.26.041002.131412.
3. Sollner, T., Whiteheart, S.W., Brunner, M., Erdjument-Bromage, H., Geromanos, S., Tempst, P., and Rothman, J.E. (1993). SNAP receptors implicated in vesicle targeting and fusion. Nature *362*, 318–324. https://doi.org/10.1038/362318a0.
4. Fasshauer, D., Bruns, D., Shen, B., Jahn, R., and Brünger, A.T. (1997). A structural change occurs upon binding of syntaxin to SNAP-25. J. Biol. Chem. *272*, 4582–4590. https://doi.org/10.1074/jbc.272.7.4582.
5. Fasshauer, D., Otto, H., Eliason, W.K., Jahn, R., and Brünger, A.T. (1997). Structural changes are associated with soluble N-ethylmaleimide-sensitive fusion protein attachment protein receptor complex formation. J. Biol. Chem. *272*, 28036–28041. https://doi.org/10.1074/jbc.272.44.28036.
6. Sutton, R.B., Fasshauer, D., Jahn, R., and Brunger, A.T. (1998). Crystal structure of a SNARE complex involved in synaptic exocytosis at 2.4 A resolution. Nature *395*, 347–353. https://doi.org/10.1038/26412.
7. Gao, Y., Zorman, S., Gundersen, G., Xi, Z., Ma, L., Sirinakis, G., Rothman, J.E., and Zhang, Y. (2012). Single reconstituted neuronal SNARE complexes zipper in three distinct stages. Science *337*, 1340–1343. https://doi.org/10.1126/science.1224492.

8. Min, D., Kim, K., Hyeon, C., Cho, Y.H., Shin, Y.K., and Yoon, T.Y. (2013). Mechanical unzipping and rezipping of a single SNARE complex reveals hysteresis as a force-generating mechanism. Nat. Commun. *4*, 1705. https://doi.org/10.1038/ncomms2692.

9. McMahon, H.T., Missler, M., Li, C., and Südhof, T.C. (1995). Complexins: cytosolic proteins that regulate SNAP receptor function. Cell *83*, 111–119. https://doi.org/10.1016/0092-8674(95)90239-2.

10. Mohrmann, R., Dhara, M., and Bruns, D. (2015). Complexins: small but capable. Cell. Mol. Life Sci. *72*, 4221–4235. https://doi.org/10.1007/s00018-015-1998-8.

11. Xu, J., Mashimo, T., and Südhof, T.C. (2007). Synaptotagmin-1, -2, and -9: Ca(2+) sensors for fast release that specify distinct presynaptic properties in subsets of neurons. Neuron *54*, 567–581. https://doi.org/10.1016/j.neuron.2007.05.004.

12. Perin, M.S., Brose, N., Jahn, R., and Südhof, T.C. (1991). Domain structure of synaptotagmin (p65). J. Biol. Chem. *266*, 623–629.

13. Perin, M.S., Fried, V.A., Mignery, G.A., Jahn, R., and Südhof, T.C. (1990). Phospholipid binding by a synaptic vesicle protein homologous to the regulatory region of protein kinase C. Nature *345*, 260–263. https://doi.org/10.1038/345260a0.

14. Fernandez, I., Araç, D., Ubach, J., Gerber, S.H., Shin, O., Gao, Y., Anderson, R.G., Südhof, T.C., and Rizo, J. (2001). Three-dimensional structure of the synaptotagmin 1 C2B-domain: synaptotagmin 1 as a phospholipid binding machine. Neuron *32*, 1057–1069. https://doi.org/10.1016/s0896-6273(01)00548-7.

15. Shao, X., Fernandez, I., Südhof, T.C., and Rizo, J. (1998). Solution structures of the Ca2+-free and Ca2+-bound C2A domain of synaptotagmin I: does Ca2+ induce a conformational change? Biochemistry *37*, 16106–16115. https://doi.org/10.1021/bi981789h.

16. Sutton, R.B., Davletov, B.A., Berghuis, A.M., Südhof, T.C., and Sprang, S.R. (1995). Structure of the first C2 domain of synaptotagmin I: a novel Ca2+/phospholipid-binding fold. Cell *80*, 929–938. https://doi.org/10.1016/0092-8674(95)90296-1.

17. Ubach, J., Zhang, X., Shao, X., Südhof, T.C., and Rizo, J. (1998). Ca2+ binding to synaptotagmin: how many Ca2+ ions bind to the tip of a C2-domain? EMBO J. *17*, 3921–3930. https://doi.org/10.1093/emboj/17.14.3921.

18. Striegel, A.R., Biela, L.M., Evans, C.S., Wang, Z., Delehoy, J.B., Sutton, R.B., Chapman, E.R., and Reist, N.E. (2012). Calcium binding by synaptotagmin's C2A domain is an essential element of the electrostatic switch that triggers synchronous synaptic transmission. J. Neurosci. *32*, 1253–1260. https://doi.org/10.1523/JNEUROSCI.4652-11.2012.

19. Ali Moussa, H.Y., and Park, Y. (2022). Electrostatic regulation of the cis- and trans-membrane interactions of synaptotagmin-1. Sci. Rep. *12*, 22407. https://doi.org/10.1038/s41598-022-26723-9.

20. Chapman, E.R., and Davis, A.F. (1998). Direct interaction of a Ca2+-binding loop of synaptotagmin with lipid bilayers. J. Biol. Chem. *273*, 13995–14001. https://doi.org/10.1074/jbc.273.22.13995.

21. Zhang, X., Rizo, J., and Südhof, T.C. (1998). Mechanism of phospholipid binding by the C2A-domain of synaptotagmin I. Biochemistry *37*, 12395–12403. https://doi.org/10.1021/bi9807512.

22. Arac, D., Chen, X., Khant, H.A., Ubach, J., Ludtke, S.J., Kikkawa, M., Johnson, A.E., Chiu, W., Sudhof, T.C., and Rizo, J. (2006). Close membrane-membrane proximity induced by Ca(2+)-dependent multivalent binding of synaptotagmin-1 to phospholipids. Nat. Struct. Mol. Biol. *13*, 209–217. https://doi.org/10.1038/nsmb1056.

23. Radhakrishnan, A., Stein, A., Jahn, R., and Fasshauer, D. (2009). The Ca2+ affinity of synaptotagmin 1 is markedly increased by a specific interaction of its C2B domain with phosphatidylinositol 4,5-bisphosphate. J. Biol. Chem. *284*, 25749–25760. https://doi.org/10.1074/jbc.M109.042499.

24. van den Bogaart, G., Meyenberg, K., Diederichsen, U., and Jahn, R. (2012). Phosphatidylinositol 4,5-bisphosphate increases Ca2+ affinity of synaptotagmin-1 by 40-fold. J. Biol. Chem. *287*, 16447–16453. https://doi.org/10.1074/jbc.M112.343418.

25. Bai, J., Tucker, W.C., and Chapman, E.R. (2004). PIP2 increases the speed of response of synaptotagmin and steers its membrane-penetration activity toward the plasma membrane. Nat. Struct. Mol. Biol. *11*, 36–44. https://doi.org/10.1038/nsmb709.

26. Bhalla, A., Tucker, W.C., and Chapman, E.R. (2005). Synaptotagmin isoforms couple distinct ranges of Ca2+, Ba2+, and Sr2+ concentration to SNARE-mediated membrane fusion. Mol. Biol. Cell *16*, 4755–4764. https://doi.org/10.1091/mbc.e05-04-0277.

27. Bradberry, M.M., Bao, H., Lou, X., and Chapman, E.R. (2019). Phosphatidylinositol 4,5-bisphosphate drives Ca(2+)-independent membrane penetration by the tandem C2 domain proteins synaptotagmin-1 and Doc2beta. J. Biol. Chem. *294*, 10942–10953. https://doi.org/10.1074/jbc.RA119.007929.

28. Nyenhuis, S.B., Thapa, A., and Cafiso, D.S. (2019). Phosphatidylinositol 4,5 Bisphosphate Controls the cis and trans Interactions of Synaptotagmin 1. Biophys. J. *117*, 247–257. https://doi.org/10.1016/j.bpj.2019.06.016.

29. Park, Y., and Ryu, J.K. (2018). Models of synaptotagmin-1 to trigger Ca(2+)-dependent vesicle fusion. FEBS Lett. *592*, 3480–3492. https://doi.org/10.1002/1873-3468.13193.

30. Llinas, R., Sugimori, M., and Silver, R.B. (1992). Microdomains of high calcium concentration in a presynaptic terminal. Science *256*, 677–679. https://doi.org/10.1126/science.1350109.

31. Landreh, M., Costeira-Paulo, J., Gault, J., Marklund, E.G., and Robinson, C.V. (2017). Effects of Detergent Micelles on Lipid Binding to Proteins in Electrospray Ionization Mass Spectrometry. Anal. Chem. *89*, 7425–7430. https://doi.org/10.1021/acs.analchem.7b00922.

32. Steinberg, M.Z., Elber, R., McLafferty, F.W., Gerber, R.B., and Breuker, K. (2008). Early structural evolution of native cytochrome c after solvent removal. Chembiochem *9*, 2417–2423. https://doi.org/10.1002/cbic.200800167.

33. Liu, X., Seven, A.B., Xu, J., Esser, V., Su, L., Ma, C., and Rizo, J. (2017). Simultaneous lipid and content mixing assays for *in vitro* reconstitution studies of synaptic vesicle fusion. Nat. Protoc. *12*, 2014–2028. https://doi.org/10.1038/nprot.2017.068.

34. Lyubimov, A.Y., Uervirojnangkoorn, M., Zeldin, O.B., Zhou, Q., Zhao, M., Brewster, A.S., Michels-Clark, T., Holton, J.M., Sauter, N.K., Weis, W.I., and Brunger, A.T. (2016). Advances in X-ray free electron laser (XFEL) diffraction data processing applied to the crystal structure of the synaptotagmin-1/SNARE complex. Elife *5*, e18740. https://doi.org/10.7554/eLife.18740.

35. Wu, E.L., Cheng, X., Jo, S., Rui, H., Song, K.C., Dávila-Contreras, E.M., Qi, Y., Lee, J., Monje-Galvan, V., Venable, R.M., et al. (2014). CHARMM-GUI Membrane Builder toward realistic biological membrane simulations. J. Comput. Chem. *35*, 1997–2004. https://doi.org/10.1002/jcc.23702.

36. Chon, N.L., Osterberg, J.R., Henderson, J., Khan, H.M., Reuter, N., Knight, J.D., and Lin, H. (2015). Membrane Docking of the Synaptotagmin 7 C2A Domain: Computation Reveals Interplay between Electrostatic and Hydrophobic Contributions. Biochemistry *54*, 5696–5711. https://doi.org/10.1021/acs.biochem.5b00422.

37. Bykhovskaia, M. (2021). SNARE complex alters the interactions of the Ca(2+) sensor synaptotagmin 1 with lipid bilayers. Biophys. J. *120*, 642–661. https://doi.org/10.1016/j.bpj.2020.12.025.

38. Herrick, D.Z., Sterbling, S., Rasch, K.A., Hinderliter, A., and Cafiso, D.S. (2006). Position of synaptotagmin I at the membrane interface: cooperative interactions of tandem C2 domains. Biochemistry *45*, 9668–9674. https://doi.org/10.1021/bi060874j.

39. Perez-Lara, A., Thapa, A., Nyenhuis, S.B., Nyenhuis, D.A., Halder, P., Tietzel, M., Tittmann, K., Cafiso, D.S., and Jahn, R. (2016). PtdInsP2 and PtdSer cooperate to trap synaptotagmin-1 to the plasma membrane in the presence of calcium. Elife *5*, e15886. https://doi.org/10.7554/eLife.15886.

40. Kundlacz, T., and Schmidt, C. (2023). Deciphering Solution and Gas-Phase Interactions between Peptides and Lipids by Native Mass Spectrometry. Anal. Chem. *95*, 17292–17299. https://doi.org/10.1021/acs.analchem.3c03428.

41. Lawrence, S.A.S., Kirschbaum, C., Bennett, J.L., Lutomski, C.A., El-Baba, T.J., and Robinson, C.V. (2024). Phospholipids Differentially Regulate Ca(2+) Binding to Synaptotagmin-1. ACS Chem. Biol. *19*, 953–961. https://doi.org/10.1021/acschembio.3c00772.

42. Brose, N., Petrenko, A.G., Südhof, T.C., and Jahn, R. (1992). Synaptotagmin: a calcium sensor on the synaptic vesicle surface. Science *256*, 1021–1025. https://doi.org/10.1126/science.1589771.

43. Honigmann, A., van den Bogaart, G., Iraheta, E., Risselada, H.J., Milovanovic, D., Mueller, V., Müllar, S., Diederichsen, U., Fasshauer, D., Grubmüller, H., et al. (2013). Phosphatidylinositol 4,5-bisphosphate clusters act as molecular beacons for vesicle recruitment. Nat. Struct. Mol. Biol. *20*, 679–686. https://doi.org/10.1038/nsmb.2570.

44. Li, L., Shin, O.H., Rhee, J.S., Araç, D., Rah, J.C., Rizo, J., Südhof, T., and Rosenmund, C. (2006). Phosphatidylinositol phosphates as co-activators of Ca2+ binding to C2 domains of synaptotagmin 1. J. Biol. Chem. *281*, 15845–15852. https://doi.org/10.1074/jbc.M600888200.

45. Park, Y., Seo, J.B., Fraind, A., Pérez-Lara, A., Yavuz, H., Han, K., Jung, S.R., Kattan, I., Walla, P.J., Choi, M., et al. (2015). Synaptotagmin-1 binds to PIP(2)-containing membrane but not to SNAREs at physiological ionic strength. Nat. Struct. Mol. Biol. *22*, 815–823. https://doi.org/10.1038/nsmb.3097.

46. van den Bogaart, G., Meyenberg, K., Risselada, H.J., Amin, H., Willig, K.I., Hubrich, B.E., Dier, M., Hell, S.W., Grubmüller, H., Diederichsen, U., and Jahn, R. (2011). Membrane protein sequestering by ionic protein-lipid interactions. Nature *479*, 552–555. https://doi.org/10.1038/nature10545.

47. Wang, Z., Liu, H., Gu, Y., and Chapman, E.R. (2011). Reconstituted synaptotagmin I mediates vesicle docking, priming, and fusion. J. Cell Biol. *195*, 1159–1170. https://doi.org/10.1083/jcb.201104079.

48. Guillen, J., Ferrer-Orta, C., Buxaderas, M., Perez-Sanchez, D., Guerrero-Valero, M., Luengo-Gil, G., Pous, J., Guerra, P., Gomez-Fernandez, J.C., Verdaguer, N., et al. (2013). Structural insights into the Ca2+ and PI(4,5)P2 binding modes of the C2 domains of rabphilin 3A and synaptotagmin 1. Proc. Natl. Acad. Sci. USA *110*, 20503–20508. https://doi.org/10.1073/pnas.1316179110.

49. Prasad, R., and Zhou, H.X. (2020). Membrane Association and Functional Mechanism of Synaptotagmin-1 in Triggering Vesicle Fusion. Biophys. J. *119*, 1255–1265. https://doi.org/10.1016/j.bpj.2020.08.008.

50. Rizo, J., Sari, L., Qi, Y., Im, W., and Lin, M.M. (2022). All-atom molecular dynamics simulations of Synaptotagmin-SNARE-complexin complexes bridging a vesicle and a flat lipid bilayer. Elife *11*, e76356. https://doi.org/10.7554/eLife.76356.

51. Larsen, A.H., and Sansom, M.S.P. (2021). Binding of Ca(2+)-independent C2 domains to lipid membranes: A multi-scale molecular dynamics study. Structure *29*, 1200–1213.e2. https://doi.org/10.1016/j.str.2021.05.011.

52. Vrljic, M., Strop, P., Ernst, J.A., Sutton, R.B., Chu, S., and Brunger, A.T. (2010). Molecular mechanism of the synaptotagmin-SNARE interaction in Ca2+-triggered vesicle fusion. Nat. Struct. Mol. Biol. *17*, 325–331. https://doi.org/10.1038/nsmb.1764.

53. Zhou, Q., Lai, Y., Bacaj, T., Zhao, M., Lyubimov, A.Y., Uervirojnangkoorn, M., Zeldin, O.B., Brewster, A.S., Sauter, N.K., Cohen, A.E., et al. (2015). Architecture of the synaptotagmin-SNARE machinery for neuronal exocytosis. Nature *525*, 62–67. https://doi.org/10.1038/nature14975.

54. Chicka, M.C., Hui, E., Liu, H., and Chapman, E.R. (2008). Synaptotagmin arrests the SNARE complex before triggering fast, efficient membrane fusion in response to Ca2+. Nat. Struct. Mol. Biol. *15*, 827–835. https://doi.org/10.1038/nsmb.1463.

55. Wang, S., Li, Y., and Ma, C. (2016). Synaptotagmin-1 C2B domain interacts simultaneously with SNAREs and membranes to promote membrane fusion. Elife *5*, e14211. https://doi.org/10.7554/eLife.14211.

56. Wu, Z., Ma, L., Courtney, N.A., Zhu, J., Landajuela, A., Zhang, Y., Chapman, E.R., and Karatekin, E. (2022). Polybasic Patches in Both C2 Domains of Synaptotagmin-1 Are Required for Evoked Neurotransmitter Release. J. Neurosci. *42*, 5816–5829. https://doi.org/10.1523/JNEUROSCI.1385-21.2022.

57. Jaczynska, K., Esquivies, L., Pfuetzner, R.A., Alten, B., Brewer, K.D., Zhou, Q., Kavalali, E.T., Brunger, A.T., and Rizo, J. (2023). Analysis of tripartite Synaptotagmin-1-SNARE-complexin-1 complexes in solution. FEBS Open Bio *13*, 26–50. https://doi.org/10.1002/2211-5463.13503.

58. Zdanowicz, R., Kreutzberger, A., Liang, B., Kiessling, V., Tamm, L.K., and Cafiso, D.S. (2017). Complexin Binding to Membranes and Acceptor t-SNAREs Explains Its Clamping Effect on Fusion. Biophys. J. *113*, 1235–1250. https://doi.org/10.1016/j.bpj.2017.04.002.

59. Zhou, Q., Zhou, P., Wang, A.L., Wu, D., Zhao, M., Südhof, T.C., and Brunger, A.T. (2017). The primed SNARE-complexin-synaptotagmin complex for neuronal exocytosis. Nature *548*, 420–425. https://doi.org/10.1038/nature23484.

60. Stein, A., Radhakrishnan, A., Riedel, D., Fasshauer, D., and Jahn, R. (2007). Synaptotagmin activates membrane fusion through a Ca2+-dependent trans interaction with phospholipids. Nat. Struct. Mol. Biol. *14*, 904–911. https://doi.org/10.1038/nsmb1305.

61. Berendsen, H.J.C., Vanderspoel, D., and Vandrunen, R. (1995). Gromacs - a Message-Passing Parallel Molecular-Dynamics Implementation. Comput. Phys. Commun. *91*, 43–56. https://doi.org/10.1016/0010-4655(95)00042-E.

62. Jo, S., Kim, T., Iyer, V.G., and Im, W. (2008). CHARMM-GUI: a web-based graphical user interface for CHARMM. J. Comput. Chem. *29*, 1859–1865. https://doi.org/10.1002/jcc.20945.

63. Lee, J., Cheng, X., Swails, J.M., Yeom, M.S., Eastman, P.K., Lemkul, J.A., Wei, S., Buckner, J., Jeong, J.C., Qi, Y., et al. (2016). CHARMM-GUI Input Generator for NAMD, GROMACS, AMBER, OpenMM, and CHARMM/OpenMM Simulations Using the CHARMM36 Additive Force Field. J. Chem. Theor. Comput. *12*, 405–413. https://doi.org/10.1021/acs.jctc.5b00935.

64. Humphrey, W., Dalke, A., and Schulten, K. (1996). VMD: visual molecular dynamics. J. Mol. Graph. *14*, 33. https://doi.org/10.1016/0263-7855(96)00018-5.

65. Nagy, G., Igaev, M., Jones, N.C., Hoffmann, S.V., and Grubmüller, H. (2019). SESCA: Predicting Circular Dichroism Spectra from Protein Molecular Structures. J. Chem. Theor. Comput. *15*, 5087–5102. https://doi.org/10.1021/acs.jctc.9b00203.

66. Marty, M.T., Baldwin, A.J., Marklund, E.G., Hochberg, G.K.A., Benesch, J.L.P., and Robinson, C.V. (2015). Bayesian deconvolution of mass and ion mobility spectra: from binary interactions to polydisperse ensembles. Anal. Chem. *87*, 4370–4376. https://doi.org/10.1021/acs.analchem.5b00140.

67. Michaud-Agrawal, N., Denning, E.J., Woolf, T.B., and Beckstein, O. (2011). MDAnalysis: a toolkit for the analysis of molecular dynamics simulations. J. Comput. Chem. *32*, 2319–2327. https://doi.org/10.1002/jcc.21787.

68. Herrick, D.Z., Kuo, W., Huang, H., Schwieters, C.D., Ellena, J.F., and Cafiso, D.S. (2009). Solution and membrane-bound conformations of the tandem C2A and C2B domains of synaptotagmin 1: Evidence for bilayer bridging. J. Mol. Biol. *390*, 913–923. https://doi.org/10.1016/j.jmb.2009.06.007.

69. Kelly, S.M., Jess, T.J., and Price, N.C. (2005). How to study proteins by circular dichroism. Biochim. Biophys. Acta *1751*, 119–139. https://doi.org/10.1016/j.bbapap.2005.06.005.

70. Sobott, F., Hernández, H., McCammon, M.G., Tito, M.A., and Robinson, C.V. (2002). A tandem mass spectrometer for improved transmission and analysis of large macromolecular assemblies. Anal. Chem. *74*, 1402–1407. https://doi.org/10.1021/ac0110552.

71. Hernandez, H., and Robinson, C.V. (2007). Determining the stoichiometry and interactions of macromolecular assemblies from mass spectrometry. Nat. Protoc. *2*, 715–726. https://doi.org/10.1038/nprot.2007.73.

72. Huang, J., Rauscher, S., Nawrocki, G., Ran, T., Feig, M., de Groot, B.L., Grubmüller, H., and MacKerell, A.D., Jr. (2017). CHARMM36m: an improved force field for folded and intrinsically disordered proteins. Nat. Methods *14*, 71–73. https://doi.org/10.1038/nmeth.4067.

73. Virtanen, P., Gommers, R., Oliphant, T.E., Haberland, M., Reddy, T., Cournapeau, D., Burovski, E., Peterson, P., Weckesser, W., Bright, J., et al. (2020). SciPy 1.0: fundamental algorithms for scientific computing in Python. Nat. Methods *17*, 261–272. https://doi.org/10.1038/s41592-019-0686-2.

STAR★METHODS

KEY RESOURCES TABLE

REAGENT or RESOURCE	SOURCE	IDENTIFIER
Antibodies		
anti-Synaptotagmin-1 cytoplasmic tail antibody, monoclonal IgG2a mouse antibody	SynapticSystems, Göttingen, Germany	cat. no. 105011; RRID: AB_2619760
anti-6xHis tag antibody, monoclonal IgG2b mouse antibody	Abcam, Cambridge, UK	cat. no. ab18184; RRID: AB_444306
peroxidase-coupled anti-mouse IgG secondary antibody, polyclonal IgG2 rabbit antibody	Sigma Aldrich. St. Louis, U.S.A.	cat. no. A9044; RRID: AB_258431
Bacterial and virus strains		
E. coli BL21 (DE3)	New England Biolabs	cat. no. C2527I
Chemicals, peptides, and recombinant proteins		
DOPS	Avanti Polar Lipids	cat. no. 840035
DOPC	Avanti Polar Lipids	cat. no. 850375
DOPE	Avanti Polar Lipids	cat. no. 850725
DOPI	Avanti Polar Lipids	cat. no. 850149
DOPI(4)P	Avanti Polar Lipids	cat. no. 850151
DOPI(4,5)P_2	Avanti Polar Lipids	cat. no. 850155
DOPI(3,4,5)P_3	Avanti Polar Lipids	cat. no. 850156
Cholesterol	Avanti Polar Lipids	cat. no. 700100
DAG	Avanti Polar Lipids	cat. no. 800815
Critical commercial assays		
Membrane lipid strips	Echelon Biosciences	cat. no. P-6002
Deposited data		
MD trajectory files	This paper	https://doi.org/10.5281/zenodo.10478556
Python scripts for MD analysis	This paper	https://github.com/cschmidtlab/syt1_membrane_md
Recombinant DNA		
pET28a Syt-1 C2A Rattus Norvegicus Syt-1 (97-263)	Stein et al.[60]	N/A
pET28a Syt-1 C2B Rattus Norvegicus Syt-1 (271-421)	Stein et al.[60]	N/A
Software and algorithms		
SpectraManager	JASCO	N/A
MassLynx v4.1	Waters	N/A
Kalliope	Anton Paar	N/A
Gromacs 2020.4	Berendsen et al.[61]	www.gromacs.org
CHARRM-Gui	Jo et al.[62]; Lee et al.[63]	www.charmm-gui.org
vmd	Humphrey et al.[64]	https://www.ks.uiuc.edu/Research/vmd/
md-python v3.0.6	www.python.org	N/A
SESCA	Nagy et al.[65]	https://www.mpinat.mpg.de/sesca
Unidec	Marty et al.[66]	https://github.com/michaelmarty/UniDec/releases
MDanalysis v2.5.0	Michaud-Agrawal et al.[67]	www.mdanalysis.org
open source PyMol	www.pymol.org	https://github.com/schrodinger/pymol-open-source

RESOURCE AVAILABILITY

Lead contact

Further information and requests for resources and reagents should be directed to and will be fulfilled by the lead contact, Carla Schmidt (carla.schmidt@uni-mainz.de).

Materials availability

This study did not generate new unique reagents.

Data and code availability

- All MD trajectories have been deposited at Zenodo and are publicly available as of the date of publication (see key resources table for details).
- The Python scripts are available at GitHub and are publicly available as of the date of publication (see key resources table for details).
- Any additional information required to reanalyze the data reported in this paper is available from the lead contact upon request.

EXPERIMENTAL MODEL AND STUDY PARTICIPANT DETAILS

Escherichia coli BL21 (DE3) cells were obtained from New England Biolabs (cat: # C2527I). Cells were first grown in LB media at 37°C and, for expression of the proteins, grown in TB medium (12 g/L tryptone, 24 g/L yeast extract, 0.4%(v/v) glycerol, 2.31 g/L KH2PO4, 12.54 g/L K2HPO4).

METHOD DETAILS

Purification of Synaptotagmin-1 C2A and C2B domains

His-tagged C2A and C2B domains of Synaptotagmin-1 from *Rattus norvegicus* were expressed in *E. coli* and purified as previously described.[39,68] Briefly, C2A and C2B expressing *E. coli* BL21 pET28a cells were disrupted by high pressure and the proteins were purified through the His-tags using a HisTrap HP 5 mL column (GE Healthcare) equilibrated in 20 mM HEPES, 300 mM NaCl, 0.1 mM TCEP, pH 7.4. Bound C2A or C2B domains were eluted with increasing amounts of imidazole. The His-tag was cleaved by thrombin and imidazole was removed during dialysis over night against 20 mM HEPES, 300 mM NaCl, 0.1 mM TCEP, pH 7.4. Cleavage of the His-tag was verified by gel electrophoresis. The His-tag and uncleaved protein were then removed by reversed affinity purification collecting the flow-through. Bound Ni^{2+} ions were removed during dialysis against 20 mM HEPES, 300 mM NaCl, 1 mM EDTA, 0.1 mM TCEP, pH 7.4.

Contaminants such as nucleic acids were removed by ion exchange chromatography using a HiTrap Q HP column (GE Healthcare) equilibrated in 20 mM HEPES, 0.1 mM TCEP, pH 7.4. The protein was eluted with increasing concentrations of NaCl. Protein purity was verified by gel electrophoresis. Peak fractions were concentrated to >1.5 mg/mL using 10 kDa MWCO filtration devices (Amicon).

Gel electrophoresis

Gel electrophoresis was performed using the NuPAGE system according to manufacturer's protocols (Thermo Fisher). The proteins were stained with colloidal Coomassie using InstantBlue Protein stain (Expedeon).

Far-UV CD spectroscopy

The protein concentration was adjusted to < 1 mg/ml with 20 mM HEPES, 300 mM NaCl, 0.1 mM TCEP, pH 7.4. 50 μl of protein solution were transferred into a 0.1 mm quartz cuvette. The ellipticity was recorded at 8°C from 250 to198 nm in continuous scanning mode with a sensitivity of 100 mdeg and a data pitch of 1 nm using a J-810 spectropolarimeter (JASCO). 64 scans, recorded at a scanning speed of 50 nm/min, were accumulated for each spectrum. A reference spectrum of the buffer was subtracted from the recorded spectrum and single binominal smoothing was applied using the SpectraManager software (JASCO). CD spectra were recorded at photomultiplier amplification voltages < 600 V to remove high noise regions. Raw ellipticity was converted to mean residue weighted ellipticity as described.[69] Theoretical reference spectra were calculated from PDB files of the respective domains obtained from full-length Synaptotagmin-1 (PDB: 5KJ7)[34] using SESCA[65] applying standard settings.

Lipid overlay assay

Membrane lipid strips (Echelon Biosciences) were first blocked with 2 mg/ml bovine serum albumin in 50 mM Tris-HCL, 150 mM NaCl, 0.1 % (v/v) Tween 20 for 1 h. Approx. 100 nM C2A or C2B-His in the same buffer containing 1 mM EGTA or 500 μM $CaCl_2$ were then added to the strips followed by incubation at 4°C overnight. The lipid strips were washed at least three times with 50 mM Tris-HCL, 150 mM NaCl, 0.1 % (v/v) Tween 20 and subsequently incubated with 1:1.000 anti-Synaptotagmin-1 cytoplasmic tail (C2A; monoclonal IgG2a mouse antibody, epitope: AA150-240 rat Synaptotagtmin-1, cat. no. 105011, SynapticSystems, Göttingen, Germany) or 1:1.000

anti-6xHis (C2B; monoclonal IgG2b mouse antibody, cat. no. ab18184, abcam, Cambridge, UK) antibodies overnight at 4°C. Again, the lipid strips were washed at least three times using 50 mM Tris-HCL, 150 mM NaCl, 0.1 % (v/v) Tween 20. Subsequently, 1:7.000 peroxidase-coupled anti-mouse IgG secondary antibody (polyclonal IgG2 rabbit antibody, cat. no. A9044, Sigma-Aldrich, St. Louis, U.S.A.) was added and incubated at 4°C overnight. Lipid strips were washed several times with 50 mM Tris-HCL, 150 mM NaCl, 0.1 % (v/v) Tween 20 before a final washing step with water was performed. Binding of the secondary antibody was visualised by chemiluminescence using the ECL detection kit according to manufacturer's protocols (Thermo Fisher Scientific).

Native mass spectrometry

Preparation of detergent-lipid micelles

Mixed detergent-lipid micelles were prepared by sonicating a 1 mM or 300 μM lipid stock solution in 200 mM ammonium acetate solution containing 2 × cmc C8E4 for 30 min.

Lipid binding to C2A and C2B

The purification buffer of the C2A or C2B domain was exchanged against 200 mM ammonium acetate solution containing 2 × cmc C8E4 using 10 kDa MWCO Amicon Ultra Centrifugal Filter according to manufacturer's protocols (Merck Millipore). 10 μM C2A or C2B were mixed with varying lipid-detergent concentrations. Protein-lipid complexes were subsequently analysed on a Synapt G1 HDMS quadrupole time-of-flight mass spectrometer modified for transmission of high-mass complexes.[70] For this, the samples were loaded into in-house prepared gold-coated emitters[71] and the source pressure was adjusted to 5 mbar. Typical instrument parameters were: capillary voltage, 1.7 kV; sampling cone voltage, 30 V; extraction cone voltage, 0.3 V; collision voltage, 10 V; nanoflow pressure, 0.0-0.5 bar; trap cell pressure, 3.5-4 bar. Mass spectra were smoothed twice with MassLynx v4.1 (Waters) applying the Savitzky–Golay filter and a smooth window of 25. Mass spectra were analysed with UniDec software[66] applying the following parameters: m/z range, 1800 to 5000; Charge range 2+ to 10+; Mass range 17000 to 22000 Da.

Lipid binding to C2A and C2B in the absence/presence of Ca^{2+}

60 μM C2A or C2B were pre-incubated for 30 mins with 1mM EGTA in 200 mM ammonium acetate, pH 7.4 (Ca^{2+}-free conditions) or 500 mM $CaCl_2$ in 200 mM AmAc, pH 7.4 (presence of Ca^{2+}) followed by dilution to 10 μM during buffer exchange against 200 mM ammonium acetate using 10 kDa MWCO Amicon Ultra Centrifugal Filter according to manufacturer's protocols (Merck Millipore). DOPC, DOPS or DOPI(4,5)P_2 were dissolved in 0.5 % (w/v) C8E4 and added at a protein:lipid ratio of 1:2.5. The samples were loaded into in-house prepared gold-coated emitters[71] and protein-lipid complexes were analysed on a Waters Micromass QToF Ultima mass spectrometer modified for native mass spectrometry[70] employing the following instrument parameters: capillary voltage, 1.5 kV; cone voltage, 80 V; collision voltage, 60 V. Mass spectra were smoothed twice applying the Savitzky-Golay filter and a smooth window of 10. Mass spectra were analysed with MassLynx v4.1 (Waters).

Liposome preparation and protein binding

Liposomes resembling the synaptic vesicle membrane contained DOPC:DOPS:DOPE:Cholesterol at a molar ratio of 38:12:20:20 and liposomes resembling the presynaptic plasma membrane contained DOPC:DOPS:DOPE:PI(4,5)P_2:DAG:Cholesterol at a molar ratio of 38:12:20:2:2:20.[33] For liposome preparation, lipid mixtures were dissolved in methanol/chloroform (2:1, vol/vol) to a final concentration of 4 mM lipids. Subsequently, the solvent was evaporated and the dry lipid film was hydrated at room temperature for 1 h to a final concentration of 2 mM lipids in 20 mM HEPES, 150 mM KCl, 0.1 mM TCEP, pH 7.4 containing 1 mM EGTA or 100 μM $CaCl_2$. Liposomes of a homogeneous size distribution were obtained by extrusion through a 100 nm polycarbonate membrane for 21 strokes. To study binding of C2A and C2B to the liposome membrane, proteins and liposomes were mixed at 1:250 and 1:1000 protein:lipid ratios followed by incubation for 1h.

Dynamic light scattering

Size distributions of the liposomes were evaluated by dynamic light scattering using a Litesizer 500 (Anton Paar) particle size analyzer equipped with a 633-nm helium-neon laser at a detection angle of 90°. For this, samples were heated for 2 min at 25°C and subsequently analysed 5 times for 15 seconds at 22°C in aqueous buffer. Autocorrelation functions were fitted by applying the Kalliope software (Anton Paar).

Liposome flotation analysis

Binding of C2A or C2B to the liposome membrane was investigated by flotation of the liposomes on a sucrose gradient. For this, liposomes pre-incubated with C2A or C2B, respectively, were mixed with sucrose in 20 mM HEPES, 150 mM KCl, 0.1 mM TCEP, pH 7.4 containing 1 mM EGTA or 100 μM $CaCl_2$ at a final concentration of 1 M. 3/4 volumes of 0.75 M sucrose in the same buffer and 0.175 volumes of buffer were layered on top followed by centrifugation at 268,000 × g for >2 h. Liposomes and bound C2A or C2B migrate to lower sucrose concentrations, while free protein remains in the bottom fraction of the gradient. Top, middle and bottom fractions were collected and top and bottom fractions were inspected by gel electrophoresis.

Molecular dynamics simulations

Equilibration of individual C2 domains

Starting coordinates of C2A (residues 141-263) and C2B (residues 272-418) in the presence of Ca^{2+} were obtained from PDB: 5KJ7 chain K.[34] For simulations in the absence of Ca^{2+}, Ca^{2+} atoms were removed from the structures. Structural models were placed in a

box of TIP3P water with 150 mM K^+ and Cl^- ions at a ratio neutralising the net charge. Structures were relaxed by energy minimization at a maximum force < 1,000 kJ mol^{-1} nm^{-1} followed by 500 ps equilibration in the NVT ensemble (i.e. at a constant number of particles (N), volume (V) and temperature (T)) at 300 K, 500 ps in the NPT ensemble (i.e. at a constant number of particles (N), pressure (P) and temperature (T)) at 1 bar pressure restraining all heavy atoms and 10 ns in the NPT ensemble removing all restraints. Simulations were performed using GROMACS version 2020.4[61] and the CHARMM36m force field.[72] The particle mesh Ewald method was used employing a 10 Å cut-off for calculating long-range electrostatics in the absence of lipids and a 12 Å cut-off in the presence of lipids. The V-rescale modified Berendsen thermostat with separate coupling groups for protein and solvent, and the Berendsen barostat were employed. H-Bonds were constrained using the LINCS algorithm enabling a time step of 2 fs. The final frame of the simulation was used for setting up the protein/membrane simulations.

Equilibration of isolated synaptic vesicle and plasma membrane bilayers

Lipid bilayer structures were obtained from CHARMM-GUI[62,63] specifying a box size of 76 Å edge length, 22.5 Å water layer thickness and a concentration of 150 mM K^+ and Cl^- ions. Membranes were composed of POPC:DOPS:POPE:Cholesterol:PIP_2:DAG (CHARMM-GUI identifiers for PIP_2 and DAG were POPI25 and POGL, respectively) at a ratio of 38:18:20:20:0:0 per leaflet for the synaptic vesicle membrane model and a ratio of 38:18:20:20:2:2 per leaflet for the plasma membrane model. This corresponds to 38 POPC, 18 DOPS, 20 POPE and 20 cholesterol molecules per leaflet for the synaptic vesicle membrane, and 38 POPC, 18 DOPS, 20 POPE, 20 cholesterol, 2 PI(4,5)P_2 (POPI25) and 2 diacylglycerol (POGL) molecules per leaflet for the plasma membrane. Relaxation and equilibration at 300 K were performed following the protocol supplied by CHARMM-GUI.[62,63] Briefly, the protocol consisted of six equilibration simulations, namely 2 x 125 ps NVT, 1 x 125 ps NPT and 3 x 500 ps NPT, gradually releasing the restraints on the lipids. Finally, a 10 ns unrestrained simulation in the NPT ensemble using the Nosé-Hoover thermostat and the Parrinello-Rahman barostat was performed. The last frame of this simulation was used for assembling the protein-lipid system.

Simulation of C2A and C2B membrane interactions

Equilibrated membrane structures were centred in the *xy*-plane and the equilibrated protein was placed at a 4 Å distance above the plane using VMD.[64] For each protein-membrane combination, three input structures with the C2 domains oriented at an angle of 0°, 30° and 60° between the *z*-axis and a vector through the main axis of the C2 domain (from the centre of mass of the protein to the centre of mass of residue 172 of C2A and residue 305 of C2B, respectively) with the Ca^{2+} binding loops facing towards the membrane were generated. Subsequently, energy minimization and a six-step equilibration protocol as described for initial equilibration of the membranes (see above) were performed. For production in the NPT ensemble the Nosé-Hoover thermostat (300K; 1 ps coupling constant for water and ions; 2.5 ps for protein and lipids) and the Parinello-Rahman barostat (semi-isotropic; 5 ps time constant). Simulations were computed until >1500 ns simulation time were accumulated.

Analysis of structural dynamics

Calculation of root-mean-square deviation and fluctuation

Root-mean-square deviation with respect to the first frame of the simulation and root-mean-square fluctuation with respect to an average structure of the last 800 ns of each simulation were calculated using functions provided by MDAnalysis.[67]

Contact angles

Trajectories of 1 ns time step per frame were generated with GROMACS and loaded into MDAnalysis.[67] The membrane interaction angle of the C2 domains was calculated between the z-axis and a vector through the main axis of the C2 domains (C2A: Tyr151 to Pro179, and C2B: Tyr282 to Pro 310). Median contact angles during the last 800 ns of the simulation were calculated for each simulation. Mean and standard deviation were reported.

Protein-lipid contacts

The most proximal lipid molecules for every amino acid residue were determined for every frame of each simulation using a k-dimensional tree[73] initialized with the centre-of-mass positions of the lipid atoms and queried with the centre-of-mass positions of the protein atoms. The resulting list was filtered and only nearest neighbours with a distance <2.6 Å were retained. Duplicate contacts (i.e. the same combination of amino acid residue number and lipid molecule) were removed. Contacts that were not observed continuously for a time span of at least 10 ns were not considered. Contact counts were summed for every simulation and averaged across the three simulations. For comparison between simulations, counts for each lipid were divided by the sum of counts of all lipids in a simulation and by the relative percentage of this lipid in the membrane lipid composition. Structural representations of lipid contacts were generated using the raw lipid contacts by mapping these values to the B-factor column of a PDB file. Visualization was performed in open source PyMol (https://github.com/schrodinger/pymol-open-source).

Local membrane reorganisation

To determine effects on local membrane organisation, all atoms were translated for each frame of the last 800 ns simulation time so that (i) the C2 domains were centred laterally and (ii) the membrane leaflets were located entirely within the simulation box. For control simulations without the proteins, only membrane leaflets were translated inside the box. Lipid atoms were wrapped inside the box for both sets of simulations. Surface positions of the phosphor atoms of the phospholipids were calculated using the membrane curvature tool of MDAnalysis (https://github.com/MDAnalysis/membrane-curvature) specifying binning into 8 x 8 bins (approx. 9 x 9 Å per bin).

Visualisation of domain insertion

Atoms for every frame of all simulations were translated so that (i) the C2 domains were centred laterally and (ii) the membrane leaflets were located completely within the simulation box. Positions of phosphor atoms of the phospholipids were calculated and visualized

using the Membrane Curvature tool implemented in MDAnalysis specifying binning into 8 x 8 bins. For comparison between simulations, surface positions were reported relative to the lowest phosphor atom coordinate.

QUANTIFICATION AND STATISTICAL ANALYSIS

Native MS measurements in the absence/presence of Ca^{2+} were performed in duplicates. All other measurements and experiments were performed at least three times. Representative results are shown. MD simulations were performed three times with different starting orientation. Relevant statistical information is provided in the figure legends and in the corresponding method details.

4. Discussion

Native MS analysis has been extensively used to study protein-lipid interactions, ranging from lipids co-purified with membrane proteins[76,79,80], protein-lipid interactions in native-like phospholipids bilayers[156–158] to binding of lipids transferred to proteins from detergent-lipid micelles[82]. In this thesis, the impact of non-covalent interactions on the lipid preferences and the lipid binding strength was investigated to characterise protein-lipid interactions. For this, native MS employing detergent-mediated lipid transfer was used and further developed. However, the effects of ionisation and gas-phase transfer on the observed lipid binding events in the gas phase as well as the mechanism of the lipid transfer from detergent-lipid micelles is still elusive. Accordingly, in this thesis, systematic interaction studies between peripheral membrane proteins (LL-37, LL-37 variants and Syt1) and lipids are conducted. These studies allow the characterisation of protein-lipid interactions and are further used to demonstrate applications and limitations of native MS and detergent-mediated lipid transfer. In publication **P4**, this approach is, together with complementary techniques, applied in a biological context. Nonetheless, the results of this study are also key for characterising protein-lipid interactions and addressing the central questions of this thesis. Here, the central questions of this thesis, whether interactions that are observed in the gas phase reflect interactions formed in solution and whether detergent-mediated lipid transfer is a reliable technique for exploring the protein-lipid interactions of peripheral membrane proteins, will be discussed.

4.1 Do interactions that are observed in the gas phase reflect interactions formed in solution?

Native MS enables the study of protein-ligand complexes, while preserving their non-covalent interactions. However, the analysis in the gas phase requires the ionisation and the gas-phase transfer of the analytes; this process may influence the observations. As an example, the transfer into the gas phase enhances electrostatic interactions[30] and complexes stabilised by the hydrophobic effect in solution are destabilised[29]. To address this central question, the contribution of non-covalent forces in solution to the ion intensity and complex stability in the gas phase will be discussed and, common errors in direct ESI MS analyses and their effects on the observations in native MS measurements will be described.

4.1.1 Are non-covalent interactions reflected in the ion intensity and gas-phase stability?

The first goal of this thesis was to evaluate whether non-covalent interactions that are formed in solution contribute to the ion intensity and the binding strength of complexes in the gas phase. Accordingly, detergent-mediated lipid transfer[82] was used in **P2** to investigate non-covalent interactions of the human AMP LL-37 with GPLs containing different head groups or varying in fatty acyl chain lengths. Specifically, the ion intensity of the peptide-lipid complexes formed by detergent-mediated lipid transfer was analysed and CID was used to probe their gas-phase stability. Studying the interactions of LL-37 with GPLs containing different head groups but identical fatty acyl chains revealed a preference for negatively charged lipids; the corresponding complexes displayed the highest ion intensities and gas-phase stabilities. The preference of LL-37 for negatively charged lipids was also previously described[118,159–161]. In contrast, complexes containing zwitterionic lipids were low abundant and showed low gas-phase stability. In both instances, ion intensity and gas-phase stability showed a high correlation, suggesting that the same non-covalent interactions that drive the formation of complexes in solution are responsible for the binding strength of the complexes in the gas phase. As the GPLs only differ in their head group, electrostatic interactions with the lipid head groups drive the interaction in solution (reflected in ion intensity) and also determine the complex stability in the gas phase.

Studying the interactions of LL-37 with GPLs containing the same PG head group but varying in fatty acyl chain lengths (ranging from PG 6:0/6:0 to PG 18:0/18:0), an increase in ion intensity with increasing fatty acyl chain length from PG 6:0/6:0 to PG 10:0/10:0 was observed. Notably, further increases of the fatty acyl chains length (i.e. PG 10:0/10:0 to PG 18:0/18:0) had only minor effects on the ion intensity of the complexes. This observation could be related to the solubility of the lipids, i.e. decreasing solubility with increasing chain lengths potentially caused precipitation of the lipids. Lowering the lipid concentration could impede complex formation, as the formation of complexes appears to be depended on the lipid concentration as demonstrated in **P4**. Alternatively, longer fatty acyl chains do not necessarily lead to more hydrophobic contacts as they are limited by the hydrophobic interface of LL-37. Finally, the transfer efficiency of lipids from detergent-lipid micelles might be influenced by their hydrophobicity. Notably, the binding strength of the LL-37-lipid complexes displayed a minor increase with fatty acyl chain length. Accordingly, compared to the interactions of LL-37 with lipids containing different head groups, the correlation between ion intensity and complex stability in the gas phase was less pronounced, suggesting that the driving force for interactions in solution and the stability of the complexes in the gas phase differs. The increase in ion intensity can be attributed to hydrophobic effect as it drives the association of hydrophobic molecules in solution[24], while not influencing the complex stability in the gas phase[29]. The

increase in complex stability with increasing fatty acyl chain length is likely caused by van der Waals interactions between LL-37 and the fatty acyl chains. Note that the strength of van der Waals interactions is increased approximately 6400 times in the gas phase[162], increasing the influence of van der Waals interactions on gas-phase stability. Furthermore, the short range of van der Waals interactions suggests direct contacts between LL-37 and the fatty acyl chains. Intriguingly, examples of complexes that are mainly stabilised by the hydrophobic effect in solution but are preserved in the gas phase, most likely through van der Waals interactions between hydrophobic contact sites, were reported previously[163–165]. An alternative explanation for the increase in complex stability with increasing chain length is the presence of different binding interfaces formed in solution. The binding interface is responsible for the formation of (directional) electrostatic interactions that stabilise the complexes in the gas phase[166]. However, binding interfaces in the gas phase cannot be determined by native MS. Future studies employing MD simulations could provide valuable insights into the binding interface in the gas phase (see Outlook).

In conclusion, the results of **P2** suggest that non-covalent interactions in solution including those that are driven by the hydrophobic effect are reflected by the ion intensities, while electrostatic interactions including van der Waals interactions determine the stability of complexes in the gas phase.

4.1.2 Do the ion intensities reflect the equilibrium concentration in solution?

The application of ESI MS to quantify protein-ligand binding events in a reliable and reproducible way has been controversially discussed since many years[38,167]. Employing optimal conditions, native MS analysis yields ion intensities that reflect the equilibrium between the free and the ligand-bound protein in solution[168]. Accordingly, native MS allows the direct quantification of protein-ligand binding events including the determination of binding constants. Loo et al. 1993[169] were the first to employ ESI MS to determine the association constant for the non-covalent interactions between the ribonuclease S-protein and the S-peptide. In recent years, direct ESI MS assays have been successfully employed to quantify many protein-ligand binding events[e.g.170–175]. Notably, by employing temperature controlled ESI devices, van't Hoff analysis can be employed to determine the binding enthalpy and entropy of protein-ligand interactions[176,177]. Nonetheless, conducting ESI MS assays employing conditions, at which the observed ratio between free and the ligand-bound protein is preserved, is challenging. Accordingly, to investigate at which conditions the ion intensity reflects the solution equilibrium, it is necessary to explore the conditions that can distort this relationship.

In publications **P2**, **P3** and **P4**, lipid preferences of peripheral membrane proteins were determined by analysing the ion intensities of protein-lipid complexes and the corresponding apo-proteins. However, there are many factors that can lead to deviation of the ion intensity from the equilibrium concentration in solution. Accordingly, avoiding these sources of deviation is a requirement for a reliable analysis of binding events using ESI MS. Common sources of deviation are (**Figure 17**)[38,167,178,179]: (i) In-source dissociation of complexes due to low gas-phase stability and harsh instrument settings (false negatives). (ii) Non-specific formation of gas-phase complexes during ESI due to high concentration of the analytes (false positives). This process is commonly referred to as non-specific aggregation. (iii) Differences in the response factors between the protein-ligand complex and the apo-protein, i.e. the response factors are non-uniform. Response factors describe the ionisation and detection efficiency of the analytes. (iv) pH and temperature changes of the sample solution during the ESI process.

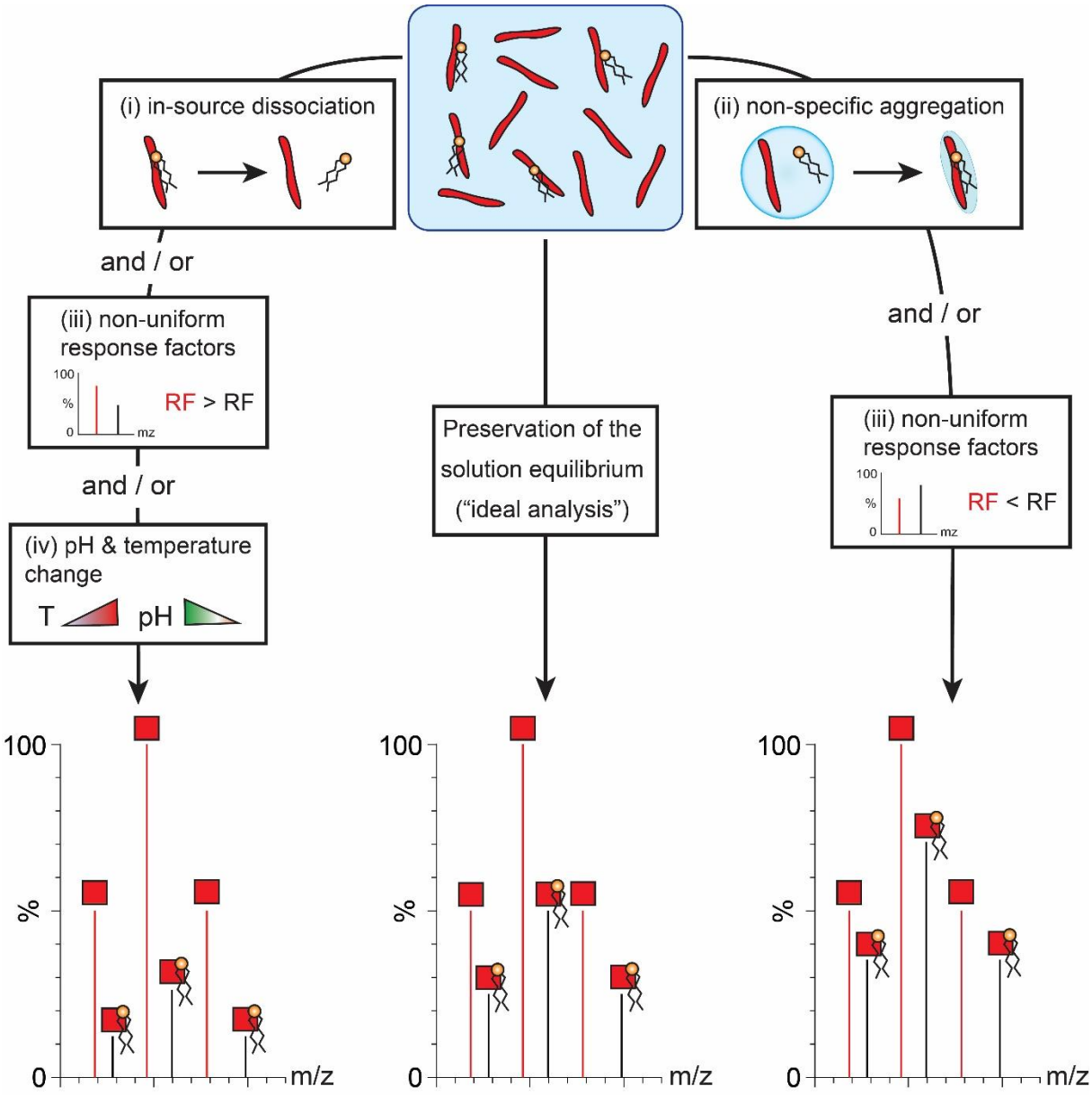

Figure 17: Schematic representation of factors that influence the observed ion intensity in ESI MS. The solution equilibrium between a protein and a protein-ligand complex is depicted (blue box). An "ideal" native MS spectrum reflects the solution equilibrium (middle). Non-uniform response factors (RF), increased pH and temperature or in-source dissociation can lower the observed relative ion intensity of the protein-ligand complexes (lhs), i.e. the complex formation in solution is underestimated. Non-uniform response factors between the protein and the protein-ligand complexes or non-specific aggregation during ESI can increase the observed ion intensity of the protein-ligand complexes (rhs), i.e. complex formation in solution is overestimated.

To address whether ion intensities presented in this thesis reflect the solution equilibrium, the influence of in-source dissociation, non-specific aggregation, non-uniform response factors and pH/temperature changes during ESI on the conducted experiments will be discussed in the following sections.

In-source dissociation

In the context of MS, the term in-source dissociation describes the dissociation of complexes in the gas phase after ionisation but before detection. Generally, the degree of in-source dissociation depends on the gas-phase stability of complexes and the instrument parameters used (e.g. cone and collision voltages). Note that both factors are not independent, i.e. employing “harsh” instrument settings might cause dissociation of stable complexes while “soft” ionisation conditions may not be able to preserve labile interactions. The stability of complexes in the gas phase does not equal their stability in solution[30]. In the gas phase, electrostatic interactions are enhanced[26,28,180] while complexes formed by the entropy driven hydrophobic effect in solution are destabilised[29]. Intriguingly, it was proposed that proteins undergo minor structural rearrangements during phase transition, involving formation of new electrostatic interactions on the protein-surface to preserve a native like structure[166]. In-source dissociation of complexes, therefore, leads to false negatives, i.e. the concentration of the protein-ligand complex in solution is underestimated. The influence of instrument parameters and the gas-phase stability on the results presented in this thesis will be discussed below.

To reduce in-source dissociation, instrument parameters used in publication **P2**, **P3** and **P4** were fine-tuned to preserve protein-lipid interactions, i.e. low cone and collision voltages were applied during measurements. Notably, analysing the interactions of LL-37 variants with different lipids in **P3** required a collision voltage of 30 V to remove detergent adducts associated with LL-37-pos. However, the analysis of interactions of the LL-37-wt with GPLs in **P2** was performed at a collisional voltage of 10 V. Accordingly, the level of activation for the three LL-37 variants and their complexes in **P3** was higher compared to **P2**. In general, collisional voltages $\leq$ 30 V are considered as low. However, CID experiments in **P2** revealed that increasing the collision voltage from 10 V to 30 V already causes a decrease in the ion intensities of the LL-37-lipid complexes that contained zwitterionic lipids. This effect was less pronounced for complexes containing negatively charged lipids as they are likely stabilised by the preferred interactions with negatively charged head groups. Notably, the abundance of peptide-lipid complexes observed for LL-37-wt was slightly lower in **P3** compared to **P2** although the same lipids and concentrations were employed. Accordingly, in-source dissociation might have a minor influence on the observed ion intensities in **P3**, however, the contribution is likely limited to an underestimation of interactions that are unstable in the gas phase. Importantly, **P3** focused on exploring the electrostatic interactions of LL-37 variants with lipids containing different lipid head groups. Since electrostatic interactions also determine the gas-phase stability of complexes (**P2**), in-source dissociation should have only minor effects on the determined lipid preferences.

In-source dissociation can also differ between instruments. Lipid-binding studies were performed on a modified[62] Waters Micromass Q-TOF Ultima spectrometer in **P2** and **P3** and on a modified[62] Synapt G1 HDMS quadrupole time-of-flight mass spectrometer in **P4.** However, without a direct comparison, e.g. by analysing the same sample on both instruments, the effects of the instruments on in-source dissociation cannot be estimated.

In publication **P2**, the stability of the formed peptide-lipid complexes was challenged by CID to determine, whether non-covalent interactions determine the stability in the gas phase. For this, the collisional voltage was increased stepwise and the intensity of the intact LL-37-lipid complexes was measured. The ion intensity, as a function of the collisional voltage, was used to compare the gas-phase stability of the different peptide-lipid complexes. However, the collisional energy that is experienced by an ion during activation in CID (also termed "effective" collision energy) not only depends on the collision voltage but also on the mass and charge of the ion[181]. Accordingly, to compare the gas-phase stability of complexes independently of their charge and mass, the centre-of-mass collision energy (also termed "effective" collision energy), which is the collisional energy experienced by an ion of a certain m/z when colliding with a neutral collision gas molecule, should be determined[182]. The centre-of-mass collisional energy E_{cm} is determined as

$$E_{cm} = E_{lab} \frac{m_{col}}{(m_{col} + m_{ion})}$$

with m_{col} as the mass of the collision gas, m_{ion} as the mass of the ion and E_{lab} as the laboratory collision energy[181]. The laboratory or nominal collision energy in eV (electron volts) describes the charge-dependent collisional energy of an ion. The calculation of the centre-of-mass collisional energy is particularly important when comparing the gas-phase stability of complexes with different m/z ratios. For probing the stability of LL-37-lipid complexes in **P2**, the centre-of-mass collision energy was not determined because the charge state distributions and the molecular weight of the LL-37-lipid complexes were similar. Accordingly, in this scenario, the collisional voltage correlates well with the centre-of-mass collisional energy and acts as a suitable metric for comparing the gas-phase stability of the different LL37-lipid complexes. Importantly, ion activation is not limited to CID experiments but all ions are activated inside the mass spectrometer. Therefore, it is important to determine potential differences in the strength of ion activation and its effect on in-source dissociation. In publication **P3**, protein-lipid interactions of supercharged cationic (LL-37-pos) and anionic (LL-37-neg) LL-37 variants were explored and compared to the wild type (LL-37-wt). Native MS analysis revealed that the average charge states of the LL-37 variants in the presence of C8E4 (required for detergent-mediated lipid transfer) were 3.1+, 2.3+ and 3.9+ for LL-37-wt, LL-37-neg and LL-37-pos, respectively. The molecular weight of the variants is similar and, therefore,

a slight increase in ion activation in the order of LL-37-neg< LL-37-wt< LL-37-pos is expected. However, it is difficult to estimate whether charge-dependent ion activation caused in-source dissociation in **P3**.

Another factor that may influence the in-source dissociation is the choice of the ionisation mode. In **P3**, the analyses of the lipid interactions of LL-37-neg by Langmuir monolayer studies and native MS in positive and negative ion mode revealed a correlation only when using negative ion mode, suggesting that the positive ion mode is not viable for the characterisation of interactions involving negatively charged peptides. One explanation might be that the negatively charged functional groups of LL-37-neg are neutralised by proton transfer during ESI in positive ion mode[183,184]. The neutralisation of negative charges could impede the electrostatically dominated peptide-lipid interactions, which stabilise the complexes in the gas phase. Accordingly, complexes that are formed by attractive electrostatic interactions between anionic residues and zwitterionic or cationic lipid head groups in solution, are likely prone to in-source dissociation when using positive ion mode. Notably, the sensitivity of protein-lipid interactions to the ionisation mode was also reported previously[185].

Non-specific aggregation

The term non-specific aggregation describes the non-specific binding of a free ligand to an apo-protein or a protein-ligand complex introduced during ESI. Non-specific aggregation leads to false positives, i.e. the concentration of the protein-ligand complexes in solution are overestimated. Note that non-specific aggregation can also lead to the formation of new protein-ligand complexes. In the past, non-specific aggregation was partially attributed to changes in the concentration of the analytes during droplet evaporation in ESI. Specifically, predictions based on the CRM assumed that the local concentration of the protein and the ligand drastically increase during droplet desolvation, thereby, shifting the solution equilibrium in the droplet between apo-protein and the protein-ligand complex towards the complex. However, the time required for droplet evaporation of small ESI droplets is significantly shorter than the equilibrium relaxation time[38]. Accordingly, this effect is reduced for nano ESI. Another assumption was that non-specific protein-ligand aggregation products are less stable in the gas phase than specific interactions formed in solution and are, therefore, lost during ion activation[38]. However, products of non-specific aggregation with a high stability in the gas phase were observed[186]. Accordingly, it is often not possible to discern non-specific interactions from specific interactions by probing the complex stability.

Non-specific aggregation in the gas phase occurs when progeny nanodroplets (i.e. the final generation of ESI droplets from which gas-phase ions are formed) contain more than one analyte. The complete evaporation of the ESI droplets causes the formation of non-specific

interactions between the analytes. The probability of trapping multiple analytes within one droplet increases with the total concentration of analytes and becomes significant above 50 µM[75,187]. To avoid concentration-dependent non-specific aggregation, in this thesis, the sum of the protein and the lipid concentration was kept below 50 µM (**P2** and **P3**) or limited to a maximum of 60 µM (**P4)**. However, in this thesis, protein-lipid complexes were formed by lipid transfer from mixed detergent-lipid micelles, a method that was proposed to facilitate non-specific interactions between soluble proteins and lipids[82]. Accordingly, the influence of detergent-mediated lipid transfer on non-specific aggregation will be discussed in chapter 4.2.1.

Non-uniform response factors

The relationship between the observed ion intensity and the concentration of the analyte in solution is described by the response factor, i.e. a combined measure for the ionisation and detection efficiency of an analyte. The response factor depends on the size and structure of the analyte as well as the properties of the ESI emitter[38,188,189]. The response factor is generally similar between the protein and the protein-ligand complex if their molecular weight is similar (i.e. $\frac{MW_{complex}}{MW_{apo-protein}} \leq 110\%$)[38,188]. However, non-uniform response factors can lead to the under- or overestimation of complex formation.

The concern of non-uniform response factors in **P4** is reduced by the fact that protein-lipid complexes differing in molecular weight by less than 10% from the apo-C2 domains were observed. In contrast, the molecular weight of peptide-lipid complexes of the LL-37-wt (**P2**) and the LL-37 variants (**P3**) generally exceeds 110% of the apo-peptide's molecular weight. However, a large proportion of the lipid mass corresponds to the fatty acyl chains which likely do not influence the response factor of the peptide-lipid complex. In contrast, the polar lipid head groups are assumed to influence the complex ionisation but are relatively small compared to the peptides. Accordingly, in publication **P2** and **P3** similar response factors of the apo-peptides and the respective peptide-lipid complexes were assumed. However, a future validation of this assumption is required.

The ionisation efficiency and, therefore, the response factor of the analytes further depends on the ESI emitter[189]. In this thesis, a gold-coated borosilicate emitter (pulled in-house) was used for each sample. The use of different ESI emitters may lead to some minor variations of the response factors between individual measurements. However, this variation was partially alleviated because only average ion intensities of (at a minimum) triplicates were used for data analyses.

pH and temperature changes during ESI

During ESI, electrochemical reactions in the ESI emitter facilitate the formation of H_3O^+, therefore, decreasing the pH of the sample solution over time[179,190]. To increase the desolvation efficiency, heated drying gas and sampling the ESI droplets in a heated metal capillary is commonly employed. However, this may cause a temperature increase of the sample[167]. These pH and temperature changes may influence the binding behaviour in solution. In this thesis, heated drying gas or heated metal capillaries was not used, therefore, an increase in solution temperature is not expected, while significant pH changes were circumvented by limiting the time for each measurement (<10 min).

4.1.3 Conclusion

In conclusion, conducting a native MS analysis is challenging as many factors distort the relationship between gas-phase observations and solution state. These factors include in-source dissociation of protein-ligand complexes, non-specific aggregation introduced during ESI, non-uniform response factors between apo-protein and protein-ligand complexes, and pH/temperature changes of the sample solution. Circumventing these factors often requires comprehensive training in native MS. However, interactions that are observed in the gas phase can indeed reflect the solution state as it is possible to maintain the solution equilibrium throughout the analysis. Importantly, all non-covalent interactions including those driven by the hydrophobic effect in solution contribute to the ion intensity, while electrostatic interactions including van der Waals interactions contribute to the gas-phase stability.

4.2 Is detergent-mediated lipid transfer a reliable technique for the investigation of the protein-lipid interactions of peripheral membrane proteins?

Exploring non-covalent interactions between proteins and lipids has become increasingly important in recent years as they form the basis for many biological processes. Native MS has been established as a valuable tool for the characterisation of proteins-lipid interactions as it preserves non-covalent interactions and resolves individual binding events[162]. In addition to the identification of co-purified, tightly bound lipids[12], the lipid binding specificity of integral membrane proteins is often probed through the addition of lipids solubilised in detergent micelles[76,80–82]. Even though lipid interactions of soluble membrane proteins can be probed by analysing their ejection from proteoliposomes[156,157], such measurements are very challenging and not viable for all protein-lipid interactions (e.g. transient interactions). Accordingly, in this thesis, protein-lipid interactions are investigated by analysing protein-lipid complexes formed

by the transfer of lipids from mixed detergent-lipid micelles to soluble membrane proteins. To characterise detergent-mediated lipid transfer as a technique for exploring protein-lipid interactions with soluble peripheral membrane proteins, the discussion will first revolve around the specificity of the protein-lipid interactions that are facilitated by the transfer from mixed detergent-lipid micelles and, second, the results of these lipid-binding studies will be compared to complementary methods in solution.

4.2.1 Specificity of detergent-mediated lipid transfer for soluble proteins

The use of mixed detergent-lipid micelles to facilitate binding of exogenous lipids to soluble proteins was demonstrated by Landreh et al. 2017[82]. In that study, the authors demonstrated the association of lipids, which are solubilised in detergent micelles, to soluble proteins through non-specific contacts during the ESI process. They observe a dependence of the lipid association on the micelle concentration in solution, indicating that protein-lipid contacts are enabled by non-specific aggregation (see section 4.1.2) occurring when the soluble protein and the mixed detergent-lipid micelle share the same ESI nanodroplet. In contrast, integral membrane proteins are embedded within the detergent micelles and likely form specific lipid interactions.

The model peptides LL-37, LL-37-pos and LL-37-neg (**P2** and **P3**) are soluble peripheral membrane proteins. The Ca^{2+}-sensor Syt1, in contrast, contains a transmembrane region that anchors the protein into the synaptic vesicle[131]. However, the lipid interactions of the individual C2 domains of Syt1 are investigated in **P4**, which are expected to behave like peripheral membrane proteins. The amphipathic peptide LL-37 is known to partially integrate into the hydrophobic core of a membrane with its preferred localisation at the interfacial region between the lipid head groups and the hydrophobic core[117]. Accordingly, LL-37 might also integrate into C8E4-lipid micelles. The amphipathic structure of LL-37-wt is retained in the supercharged LL-37-pos and LL-37-neg variants, which may also integrate into detergent micelles. In addition, secondary structure analyses of LL-37-wt and the LL-37 variants by CD spectroscopy (**P2** and **P3**) indicate that the presence of C8E4 molecules induces transition from a random coil structure to an alpha helix, suggesting direct interactions with C8E4 in solution; although, it is unclear whether their interactions involve integration into the micelle or simply interactions with individual detergent molecules in solution. The analysis of proteins embedded in detergent micelles generally requires high collisional activation to release the proteins from the detergent micelles[77]. Accordingly, integration of the peptides into C8E4 micelles would contradict this fact as low activation energies were employed for the analysis. Thus, an integration of the peptides into the micelles is not expected. For the C2 domains (**P4**), integration into the micelles is not

expected as the interactions with lipids are mainly driven by electrostatic interactions[191] and, again, analysis in the presence of C8E4 micelles was conducted at low activation energies.

Assuming that integration of the LL-37 variants and the C2 domains into the micelles does not occur, lipid transfer from detergent-lipid micelles is expected to be driven by concentration-dependent non-specific aggregation during the ESI process[82]. Non-specific aggregation occurs when multiple analytes are present within the same ESI nanodroplet. The probability of trapping multiples analytes within one ESI nanodroplet increases with the total concentration of analytes and becomes significant above 50 µM[75,187]. In this thesis, two times the critical micelle concentration (cmc) of C8E4 was employed for lipid-binding studies by native MS. The cmc of C8E4 is 0.25% (w/v) or approximately 8.15 mM[192]. Two times the cmc with an aggregation number of 82 results in the micelle concentration of approximately 100 µM. Notably, 8.15 mM of C8E4 are present as dissolved molecules in solution while the detergent concentrations above the cmc contribute to the formation of micelles. In order to quantify the degree of non-specific aggregation for experiments in **P2** and **P3**, a Monte Carlo simulation as presented by Benesch et al. 2007[75] was performed (**Figure 18**). However, it should be stressed that this method does not take evaporation of the droplet or excluded volume into account[75]. Here, 220 particles were randomly placed in a sphere with a diameter of 180 nm (**Figure 18 A**). A sphere of these proportions corresponds to the size of an initial droplet (i.e. droplet before the asymmetric fission event) formed during nano ESI[193]; 220 particles are approximately equal to the number of particles expected in the droplet at a total analyte concentration of 120 µM (20 µM peptide +100 µM C8E4 micelles). Subsequently, the number of particles within a randomly placed sphere with a diameter of 18 nm (i.e. a sphere corresponding in size to ESI nanodroplets after the fission event[193]) were counted. This process was repeated 100,000 times and the average value was calculated. Notably, in **P2** and **P3**, a lipid concentration of 25 µM was used, assuming complete solubilisation and a uniform distribution of the lipids, 25% of the C8E4 micelles contain 1 lipid molecule. The python script of the Monte Carlo simulation was developed with the assistance of OpenAI's ChatGPT (December 2024 version).

The simulation reveals that under these conditions, 80.2% of the ESI nanodroplets remain empty, 17.73% contain one analyte and 1.19% two analytes (**Figure 18 B**). Of the droplets containing one analyte, 16.66% contain a protein molecule (**Figure 18 C**). Accordingly, 2.96% of all progeny droplets contain exactly one protein molecule. Of the droplets containing two analytes, 6.94% contain one protein molecule and one mixed detergent-lipid micelle (**Figure 18 D**), which equals approximately 0.135% of all progeny droplets. If interactions were solely driven by non-specific aggregation during ESI and assuming similar response factors between the apo-protein and the protein-lipid complexes, the ion intensity of the protein-lipid complex containing one lipid should only be 4.57% of the apo-protein. Notably, the protein concentration

used in **P4** was lower (10 µM) and the lipid concentrations ranged from 12.5 µM up to 50 µM but the complex intensity caused by non-specific aggregation should be < 10% of the apo-proteins for all lipid concentrations. The ratios of the protein-lipid complex to apo-protein observed for LL-37 (**P2**), the LL-37 variants (**P3**) and the C2 domains of Syt1 (**P4**) were for many interactions significantly higher than 5%. This suggests that protein-lipid interactions facilitated by the presence of detergent micelles are not solely driven by the concentration-dependent non-specific aggregation during ESI. Instead, protein-lipid interactions in solution are likely responsible for the observed lipid binding events. In conclusion, protein-lipid interactions facilitated by the presence of detergent micelles appear to be driven mostly by interactions in solution; however, non-specific aggregation during ESI might affect the measurements.

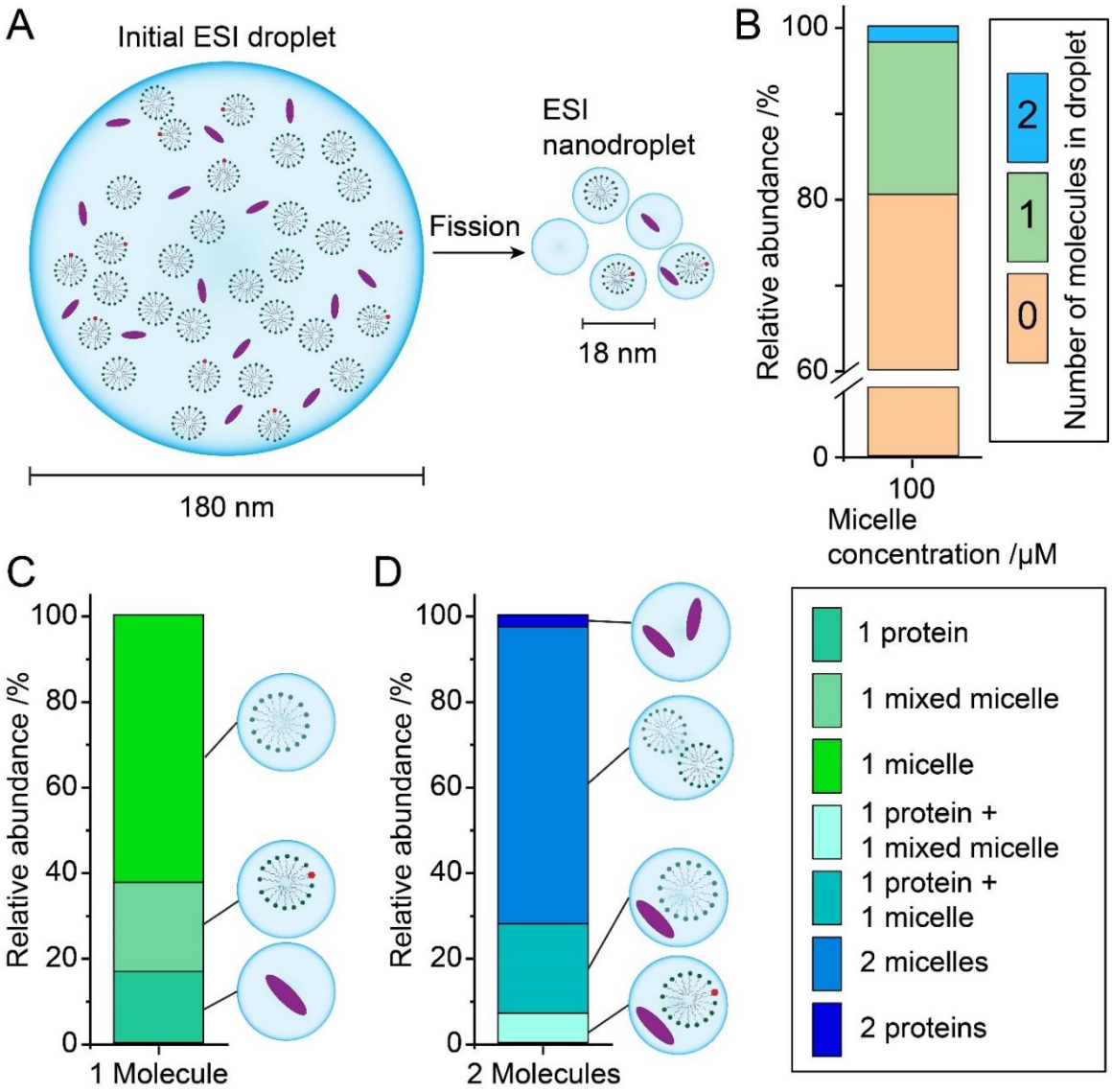

Figure 18: Quantification of non-specific aggregation during the nano ESI process. (**A**) Schematic representation of ESI nanodroplets formed through the fission of an initial nano ESI droplet with their expected sizes[193]. Non-specific aggregates form during the ionisation when more than one analyte is present in the final ESI nanodroplets. (**B**) Relative abundances of ESI nanodroplets containing zero, one and two molecules at a protein concentration of 20 µM and a micelle concentration of 100 µM was estimated via a Monte Carlo simulation as demonstrated by Benesch et al. 2007[75]. 220 particles (at a total analyte concentration of 120 µM) were randomly placed into a spherical volume corresponding to the initial ESI droplets and the number of particles were counted in a randomly placed volume corresponding to the final ESI nanodroplets. Shown are the averages after 100,000 repetitions. (**C**) Relative abundance of nanodroplets containing one protein molecule, one mixed detergent-lipid micelle or one detergent micelle. (**D**) Relative abundance of nanodroplets containing two micelles, two protein molecules or a mixture of one protein molecule and one detergent micelle is shown. The figure was adapted from Benesch et al. 2007[75].

4.2.2 Comparison of detergent-mediated lipid transfer with complementary methods in solution

Detergent-mediated lipid transfer has been established as a suitable method for probing the lipid interaction of integral membrane proteins[76,80–82]. Notably, this approach revealed thermodynamic parameters for individual lipid binding events similar to those determined by surface plasmon resonance and isothermal titration calorimetry[177]. To determine whether protein-lipid interactions of peripheral membrane proteins facilitated by the transfer of lipids from mixed detergent-lipid micelles reflect interactions formed in solution, lipid binding preferences determined by native MS were compared with binding preferences determined by complementary methods in solution. Bindings constants (e.g. dissociation constants) were not determined in this thesis and the comparison is based on lipid preferences. Importantly, common sources for errors that influence direct ESI MS assays (see section 4.1.2) also influence protein-lipid binding studies facilitated by the detergent-mediated lipid transfer.

The interactions of LL-37 with GPLs containing different head groups or varying fatty acyl chain lengths were explored in **P2**. In this study, complementary in solution methods were not employed. However, native MS analysis revealed a preference for negatively charged lipids, which is in agreement with previous observations by nuclear magnetic resonance spectroscopy[118], sum-frequency generation spectroscopy[159], Langmuir film techniques[160] and interaction studies using liposomes[161]. Furthermore, a preference of LL-37 for longer fatty acyl chains was observed. This preference was previously demonstrated by Walker et al. 2022[194] for the incorporation of LL-37 into lipid nanodiscs. However, using a Langmuir film balance revealed that the affinity of LL-37-wt for the zwitterionic PC 14:0/14:0 was likely underestimated in the native MS analysis (**P3**). In conclusion, the head group and fatty acyl chain selectivity determined for LL-37 were generally in agreement with previous findings, although interactions with PC 14:0/14:0 were underestimated.

In **P3**, three LL-37 variants (LL-37-wt, LL-37-pos and LL-37-neg) were employed to assess the effects of peptide surface charge on protein-lipid interactions in the gas phase and in solution. For this, interactions with three negatively charged GPLs (PS 14:0/14:0, PG 14:0/14:0, PA 14:0/14:0), two zwitterionic GPLs (PE 14:0/14:0, PC 14:0/14:0) and one positively charged artificial lipid analogue (TAP 14:0/14:0) were analysed by native MS in positive ion mode. The interactions of LL-37-neg with PG 14:0/14:0, PC 14:0/14:0 and TAP 14:0/14:0 were also analysed in negative ion mode. In addition, a Langmuir film balance was employed to study the interactions of the LL-37 variants with lipid monolayers (PG 14:0/14:0, PC 14:0/14:0 and TAP 14:0/14:0) in solution.

Native MS analysis in positive ion mode revealed a preference of LL-37-wt and LL-37-pos for negatively charged lipids, a low affinity for zwitterionic lipids and no binding of the cationic TAP.

These results are in agreement with previous reports on the preferences of LL-37-wt for negatively charged lipids[118,159–161]. In contrast, all peptide-lipid complexes involving LL-37-neg showed low ion intensities in positive ion mode. Notably, LL-37-neg appeared to be unstable as a small population of LL-37-neg was observed that lost the coil region at the C-terminus through fragmentation. Surprisingly, despite different electrostatic properties of the LL-37 variants, the trend of the lipid preferences was the same, namely positively charged lipids < zwitterionic lipids < negatively charged lipids. While this trend is largely attributed to attractive electrostatic interactions with the lipid head groups in the case of LL-37-wt and LL-37-pos, this is not the case for the negatively charged LL-37-neg variant. Surprisingly, using negative ion mode, the lipid preferences of LL-37-neg were reversed, namely PG 14:0/14:0 < PC 14:0/14:0 < TAP 14:0/14:0. Furthermore, fragmentation of the C-terminus was no longer observed indicating stabilisation of the peptide in negative ion mode, a phenomenon that was previously reported for membrane proteins[195]. The analysis of protein-lipid interactions using a Langmuir film balance revealed a similar trend for LL-37-pos: positively charged lipids < zwitterionic lipids < negatively charged lipids. Surprisingly, LL-37-wt showed a comparably high affinity for PC 14:0/14:0 and PG 14:0/14:0 while the affinity for TAP 14:0/14:0 was low. These findings indicate a more favourable interaction of LL-37-wt with PC 14:0/14:0 in solution or an underestimated affinity by native MS. In solution, LL-37-wt is able to occupy its preferred location in the interfacial region between the lipid head groups and the hydrophobic core[117]. This location might facilitate favourable electrostatic interactions with the negatively charged phosphate group of PC 14:0/14:0. Furthermore, compared to LL-37-pos, LL-37-wt contains cationic and anionic amino acids enabling attractive interactions with the phosphate and the choline group of PC 14:0/14:0, potentially allowing a more efficient insertion into the lipid monolayer. In the gas phase, as discussed in 4.1.2, in-source dissociation of complexes containing PC 14:0/14:0 might lead to an underestimation of the affinity determined by native MS. In addition, in-source dissociation may be facilitated by the neutralisation of negative charges of LL-37-wt during ESI[183,184] by impeding favourable electrostatic interactions. For LL-37-neg, lipid preferences determined when using a Langmuir film balance only correlated with the preferences determined in negative ion mode. Accordingly, the analysis in positive ion mode is not suitable for the characterisation of interactions involving negatively charged peptides. This could be related to the use of detergent-mediated lipid transfer, as the transfer efficiency of lipids from mixed detergent-lipid micelles could be influenced by the ion mode. Alternatively, in-source dissociation of complexes containing zwitterionic and cationic lipids in positive ion mode might influence the observations in the gas phase. Again, neutralisation of negative charges during proton transfer in ESI[183,184] (positive ion mode) may facilitate in-source dissociation.

In conclusion, the comparison between the variants using a Langmuir film balance and native MS revealed, for both approaches, a strong effect of surface charge on the electrostatic interactions with lipids. Importantly, a preference of LL-37-pos and LL-37-neg for lipids containing the opposite charge was observed. The analysis of LL-37-neg required the use of the negative ion mode revealing a major influence of the ionisation. For LL-37-wt, a lack of correlation between the analysis by native MS and Langmuir film balance measurements was revealed for the interaction with zwitterionic PC 14:0/14:0 with analysis by native MS revealing a low affinity and the Langmuir film balance measurements revealing a high affinity. This discrepancy potentially originates from different binding interfaces in the two approaches or due to in-source dissociation of the peptide-lipid complexes in positive ion mode.

The goal of **P4** was to determine how membrane interactions shape the functional mechanism of the Ca^{2+}-sensor Syt1. For this, lipid and membrane interactions of the isolated C2 domains (C2A and C2B) of Syt1 were characterised. This project employed native MS and lipid overlay assays to explore interactions with individual lipid species, liposome flotation assays to study the interactions with model membranes and MD simulations to gain detailed insights into the mechanism of the membrane interaction. Lipid overlay assays revealed a high affinity of the C2 domains for negatively charged lipids, especially for phosphatidylinositol phosphates. Intriguingly, the affinity for negatively charged lipids increased in the presence of Ca^{2+} and both C2 domains showed an high affinity towards $PI(4,5)P_2$, which is as a key lipid for driving Ca^{2+}-dependent membrane interactions of Syt1[196]. In addition, a preference of C2B for PS (in the absence and presence of Ca^{2+}) was observed, as previously reported[197]. Liposome flotation assays (performed by Melissa Frick) using liposomes mimicking the synaptic vesicle or the plasma membrane revealed minimal binding of the C2 domains in the absence of Ca^{2+}. In the presence of Ca^{2+}, C2A bound to the membranes in a non-selective manner, while, a preference of C2B for the $PI(4,5)P_2$ containing plasma membrane was observed. Importantly, association of the C2B domain to the plasma membrane agrees well with previous findings[196,198]. MD simulations (performed by Julian Bender) were employed to characterise the interactions of the C2 domains with membranes resembling the synaptic vesicle and the plasma membrane in the absence and presence of Ca^{2+}. These simulations suggest that the C2A domain is not selective towards a specific membrane composition but is sensitive to the presence of Ca^{2+}, while the C2B domain associates to the plasma membrane in the absence and presence of Ca^{2+}. Notably, the determined lipid contacts for both C2 domains were similar with both domains showing a preference for the negatively charged $PI(4,5)P_2$ in the plasma membrane. Importantly, MD simulation revealed different orientations for the two C2 domains on the membrane with C2A undergoing a Ca^{2+}-dependent shift to a perpendicular orientation.

The interactions of C2A and C2B with five negatively charged lipids (PS, DOPI, DOPI(4)P, $DOPI(4,5)P_2$ and $DOPI(3,4,5)P_3$) and one zwitterionic lipid (DOPC) at different concentrations

were explored by native MS. Intriguingly, native MS analysis revealed binding of up to three lipid molecules for all lipid species, including the zwitterionic lipid DOPC, with complex intensities increasing with the lipid concentration. Nonetheless, the ion intensities indicate a preference for negatively charged lipids with complexes containing DOPI(3,4,5)P_3 displaying the highest intensities for both C2 domains. In contrast to the results of the lipid overlay assay, C2A generally displayed a higher lipid affinity compared to C2B in the native MS analysis. In addition, a major preference of C2B for DOPI(4,5)P_2 or DOPS could not be observed by native MS analysis. Binding of DOPC was surprising, as lipid overlay assays revealed that binding of both C2 domains was not observed in the presence or absence of Ca^{2+}. These interactions are likely transient and facilitated by interactions of the aspartate-rich Ca^{2+}-binding loops of the C2 domains[134,135] with the choline head group of DOPC. Notably, CID of protein-lipid complexes revealed a low gas-phase stability of complexes containing DOPC compared to complexes containing DOPI(4,5)P_2 supporting a potential transient nature of these interactions. The ability to preserve transient interactions in the gas phase is facilitated by the charge reducing effects of C8E4 as demonstrated in **P1**. The use of other charge reducing agents like imidazole was shown to prevent in-source dissociation of protein-ligand complexes[170,171]. Furthermore, low amounts of normalised lipid contacts to PC were detected in MD simulations supporting the possibility of transient interactions. Lipid overlay assays are likely not suited to detect transient interactions, as proteins need to remain stably associated throughout the washing steps and long incubation times. Nonetheless, lipid overlay assays, liposome flotation assays and MD simulations revealed a major influence of Ca^{2+} on the lipid interactions of the C2 domains. These observations agree well with previous findings that Ca^{2+} acts as a regulator of phospholipid binding by Syt1[142,198,199]. In contrast, pre-incubation of the C2 domains with Ca^{2+} or ethylene glycol-bis(β-aminoethyl ether)-N,N,N',N'-tetraacetic acid (EGTA) (to mimic the Ca^{2+} "free" state) did not affect observed lipid binding events by native MS (performed by Julia Bieber). The absence of a lipid membrane in the native MS analysis might be responsible for these findings. However, in a recent study, Lawrence et al. 2024[200] employed a similar approach and showed that GPL interactions regulate the Ca^{2+} binding by Syt1. Accordingly, analytical challenges might be the reason for the lack of Ca^{2+}-dependence observed by native MS. For instance, lipid binding studies in the presence of Ca^{2+} required harsh instruments parameters, which promote in-source dissociation.

In conclusion, native MS analysis revealed a clear preference of the C2 domains for negatively charged lipids, especially for phosphatidylinositol phosphates, which is in agreement with the results obtained from the complementary techniques. Notably, a major selectivity of C2B towards DOPI(4,5)P_2 over other GPLs was not detected. In addition, the influence of Ca^{2+} on the protein-lipid interactions of the C2 domains could not be assessed by native MS; methodological limitations might be the reason for this limitation.

4.2.3 Conclusion

In conclusion, detergent-mediated lipid transfer could be a suitable technique for the investigation of the protein-lipid interactions of peripheral membrane proteins; the approach is not entirely driven by non-specific aggregation during ESI and determined binding preferences are generally in agreement with complementary techniques. However, as required for all direct ESI MS assays, the experimental conditions including the ion mode should be selected with care. Furthermore, the underestimation of the affinity of LL-37-wt for PC 14:0/14:0 in **P3** and the inability to determine the influence of Ca^{2+} on the lipid interactions of the C2 domains in **P4** requires further investigation. Nonetheless, the approach is suitable for many electrostatically dominated interactions, although, further insights into the mechanism of lipid transfer are required.

5. Conclusion and Outlook

In this thesis, the interactions of peripheral membrane proteins (LL-37, LL-37 variants and Syt1) with GPLs were investigated to characterise the impact of non-covalent interactions on the formation of protein-lipid interactions and to determine whether interactions observed in the gas phase reflect interactions observed in solution. In addition, native MS analysis of protein-lipid complexes formed by detergent-mediated lipid transfer as a method for probing the lipid interactions of soluble peripheral membrane proteins was characterised. A graphical overview of the different methods employed in projects **P2**, **P3** and **P4** is given in **Figure 19**.

The aim of publication **P2** was to identify whether non-covalent interactions in solution contribute to the ion intensity and the binding strength of protein-lipid complexes in the gas phase. For this, interactions of the human AMP LL-37 with GPLs containing different head groups or varying in fatty acyl chain lengths were investigated by native MS. The results suggest that non-covalent interactions in solution including those that are driven by the hydrophobic effect are reflected by ion intensities, while electrostatic interactions determine the stability of the complexes in the gas phase. Furthermore, the determined preferences of LL-37 for negatively charged GPLs agree well with the literature. An increase in protein-lipid complex stability with increasing fatty acyl chain length was observed, which can likely be attributed to van der Waals interactions. Notably, stabilisation of protein-ligand complexes in the gas phase by van der Waals interactions between hydrophobic contact sites has been previously reported[163–165]. However, the binding interface of the LL-37-lipid complexes and, therefore, the presence of hydrophobic contact sites is currently unknown. To uncover the structure and binding interfaces of the complexes in the gas phase in future studies, MD

simulations could be used as recently demonstrated by Oh et al. 2017[201] and Konermann et al. 2018[202].

The effects of peptide surface charge on protein-lipid interactions in solution and in the gas phase was explored in publication **P3**. The interactions of three LL-37-variants (with different electrostatic properties) with lipids were analysed by native MS (positive and negative ion mode) and using a Langmuir film balance. Both techniques reveal strong effects of the surface charge on the protein-lipid interactions. LL-37-pos and LL-37-neg displayed a high affinity for lipids with opposite charge. Surprisingly, only the analysis of LL-37-neg in negative ion mode correlated with the analysis using a Langmuir film balance, demonstrating a great influence of the ion mode. The investigation of the peptide-lipid interactions of LL-37-wt by Langmuir film balance revealed a high affinity of LL-37-wt towards negatively charged lipids and zwitterionic PC 14:0/14:0, likely due to its more “balanced" surface charge. However, compared to the analysis using a Langmuir film balance, the affinity towards PC 14:0/14:0 was low in native MS, suggesting a more favourable interaction in solution or an underestimation of the complex formation in the gas phase (see section 4.1.2 and **Figure 17**). Probing the interactions of LL-37-wt with PC 14:0/14:0 solubilised in detergent micelles in solution could provide further insights into the origin of this discrepancy.

The goal of **P4** was to characterise lipid and membrane interactions of the isolated cytosolic C2 domains of the Ca^{2+}-sensor Syt1 to uncover its mechanism during synaptic vesicle fusion. This study followed a multidisciplinary approach employing native MS, lipid overlay assays, liposome flotation assays and MD simulations to uncover interactions with individual lipid species, model membranes and to gain detailed insights into the mechanism. Native MS analysis and lipid overlay assays revealed a preference of the C2 domains for negatively charged phospholipids, especially phosphatidylinositol phosphates. Notably, the lipid overlay assays revealed enhanced binding to negatively charged lipids in the presence of Ca^{2+}. Liposome flotation assays with liposomes, mimicking the synaptic vesicle or the plasma membrane, demonstrated Ca^{2+}-dependent membrane interactions of the C2 domains. Specifically, C2A was not selective in its membrane interaction in the presence of Ca^{2+}, while C2B displayed a preference for the plasma membrane. MD simulations provided detailed insights into the dynamics of the interactions of the C2 domains with the two membranes. Lipid contacts and membrane selectivity were similar between the C2 domains. However, different orientations of the C2 domains on the membrane and their Ca^{2+}-dependent membrane insertion were identified. Remarkably, the presence of Ca^{2+} has major effects on the observed lipid interactions in lipid overlay assays, liposome flotation assays and MD simulations, however, an effect of Ca^{2+} was not detected by native MS analysis. As many protein-lipid interactions of peripheral membrane proteins depend on co-factors (e.g. phospholipase A2[203]

or phosphoinositide 3-kinase[204]), it is of great interest in the future to uncover the effects of co-factors during detergent-mediated lipid transfer.

The combined results suggest the following mechanism for Syt1: C2B binds to the presynaptic membrane in the absence and in the presence of Ca^{2+}, while C2A associates with the synaptic vesicle membrane and undergoes a Ca^{2+}-dependent shift from a parallel contact angle to a perpendicular orientation. This process causes tension in the flexible linker that connects the C2 domains, thereby pulling the two membranes together.

Unravelling the mechanism of lipid transfer from detergent-lipid micelles to peripheral membrane proteins would be of great benefit in the interpretation of observed protein-lipid interactions. A first step towards the elucidation of the mechanism will be investigating the interactions of the mixed detergent-lipid micelles with peripheral membrane proteins in solution. For instance, tryptophan fluorescence spectroscopy could be used to detect the integration into the hydrophobic interior of the micelle. There are many open questions concerning the mechanism; questions that arose from this thesis are: (i) Why does increasing the micelle concentration also increase complex formation, as previously demonstrated by Landreh et al. 2017[82], if non-specific aggregation is not the driving force behind protein-lipid complex formation? (ii) Does the efficiency of lipid transfer from mixed micelles depend on the detergent and lipid properties as well as the ion mode? (iii) What are the binding interfaces of the protein-lipid complexes? (iv) Would integration of a peripheral membrane protein into a detergent-lipid micelle influence the observed interactions? Addressing these questions in future studies would further evaluate the application of lipid transfer from detergent-lipid micelles as a suitable approach.

In conclusion, combining the results of **P2**, **P3** and **P4** suggests that protein-lipid interactions of peripheral membrane proteins can be successfully probed by native MS in combination with detergent-mediated lipid transfer. However, interactions involving both, a mixture of attractive and repulsive electrostatic interactions, like the interactions of LL-37-wt with zwitterionic PC 14:0/14:0 were not accurately assessed by native MS analysis. Furthermore, compared to complementary methods in solution, the technique was not able to determine the influence of Ca^{2+} on the lipid interactions of the C2 domains. A factor that was not discussed in detail, but which may be a concern, is the absence of a membrane in this technique. Notably, as for all direct ESI MS assays, special care should be taken in the selection of experimental conditions, including the ion mode, as they may distort the correlation between ion intensity and solution equilibrium. Accordingly, its broad applicability and reliability still requires further verification. Nonetheless, the results revealed that all non-covalent interactions in solution, including the hydrophobic effect, contribute to the ion intensity. Furthermore, native MS appears to be reliable for exploring interactions dominated by “simple” electrostatic interactions as revealed

by the lipid interactions of LL-37-pos and LL-37-neg. Finally, it must be stressed that this approach has the potential to become a valuable tool for the exploration of protein-lipid interactions formed by a variety of different non-covalent interactions.

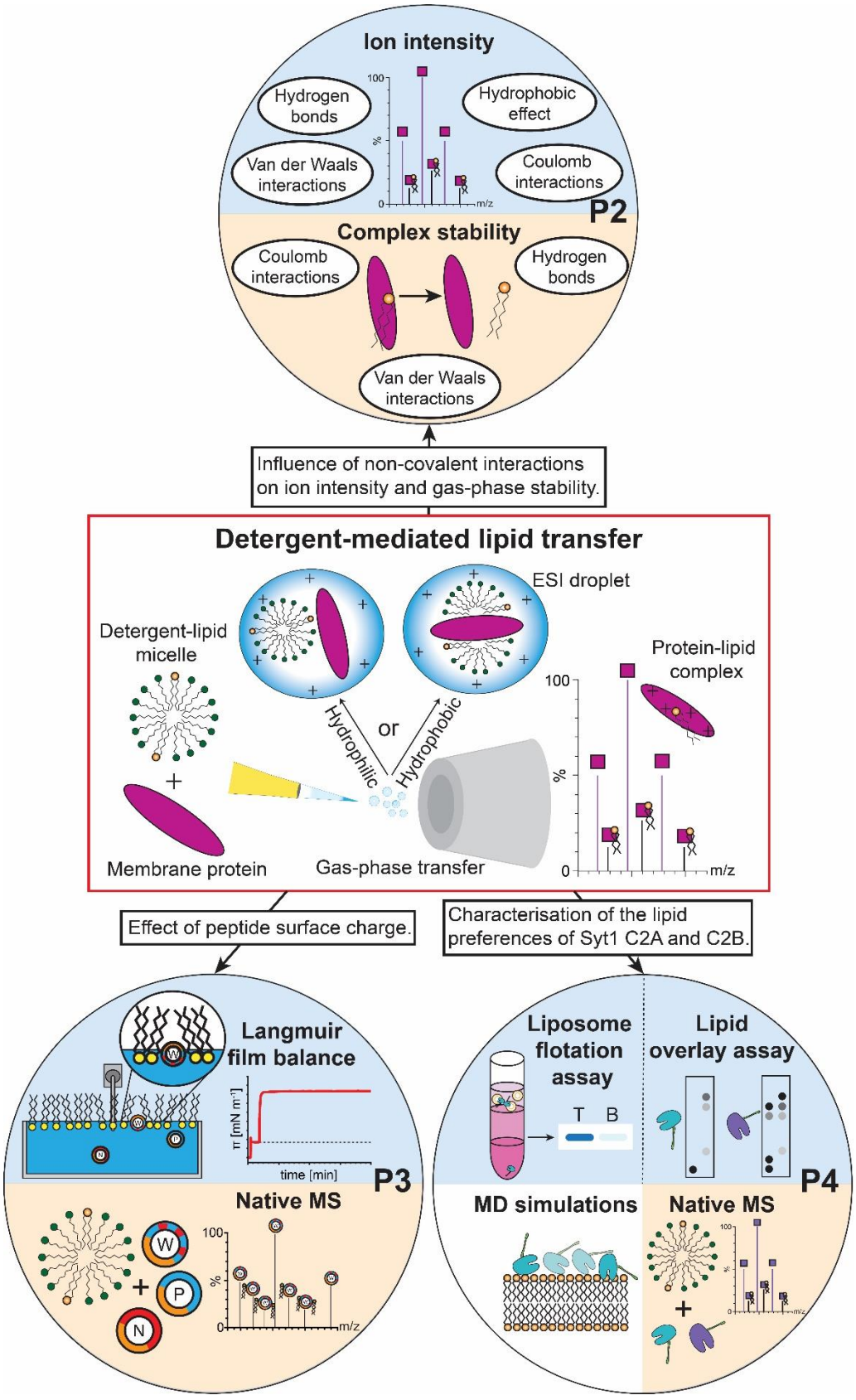

Figure 19: Graphical representation of the main topics of this thesis. Detergent-mediated lipid transfer[82] represents the central method of this thesis, which was employed and characterised in all publications. The employed methods can be further divided into gas phase (orange background), solution (blue background) or *in sillico* methods (white background).

Curriculum Vitae

Name: Til Erik Kundlacz

Date of birth: [redacted]

Place of birth: [redacted]

Nationality: German

Education

09/2021 - now	**PhD student** in Chemistry, Martin Luther University Halle-Wittenberg, Halle (Saale) Thesis: "On the impact of non-covalent interactions on the formation of protein-lipid complexes in the gas phase and in solution" Supervisor: Prof. Dr. Carla Schmidt & Prof. Dr. Dariush Hinderberger
10/2018 – 02/2021	**Master's degree** in Biochemistry, Martin Luther University Halle-Wittenberg, Halle (Saale) Thesis: "Lipid binding of Synaptotagmin-1 probed by native and ion mobility-mass spectrometry" Supervisor: Prof. Dr. Carla Schmidt
10/2015 – 10/2018	**Bachelor's degree** in Biochemistry, Martin Luther University Halle-Wittenberg, Halle (Saale) Thesis: "Hefe-Zwei-Hybrid Studien mit Rezeptorkinasen und ubiquitär exprimierten Phosphatidylinositol-4-Phosphat 5-kinasen aus *Arabidopsis*" Supervisor: Prof. Dr. Ingo Heilmann
2007 - 2015	**Abitur**, Geschwister-Scholl-Gymnasium, Sangerhausen

Complete publication list

Marie Barth, Julian Bender, **Til Kundlacz**, and Carla Schmidt (2020) Evaluation of different labelling strategies for structural analysis of protein complexes. *Journal of Proteomics*, vol. 222, p. 103793, https://doi.org/10.1016/j.jprot.2020.103793

Til Kundlacz*, Julian Bender*, Carla Schmidt (2021) Effects of non-ionic and zwitterionic detergents on soluble proteins during native mass spectrometry experiments. *International Journal of Mass Spectrometry*, vol. 468, p. 116652, https://doi.org/10.1016/j.ijms.2021.116652

Til Kundlacz, Carla Schmidt (2023) Deciphering Solution and Gas-Phase Interactions between Peptides and Lipids by native Mass Spectrometry. *Anal. Chem.*, 95, 47, 17292-17299. https://doi.org/10.1021/acs.analchem.3c03428

Julian Bender*, **Til Kundlacz***, Lucas S. P. Rudden, Melissa Frick, Julia Bieber, Matteo T. Degiacomi, Carla Schmidt (2024) Ca^{2+}-dependent lipid preferences shape synaptotagmin-1 C2A and C2B dynamics: Insights from experiments and simulations. *Structure*, vol. 32, issue 10, p. 1691-1704.e5, https://doi.org/10.1016/j.str.2024.07.017

Til Kundlacz, Christian Schwieger, Carla Schmidt (2025) Effects of Surface Charge of Amphiphilic Peptides on Peptide-Lipid Interactions in the Gas Phase and in Solutions. *Anal. Chem.*, https://doi.org/10.1021/acs.analchem.5c00283

Oral presentations

1st BEAM Retreat, 07. - 08.04.2022 (Location: Dessau, Germany)

Investigation of protein-lipid interactions by native mass spectrometry

HALOmem International Meeting: Membrane protein structure and dynamics, 15. - 16.09.2022 (Location: Halle (Saale), Germany)

Deciphering solution and gas-phase interactions between proteins and lipids by native mass spectrometry

33rd Sanibel Conference of Mass Spectrometry: Membrane Proteins and Their Complexes: MS and Beyond (by American society for mass spectrometry), 20. - 22.01.2023 (Location: St. Pete Beach, Florida, USA)

Deciphering solution and gas-phase interactions using native mass spectrometry

1st Beam Symposium, 06. - 08.09.2023 (Location: Halle (Saale), Germany)

Deciphering solution and gas-phase interactions between proteins and lipids by native mass spectrometry

3rd BEAM Retreat, 18. - 19.04.2024 (Location: Erfurt, Germany)

Deciphering Solution and Gas-Phase Interactions between Peptides and Lipids

DFG Defence of RTG 2670 (BEAM), 13. – 14.02.2025 (Location: Halle (Saale), Germany)

On the Effects of Surface Charge of Amphiphilic Peptides on Peptide-Lipid Interactions in the Gas Phase and in Solution

Poster presentations

EMBO Conference: Recent advances in structural biology of membrane proteins, 29.11 - 01.12.2021 (Location: Online)

Characterising the interaction of proteins with polyphilic detergents and lipids and their impact on membrane self-assembly

33rd Sanibel Conference of Mass Spectrometry: Membrane Proteins and Their Complexes: MS and Beyond **(**by American society for mass spectrometry), 20. - 22.01.2023 (Location: St. Pete Beach, Florida, USA)

Deciphering solution and gas-phase interactions using native mass spectrometry

55th Annual conference of the DGMS (German Society of Mass Spectrometry), 10. - 13.03.2024 (Location: Freising, Germany)

Deciphering Solution and Gas-phase Interactions between Peptides and Lipids by Native Mass Spectrometry

72nd Annual conference of the ASMS (American society for mass spectrometry), 01. - 06.06.2024 (Location: Anaheim, California, USA)

Exploring Interactions Between Differently Charged LL-37 Variants and Lipids by Native Mass Spectrometry

DFG Defence of RTG 2670 (BEAM), 13. – 14.02.2025 (Location: Halle (Saale), Germany)

On the Effects of Surface Charge of Amphiphilic Peptides on Peptide-Lipid Interactions in the Gas Phase and in Solution.

Eidesstattliche Erklärung

Ich versichere hiermit, dass die vorliegende Dissertation unabhängig und ohne fremde Hilfe angefertigt wurde. Es wurden keine Quellen oder Hilfsmittel außer die angegebenen verwendet. Von anderen Personen bereitgestellte Materialien und durchgeführte Experimente wurden als solche erkenntlich gemacht. Weiterhin entspricht die vorgelegte Arbeit der elektronischen Version. Ich versichere, dass diese oder eine ähnliche Dissertation nicht bereits zum Zwecke einer Promotion eingereicht wurde. Vor dieser Arbeit habe ich keine früheren Promotionsversuche unternommen.

Til Erik Kundlacz
Halle (Saale)
11.03.2025

Acknowledgement

First and foremost, I would like to thank Prof. Dr. Carla Schmidt for her support and for giving me the opportunity to work in the fascinating field of mass spectrometry. I am very grateful for her guidance, our insightful discussions, her valuable feedback and her open-door policy that helped me learn and grow as a scientist during this work. I also wish to express my gratitude for the opportunities to participate in national and international conferences and to publish our work in prestigious journals. I am especially grateful that Carla continued to be my scientific supervisor despite her move to Mainz and despite starting a new group.

Second, I would like to thank all reviewers for reviewing this thesis.

I would also like to thank former and current group members of AG Schmidt: Julia, Julian, Marie, Melissa, Tommy, Christian, Sarah, Elisa, Gihyun, Zahra, Federico, Rita, Leonie, Lea and Toni for the thoughtful scientific discussions and for creating an overall great working environment. I am also grateful for the time I spend with everyone outside the lab, be it on away days, conferences, cake breaks, paper parties, Carla's famous Christmas dinners or simply over lunch. A special thank you to Julia for the camaraderie we have shared throughout all this time, for insightful discussions, and for being a beacon of positivity. My special thanks also go to Julian, who had a major part in setting me on the path of native MS during my Master's thesis and provided me with a solid foundation to build on during my PhD.

I would also like to express my gratitude to Prof. Dr. Dariush Hinderberger for taking over the official supervision of my dissertation, for great scientific discussions and encouraging scientific collaborations. I am also grateful to Prof. Dr. Milton Stubbs and his group for not only sharing their lab and office space with me, but also for the great time and the cakes we enjoyed together. I am particularly thankful to Dr. Annette Meister and Dr. Christian Schwieger for their support, great scientific exchange and for sharing their expertise in the fields of lipids and biophysics. I would also like to thank Ulla and Luise for their support in navigating the university bureaucracy and fun conversations.

I consider myself fortunate to have been part of a great scientific environment in the RTG 2670 "Beyond Amphiphilicity: Self-Organization of Soft Matter via Multiple Noncovalent Interactions" (BEAM). Therefore, I would like to thank all BEAM members, the speaker of the RTG Dariush as well as the former and current scientific and administrative coordinators: Kristin, Imme and Nicole. I greatly benefited from the wide variety of lectures, workshops and events offered by BEAM. This project was generously funded by the Deutsche Forschungsgemeinschaft (DFG project number 436494874).

Finally, I am very grateful for the love and support of my family and friends over the years. I am particularly grateful to my girlfriend Danila for her encouragement, support and belief in me.

Til Erik Kundlacz

References

(1) Nakamura, Y. Plant Phospholipid Diversity: Emerging Functions in Metabolism and Protein-Lipid Interactions. *Trends Plant Sci* **2017**, *22*, 1027–1040.
(2) Cho, W.; Stahelin, R. V. Membrane-protein interactions in cell signaling and membrane trafficking. *Annu Rev Biophys Biomol Struct* **2005**, *34*, 119–151.
(3) Maffeo, C.; Bhattacharya, S.; Yoo, J.; Wells, D.; Aksimentiev, A. Modeling and simulation of ion channels. *Chem Rev* **2012**, *112*, 6250–6284.
(4) Pawson, T.; Nash, P. Protein–protein interactions define specificity in signal transduction. *Genes Dev.* **2000**, *14*, 1027–1047.
(5) Oren, Z.; Lerman, J. C.; Gudmundsson, G. H.; Agerberth, B.; Shai, Y. Structure and organization of the human antimicrobial peptide LL-37 in phospholipid membranes: relevance to the molecular basis for its non-cell-selective activity. *Biochem J* **1999**, *341 (Pt 3)*, 501–513.
(6) Saliba, A.-E.; Vonkova, I.; Gavin, A.-C. The systematic analysis of protein-lipid interactions comes of age. *Nat Rev Mol Cell Biol* **2015**, *16*, 753–761.
(7) Mulgrew-Nesbitt, A.; Diraviyam, K.; Wang, J.; Singh, S.; Murray, P.; Li, Z.; Rogers, L.; Mirkovic, N.; Murray, D. The role of electrostatics in protein-membrane interactions. *Biochim Biophys Acta* **2006**, *1761*, 812–826.
(8) Dathe, M.; Schümann, M.; Wieprecht, T.; Winkler, A.; Beyermann, M.; Krause, E.; Matsuzaki, K.; Murase, O.; Bienert, M. Peptide helicity and membrane surface charge modulate the balance of electrostatic and hydrophobic interactions with lipid bilayers and biological membranes. *Biochemistry* **1996**, *35*, 12612–12622.
(9) White, S. H.; Wimley, W. C. Hydrophobic interactions of peptides with membrane interfaces. *Biochim Biophys Acta* **1998**, *1376*, 339–352.
(10) Zhao, H.; Lappalainen, P. A simple guide to biochemical approaches for analyzing protein-lipid interactions. *Mol Biol Cell* **2012**, *23*, 2823–2830.
(11) Gault, J.; Donlan, J. A. C.; Liko, I.; Hopper, J. T. S.; Gupta, K.; Housden, N. G.; Struwe, W. B.; Marty, M. T.; Mize, T.; Bechara, C.; Zhu, Y.; Wu, B.; Kleanthous, C.; Belov, M.; Damoc, E.; Makarov, A.; Robinson, C. V. High-resolution mass spectrometry of small molecules bound to membrane proteins. *Nat Methods* **2016**, *13*, 333–336.
(12) Zhou, M.; Morgner, N.; Barrera, N. P.; Politis, A.; Isaacson, S. C.; Matak-Vinković, D.; Murata, T.; Bernal, R. A.; Stock, D.; Robinson, C. V. Mass spectrometry of intact V-type ATPases reveals bound lipids and the effects of nucleotide binding. *Science* **2011**, *334*, 380–385.
(13) Barrera, N. P.; Isaacson, S. C.; Zhou, M.; Bavro, V. N.; Welch, A.; Schaedler, T. A.; Seeger, M. A.; Miguel, R. N.; Korkhov, V. M.; van Veen, H. W.; Venter, H.; Walmsley, A. R.; Tate, C. G.; Robinson, C. V. Mass spectrometry of membrane transporters reveals subunit stoichiometry and interactions. *Nat Methods* **2009**, *6*, 585–587.
(14) Demmers, J. A. A.; van Dalen, A.; Kruijff, B. de; Heck, A. J. R.; Killian, J. A. Interaction of the K+ channel KcsA with membrane phospholipids as studied by ESI mass spectrometry. *FEBS Lett* **2003**, *541*, 28–32.
(15) Israelachvili, J. N. *Intermolecular and Surface Forces*; Elsevier, 2011.
(16) Davies, M. In Some Electrical and Optical Aspects of Molecular Behaviour; Elsevier, 1965; pp. 8–40.
(17) Lee, A. G. Lipid-protein interactions in biological membranes: a structural perspective. *Biochim Biophys Acta* **2003**, *1612*, 1–40.
(18) Lennard-Jones, J. E. Cohesion. *Proc. Phys. Soc.* **1931**, *43*, 461–482.
(19) Pauli, W. Über den Zusammenhang des Abschlusses der Elektronengruppen im Atom mit der Komplexstruktur der Spektren. *Z. Physik* **1925**, *31*, 765–783.
(20) Kimmich, R. *Principles of Soft-Matter Dynamics*; Springer Netherlands: Dordrecht, 2012.

(21) Bhushan, B.; Israelachvili, J. N.; Landman, U. Nanotribology: friction, wear and lubrication at the atomic scale. *Nature* **1995**, *374*, 607–616.
(22) Baker, E. N.; Hubbard, R. E. Hydrogen bonding in globular proteins. *Prog Biophys Mol Biol* **1984**, *44*, 97–179.
(23) Hubbard, R. E.; Kamran Haider, M. In Encyclopedia of Life Sciences; Wiley, 2005.
(24) Chandler, D. Interfaces and the driving force of hydrophobic assembly. *Nature* **2005**, *437*, 640–647.
(25) Tanford, C. *The hydrophobic effect*; Wiley: New York, 1973.
(26) Erba, E. B.; Zenobi, R. Mass spectrometric studies of dissociation constants of noncovalent complexes. *Annu. Rep. Prog. Chem., Sect. C: Phys. Chem.* **2011**, *107*, 199.
(27) Schalley, C. A. Molecular recognition and supramolecular chemistry in the gas phase. *Mass Spectrom. Rev.* **2001**, *20*, 253–309.
(28) Kohtani, M.; Jones, T. C.; Schneider, J. E.; Jarrold, M. F. Extreme stability of an unsolvated alpha-helix. *J Am Chem Soc* **2004**, *126*, 7420–7421.
(29) Robinson, C. V.; Chung, E. W.; Kragelund, B. B.; Knudsen, J.; Aplin, R. T.; Poulsen, F. M.; Dobson, C. M. Probing the Nature of Noncovalent Interactions by Mass Spectrometry. A Study of Protein−CoA Ligand Binding and Assembly. *J Am Chem Soc* **1996**, *118*, 8646–8653.
(30) Yin, S.; Xie, Y.; Loo, J. A. Mass spectrometry of protein-ligand complexes: enhanced gas-phase stability of ribonuclease-nucleotide complexes. *J Am Soc Mass Spectrom* **2008**, *19*, 1199–1208.
(31) Karas, M.; Bachmann, D.; Bahr, U.; Hillenkamp, F. Matrix-assisted ultraviolet laser desorption of non-volatile compounds. *Int J Mass Spectrom Ion Processes* **1987**, *78*, 53–68.
(32) Fenn, J. B.; Mann, M.; Meng, C. K.; Wong, S. F.; Whitehouse, C. M. Electrospray ionization for mass spectrometry of large biomolecules. *Science* **1989**, *246*, 64–71.
(33) Yamashita, M.; Fenn, J. B. Electrospray ion source. Another variation on the free-jet theme. *J. Phys. Chem.* **1984**, *88*, 4451–4459.
(34) Taylor, G. I. Disintegration of water drops in an electric field. *Proc. R. Soc. Lond. A* **1964**, *280*, 383–397.
(35) Wu, X.; Oleschuk, R. D.; Cann, N. M. Characterization of microstructured fibre emitters: in pursuit of improved nano electrospray ionization performance. *Analyst* **2012**, *137*, 4150–4161.
(36) Rayleigh. XX. On the equilibrium of liquid conducting masses charged with electricity. *The London, Edinburgh, and Dublin Philosophical Magazine and Journal of Science* **1882**, *14*, 184–186.
(37) Konermann, L.; Ahadi, E.; Rodriguez, A. D.; Vahidi, S. Unraveling the mechanism of electrospray ionization. *Anal Chem* **2013**, *85*, 2–9.
(38) Peschke, M.; Verkerk, U. H.; Kebarle, P. Features of the ESI mechanism that affect the observation of multiply charged noncovalent protein complexes and the determination of the association constant by the titration method. *J Am Soc Mass Spectrom* **2004**, *15*, 1424–1434.
(39) Kebarle, P.; Verkerk, U. H. Electrospray: from ions in solution to ions in the gas phase, what we know now. *Mass Spectrom Rev* **2009**, *28*, 898–917.
(40) Wilm, M.; Mann, M. Analytical properties of the nanoelectrospray ion source. *Anal Chem* **1996**, *68*, 1–8.
(41) Wilm, M. S.; Mann, M. Electrospray and Taylor-Cone theory, Dole's beam of macromolecules at last? *Int J Mass Spectrom Ion Processes* **1994**, *136*, 167–180.
(42) Iribarne, J. V. On the evaporation of small ions from charged droplets. *The Journal of Chemical Physics* **1976**, *64*, 2287.
(43) Dole, M.; Mack, L. L.; Hines, R. L.; Mobley, R. C.; Ferguson, L. D.; Alice, M. B. Molecular Beams of Macroions. *The Journal of Chemical Physics* **1968**, *49*, 2240–2249.

(44) Mack, L. L.; Kralik, P.; Rheude, A.; Dole, M. Molecular Beams of Macroions. II. *The Journal of Chemical Physics* **1970**, *52*, 4977–4986.
(45) Thomson, B. A.; Iribarne, J. V. Field induced ion evaporation from liquid surfaces at atmospheric pressure. *The Journal of Chemical Physics* **1979**, *71*, 4451–4463.
(46) Wilm, M. Principles of electrospray ionization. *Mol Cell Proteomics* **2011**, *10*, M111.009407.
(47) Daub, C. D.; Cann, N. M. How are completely desolvated ions produced in electrospray ionization: insights from molecular dynamics simulations. *Anal Chem* **2011**, *83*, 8372–8376.
(48) Iavarone, A. T.; Williams, E. R. Mechanism of charging and supercharging molecules in electrospray ionization. *J Am Chem Soc* **2003**, *125*, 2319–2327.
(49) Hogan, C. J.; Carroll, J. A.; Rohrs, H. W.; Biswas, P.; Gross, M. L. Combined charged residue-field emission model of macromolecular electrospray ionization. *Anal Chem* **2009**, *81*, 369–377.
(50) Testa, L.; Brocca, S.; Grandori, R. Charge-surface correlation in electrospray ionization of folded and unfolded proteins. *Anal Chem* **2011**, *83*, 6459–6463.
(51) La Fernandez de Mora, J. Electrospray ionization of large multiply charged species proceeds via Dole's charged residue mechanism. *Analytica Chimica Acta* **2000**, *406*, 93–104.
(52) McAllister, R. G.; Metwally, H.; Sun, Y.; Konermann, L. Release of Native-like Gaseous Proteins from Electrospray Droplets via the Charged Residue Mechanism: Insights from Molecular Dynamics Simulations. *Journal of the American Chemical Society* **2015**, *137*, 12667–12676.
(53) Chowdhury, S. K.; Katta, V.; Chait, B. T. Probing conformational changes in proteins by mass spectrometry. *Journal of the American Chemical Society* **1990**, *112*, 9012–9013.
(54) Ahadi, E.; Konermann, L. Modeling the behavior of coarse-grained polymer chains in charged water droplets: implications for the mechanism of electrospray ionization. *J Phys Chem B* **2012**, *116*, 104–112.
(55) Paul, W.; Steinwedel, H. Notizen: Ein neues Massenspektrometer ohne Magnetfeld. *Zeitschrift für Naturforschung A* **1953**, *8*, 448–450.
(56) Wolff, M. M.; Stephens, W. E. A Pulsed Mass Spectrometer with Time Dispersion. *Review of Scientific Instruments* **1953**, *24*, 616–617.
(57) Makarov, A. Electrostatic axially harmonic orbital trapping: a high-performance technique of mass analysis. *Anal Chem* **2000**, *72*, 1156–1162.
(58) Paul, W. Electromagnetic traps for charged and neutral particles. *Rev. Mod. Phys.* **1990**, *62*, 531–540.
(59) Marshall, A. G.; Hendrickson, C. L.; Jackson, G. S. Fourier transform ion cyclotron resonance mass spectrometry: A primer. *Mass Spectrom. Rev.* **1998**, *17*, 1–35.
(60) Cotter, R. J. Peer Reviewed: The New Time-of-Flight Mass Spectrometry. *Anal Chem* **1999**, *71*, 445A-51A.
(61) Mamyrin, B. A.; Karataev, V. I.; Shmikk, D. V.; Zagulin, V. A. The mass-reflectron, a new nonmagnetic time-of-flight mass spectrometer with high resolution. *Soviet Physics JETP* **1973**, 82–89.
(62) Sobott, F.; Hernández, H.; McCammon, M. G.; Tito, M. A.; Robinson, C. V. A tandem mass spectrometer for improved transmission and analysis of large macromolecular assemblies. *Anal Chem* **2002**, *74*, 1402–1407.
(63) Allen, J. S. An Improved Electron Multiplier Particle Counter. *Review of Scientific Instruments* **1947**, *18*, 739–749.
(64) Ladislas Wiza, J. Microchannel plate detectors. *Nuclear Instruments and Methods* **1979**, *162*, 587–601.
(65) Olsen, J. V.; Macek, B.; Lange, O.; Makarov, A.; Horning, S.; Mann, M. Higher-energy C-trap dissociation for peptide modification analysis. *Nat Methods* **2007**, *4*, 709–712.

(66) Syka, J. E. P.; Coon, J. J.; Schroeder, M. J.; Shabanowitz, J.; Hunt, D. F. Peptide and protein sequence analysis by electron transfer dissociation mass spectrometry. *PNAS* **2004**, *101*, 9528–9533.
(67) Jennings, K. R. Collision-induced decompositions of aromatic molecular ions. *International Journal of Mass Spectrometry and Ion Physics* **1968**, *1*, 227–235.
(68) Senko, M. W.; Speir, J. P.; McLafferty, F. W. Collisional activation of large multiply charged ions using Fourier transform mass spectrometry. *Anal Chem* **1994**, *66*, 2801–2808.
(69) Ruotolo, B. T.; Giles, K.; Campuzano, I.; Sandercock, A. M.; Bateman, R. H.; Robinson, C. V. Evidence for macromolecular protein rings in the absence of bulk water. *Science* **2005**, *310*, 1658–1661.
(70) Pan, P.; McLuckey, S. A. The effect of small cations on the positive electrospray responses of proteins at low pH. *Anal Chem* **2003**, *75*, 5468–5474.
(71) Hernández, H.; Dziembowski, A.; Taverner, T.; Séraphin, B.; Robinson, C. V. Subunit architecture of multimeric complexes isolated directly from cells. *EMBO Rep* **2006**, *7*, 605–610.
(72) Sobott, F.; Robinson, C. V. Characterising electrosprayed biomolecules using tandem-MS—the noncovalent GroEL chaperonin assembly. *Int J Mass Spectrom* **2004**, *236*, 25–32.
(73) Marty, M. T.; Baldwin, A. J.; Marklund, E. G.; Hochberg, G. K. A.; Benesch, J. L. P.; Robinson, C. V. Bayesian deconvolution of mass and ion mobility spectra: from binary interactions to polydisperse ensembles. *Anal Chem* **2015**, *87*, 4370–4376.
(74) Morgner, N.; Robinson, C. V. Massign: an assignment strategy for maximizing information from the mass spectra of heterogeneous protein assemblies. *Anal Chem* **2012**, *84*, 2939–2948.
(75) Benesch, J. L. P.; Ruotolo, B. T.; Simmons, D. A.; Robinson, C. V. Protein complexes in the gas phase: technology for structural genomics and proteomics. *Chem Rev* **2007**, *107*, 3544–3567.
(76) Laganowsky, A.; Reading, E.; Allison, T. M.; Ulmschneider, M. B.; Degiacomi, M. T.; Baldwin, A. J.; Robinson, C. V. Membrane proteins bind lipids selectively to modulate their structure and function. *Nature* **2014**, *510*, 172–175.
(77) Barrera, N. P.; Di Bartolo, N.; Booth, P. J.; Robinson, C. V. Micelles protect membrane complexes from solution to vacuum. *Science* **2008**, *321*, 243–246.
(78) Reading, E.; Liko, I.; Allison, T. M.; Benesch, J. L. P.; Laganowsky, A.; Robinson, C. V. The role of the detergent micelle in preserving the structure of membrane proteins in the gas phase. *Angew Chem Int Ed Engl* **2015**, *54*, 4577–4581.
(79) Gupta, K.; Li, J.; Liko, I.; Gault, J.; Bechara, C.; Di Wu; Hopper, J. T. S.; Giles, K.; Benesch, J. L. P.; Robinson, C. V. Identifying key membrane protein lipid interactions using mass spectrometry. *Nat Protoc* **2018**, *13*, 1106–1120.
(80) Reading, E.; Walton, T. A.; Liko, I.; Marty, M. T.; Laganowsky, A.; Rees, D. C.; Robinson, C. V. The Effect of Detergent, Temperature, and Lipid on the Oligomeric State of MscL Constructs: Insights from Mass Spectrometry. *Chem Biol* **2015**, *22*, 593–603.
(81) Laganowsky, A.; Reading, E.; Hopper, J. T. S.; Robinson, C. V. Mass spectrometry of intact membrane protein complexes. *Nat Protoc* **2013**, *8*, 639–651.
(82) Landreh, M.; Costeira-Paulo, J.; Gault, J.; Marklund, E. G.; Robinson, C. V. Effects of Detergent Micelles on Lipid Binding to Proteins in Electrospray Ionization Mass Spectrometry. *Anal Chem* **2017**, *89*, 7425–7430.
(83) Einstein, A. Über die von der molekularkinetischen Theorie der Wärme geforderte Bewegung von in ruhenden Flüssigkeiten suspendierten Teilchen. *Annalen der Physik* **1905**, *322*, 549–560.
(84) Hassan, P. A.; Rana, S.; Verma, G. Making sense of Brownian motion: colloid characterization by dynamic light scattering. *Langmuir* **2015**, *31*, 3–12.
(85) Wyatt, P. J. Light scattering and the absolute characterization of macromolecules. *Analytica Chimica Acta* **1993**, *272*, 1–40.

(86) Stetefeld, J.; McKenna, S. A.; Patel, T. R. Dynamic light scattering: a practical guide and applications in biomedical sciences. *Biophys Rev* **2016**, *8*, 409–427.
(87) Einstein, A. Zur Theorie der Brownschen Bewegung. *Annalen der Physik* **1906**, *324*, 371–381.
(88) Möhwald, H. Phospholipid and phospholipid-protein monolayers at the air/water interface. *Annu Rev Phys Chem* **1990**, *41*, 441–476.
(89) Brockman, H. Lipid monolayers: why use half a membrane to characterize protein-membrane interactions? *Curr Opin Struct Biol* **1999**, *9*, 438–443.
(90) Blume, A. Lipids at the air–water interface. *ChemTexts* **2018**, *4*.
(91) Maget-Dana, R. The monolayer technique: a potent tool for studying the interfacial properties of antimicrobial and membrane-lytic peptides and their interactions with lipid membranes. *Biochim Biophys Acta* **1999**, *1462*, 109–140.
(92) Calvez, P.; Bussières, S.; Eric, D.; Salesse, C. Parameters modulating the maximum insertion pressure of proteins and peptides in lipid monolayers. *Biochimie* **2009**, *91*, 718–733.
(93) Demel, R. A.; van Geurts Kessel, W. S.; Zwaal, R. F.; Roelofsen, B.; van Deenen, L. L. Relation between various phospholipase actions on human red cell membranes and the interfacial phospholipid pressure in monolayers. *Biochim Biophys Acta* **1975**, *406*, 97–107.
(94) Marsh, D. Lateral pressure in membranes. *Biochim Biophys Acta* **1996**, *1286*, 183–223.
(95) Seelig, A. Local anesthetics and pressure: a comparison of dibucaine binding to lipid monolayers and bilayers. *Biochim Biophys Acta* **1987**, *899*, 196–204.
(96) Blume, A.; Eibl, H. The influence of charge on bilayer membranes. Calorimetric investigations of phosphatidic acid bilayers. *Biochim Biophys Acta* **1979**, *558*, 13–21.
(97) Giehl, A.; Lemm, T.; Bartelsen, O.; Sandhoff, K.; Blume, A. Interaction of the GM2-activator protein with phospholipid-ganglioside bilayer membranes and with monolayers at the air-water interface. *Eur J Biochem* **1999**, *261*, 650–658.
(98) van Meer, G.; Voelker, D. R.; Feigenson, G. W. Membrane lipids: where they are and how they behave. *Nat Rev Mol Cell Biol* **2008**, *9*, 112–124.
(99) Harayama, T.; Riezman, H. Understanding the diversity of membrane lipid composition. *Nat Rev Mol Cell Biol* **2018**, *19*, 281–296.
(100) Lemmon, M. A.; Ferguson, K. M. Signal-dependent membrane targeting by pleckstrin homology (PH) domains. *Biochem J* **2000**, *350*, 1–18.
(101) Radek, K.; Gallo, R. Antimicrobial peptides: natural effectors of the innate immune system. *Semin Immunopathol* **2007**, *29*, 27–43.
(102) Boman, H. G. Antibacterial peptides: key components needed in immunity. *Cell* **1991**, *65*, 205–207.
(103) Huan, Y.; Kong, Q.; Mou, H.; Yi, H. Antimicrobial Peptides: Classification, Design, Application and Research Progress in Multiple Fields. *Front Microbiol* **2020**, *11*, 582779.
(104) Brogden, K. A.; Ackermann, M.; McCray, P. B.; Tack, B. F. Antimicrobial peptides in animals and their role in host defences. *Int J Antimicrob Agents* **2003**, *22*, 465–478.
(105) Sohlenkamp, C.; Geiger, O. Bacterial membrane lipids: diversity in structures and pathways. *FEMS Microbiology Reviews* **2016**, *40*, 133–159.
(106) Shai, Y. Mechanism of the binding, insertion and destabilization of phospholipid bilayer membranes by alpha-helical antimicrobial and cell non-selective membrane-lytic peptides. *Biochim Biophys Acta* **1999**, *1462*, 55–70.
(107) Zasloff, M. Antimicrobial peptides of multicellular organisms. *Nature* **2002**, *415*, 389–395.
(108) Henzler-Wildman, K. A.; Martinez, G. V.; Brown, M. F.; Ramamoorthy, A. Perturbation of the hydrophobic core of lipid bilayers by the human antimicrobial peptide LL-37. *Biochemistry* **2004**, *43*, 8459–8469.
(109) Sani, M.-A.; Separovic, F. How Membrane-Active Peptides Get into Lipid Membranes. *Acc Chem Res* **2016**, *49*, 1130–1138.

(110) Dürr, U. H. N.; Sudheendra, U. S.; Ramamoorthy, A. LL-37, the only human member of the cathelicidin family of antimicrobial peptides. *Biochim Biophys Acta* **2006**, *1758*, 1408–1425.
(111) Wang, G. Structures of human host defense cathelicidin LL-37 and its smallest antimicrobial peptide KR-12 in lipid micelles. *J Biol Chem* **2008**, *283*, 32637–32643.
(112) Sato, H.; Feix, J. B. Peptide-membrane interactions and mechanisms of membrane destruction by amphipathic alpha-helical antimicrobial peptides. *Biochim Biophys Acta* **2006**, *1758*, 1245–1256.
(113) Dathe, M.; Wieprecht, T. Structural features of helical antimicrobial peptides: their potential to modulate activity on model membranes and biological cells. *Biochim Biophys Acta* **1999**, *1462*, 71–87.
(114) Ladokhin, A. S.; White, S. H. Folding of amphipathic alpha-helices on membranes: energetics of helix formation by melittin. *J Mol Biol* **1999**, *285*, 1363–1369.
(115) Johansson, J.; Gudmundsson, G. H.; Rottenberg, M. E.; Berndt, K. D.; Agerberth, B. Conformation-dependent antibacterial activity of the naturally occurring human peptide LL-37. *J Biol Chem* **1998**, *273*, 3718–3724.
(116) Li, J.; Koh, J.-J.; Liu, S.; Lakshminarayanan, R.; Verma, C. S.; Beuerman, R. W. Membrane Active Antimicrobial Peptides: Translating Mechanistic Insights to Design. *Front Neurosci* **2017**, *11*, 73.
(117) Sood, R.; Domanov, Y.; Pietiäinen, M.; Kontinen, V. P.; Kinnunen, P. K. J. Binding of LL-37 to model biomembranes: insight into target vs host cell recognition. *Biochim Biophys Acta* **2008**, *1778*, 983–996.
(118) Henzler Wildman, K. A.; Lee, D.-K.; Ramamoorthy, A. Mechanism of lipid bilayer disruption by the human antimicrobial peptide, LL-37. *Biochemistry* **2003**, *42*, 6545–6558.
(119) Eisenberg, D.; Schwarz, E.; Komaromy, M.; Wall, R. Analysis of membrane and surface protein sequences with the hydrophobic moment plot. *J Mol Biol* **1984**, *179*, 125–142.
(120) Gautier, R.; Douguet, D.; Antonny, B.; Drin, G. HELIQUEST: a web server to screen sequences with specific alpha-helical properties. *Bioinformatics* **2008**, *24*, 2101–2102.
(121) Kundlacz, T.; Schmidt, C. Deciphering Solution and Gas-Phase Interactions between Peptides and Lipids by Native Mass Spectrometry. *Anal Chem* **2023**, *95*, 17292–17299.
(122) Katz, B. *The release of neutral transmitter substances*; Liverpool University Press: [Liverpool], 1969.
(123) Takamori, S.; Holt, M.; Stenius, K.; Lemke, E. A.; Grønborg, M.; Riedel, D.; Urlaub, H.; Schenck, S.; Brügger, B.; Ringler, P.; Müller, S. A.; Rammner, B.; Gräter, F.; Hub, J. S.; Groot, B. L. de; Mieskes, G.; Moriyama, Y.; Klingauf, J.; Grubmüller, H.; Heuser, J.; Wieland, F.; Jahn, R. Molecular anatomy of a trafficking organelle. *Cell* **2006**, *127*, 831–846.
(124) Südhof, T. C. The synaptic vesicle cycle. *Annu Rev Neurosci* **2004**, *27*, 509–547.
(125) Söllner, T.; Whiteheart, S. W.; Brunner, M.; Erdjument-Bromage, H.; Geromanos, S.; Tempst, P.; Rothman, J. E. SNAP receptors implicated in vesicle targeting and fusion. *Nature* **1993**, *362*, 318–324.
(126) Söllner, T.; Bennett, M. K.; Whiteheart, S. W.; Scheller, R. H.; Rothman, J. E. A protein assembly-disassembly pathway in vitro that may correspond to sequential steps of synaptic vesicle docking, activation, and fusion. *Cell* **1993**, *75*, 409–418.
(127) Sutton, R. B.; Fasshauer, D.; Jahn, R.; Brunger, A. T. Crystal structure of a SNARE complex involved in synaptic exocytosis at 2.4 A resolution. *Nature* **1998**, *395*, 347–353.
(128) Fernández-Chacón, R.; Königstorfer, A.; Gerber, S. H.; García, J.; Matos, M. F.; Stevens, C. F.; Brose, N.; Rizo, J.; Rosenmund, C.; Südhof, T. C. Synaptotagmin I functions as a calcium regulator of release probability. *Nature* **2001**, *410*, 41–49.
(129) Xu, J.; Mashimo, T.; Südhof, T. C. Synaptotagmin-1, -2, and -9: Ca(2+) sensors for fast release that specify distinct presynaptic properties in subsets of neurons. *Neuron* **2007**, *54*, 567–581.

(130) Perin, M. S.; Fried, V. A.; Mignery, G. A.; Jahn, R.; Südhof, T. C. Phospholipid binding by a synaptic vesicle protein homologous to the regulatory region of protein kinase C. *Nature* **1990**, *345*, 260–263.
(131) Fuson, K. L.; Montes, M.; Robert, J. J.; Sutton, R. B. Structure of human synaptotagmin 1 C2AB in the absence of Ca2+ reveals a novel domain association. *Biochemistry* **2007**, *46*, 13041–13048.
(132) Shao, X.; Fernandez, I.; Südhof, T. C.; Rizo, J. Solution structures of the Ca2+-free and Ca2+-bound C2A domain of synaptotagmin I: does Ca2+ induce a conformational change? *Biochemistry* **1998**, *37*, 16106–16115.
(133) Sutton, R.B.; Davletov, B. A.; Berghuis, A. M.; Sudhof, T. C.; Sprang, S. R. Structure of the first C2 domain of synaptotagmin I: A novel Ca2+/phospholipid-binding fold. *Cell* **1995**, *80*, 929–938.
(134) Fernandez, I.; Araç, D.; Ubach, J.; Gerber, S. H.; Shin, O.-H.; Gao, Y.; Anderson, R. G.W.; Südhof, T. C.; Rizo, J. Three-Dimensional Structure of the Synaptotagmin 1 C2B-Domain. *Neuron* **2001**, *32*, 1057–1069.
(135) Ubach, J.; Zhang, X.; Shao, X.; Südhof, T. C.; Rizo, J. Ca2+ binding to synaptotagmin: how many Ca2+ ions bind to the tip of a C2-domain? *EMBO J* **1998**, *17*, 3921–3930.
(136) Pérez-Lara, Á.; Thapa, A.; Nyenhuis, S. B.; Nyenhuis, D. A.; Halder, P.; Tietzel, M.; Tittmann, K.; Cafiso, D. S.; Jahn, R. PtdInsP2 and PtdSer cooperate to trap synaptotagmin-1 to the plasma membrane in the presence of calcium. *Elife* **2016**, *5*.
(137) Zhang, X.; Rizo, J.; Südhof, T. C. Mechanism of phospholipid binding by the C2A-domain of synaptotagmin I. *Biochemistry* **1998**, *37*, 12395–12403.
(138) Schiavo, G.; Gu, Q. M.; Prestwich, G. D.; Söllner, T. H.; Rothman, J. E. Calcium-dependent switching of the specificity of phosphoinositide binding to synaptotagmin. *Proc Natl Acad Sci U S A* **1996**, *93*, 13327–13332.
(139) Bai, J.; Tucker, W. C.; Chapman, E. R. PIP2 increases the speed of response of synaptotagmin and steers its membrane-penetration activity toward the plasma membrane. *Nat Struct Mol Biol* **2004**, *11*, 36–44.
(140) Chapman, E. R.; Davis, A. F. Direct interaction of a Ca2+-binding loop of synaptotagmin with lipid bilayers. *J Biol Chem* **1998**, *273*, 13995–14001.
(141) Vennekate, W.; Schröder, S.; Lin, C.-C.; van den Bogaart, G.; Grunwald, M.; Jahn, R.; Walla, P. J. Cis- and trans-membrane interactions of synaptotagmin-1. *PNAS* **2012**, *109*, 11037–11042.
(142) van den Bogaart, G.; Thutupalli, S.; Risselada, J. H.; Meyenberg, K.; Holt, M.; Riedel, D.; Diederichsen, U.; Herminghaus, S.; Grubmüller, H.; Jahn, R. Synaptotagmin-1 may be a distance regulator acting upstream of SNARE nucleation. *Nat Struct Mol Biol* **2011**, *18*, 805–812.
(143) Hui, E.; Johnson, C. P.; Yao, J.; Dunning, F. M.; Chapman, E. R. Synaptotagmin-mediated bending of the target membrane is a critical step in Ca(2+)-regulated fusion. *Cell* **2009**, *138*, 709–721.
(144) Martens, S.; Kozlov, M. M.; McMahon, H. T. How synaptotagmin promotes membrane fusion. *Science* **2007**, *316*, 1205–1208.
(145) Brewer, K. D.; Bacaj, T.; Cavalli, A.; Camilloni, C.; Swarbrick, J. D.; Liu, J.; Zhou, A.; Zhou, P.; Barlow, N.; Xu, J.; Seven, A. B.; Prinslow, E. A.; Voleti, R.; Häussinger, D.; Bonvin, A. M. J. J.; Tomchick, D. R.; Vendruscolo, M.; Graham, B.; Südhof, T. C.; Rizo, J. Dynamic binding mode of a Synaptotagmin-1-SNARE complex in solution. *Nat Struct Mol Biol* **2015**, *22*, 555–564.
(146) Xu, J.; Brewer, K. D.; Perez-Castillejos, R.; Rizo, J. Subtle Interplay between synaptotagmin and complexin binding to the SNARE complex. *J Mol Biol* **2013**, *425*, 3461–3475.

(147) Chicka, M. C.; Hui, E.; Liu, H.; Chapman, E. R. Synaptotagmin arrests the SNARE complex before triggering fast, efficient membrane fusion in response to Ca2+. *Nat Struct Mol Biol* **2008**, *15*, 827–835.
(148) Bender, J.; Kundlacz, T.; Rudden, L. S. P.; Frick, M.; Bieber, J.; Degiacomi, M. T.; Schmidt, C. Ca2+-dependent lipid preferences shape synaptotagmin-1 C2A and C2B dynamics: Insights from experiments and simulations. *Structure* **2024**.
(149) Singer, S. J.; Nicolson, G. L. The fluid mosaic model of the structure of cell membranes. *Science* **1972**, *175*, 720–731.
(150) Nicolson, G. L. The Fluid-Mosaic Model of Membrane Structure: still relevant to understanding the structure, function and dynamics of biological membranes after more than 40 years. *Biochim Biophys Acta* **2014**, *1838*, 1451–1466.
(151) Hannich, J. T.; Umebayashi, K.; Riezman, H. Distribution and functions of sterols and sphingolipids. *Cold Spring Harb Perspect Biol* **2011**, *3*.
(152) Yamashita, A.; Hayashi, Y.; Nemoto-Sasaki, Y.; Ito, M.; Oka, S.; Tanikawa, T.; Waku, K.; Sugiura, T. Acyltransferases and transacylases that determine the fatty acid composition of glycerolipids and the metabolism of bioactive lipid mediators in mammalian cells and model organisms. *Prog Lipid Res* **2014**, *53*, 18–81.
(153) Antonny, B.; Vanni, S.; Shindou, H.; Ferreira, T. From zero to six double bonds: phospholipid unsaturation and organelle function. *Trends Cell Biol* **2015**, *25*, 427–436.
(154) Israelachvili, J. N.; Mitchell, D. J.; Ninham, B. W. Theory of self-assembly of hydrocarbon amphiphiles into micelles and bilayers. *J. Chem. Soc., Faraday Trans. 2* **1976**, *72*, 1525.
(155) Quinn, P. J.; Joo, F.; Vigh, L. The role of unsaturated lipids in membrane structure and stability. *Prog Biophys Mol Biol* **1989**, *53*, 71–103.
(156) Frick, M.; Schwieger, C.; Schmidt, C. Liposomes as Carriers of Membrane-Associated Proteins and Peptides for Mass Spectrometric Analysis. *Angew Chem Int Ed Engl* **2021**, *60*, 11523–11530.
(157) Zhu, Y.; Yun, S. D.; Zhang, T.; Chang, J.-Y.; Stover, L.; Laganowsky, A. Native mass spectrometry of proteoliposomes containing integral and peripheral membrane proteins. *Chem Sci* **2023**, *14*, 14243–14255.
(158) Kostelic, M. M.; Zak, C. K.; Jayasekera, H. S.; Marty, M. T. Assembly of Model Membrane Nanodiscs for Native Mass Spectrometry. *Anal Chem* **2021**, *93*, 5972–5979.
(159) Ding, B.; Soblosky, L.; Nguyen, K.; Geng, J.; Yu, X.; Ramamoorthy, A.; Chen, Z. Physiologically-relevant modes of membrane interactions by the human antimicrobial peptide, LL-37, revealed by SFG experiments. *Sci Rep* **2013**, *3*, 1854.
(160) Neville, F.; Cahuzac, M.; Konovalov, O.; Ishitsuka, Y.; Lee, K. Y. C.; Kuzmenko, I.; Kale, G. M.; Gidalevitz, D. Lipid headgroup discrimination by antimicrobial peptide LL-37: insight into mechanism of action. *Biophys J* **2006**, *90*, 1275–1287.
(161) Zhang, X.; Oglęcka, K.; Sandgren, S.; Belting, M.; Esbjörner, E. K.; Nordén, B.; Gräslund, A. Dual functions of the human antimicrobial peptide LL-37-target membrane perturbation and host cell cargo delivery. *Biochim Biophys Acta* **2010**, *1798*, 2201–2208.
(162) Loo, J. A. Studying noncovalent protein complexes by electrospray ionization mass spectrometry. *Mass Spectrom. Rev.* **1997**, *16*, 1–23.
(163) Liu, L.; Bagal, D.; Kitova, E. N.; Schnier, P. D.; Klassen, J. S. Hydrophobic protein-ligand interactions preserved in the gas phase. *Journal of the American Chemical Society* **2009**, *131*, 15980–15981.
(164) Barylyuk, K.; Balabin, R. M.; Grünstein, D.; Kikkeri, R.; Frankevich, V.; Seeberger, P. H.; Zenobi, R. What happens to hydrophobic interactions during transfer from the solution to the gas phase? The case of electrospray-based soft ionization methods. *J Am Soc Mass Spectrom* **2011**, *22*, 1167–1177.
(165) Gabelica, V.; Galic, N.; Pauw, E. de. On the specificity of cyclodextrin complexes detected by electrospray mass spectrometry. *J Am Soc Mass Spectrom* **2002**, *13*, 946–953.

(166) Steinberg, M. Z.; Elber, R.; McLafferty, F. W.; Gerber, R. B.; Breuker, K. Early structural evolution of native cytochrome c after solvent removal. *Chembiochem* **2008**, *9*, 2417–2423.
(167) Kitova, E. N.; El-Hawiet, A.; Schnier, P. D.; Klassen, J. S. Reliable determinations of protein-ligand interactions by direct ESI-MS measurements. Are we there yet? *J Am Soc Mass Spectrom* **2012**, *23*, 431–441.
(168) Benesch, J. L. P.; Ruotolo, B. T. Mass spectrometry: come of age for structural and dynamical biology. *Curr Opin Struct Biol* **2011**, *21*, 641–649.
(169) Loo, R. R. O.; Goodlett, D. R.; Smith, R. D.; Loo, J. A. Observation of a noncovalent ribonuclease S-protein/S-peptide complex by electrospray ionization mass spectrometry. *Journal of the American Chemical Society* **1993**, *115*, 4391–4392.
(170) Liu, L.; Kitova, E. N.; Klassen, J. S. Quantifying protein-fatty acid interactions using electrospray ionization mass spectrometry. *J Am Soc Mass Spectrom* **2011**, *22*, 310–318.
(171) Sun, J.; Kitova, E. N.; Wang, W.; Klassen, J. S. Method for distinguishing specific from nonspecific protein-ligand complexes in nanoelectrospray ionization mass spectrometry. *Anal Chem* **2006**, *78*, 3010–3018.
(172) Schulte, J.; Tants, J.-N.; Ehr, J. von; Schlundt, A.; Morgner, N. Determination of dissociation constants via quantitative mass spectrometry. *Front. Anal. Sci.* **2023**, *3,* No. 1119489 vols.
(173) Tjernberg, A.; Carnö, S.; Oliv, F.; Benkestock, K.; Edlund, P.-O.; Griffiths, W. J.; Hallén, D. Determination of dissociation constants for protein-ligand complexes by electrospray ionization mass spectrometry. *Anal Chem* **2004**, *76*, 4325–4331.
(174) Sannes-Lowery, K. A.; Griffey, R. H.; Hofstadler, S. A. Measuring dissociation constants of RNA and aminoglycoside antibiotics by electrospray ionization mass spectrometry. *Anal Biochem* **2000**, *280*, 264–271.
(175) Schrecke, S.; Zhu, Y.; McCabe, J. W.; Bartz, M.; Packianathan, C.; Zhao, M.; Zhou, M.; Russell, D.; Laganowsky, A. Selective regulation of human TRAAK channels by biologically active phospholipids. *Nat Chem Biol* **2021**, *17*, 89–95.
(176) Lyu, J.; Zhang, T.; Marty, M. T.; Clemmer, D.; Russell, D. H.; Laganowsky, A. Double and triple thermodynamic mutant cycles reveal the basis for specific MsbA-lipid interactions. *Elife* **2024**, *12,* No. RP91094.
(177) Cong, X.; Liu, Y.; Liu, W.; Liang, X.; Russell, D. H.; Laganowsky, A. Determining Membrane Protein-Lipid Binding Thermodynamics Using Native Mass Spectrometry. *Journal of the American Chemical Society* **2016**, *138*, 4346–4349.
(178) Benkestock, K.; Sundqvist, G.; Edlund, P.-O.; Roeraade, J. Influence of droplet size, capillary-cone distance and selected instrumental parameters for the analysis of noncovalent protein-ligand complexes by nano-electrospray ionization mass spectrometry. *J. Mass Spectrom.* **2004**, *39*, 1059–1067.
(179) Wang, W.; Kitova, E. N.; Klassen, J. S. Influence of solution and gas phase processes on protein-carbohydrate binding affinities determined by nanoelectrospray Fourier transform ion cyclotron resonance mass spectrometry. *Anal Chem* **2003**, *75*, 4945–4955.
(180) van der Spoel, D.; Marklund, E. G.; Larsson, D. S. D.; Caleman, C. Proteins, lipids, and water in the gas phase. *Macromol Biosci* **2011**, *11*, 50–59.
(181) Shukla, A. K.; Futrell, J. H. Tandem mass spectrometry: dissociation of ions by collisional activation. *J. Mass Spectrom.* **2000**, *35*, 1069–1090.
(182) Douglas, D. J. Applications of collision dynamics in quadrupole mass spectrometry. *J Am Soc Mass Spectrom* **1998**, *9*, 101–113.
(183) Grandori, R. Origin of the conformation dependence of protein charge-state distributions in electrospray ionization mass spectrometry. *J. Mass Spectrom.* **2003**, *38*, 11–15.
(184) Cole, R. B. In Electrospray ionization mass spectrometry: fundamentals, instrumentation, and applications; Cole, Richard B., Ed., 1997; p. 577.

(185) Liko, I.; Degiacomi, M. T.; Lee, S.; Newport, T. D.; Gault, J.; Reading, E.; Hopper, J. T. S.; Housden, N. G.; White, P.; Colledge, M.; Sula, A.; Wallace, B. A.; Kleanthous, C.; Stansfeld, P. J.; Bayley, H.; Benesch, J. L. P.; Allison, T. M.; Robinson, C. V. Lipid binding attenuates channel closure of the outer membrane protein OmpF. *PNAS* **2018**, *115*, 6691–6696.
(186) Wang, W.; Kitova, E. N.; Klassen, J. S. Bioactive recognition sites may not be energetically preferred in protein-carbohydrate complexes in the gas phase. *J Am Chem Soc* **2003**, *125*, 13630–13631.
(187) Wang, W.; Kitova, E. N.; Klassen, J. S. Nonspecific protein-carbohydrate complexes produced by nanoelectrospray ionization. Factors influencing their formation and stability. *Anal Chem* **2005**, *77*, 3060–3071.
(188) Kitova, E. N.; Kitov, P. I.; Paszkiewicz, E.; Kim, J.; Mulvey, G. L.; Armstrong, G. D.; Bundle, D. R.; Klassen, J. S. Affinities of Shiga toxins 1 and 2 for univalent and oligovalent Pk-trisaccharide analogs measured by electrospray ionization mass spectrometry. *Glycobiology* **2007**, *17*, 1127–1137.
(189) El-Faramawy, A.; Siu, K. W. M.; Thomson, B. A. Efficiency of nano-electrospray ionization. *J Am Soc Mass Spectrom* **2005**, *16*, 1702–1707.
(190) van Berkel, G. J.; Asano, K. G.; Schnier, P. D. Electrochemical processes in a wire-in-a-capillary bulk-loaded, nano-electrospray emitter. *J Am Soc Mass Spectrom* **2001**, *12*, 853–862.
(191) Striegel, A. R.; Biela, L. M.; Evans, C. S.; Wang, Z.; Delehoy, J. B.; Sutton, R. B.; Chapman, E. R.; Reist, N. E. Calcium binding by synaptotagmin's C2A domain is an essential element of the electrostatic switch that triggers synchronous synaptic transmission. *J Neurosci* **2012**, *32*, 1253–1260.
(192) Le Maire, M.; Champeil, P.; Moller, J. V. Interaction of membrane proteins and lipids with solubilizing detergents. *Biochim Biophys Acta* **2000**, *1508*, 86–111.
(193) Kebarle, P.; Tang, L. From ions in solution to ions in the gas phase - the mechanism of electrospray mass spectrometry. *Anal Chem* **1993**, *65*, 972A-986A.
(194) Walker, L. R.; Marty, M. T. Lipid tails modulate antimicrobial peptide membrane incorporation and activity. *Biochim Biophys Acta Biomembr* **2022**, *1864*, 183870.
(195) Liko, I.; Hopper, J. T. S.; Allison, T. M.; Benesch, J. L. P.; Robinson, C. V. Negative Ions Enhance Survival of Membrane Protein Complexes. *J Am Soc Mass Spectrom* **2016**, *27*, 1099–1104.
(196) Nyenhuis, S. B.; Thapa, A.; Cafiso, D. S. Phosphatidylinositol 4,5 Bisphosphate Controls the cis and trans Interactions of Synaptotagmin 1. *Biophys J* **2019**, *117*, 247–257.
(197) Honigmann, A.; van den Bogaart, G.; Iraheta, E.; Risselada, H. J.; Milovanovic, D.; Mueller, V.; Müllar, S.; Diederichsen, U.; Fasshauer, D.; Grubmüller, H.; Hell, S. W.; Eggeling, C.; Kühnel, K.; Jahn, R. Phosphatidylinositol 4,5-bisphosphate clusters act as molecular beacons for vesicle recruitment. *Nat Struct Mol Biol* **2013**, *20*, 679–686.
(198) Araç, D.; Chen, X.; Khant, H. A.; Ubach, J.; Ludtke, S. J.; Kikkawa, M.; Johnson, A. E.; Chiu, W.; Südhof, T. C.; Rizo, J. Close membrane-membrane proximity induced by Ca(2+)-dependent multivalent binding of synaptotagmin-1 to phospholipids. *Nat Struct Mol Biol* **2006**, *13*, 209–217.
(199) Radhakrishnan, A.; Stein, A.; Jahn, R.; Fasshauer, D. The Ca2+ affinity of synaptotagmin 1 is markedly increased by a specific interaction of its C2B domain with phosphatidylinositol 4,5-bisphosphate. *J Biol Chem* **2009**, *284*, 25749–25760.
(200) Lawrence, S. A. S.; Kirschbaum, C.; Bennett, J. L.; Lutomski, C. A.; El-Baba, T. J.; Robinson, C. V. Phospholipids Differentially Regulate Ca2+ Binding to Synaptotagmin-1. *ACS Chem. Biol.* **2024**, *19*, 953–961.
(201) Oh, M. in; Consta, S. Stability of a Transient Protein Complex in a Charged Aqueous Droplet with Variable pH. *J Phys Chem Lett* **2017**, *8*, 80–85.

(202) Konermann, L.; Metwally, H.; McAllister, R. G.; Popa, V. How to run molecular dynamics simulations on electrospray droplets and gas phase proteins: Basic guidelines and selected applications. *Methods* **2018**, *144*, 104–112.
(203) Murakami, M.; Nakatani, Y.; Atsumi, G.-I.; Inoue, K.; Kudo, I. Regulatory Functions of Phospholipase A2. *Crit Rev Immunol* **2017**, *37*, 127–195.
(204) Arcaro, A.; Volinia, S.; Zvelebil, M. J.; Stein, R.; Watton, S. J.; Layton, M. J.; Gout, I.; Ahmadi, K.; Downward, J.; Waterfield, M. D. Human phosphoinositide 3-kinase C2beta, the role of calcium and the C2 domain in enzyme activity. *J Biol Chem* **1998**, *273*, 33082–33090.